BEARING CAPACITY OF CONCRETE

KIAN LAYEGHI

A THESIS SUBMITTED FOR THE DEGREE

OF

MASTER OF PHILOSOPHY

DEPARTMENT OF CIVIL ENGINEERING

UNIVERSITY OF ASTON IN BIRMINGHAM

MAY 1984

TO MY

MOTHER AND FATHER

BEARING CAPACITY OF CONCRETE

BY

KIAN LAYEGI

THESIS SUBMITTED FOR THE DEGREE OF MASTER OF PHILOSOPHY, APRIL 1984

SYNOPSIS

A review of relevant papers and codes of practice from several countries on the bearing capacity of concrete lead to the conclusion that there was a need for a study of existing data in order to be able to develop a simple yet reasonably accurate general formula to predict failure.

Initially 36 cubes were axially loaded through rigid plates and the results were compared with approximately 600 tests by investigators from other countries. In the second series of tests cubes were loaded concentrically through strip, rectangular and knife edge loading pieces with base plates of different thicknesses (4 to 40mm). These results were also compared with 85 available tests by other investigators. The distribution of axial stresses in the concrete and bending stresses in the steel base plate were measured using strain gauges fixed to both the concrete and the steel base plate.

The third series of tests was concerned with loading through universal columns of different sizes, as used in practice. Tests to failure were carried out on both 150 and 250mm cubes through three thicknesses of steel base plate (4, 8 and 12mm). The results from this series of tests could not be compared with any other test results, as none were available.

An empirical formula for the bearing capacity of concrete was produced from the first series of tests and then developed for strip, rectangular and square concentric loading pieces applied to a concrete cube through flexible plates. The formula was also used to predict the failure load in the third series of tests with universal columns. The test results from this series were also compared with the the design loads recommended by: AISC(29),Draft of Steel Code(30) and BS 449(31).

In the fourth series of tests concrete cubes were loaded eccentrically through stiff bearings of various sizes. The empirical formula obtained for concentric loading conditions was extended to predict the failure load for cubes loaded eccentrically through stiff bearings.

Finally a linear finite element plane-stress analysis was used to investigate the axial and lateral stress distribution in the concrete and steel base plate loaded through a knife edge loading piece. The theoretical model was chosen to resemble the tests carried out in this investigation on flexible steel base plate; presented in Chapter 3.

CONCRETE   BEARING CAPACITY   STEEL BASE PLATE   UNIVERSAL COLUMN

ACKNOWLEDGEMENTS

The author would like to thank Dr L H Martin for his help during the course of this research. His thanks are also due to Dr D J Just for his supervision of the work on the finite element analysis.

Thanks also go to Mr J H Hollins and all the technical staff who helped during the experimental work.

The author is indebted to Miss A K Holloway for her help in typing of the manuscript.

NOTATION

A	Area of specimens, part of which is subjected to load.
A_s	Stiff bearing or rigid plate surface area.
A_{se}	Effective area that is in contact with the specimen.
A_I	I-shape bearing area.
A_{Rec}	Rectangular bearing area.
a_e, b_e	Effective cantilever length.
B	Width of Universal Column.
b_x	Width of concrete specimen (see Fig. 2.2).
b_y	Length of concrete specimen (see Fig. 2.2).
D	Depth of Universal Column.
d	Diameter of circular specimen.
d_s	Diameter of stiff bearing.
e_x, e_y	Eccentricities of applied load, or bearing plate, with reference to centroid of specimen .
F	Load at failure.
F_e	Load at failure for an eccentricity of e.
F_c	Load at first cracking of specimen.
F_h	Horizontal component of load.
F_w	Design working load.
F_u	Design ultimate load.
f_b	Allowable bending stress of steel base plate.
f_{cb}	Bearing stress of concrete defined as (F/A_{se}).
f_{cp}	Prism or cylinder strength of concrete.
f_{cr}	Cracking strength of concrete.
f_{cu}	Cube strength of concrete.
f_N	Nominal bending stress of steel base plate.
f_p	Allowable bearing pressure.

f_{sp}	Splitting strength of concrete (cylinder-splitting test).
f_y	Yield stength of steel base plate.
H	Height of specimen.
L	Cantilever contact length between the concrete and plate.
R	Ratio of bearing area in contact with specimen (A_{se}), to the total area of the specimen (A).
R_1	Ratio of f_{cb} to f_{cu}.
R_2	Ratio of total area of the specimen (A), to bearing area in contact with specimen (A_{se}).
n	Ratio of (failure load) to (area of specimen x cube crushing stress) i.e.(F/Af_{cu})
n_e	Ratio of (failure load for eccentricity of e) to (area of specimen x cube crushing stress) i.e.(F_e/Af_{cu})
n_1	Ratio of (experimental failure load)/(theoretical failure load)
S_x	Width of stiff bearing, punch or rigid plate (see Fig. 2.2).
S_y	Length of stiff bearing, punch or rigid plate (see Fig. 2.2).
t	Thickness of base plate.
t_f	Thickness of the flange.
t_w	Thickness of the web.
Z_p	Plastic section modulus.
ϕ	Angle of internal friction.
a_1-a_8	Constants of displacement function.
u,v	Global degrees of freedom.
X,Y	Global reference axix.

Note : Some notations not included in the above list, will be specifically defined when they are first itroduced.

CONTENTS

PAGE No

PAGE No

LIST of TABLES

PAGE No

LIST of FIGURE

CHAPTER 6

PAGE No

LIST of PLATES

CHAPTER ONE

REVIEW OF PREVIOUS RESEARCH

1.1 Introduction

An important problem in the field of structural engineering design occurs when a concrete block is subjected to a concentrated load, eg : columns on concrete pedestals, bridge bearings on concrete piers, foundations of some hydraulic structures, anchor plates in prestressed concrete, concrete hinges, bearing blocks, and pile heads. To prevent crushing of the concrete, base plates are inserted between the steel and concrete to distribute the load.

The material in the region of the localized force is subjected to stresses of a very complex nature, and study of the problem is further complicated by the non-homogeneity and non-elasticity of concrete. Other factors which influence the accurate assessment of the bearing capacity of concrete are:

i) the influence of frictional restraint on the bearing surfaces.

ii) the distribution of compressive stresses at the bearing surface.

iii) the geometry of a loaded surface of a specimen relative to that of a bearing plate.

iv) the support medium, and the dimensions of a specimen.

v) the material properties and strength of concrete.

vi) the positioning and the amount of reinforcement.

vii) the position and existence of other forms of loads acting in addition to the normal load.

viii) the effect of different loading configuration and the effect of cracking and shrinkage.

Under current design methods based on the codes of practice, such as CP 110: 1972 and ACI 318: 77, the main factor in designing for bearing capacity is the allowable bearing stress. However, a comparison of the design codes (discussed in Chapter 1) for a square loaded area, shows a wide variation in permissible bearing stresses.

Almost all the papers published so far, detailing both theoretical and experimental investigations, have, with the exception of a few (4,13,20), dealt with rigid plates and their effect on bearing capacity. Theoretical works to date (7,10,14),which between them give a wide divergence of results, are based on the internal friction theory. This assumes failure as a sliding action of a single cone along planes inclined to the direction of principal stress. The resistance to sliding consists of two parts: a constant shearing strength or internal cohesion, and a resistance which is proportional to the normal stress on the plane of sliding, and may be considered as due to internal friction.

In practice, however, the loaded area of a plate is quite often less than its total area, therefore the bending of the plate and consequently its stiffness affects the ultimate capacity. Only Hawkins(13) has carried out a detailed analysis and considered the influence of bending of the base plate on bearing capacity, for concentric loading. He developed two discontinuous quadratic equations for flexible and semi-flexible plates. The Draft of the Steel Code 8.8.2 (28), proposed an empirical elastic solution which is based on an allowable bearing pressure of $0.4f_{cu}$ for concrete and an allowable bending stress of 267 N/mm^2 for the steel base plate. The code assumes that when concrete reaches the strength of $0.4f_{cu}$ the base plate has a strength of 267 N/mm^2. There is no experimental evidence which supports this supposition.

The experimental works reported so far, while of considerable interest, does not explain the factors affecting the bearing capacity of concrete especially the effect due to the bending of steel the base plate. There is a need for an investigation of this effect on bearing capacity, both in concentric and eccentric loading conditions. In addition, experiments are required to determine the effects of the more commonly used loading pieces, such as I and H sections.

1.2 Literature Review

Bauschinger's(1) tests in 1876 were on a limited number of sandstone cubes, but nevertheless the well known cube root formula ($f_{cb}=f_{cp}\sqrt[3]{A/A_s}$) for localised pressure was based on his work. Bauschinger's tests were over a narrow range of ratios of footing area to bearing area (1:1 to 7:1). His tests demonstrated that the maximum bearing pressure that may be applied to rock and concrete footings increases as the ratio of footing area to loaded area (R_2) increases.

Meyerhof(2) in 1953 tested 20 cubes and prism specimens, the depths of which varied from 38 mm to 152 mm. Concentric loading was applied through a short, high-tensile steel cylinder, 32 mm in diameter with thick plates as the support medium. The concrete cube strength varied from 20 to $27N/mm^2$, and the tests were carried out after six to eight days.

Based on the Coulomb-Mohr theory of rupture, Meyerhof developed a theory for a two-dimensional case of strip-loading with large ratios of block depth to width ($H/b_x > 1$). This showed a high correlation for small ratios of the block width to footing width (b_x/S_x =2 to 6) when compared to tests by Graf (3). Meyerhof extended his theory to apply to circular punch loading, but the correlation of the theory to the experimental work was unsatisfactory.

The blocks tested by Meyerhof exhibited a sliding failure in concrete due to the formation of a distinct cone under the circular base plate. Meyerhof suggested that for strip footings the bearing capacity increased in direct proportion to the ratio of block thickness to footing width (H/S_x). He also suggested that the angle of internal friction of concrete and rock decreased with greater pressure on the shear plane.

Although Meyerhof's theory for strip loading agreed closely with tests by Graf (3) for a limited ratio of block width to footing width (b_x/S_x), it should be pointed out that Meyerhof assumed $f_{sp}/C = 1$.

where C is unit cohesion

Shelson(4) in 1957 was one of the first to consider the effect of flexible plates. He tested twenty-one 203mm cubes which were loaded through 6mm thick mild steel base plates. In four groups (each group consisted of three tests), the load was applied to the plate through a loading column which terminated in a bearing surface 25mm square on the base plate. In the remainder of the tests, the load was applied over the entire surface area of the base plate. The base plate itself was bedded on top of the block in plaster of paris, and positioned at the centre with its edges parallel to those of the block. The concrete strength of Shelson's specimens varied from

$50N/mm^2$ to around $57N/mm^2$.

Shelson (4) compared his results to those of Baushinger(1), Meyerhof(2) and Parker(5), as shown in Fig. 1.1. He made a minor alteration to the formula recommended by ACI Building Code (ACI 318-56) Section 305 and compared this to the experimental results as shown in Fig. 1.2. Shelson suggested that in the shallow blocks ($H/b_x < 1$) a uniform compressive stress covering the region directly beneath the loaded area extended throughout the total depth. A wedge did not form beneath the loaded area and therefore failure was not due to splitting of the block. While his tests had a depth to width (H/b_x) ratio equal to one, Shelson concluded that for a given ratio of footing area to loaded area (A/A_s) the maximum bearing pressure increases as the depth to width (H/b_x) ratio decreases.

Shelson then compared his version of the ACI formula to the specifications of the ACI Building Code (Fig. 1.2). He claimed that for lower ratios of footing area to loaded area (A/A_s), the ACI code may result in a slightly lower factor of safety than anticipated, while for ratios higher than 10:1 the specifications were too conservative.

In 1958 a four part paper by Tung Au, Campbell-Allen, W.G. Plewes and Maurice Royer(6) was published discussing Shelson's work.

i) Au pointed out that within the range of the test results, the allowable concrete bearing stress might be increased with an increase in the A/A_s ratio, and that the test data did not include ratios of A/A_s (1:1 to 1:8) which occur more often in practice. Au was not convinced that the bearing pressure on concrete at $A/A_s = 1$ should

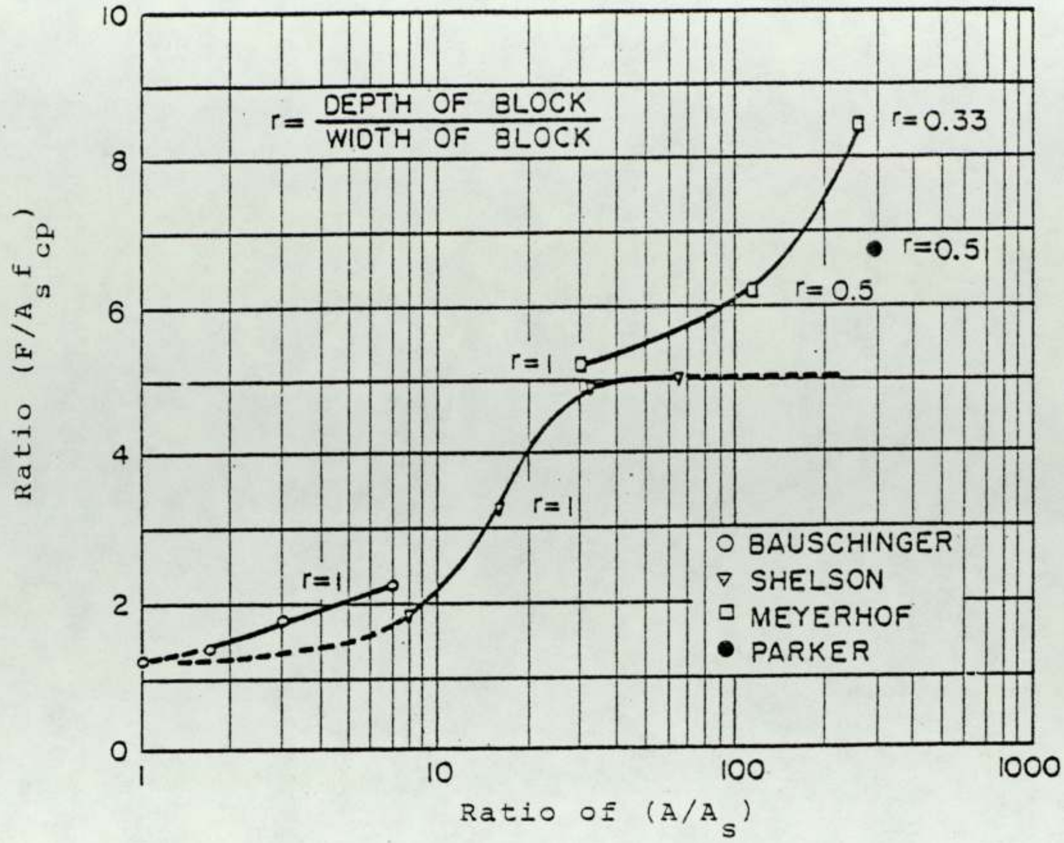

Fig. 1.1 Test results on the bearing capacity of stone and concrete footings.

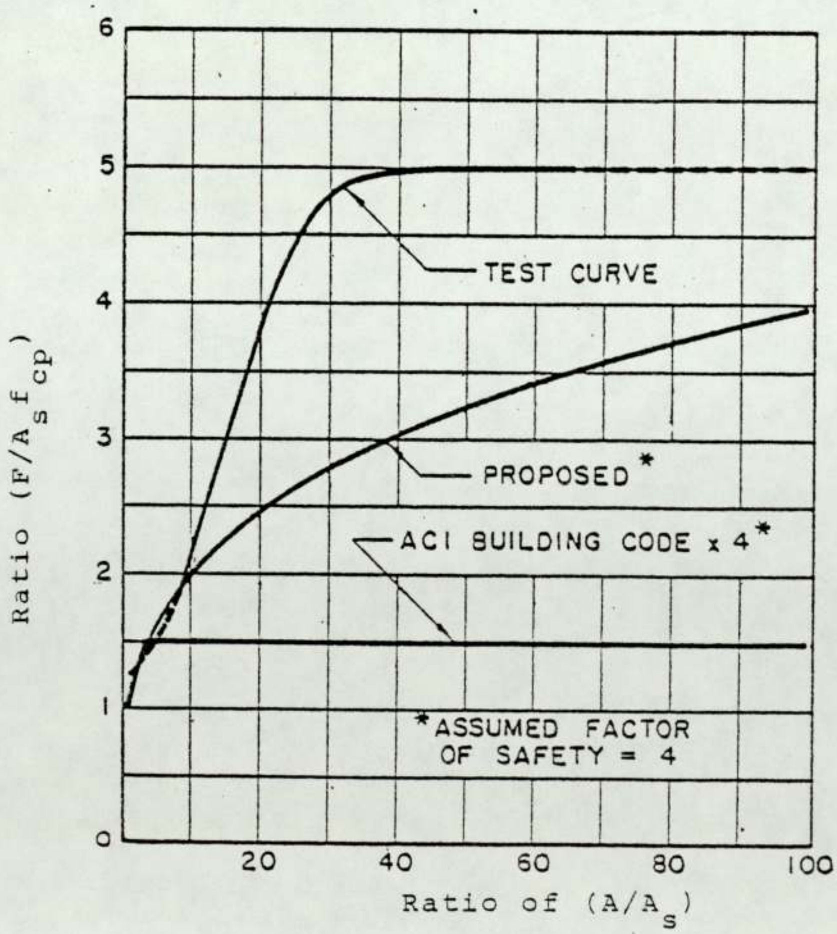

Fig. 1.2 Comparison of Shelson's test results to permissible bearing capacity of concrete as recommended by ACI

be taken as high as that shown in Fig. 1.2, and suggested that there was not sufficient evidence to propose a revision of ACI Building Code (ACI 318-56) Section 305.

ii) Campbell-Allen supported his own argument using tests carried out at the University of Sydney on 18 mortar and concrete cylinders loaded axially by circular steel punches over a part of their areas. The ratio of concrete area to loaded area varied from 1.8:1 to 28:1, with the majority of tests having a ratio of less than 8:1. The mix had a 3:1 sand-cement ratio with a w/c ratio ranging from 0.62 to 0.5. Tests were carried out at 7 days' age and the concrete strength varied from 9 to 20 N/mm^2. From the results of these tests and a comparison (Fig .1.3) with those carried out by Shelson, Campbell-Allen noted that the values of bearing pressure in his tests were greater than in Shelson's. This he suspected to be due to the change of shape, from square to circular cross-section. In three cases where the depth to diameter ratios were less than 1:1, a substantial reduction in bearing pressure was observed, conflicting with Shelson's findings. Campbell-Allen added that Shelson's tests were all on centrally-loaded footings, while ACI 318-56 allowed considerable eccentricity. A small number of tests at the University of Sydney, in which 102mm diameter cylinders were loaded through 25mm diameter discs with various eccentricities, indicated that, for the maximum eccentricity for which any stress was permitted by ACI 318-56, the bearing pressure was only 52 percent of the pressure when loading was concentric. If these reductions due to eccentricity were considered in the curve proposed by Shelson, the curve would no longer be conservative.

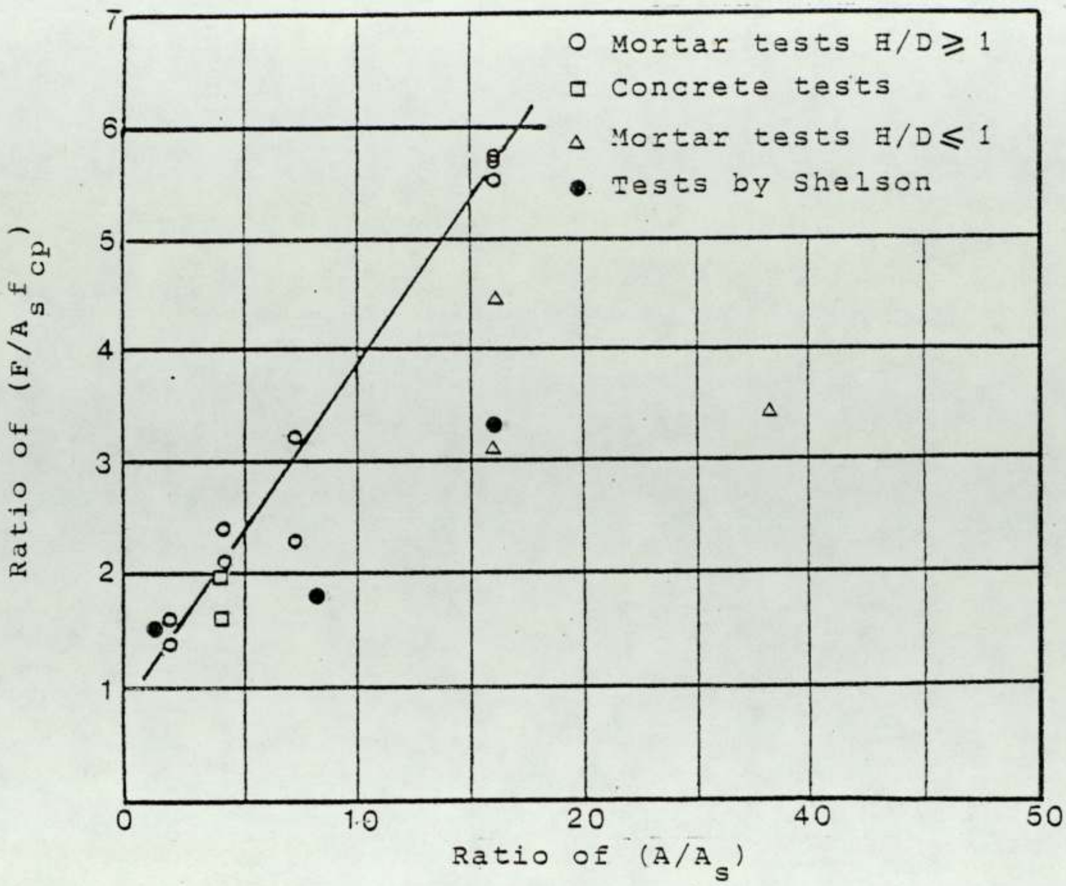

Fig. 1.3 Concentric loading tests on mortar and concrete cylinders, carried out at the University of Sydney.

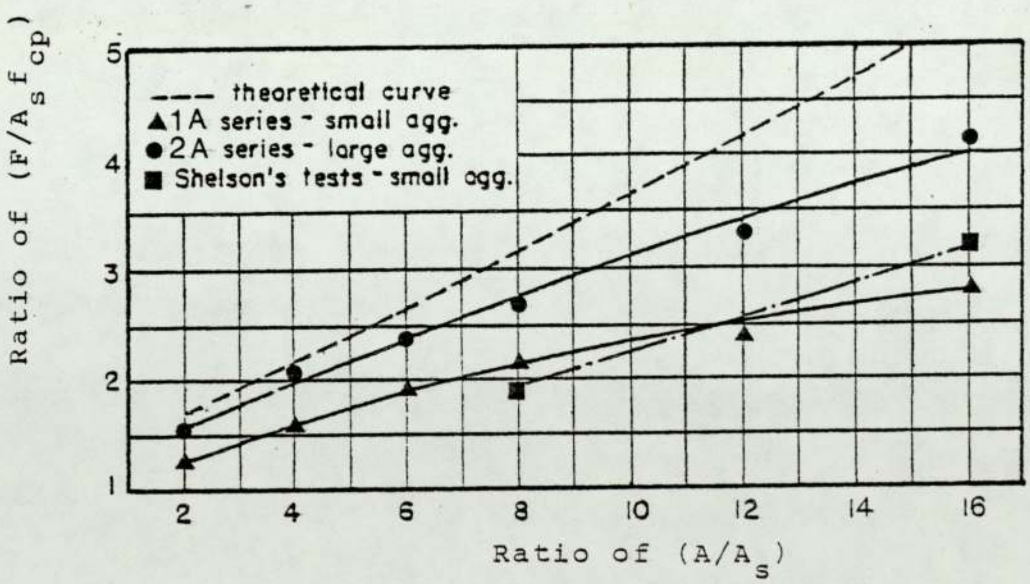

Fig. 1.4 Comparative study of results for 203 mm cubes by Au and Baird.

iii) Plewes indicated the importance of the depth to width ratio which was neglected by Shelson. He argued that it was not possible to decide, from the given data, whether the effect of varying the depth to width ratio could be ignored. Plewes argued that Shelson's assumptions were not clear, but he himself did not present any experimental work to support his own statements.

iv) Royer studied the formula presented by Shelson(4), claiming it was practically identical to Bauschinger's test(1), with a safety factor of four. Using Shelson's test results, Royer developed a similar formula which he suggested would be closer, to the test curve.

Further relevant work in this field was done in 1960 by Au and Baird (7). Sixty concrete blocks, whose area was 2 to 16 times the contact area and whose depth equalled either half or the total width of the block (203mm), were tested. A concentric load was applied through steel base plates placed on top of concrete blocks in plaster of paris. The concrete blocks were embedded in plaster of paris, on steel shoe plates 6mm thick, which provided smooth bottom surfaces. The specimens were cast from two mixes with maximum aggregate sizes of 6 and 12mm respectively. Two concrete strengths of 68 and 38 N/mm^2 were used (Mix 1 and Mix 2). AU and Baird used the internal friction theory of sliding failure as their working hypothesis, and developed a theoretical solution which was not in good correlation with the experimental results, as shown in Fig. 1.4. The formula presented was sensitive to half the apex angle on a vertical plane passing through the apex of the inverted pyramid. Since this angle varied by several degrees in experiments, the results could be misleading. The effect of aggregate size on bearing capacity is shown in Fig.1.5. The results

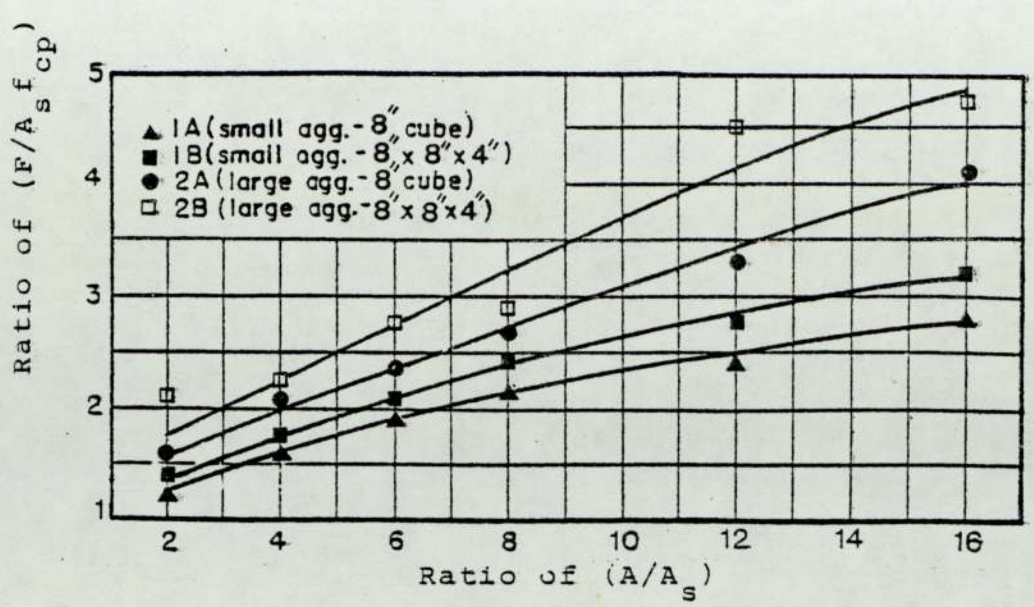

Fig. 1.5 Plotted experimental results of Au-Baird, central loading on concrete specimens.

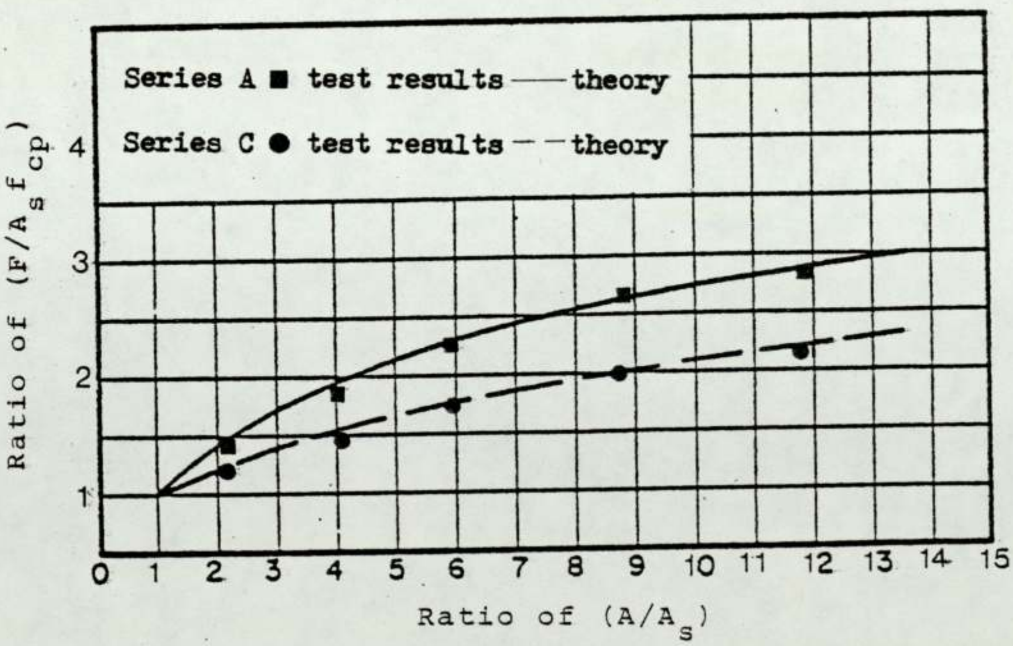

Fig. 1.6 Comparison of the test carried out at the University of Illinois and the theory recommended by Hawkins.

indicated that the maximum load was usually reached shortly after the crack appeared, and then the load-carrying capacity immediately reduced to a small value. In examining the shallow specimens (203 x 203 x 101), no clear cut pyramids were found. The absence of pyramids was attributed to a resistance to the sliding failure.

In a two part paper published in 1960 by Ugur Ersoy and Neil Hawkins(8), the work done by AU and Baird was discussed. Ersoy pointed out that the theory by Au and Baird was based on the formation of an inverted pyramid underneath the loading plate at failure. This Ersoy indicated, did not occur in specimens having small ratios of H/b_x, and claimed that specimens failed because of the crushing of the concrete underneath the loading plate. Au suggested that for a fixed value of R, the bearing capacity is constant for a block having a high ratio of depth to the side dimension of loading plate (H/S_x) and decreases for small ratios. However, no theoretical or experimental work was given to support this statement.

Hawkins(8) argued that the assumption made by Au et al., that the final failure by splitting was the result of combined tension and bending in the surrounding concrete block did not seem reasonable. Hawkins stated that Au and Baird's theoretical equation implied that f_{cb}/f_{cp} was sensitive to the depth of the block, and also that f_{cb}/f_{cp} continued to increase without limit as the ratio of contact area to block area increased. Neither of these assumptions, Hawkins asserted, had been confirmed by tests.

Hawkins(8) extended the formula presented by Au et.al. by assuming that a uniform pressure was distributed over the interface between the cone underneath the stiff bearing and the confining concrete. Hence he showed that horizontal splitting pressure was a function of C and R_2 . He substituted his own expression for horizontal splitting pressure in the equation developed by Au et.al. To support his theoretical formula, Hawkins used the tests carried out at the University of Illinois on seventy-one 152mm and 229mm cubes with a concrete strength varying from 27 to 65 N/mm^2 . The specimens were loaded concentrically, using square steel bearing plates 19mm thick. The comparison is shown in Figs. 1.6 and 1.7. Although the figures indicate a good correlation between the test results and the theory, Hawkins assumed a constant angle of internal friction of 43 degrees, which was unsupported by any experimental results. Test series A, C and D in the figures 1.6 and 1.7 were on 150mm cubes of cube stengths 23.7, 51.9 and 36.1 N/mm^2 respectively. A more detail of these test results is shown in Table 4.2 of Chapter 4.

Hawkins claimed that he determined the value of C from a Mohr's circle construction, but again there were no published results. Hawkins stated that "The bearing capacity of concrete is independent of the depth of the block", a statement in conflict with the tests carried out by Au and Baird on cubes (203mm) and prisms (203 x 203 x 102mm).

Muguruma and Okamoto(9) in 1965 tested fifty-two cubes and prisms of rectangular and square cross-section in two series of two and three dimensional concentric loadings. In series one, the specimens had a rectangular cross-section (250 x 150), with three different heights of 500, 250 and 150mm; the ratios of concrete area to loaded area were 1:1 to 1:25. In series two, the specimens were

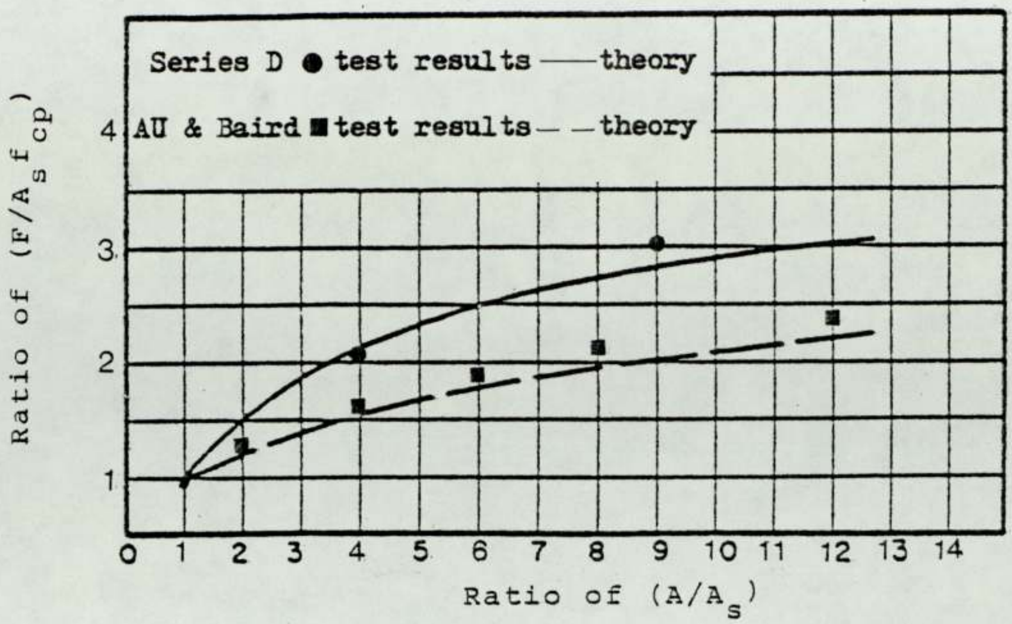

Fig. 1.7 Comparison between the test results of Au - Baird and the University of Illinois to the theory recommended by Hawkins.

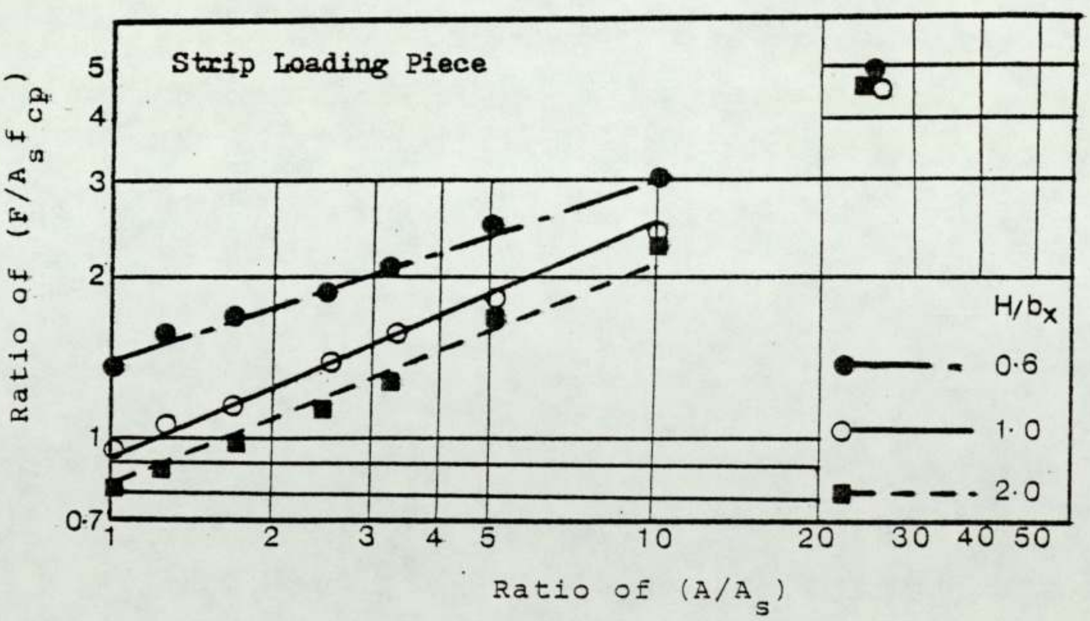

Fig. 1.8 Plotted experimental results of Muguruma et al, central loading through strip loading piece.

loaded three dimensionally, through square steel base plates. The blocks were of square cross-section (200 x 200mm) with five different heights varying from 100 to 400mm. The concrete area to loaded area varied from 1:1 to 1:100, and the concrete strength varied from 48 to $52N/mm^2$. For different ratios of height to width of block (H/b_x), the results are shown in Figs. 1.8 and 1.9. Muguruma and Okamoto developed an empirical formula which was a function of height and width of concrete, for both two and three dimensional concentrated loading conditions. The formula, however, should only be applied to high concrete strengths ($40-50N/mm^2$) and low values of concrete area to loaded area ($A/A_s < 10$). The correlation of the theoretical and the experimental results was not shown in the paper.

Extensive analytical work by Hawkins(10) in 1968 resulted in approximate expressions for the bearing strength of concrete blocks loaded both concentrically and eccentrically through rigid plates. The expressions were based on 230 tests using mainly 152mm cubes with a cube strength of 27 to $67N/mm^2$. Cowan's(11) dual failure criterion for concrete was adopted for the theoretical work.

The expressions produced were a function of the apex angle related to a vertical plane passing through the apex of the inverted pyramid formed underneath the bearing plate. A similar approach was adopted by Au and Baird(7). A good correlation between test results and theory was observed when the loading was concentric and through a square loading plate. Hawkins' equation for rectangular plates did not predict the test results accurately.

Having produced three equations for eccentric loading,

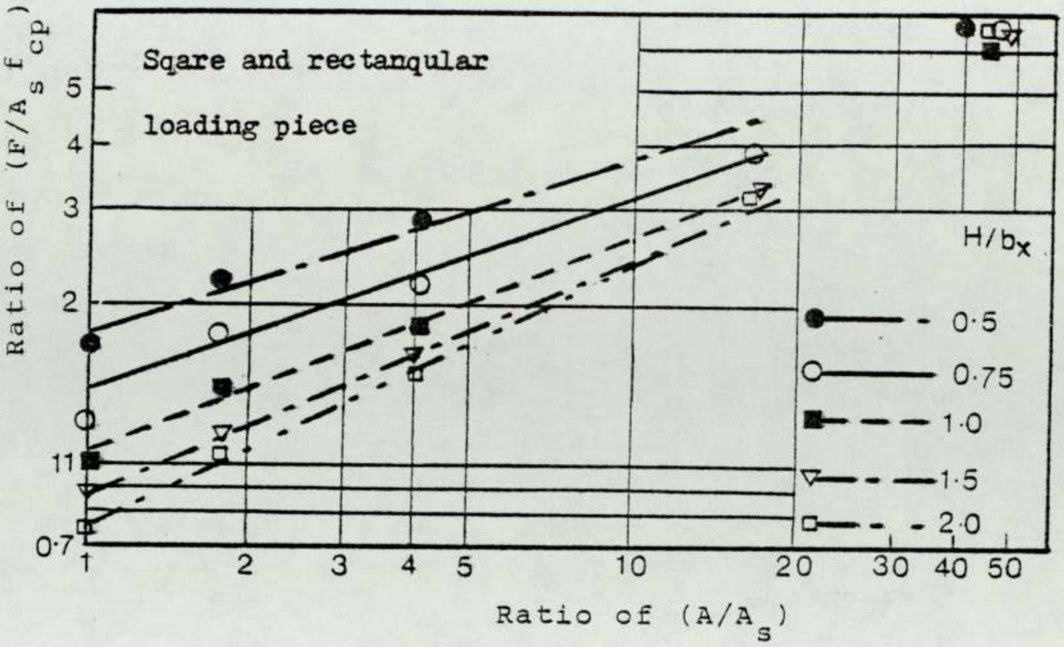

Fig. 1.9 Plotted experimental results by Muguruma et al, central loading through square and rectangular loading piece.

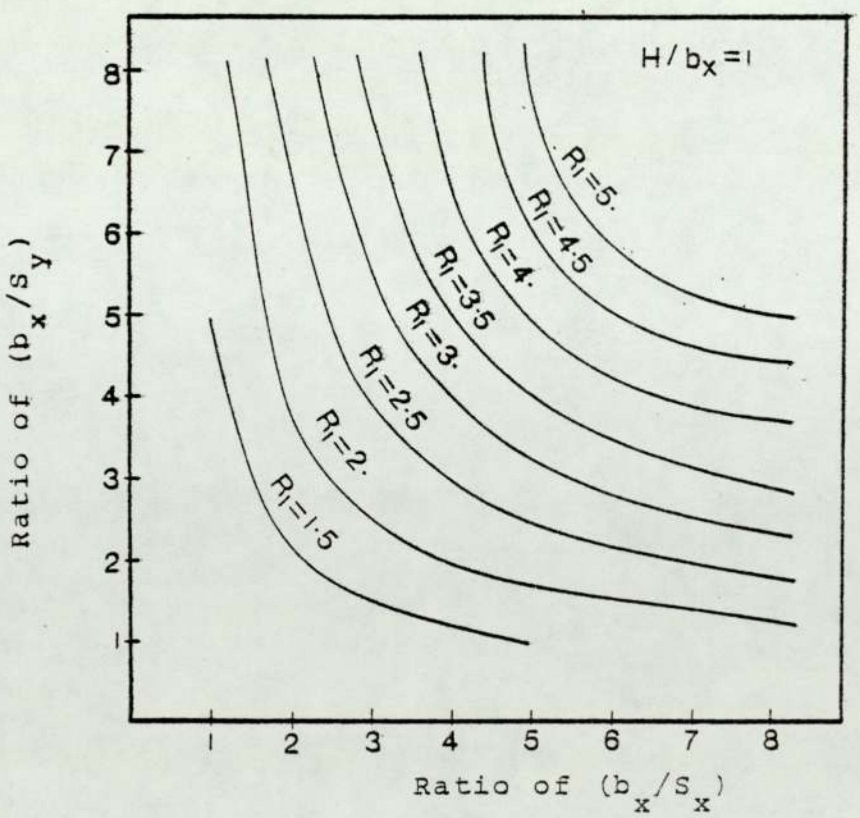

Fig. 1.10 Relationship of R_1 and relative dimensions of specimen and loaded area (b_x/S_x, b_x/S_y). By Niyogi

Hawkins recommended that the one with the least failure load be used. The ratio of the test results to the theory , for loading on the corner of the concrete varied from 1.29 to 1.55. For this kind of load, Hawkins recommended a maximum ratio of R_2 of unity, without presenting a reasonable explanation.

In 1968 Hawkins(12) was one of the first to make a detailed investigation into the effect of the bending of the base plate on the bearing strength of concrete. Eight series of tests, mainly on 152mm cubes with cube strength varying from 24 to 51N/mm^2 , were carried out, in which base plates of different thicknesses (.75 to 25mm) were used. Loading was concentric and through square punches with sides varying from 51 to 58 mm.

Hawkins suggested that failure models changed depending on whether the base plate was flexible, semi-flexible or rigid. For both flexible and semi-flexible plates, Hawkins developed two quartic independent equations in which the ultimate capacity increased linearly with the plate thickness, but these equations were discontinuous. The correlation of the test results to the theory using three variation for flexible, semi-flexible and rigid plates had a mean deviation of $\mp$ .089(8.7%).

Hawkins also compared his theory to Shelson's tests(4), and the correlation had a mean of 1.06 $\mp$ .06(0.5%). Hawkins used a value of the angle of internal friction of 51° for these calculations.

Chen and Drucker(14) in 1969 developed upper-bound equations for both two and three dimensional loading. Their analysis was based on a modified Mohr-Coulomb failure criterion with small tension cut-off and a limit-state theorem . Separate equations were introduced for short ($H<b_x$) and long ($H>b_x$) blocks for both cases of loading. The analysis for ($H>b_x$), however, was based on a trial and error method. The theory showed a good correlation for small ratios of H/S_x (3 to 6), with test data for strip loading by Graf(16) in 1934. The parameter of $\psi = 20^{\circ}$ and $f_{cp} = 5f_{sp}$ was used for this comparison. Chen and Drucker(14) compared their theory to the tests done by Campbell(6) and Meyerhof(2), suggesting that using $f_{cp} = 10f_{sp}$ and $\psi=20^{\circ}$ gave good upper-bound values. However, this comparison was not shown. For ratios of specimen width to width of the stiff bearing (b_x/S_x) over 5, the Chen and Drucker proposed that the local deformability of concrete in tension was not sufficient to permit the application of limit state analysis

In 1970 Hyland and Chen(17) tested 210 mortar and concrete cylinders (152mm diameter) with three different lengths of 153, 76 and 51mm. Half of the specimens (mortar and concrete) had a 16mm diameter hole beneath the loading plate of diameters 38 and 51mm. Tests were carried out at about 34 days, with the concrete cube strength varying from 35 to 55N/mm^2 . Three different base conditions were used. A 178x178x9.5mm steel plate provided high base friction, and a plastic base and double punch were used to provide low friction.

The predicted values of Chen and Drucker(14) for a smooth base condition were compared to the experimental results, and it was suggested that Chen and Drucker's solution gave an accurate upperbound only when H/S_x was less than two. The internal friction angle of concrete for this comparison was taken to be 30 degrees. Hyland and

Chen(17) indicated that concrete could be strained sufficiently to develop almost complete plasticity throughout a concrete cylinder for $H/D_s < 2$ and $D/D_s < 4$ loaded by a concentric punch. Their results revealed that the presence of a central hole (16mm diameter) in specimens did not have a significant effect on the observed bearing strength.

The most extensive and comprehensive tests, which contained 1422 specimens, were carried out by Niyogi(18,19). Most of the specimens were 203mm cubes and 203mm square prisms of varying height (102mm to 610mm). Concentric loading was applied through square, rectangular and strip bearing plates 12.7mm thick and of mild steel, except for the smaller sizes, where high tensile steel was used. Niyogi considered the effect of the following variables on bearing capacity :

i) the size of the specimen and the plate size,

ii) the supporting medium,

iii) the concentrated load applied from opposite ends of the specimen,

iv) the mix proportions and strength of concrete,

v) the dimension of the specimen,

vi) the form and quantity of reinforcement.

In his first paper Niyogi(18) in 1973, only considered the effect of the first variable above, using 440 specimens with concrete cube strength varying from 23 to $35N/mm^2$. With the results given in Fig. 1.10 he developed an empirical formula for cubic specimens loaded concentrically through square, rectangular and strip loading. Except for both large and small relative side ratios (b_x/S_x, b_y/S_y), a good correlation of formula and experimental results was shown. Niyogi developed an expression for a correction factor for eccentric loading which was derived from test data for square plates only.

Niyogi suggested that the ratio of the dimensions of the specimen surface and bearing plate (b_x/S_x, b_y/S_y) were more important parameters than R_2 i.e. (A/A_s). The importance of these parameters is shown in Fig. 1.10. He indicated that the bearing strength decreased as the height increased, particularly when $R_2 \simeq$ 8 or less . From the results plotted in Fig. 1.11, Niyogi suggested that in the case of three dimensional loading, the bearing capacity decreased for increasing ratios of H/b_x with ratios of $R_2 < 8$. On the other hand, the bearing capacity increased for increasing ratios of H/b_x and ratios of $R_2 > 8$. This was in direct conflict with Shelson's conclusion. One important point which can be drawn from Niyogi's plotted results in Figs. 1.11 and 1.12 is that the rate of increase in bearing capacity changes for ratios of R_2 greater and less than 8:1, which suggests a change in failure criteria.

Niyogi's second paper(19) in 1974 considered the effect of support media, mix and size of specimen. His tests included 203mm cubes and square prisms of varying heights, with mix proportions : 1:1:2, 1:1:1.5, 1:2:4, 1:3:4 and 1:4:8. Some four hundred and five specimens were loaded concentrically through steel plates (strip-square) and, apart from those tests which underwent concentric loading from both ends, the rest were seated on the machine bed, on rubber, or on sand.

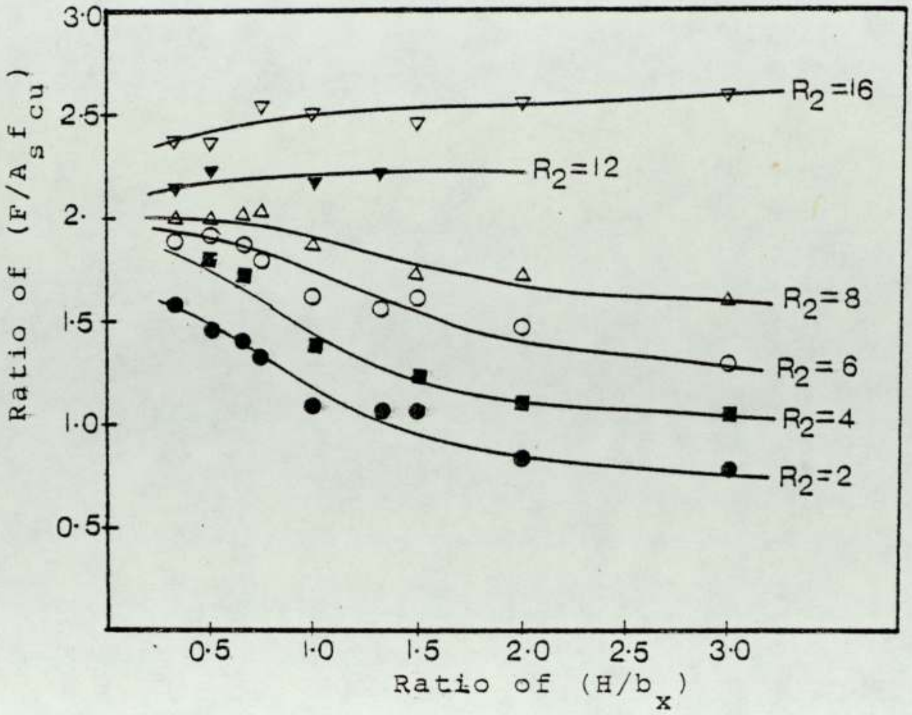

Fig. 1.11 plotted test results by Niyogi, central loading through strip loading piece.

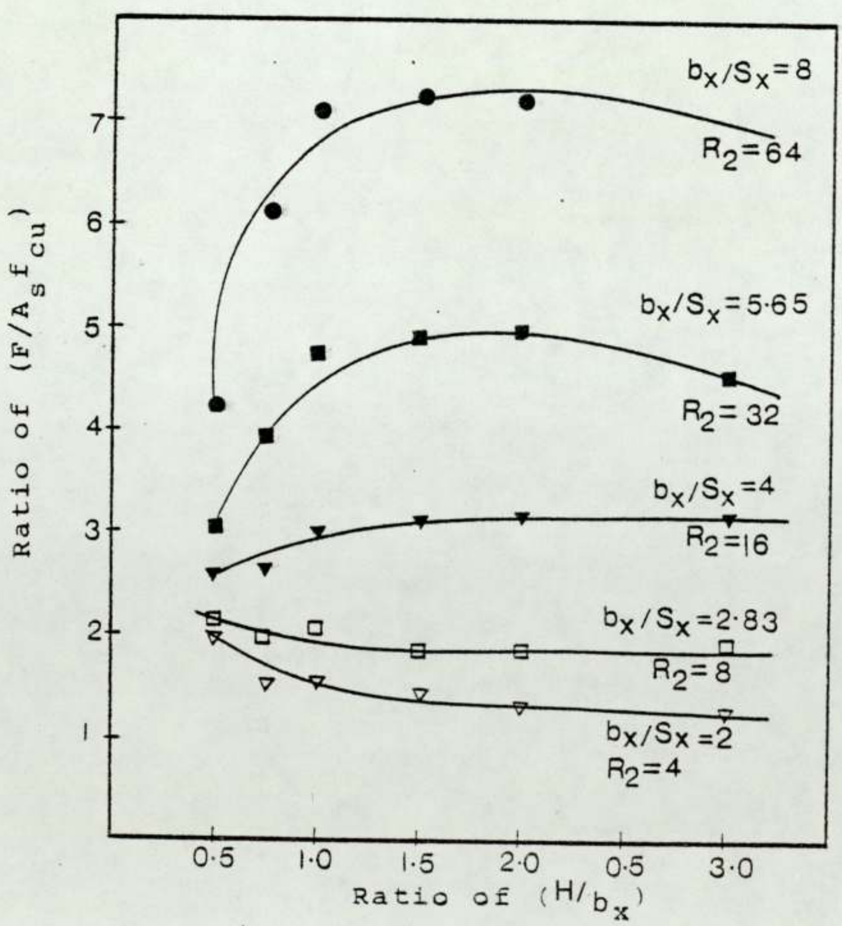

Fig. 1.12 Plotted test results by Niyogi, central loading on square prisms.

Niyogi drew the following conclusions :

i) that the compressible bed reduced the bearing strength of blocks (particularly for $H/b_x < 2$); the nature of the bed had no effect if the relative depth (H/b_x) was above 2.

ii) that concentric loading from both ends had the effect of reducing the bearing strength compared to localised loading from one end only. This reduction in bearing strength depended on the height of a specimen and the support media.

iii) that the bearing strength could be affected to some extent by variations in mix proportions and strength of concrete. The richer the mix, and the higher the strength of concrete, the lower the value of bearing strength for a given ratio of R_2.

De-Wolf(20) in 1978 carried out a series of tests in which he used different thicknesses of base plate (16 to 29 mm). Nineteen cubes of varying sizes (175 to 279mm) were concentrically loaded through a square punch, which was centred on a square base plate, for three ratios of concrete area to base plate(1.0,2.0,4.0). The concrete strength was approximatly 20 N/mm^2 and the mild steel base plate had a yield strength of 250 to 300 N/mm^2.

De-Wolf developed a simple empirical formula and the correlation with the tests results was $1.01 \pm .0813$ (8.0 %). While the method adequately predicted the failure load for the series of tests carried out by De-Wolf himself, he suggested that the formula could not be directly applied to other tests. Using Hawkins (10) formula De-Wolf set upper and lower limits to the proposed formula.

In developing the formula, De-Wolf assumed that the concrete strength(f_{cu}) and the ultimate load had a linear relation, which was in conflict with Hawkins' finding(13). De-Wolf also stated that the yield strength of the base plate had a negligible effect, contradicting Hawkins' suggestion that the bearing capacity increased in direct proportion to the square root of the steel base plate's yield strength.

In 1979 Williams(21) carried out a comprehensive investigation, reviewing and correlating almost all the available data. To fill the existing gaps between the published results, he carried out an extensive series of tests (1152 specimens) of five basic concrete mixes with cube strength varying from 20 to 75N/mm^2 and maximum aggregate size ranging from 2.4 to 20mm. The specimens were mainly 152mm cubes and 152mm square prisms of varying heights (25 to 475mm), loaded concentrically under a variety of loading configurations, two and three dimensional. A series of cubes was tested, in which a thick steel punch was positioned on a steel plate with three different thicknesses (6, 12, 25mm). The yield strength of the base plate was not published. Williams(21) used several different supporting media, such as steel platens, resin sandwich, plaster, 3mm rubber sheet and 3mm plywood.

All the available data was plotted as shown in Fig. 1.13. Having applied a correction factor to the data in Fig. 1.13 and having removed the data for depth/width ratio of less than .5, Williams plotted the results shown in Fig. 1.14. The following conclusions were drawn.

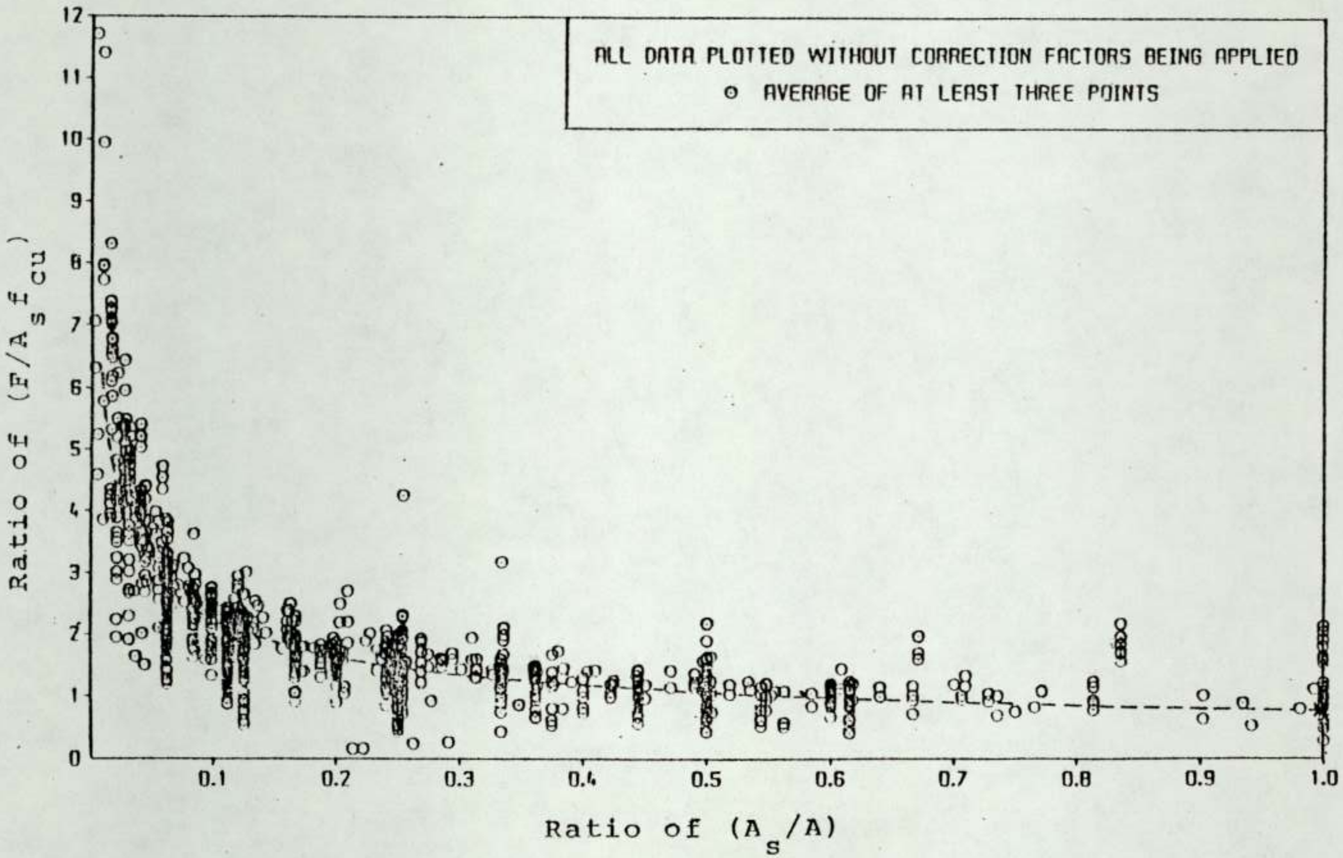

Fig. 1.13 Graph plotted by Williams, using all the available data as presented in his paper.

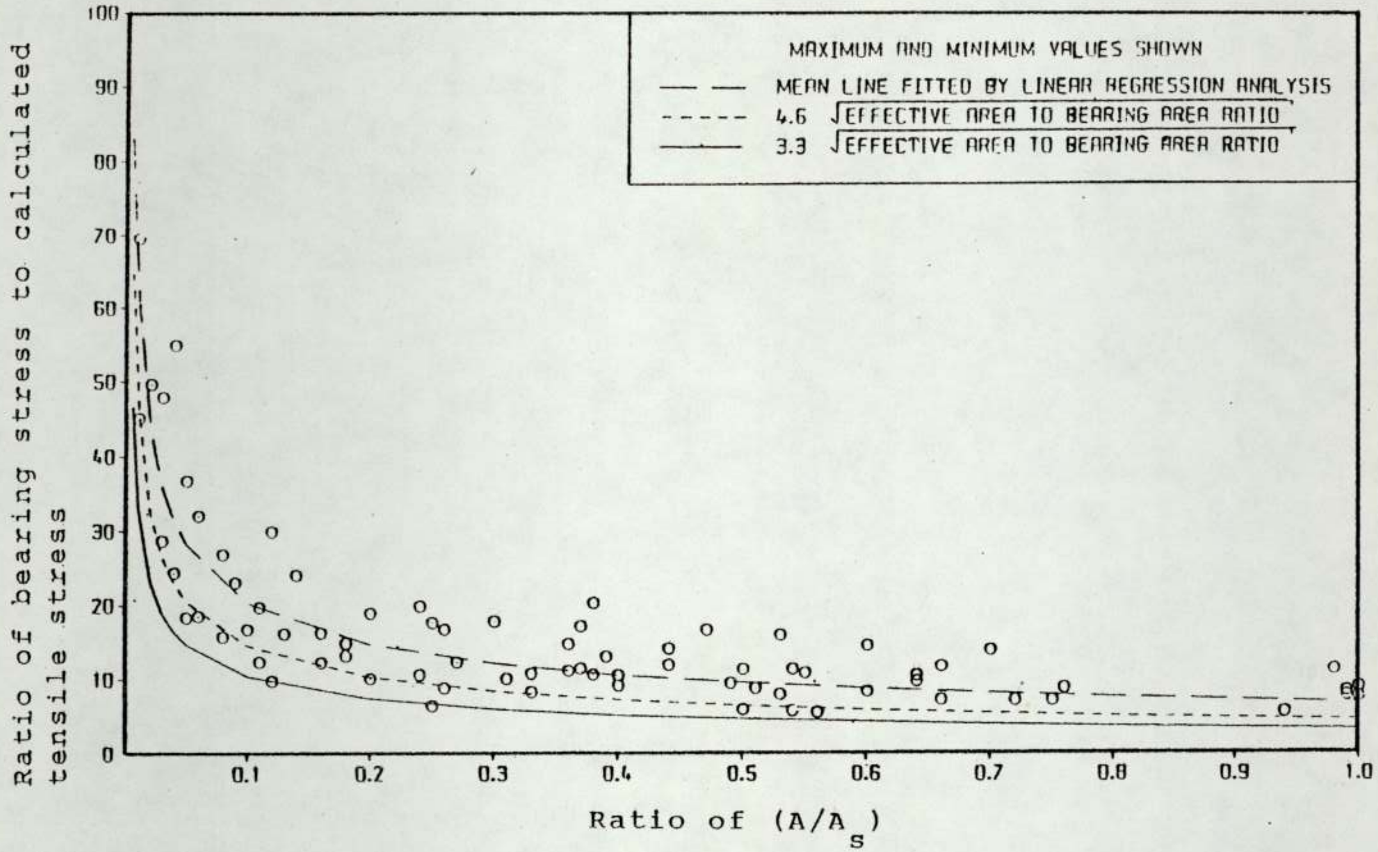

Fig. 1.14 Graph plotted by Williams, using all the available data, corrected for varying loading conditions, maximum and minimum values are only shown.

i) That the localised bearing capacity of concrete could be calculated on an "effective area" basis, using an equation of the form :

$$\frac{f_{cb}}{f_{sp}} = K \left[\frac{A_s}{A_e}\right]^n$$

from experimental results for $H/b_x > .5$ $k=6.92$

$n= -0.47$

ii) That using the effective loaded area as a basis for determining the bearing capacity, the existing codes limit the allowable bearing strength to :

CEB.FIP (23)	$1.76f_{cu}$	Where ν_r is the design value for concrete strength Table 1.1
DIN 1045 (24)	$1.4\ \nu_r$	
ACI 318.77 (27)	$1.19f_{cp}$	

iii) That specimens with a depth/width ratio greater than 1.5 would not be affected by the supporting materials. This ratio was suggested by Niyogi(18) to be two.

iv) That in the case of thin steel plates loaded via a thick steel punch, an effective area of plate could be calculated using the 45 projected punch area, as suggested by Shelson(4).

v) That the failure was of a tensile nature and variations in bearing strength were not directly proportional to the cube strength but were more closely related to the tensile strength of the concrete.

vi) That for edge loading on deep specimens, the effective width of concrete contributing to the bearing strength could be as high as eight times the width of the loaded area. The allowable effective area in the existing design codes are :

ACI 318.77	$\sqrt{A/A_s}$	$\leqslant 2.0$
DIN 1045	$\sqrt{A_F/A_s}$	$\leqslant 2.0$
CEB-FIP	$\sqrt{A_e/A_s}$	$\leqslant 3.3$

1.3 Design Codes

Williams(21) compared the allowable bearing stress given in several codes of practice and showed that the recommendations were based mainly on the compressive strength of concrete (cube, cylinder or prism test). Some of the codes allowed for the geometry of the loaded area relative to the total surface area.

CP110, clause 5.2.4.4 (22) recommended that for contact surfaces that neither had large irregularities nor adequate intermediate padding, bearing stresses should not normally exceed 0.4 times the characteristic cube strength. This is the value recommended in the draft steel code.

Bearing stresses up to $0.8f_{cu}$ were permitted when adequate binding reinforcements were supplied. The high stresses ($0.8f_{cu}$) could only be used when justified by prototype testing.

CEB-FIP Model Code, clause18.2.1.2 (23) recommemded the formula:

$$F_{Rdu} = f_{cd} \quad \sqrt{A_c\ A_s} \ \leqslant 3.3\ f_{cd}\ A_s$$

where F_{Rdu} = normal force for ultimate state;

f_{cd} = design strength of concrete in compression $= f_{ck}/\gamma_c$

where f_{ck} = characteristic strength of 150mm diameter x 300mm high cylinder;

γ_c = 1.5 for the ultimate limit state.

Therefore, the bearing strength = F_{Rdu}/A_s, so that

$$f_{cb} = (f_{ck}/1.5)\ \sqrt{A_e/A_s} \ \leqslant 3.3(f_{ck}/1.5)$$

$$f_{cb} = (f_{ck}/1.5)\ \sqrt{A_e/A_s} \ \leqslant 2.2f_{ck}.$$

Or, taking f_{ck} as $.8f_{cu}$,

$fcb \leqslant 1.76f_{cu}$.

DIN 1045, clause 17.3.3 (24) recommends the following formula for partial loading :

$$f_{cb} = \gamma_r/2.1\ \sqrt{A_f/A_s} \ < 1.4\ \ \gamma_r$$

where

γ_r = the design value for concrete strength (Table 1.1)

A_f is calculated from Fig.10 of DIN 1045 (24)

Provided that tensile force could be resisted (e.g. reinforcement), then the equation was applicable.

Concrete group	Strength class of concrete	Nominal strength* (N/mm^2)	Design value (N/mm^2) γ_r	Safety factor γ
1 BI	Bn 50	4.9	3.43	1.43
2	Bn 100	9.8	6.87	1.43
3	Bn 150	14.7	10.30	1.43
4	Bn 250	24.5	17.20	1.43
5 BII	Bn 350	34.3	22.60	1.52
6	Bn 450	44.1	26.50	1.67
7	Bn 550	53.9	29.40	1.83

Table 1.1 Concrete strength tables (DIN 1045)

* The nominal strength is the same as the characteristic strength used in CP 110.

French rules CC13A 68 for reinforced concrete (25) and Provisional Instruction(1973) for prestressed concrete (26) give the allowable bearing stress as the product of compressive stress and the ratio of the loaded area to a geometrically similar surface area, with a maximum value of four times the compressive strength. The same allowable stress is recommended for prestressed anchorages. The formula to be used is :

$$f_{bu} = (K/\gamma_b) * f_{cj}$$

where f_{cj} = the characteristic concrete strength at an age of j days.

$\gamma_b = 1.6$

K = increase coefficient (maximum 4).

ACI Code 318.77 (27) states that the bearing strength for concrete without lateral reinforcement should not exceed 0.85 ψ times the compressive strength. For partial area loading, the bearing stress may be increased by a factor of $\sqrt{A/A_s}$, provided this ratio does not exceed 2. A minimum thickness is also recommended for the steel bearing plates :

$$t_e \geqslant 2f_{cu}/f_y \sqrt{A/A_s}.$$

For a lesser thickness of plate, A_s should be taken as the area enclosed within the perimeter located at a distance te outside the perimeter of anchorage.

Williams' Fig. 1.15 compared the design codes for a square section block subjected to a concentric load distributed over a square area.

1.4 Conclusion

The preceding review of the existing literature indicates that in only three papers, Shelson(4), De-Wolf(20) and Hawkins(10,12), was the bending effect of the base plate considered. Since Shelson(4) only considered one thickness (6mm) of base plate, the results of his tests therefore provide no information on the effect of varying the base plate thickness on the bearing capacity.

De-Wolf(20) did consider plates of varying thicknesses ranging from 16 to 32mm and introduced an empirical equation for cubes loaded through a square bearing plate. His empirical theory, however, was related to Hawkins' theoretical work.

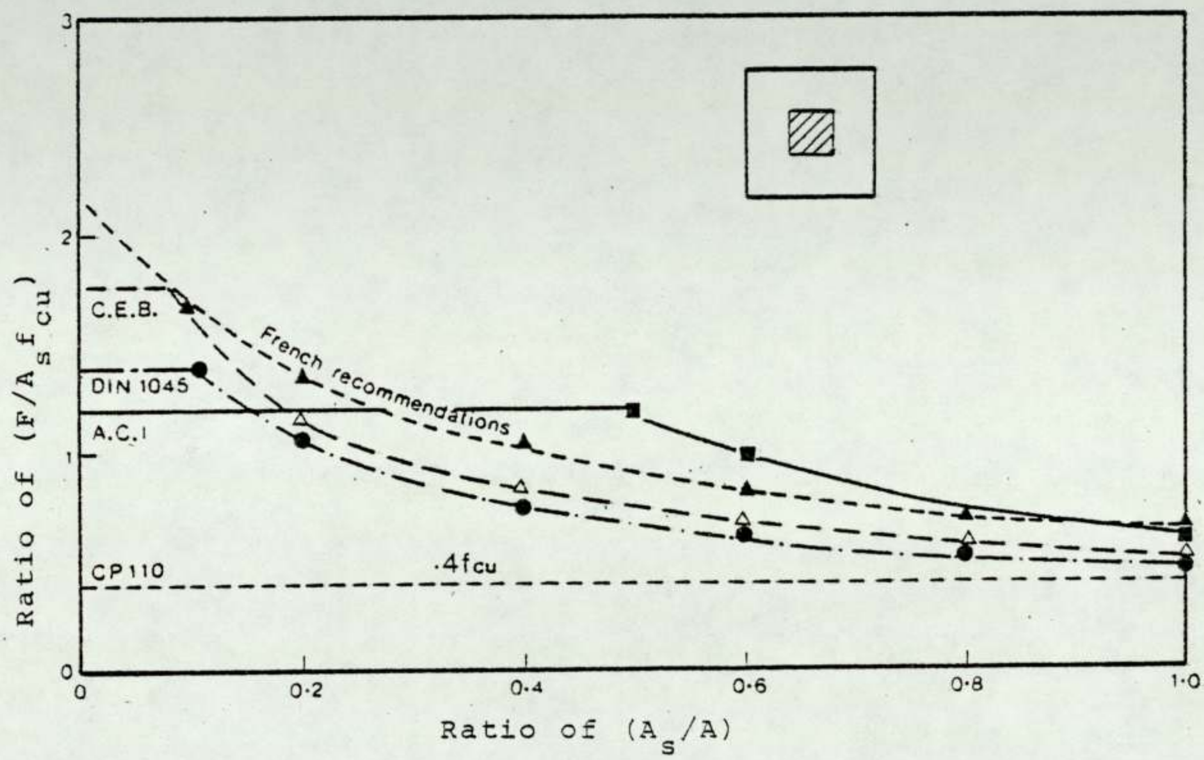

Fig. 1.15 Comparison of design codes for a square loaded area.

Hawkins(10,12) carried out a detailed analysis using rigid and flexible plates, and introduced a theoretical formula which showed a good correlation with the experimental results when applied to a square-shaped loading piece. However, this correlation was poor when the theory was applied to rectangular stiff bearings, which are frequently used in practice.

Finally, in none of the existing work was the load applied through universal columns to investigate the effect of varying the geometry of the column and plate on the bearing capacity of the concrete.

CHAPTER TWO

EXPERIMENTAL WORK ON RIGID BEARING PLATE

2.1 Introduction

From the review of previous research work concerning the bearing capacity of concrete it was evident that a considerable number of experiments had already been carried out on loading through different sizes and shapes of stiff bearings on various concrete strengths and support media. Therefore, it was not necessary to perform a vast number of tests to

a) confirm the available experimental results,

b) obtain a better understanding of the behaviour and mode of failure of concrete loaded through different sizes of stiff bearing,

c) standardise the test results of previous research and the present work.

Tests in twelve series were carried (11 and 25 days after casting) on thirty six concrete cubes of mean cube strengths of 25.8, and 28.15 N/mm^2 with standard deviations of ± 3.7 and 1.5% respectively. These cubes (150 mm) were loaded concentrically through rigid plates for ratios of (loaded area)/ (concrete area) ranging from 0.0044 to 1.0. The results of the 12 test series are given in Table 2.1.

2.2 Concrete Specification

A mix design of 1:2.5:3.5 with a water cement ratio 0.65 was used throughout this research. All the batching was done by weight. The cube strength of this concrete, for seven and for twenty eight days in dry air condition, was 21.4 N/mm^2 and 29.4 N/mm^2

respectively.

2.3 Materials

Throughout the experimental work in this research the following materials were used.

Cement.- Ordinary Portland Cement (O.P.C) from a local supplier.

Fine Aggregate.- Local zone 3 sand.

Coarse Aggregate.- Crushed aggregate with a maximum size of 10 mm .

Both fine and coarse aggregate, supplied from local pits in the Birmingham area, were dried and stored in the laboratory before mixing.

2.4 Manufacture of Specimens

The materials were mixed in a "Linear Cumflow 1A" mixer of $0.25 m^3$ capacity. The 150 mm cubes were cast in steel moulds on a vibrating table. After one day the specimens were stripped down and stored in the laboratory in the open on wooden racks to ensure that air could circulate freely over all surfaces. To ease the handling of the concrete mix, two batches of 150 mm cube specimens were cast on separate days.

2.5 Control Tests

Control specimens were also cast from each mix, cured in the same way and tested in order to determine the physical properties of material used. Three 100mm cubes were tested in order to determine the cube strength of the specimens. The tensile strength was calculated from the average splitting load of three cylinders 200mm long by 100mm diameter. These control tests were carried in accordance to the recommendations in BS. 1881: 1970 (28).

To determine Young's Modulus three 200x100mm cylinders were placed in a central position on the machine and loaded axially. As the cylinder required capping, the mould in which the cylinder was cast was filled to within 15mm of the top and, after the concrete had started to set, the remaining space was made up with plaster of paris and carefully levelled off. Before loading, two type (PL-60-11) electrical resistance strain gauges were fixed longitudinally to the surface, at opposite ends of a diameter and parallel to the axis of the cylinder at mid-height. Readings of each gauge were taken before loading commenced and at each half ton increment until it became impossible to take readings. After this stage, the strain recorder was then disconnected from the extension box and the loading was continued until failure. The strain readings at each value of the applied load were averaged and the modulus of elasticity for the concrete in compression was calculated.

2.6 Test Procedure

The bearing specimens were placed in a central position on the machine, at right-angles to the direction in which they were cast, and loaded concentrically through a square mild steel bearing plate 20mm thick. To produce a range of ratios of (loaded area)/(concrete area), thirty-six 150mm cubes were tested through 12 different size bearing plates, the smallest being 10x10mm (R = .0044) and the largest 150x150mm (R = 1.0). Few tests were also carried out in which load was applied through a rigid strip loading piece. The purpose of carrying these tests was to establish a clear pattern of mode of failure and its comparison to those of square loading piece.

The thick upper platen of the testing machine was in contact over the entire area of the bearing plate and the load was applied at an average rate of one ton every thirty seconds . The specimens were loaded until failure occurred i.e. load dropped off. The bearing plates after use did not indicate any flexural or other deformation, except in rare cases where some minute local deformations were observed at the edge of the plates. This local deformation could be the result of the testing machine not being in contact over the entire area of the bearing plate, which in turn had caused the over-stressing of one of the edges of the plate. The deformed plates were then replaced by new ones. For each specimen the load at first crack, the progress of cracking, the mode of failure and the maximum load were recorded. For some specimens photographs were taken.

2.7 Mode of Failure

A typical appearance of the cubes at failure for strip and square loading is shown in Photographs 2.1 and 2.2 respectively. With concentric loading, for small ratios of loaded area to concrete area (R), cracks formed on the top of the block around the edges of the rigid plate as the specimen was loaded. The fracture continued downwards and inwards, and its appearance indicated splitting and sliding at failure. As loading increased and failure approached,

Plate 2.1 Typical crack formation at failure under strip loading condition on 150mm cubes. Scale 1 : 3.95

Plate 2.2 Typical crack formation at failure under square loading condition on 150mm cubes. Scale 1 : 3.95

cracks occasionally developed from the corners of the bearing plate, extending outwards. Failure occurred with the punching out of an inverted cone (Photograph 2.2) or wedge (Photograph 2.1). For large values of R the pattern of failure changed from that above to one of crushing, similar to a cube crushing test (Photograph 2.3). In this case, failure was always accompanied by the formation of debris. The difference between the failure and the initial cracking loads increased as the ratio R increased, and this difference was a maximum for R = 1.0, a fact noted previously by Niyogi(18).

2.8 Presentation of Test Results

In almost every paper reviewed, the results of the tests were plotted with a dimensionless ratio of bearing capacity (failure load divided by loaded area, F/A_s) to concrete strength (cube or prism) as the ordinate, and the ratio of concrete area to loaded area (A/A_s) as the abscissa. This method has the disadvantage that when $A_s \longrightarrow 0$, $F/A_s \longrightarrow \infty$.

An alternative method of plotting the results is suggested in this investigation. The ratio of failure load divided by concrete surface area F/A to concrete cube strength (f_{cu}) is the ordinate and the ratio of loaded area to concrete surface area (A_s/A) is the abscissa. It should be pointed out that a distinct advantage of this plotting method is that both the ordinate and the abscissa have a maximum value of unity. This is reached when a concrete cube is loaded through a rigid plate covering the entire upper surface of the specimen (A_s/A = 1), which corresponds to the standard crushing test for concrete.

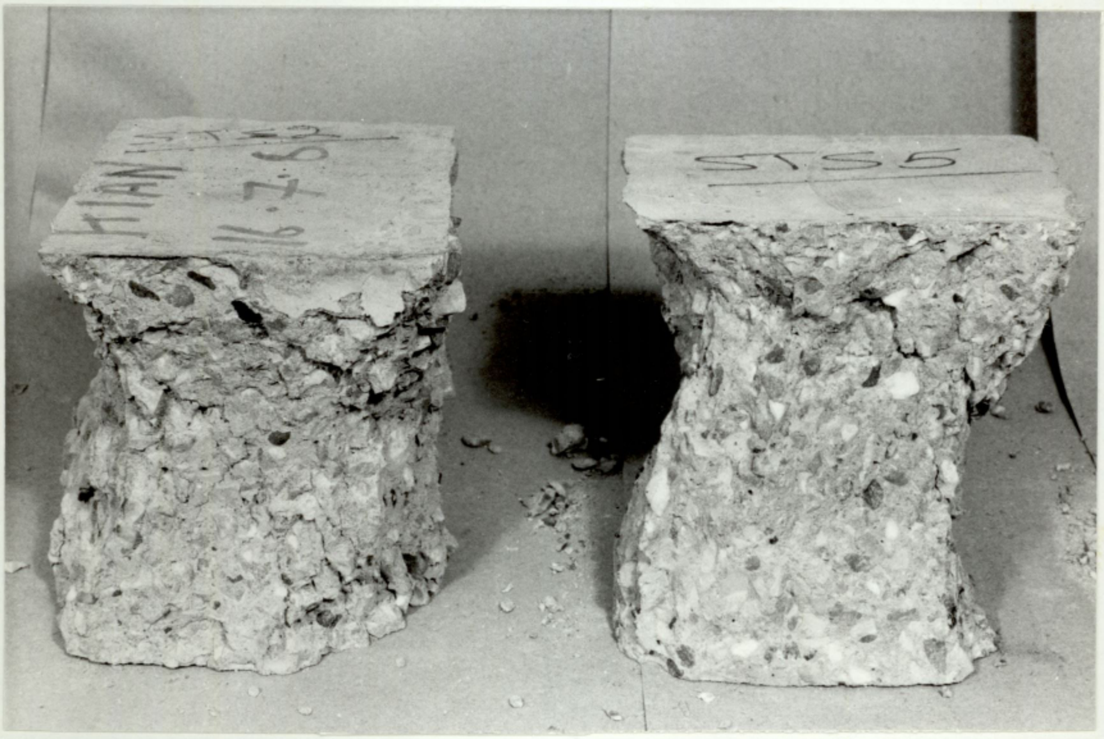

Plate 2.3 Typical formation of double cone after failure under concentric loading condition on 150mm cubes.

Scale 1 : 3.95

Test No	Concrete Properties			Loading Plate		Load at Failure	Ratio $F/f_{cu}A$	Ratio A_s/A	No of Tests	Coeff. Of Variation Of Failure Load In Each Group
	f_{cu}	f_{sp}	E_c	b_x	b_y	F	n	R		
	N/mm^2	N/mm^2	KN/mm^2	mm	mm	KN	Dimensionless			
1	25.80	1.68	24.2	10.0	10.0	44.64	0.08	0.004	3	+ 0.087, (1.9)%
2	28.15	1.83	26.4	30.0	30.0	94.67	0.15	0.040	3	+ 0.353, (3.6)%
3	28.15	1.83	26.4	40.0	40.0	126.55	0.20	0.071	3	+ 0.265, (2.05)%
4	28.15	1.83	26.4	50.0	50.0	142.25	0.22	0.110	3	+ 0.707, (4.87)%
5	25.80	1.68	24.2	60.0	60.0	185.80	0.32	0.160	3	+ 0.513, (2.70)%
6	28.15	1.83	26.4	80.0	80.0	289.40	0.46	0.284	3	+ 0.551, (1.87)%
7	28.15	1.83	26.4	100.0	100.0	329.42	0.52	0.440	3	+ 0.600, (1.79)%
8	25.80	1.68	24.2	108.0	108.0	324.20	0.56	0.520	3	+ 1.480, (4.49)%
9	25.80	1.68	24.2	120.0	120.0	377.20	0.65	0.640	3	+ 0.636, (1.65)%
10	25.80	1.68	24.2	130.0	130.0	433.00	0.74	0.750	3	+ 0.408, (0.93)%
11	25.80	1.68	24.2	140.0	140.0	510.12	0.88	0.870	3	+ 0.0 , (0.0) %
12	25.80	1.68	24.2	150.0	150.0	569.50	1.00	1.000	3	+ 0.141, (0.24)%

Table 2.1- Results of tests carried out by Author for concentric loading through rigid square plates on 150 mm cubes.

The results of the 12 test series (each series comprising three tests) are given in Table 2.1. In this table, the concrete cube strength and tensile strength are expressed in N/mm^2, the size of the square plates are given in mm and the ratios of R and n are dimensionless.

Figure 2.1 shows the results plotted in the manner proposed above. The results show that the rate of increase in bearing capacity decreases as the ratio of loading to concrete area ($R = A_s/A$) increases. This was also observed by Niyogi (18) who suggested that the rate of increase in bearing capacity changes at the point where A_s/A is greater than 1:8.

Using the least-square-curve fit method for the first four test series with R less than 0.125 (1:8), the best fit is a straight line with the index of determination equal to 0.93. The equation of this line is :

$$n = 0.085 + 1.36R \qquad (2.1)$$

The best fit for the eight test results with a ratio of loaded area to surface area ($R=A_s/A$) greater than 1:8 is a straight line with the equation of $n = 0.19 + 0.77R$ and of index determination equal to 0.98. However, this equation does not quite satisfy the boundary condition at R = 1. Therefore the following steps were taken in order to find the equation which satisfies the boundary condition yet is close to the best fit equation :-

1) When A_s/A equals unity, the value for $n = F/(Af_{cu})$ also equals unity since F/A is the crushing strength of the concrete -(f_{cu}).

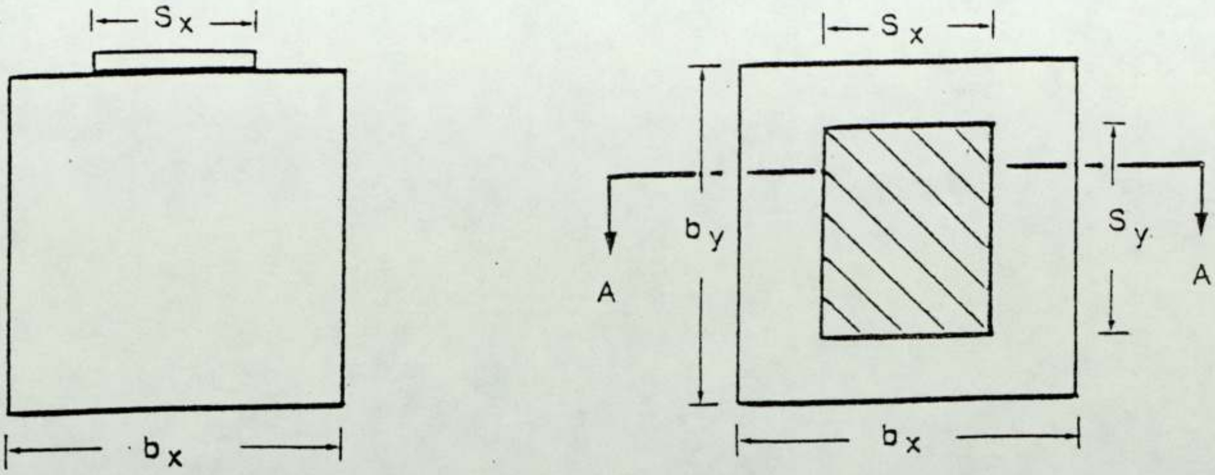

Section AA

Plan view

Square specimens loaded concentrically.

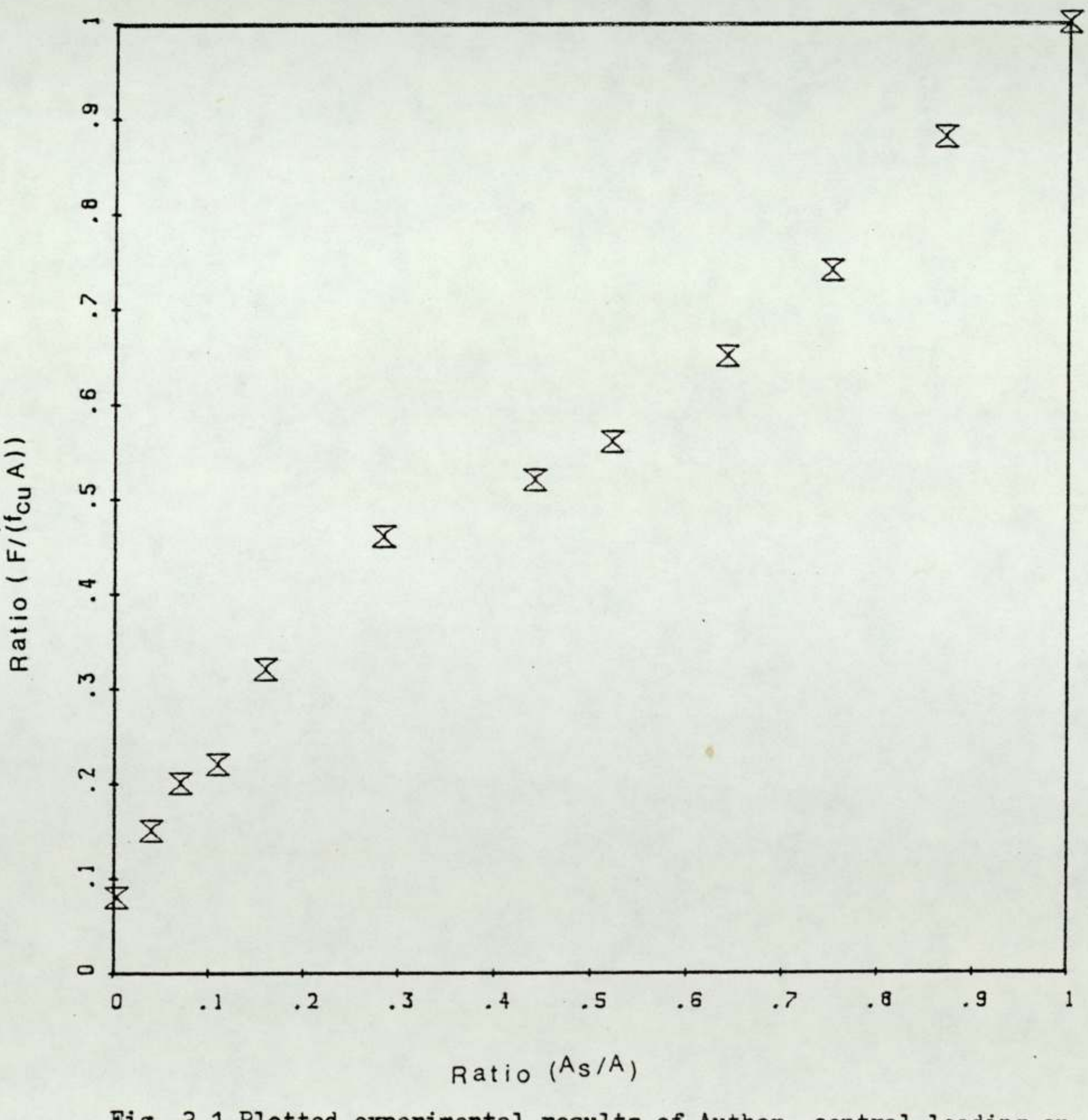

Fig. 2.1 Plotted experimental results of Author, central loading on 150 mm cubes.

2) Another point is found using the above equation and solving for n when $R=(A_s/A)$ is equal to 0.125(1:8).

The straight line which is found in this way has an equation of :

$$n = 0.15 + 0.85R \qquad (2.2)$$

This satisfies the boundary condition and approximate to the equation found using the least-square-curve fit method. Using Equations (2.1) and (2.2), Fig 2.2 is plotted ; in the same figure the twelve test results are also plotted for comparison.

The difference in the gradient of the two straight lines can be explained as follows. For the loaded area to concrete area ($R=A_s/A$) less than 1:8, visual observation suggested that a single cone and splitting of the cube occurred. However, for ratios higher than 1:8, cubes showed a double cone with multiple vertical crack followed by crushing.

In the same way, data from approximately 600 available tests by other investigators (8,9,18,19,21) was plotted in order to confirm the validity of Equations (2.1) and (2.2). These results, shown in Table A.1, came from experiments involving cube specimens of sizes 102-305mm. The cubes were loaded concentrically through bearing plates of various areas and of three shapes : strip (bearing over the full breadth of the specimen), rectangular and square. The 600 test results are plotted in two Figs. 2.3 and 2.4 for R less and greater than 1:8 respectively. The solid and dotted lines in the figures correspondingly represent the lines suggested by Author (Equations 2.1, 2.2) and the best fit lines obtained for the tests by other

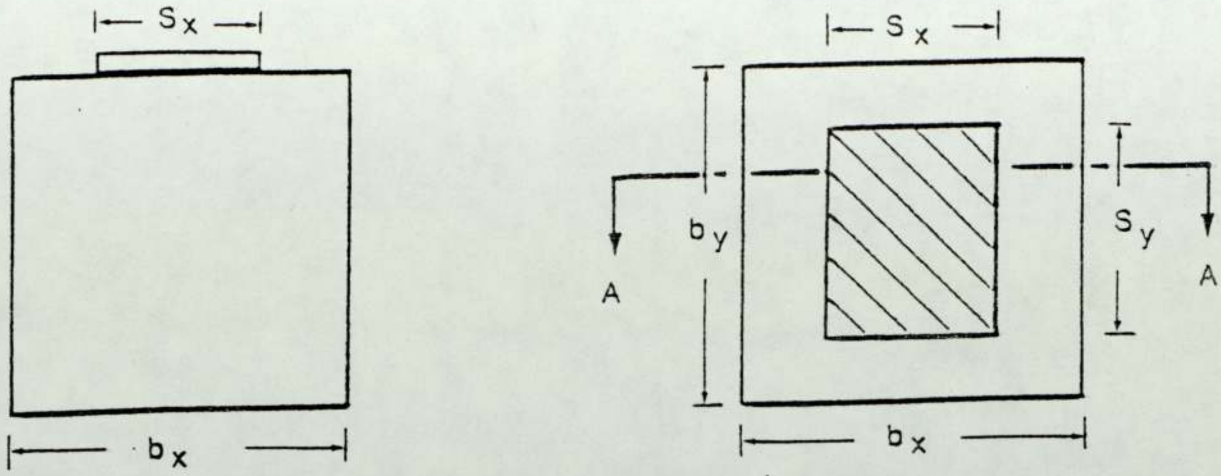

Square specimens loaded concentrically.

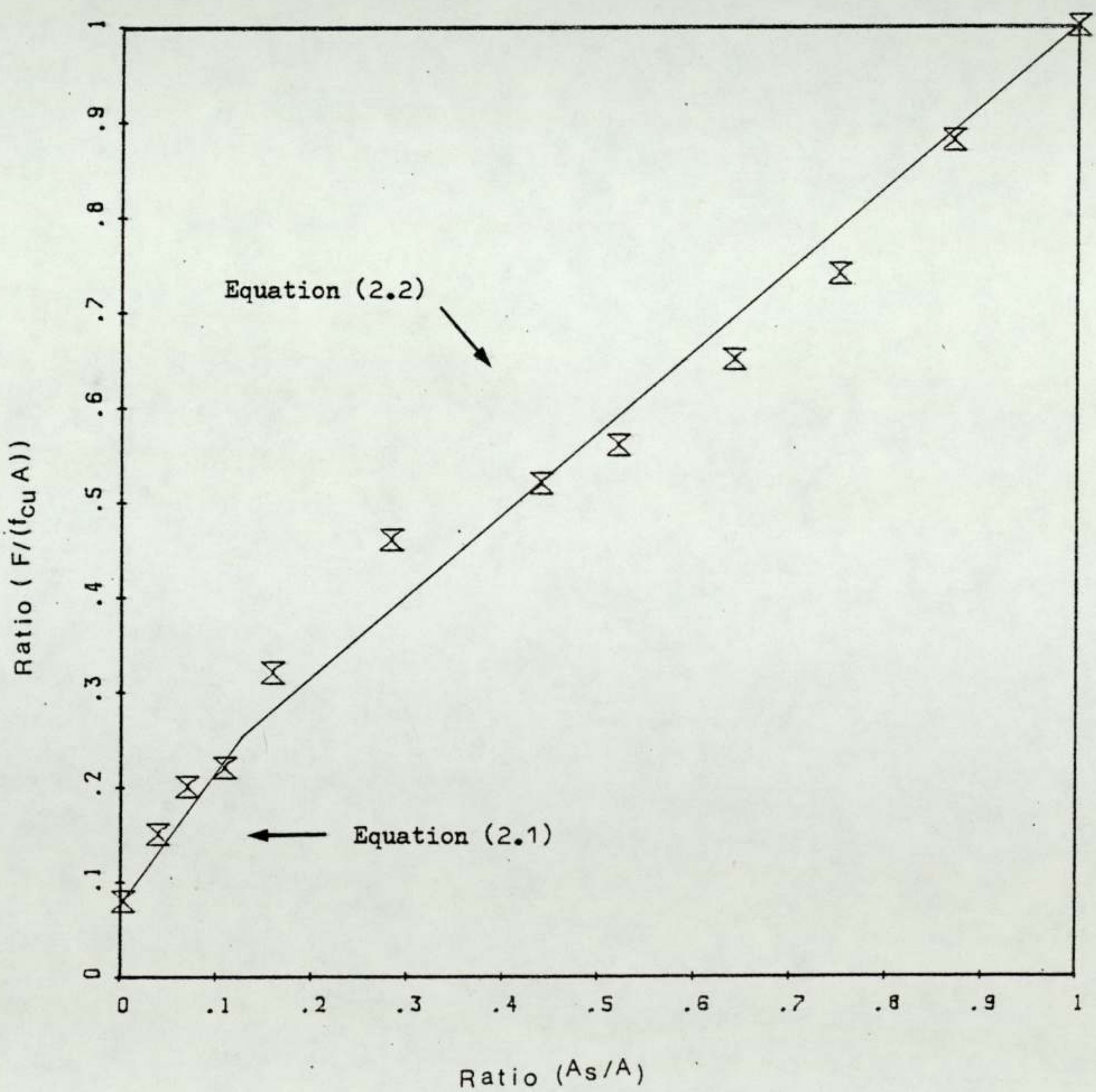

Fig. 2.2 Plotted experimental and theoretical results of Author, central loading on 150 mm cubes.

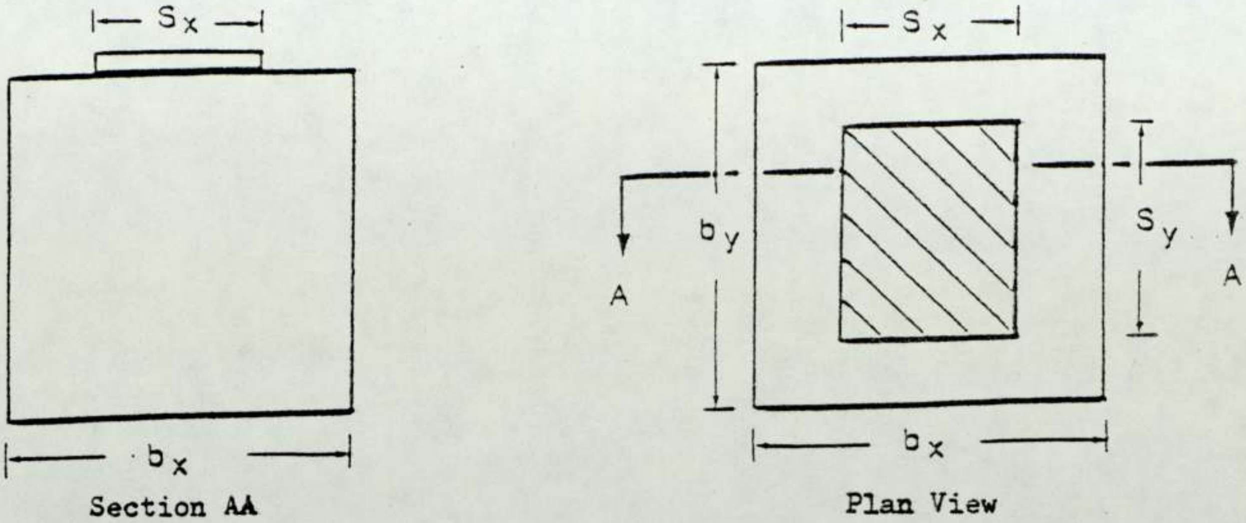

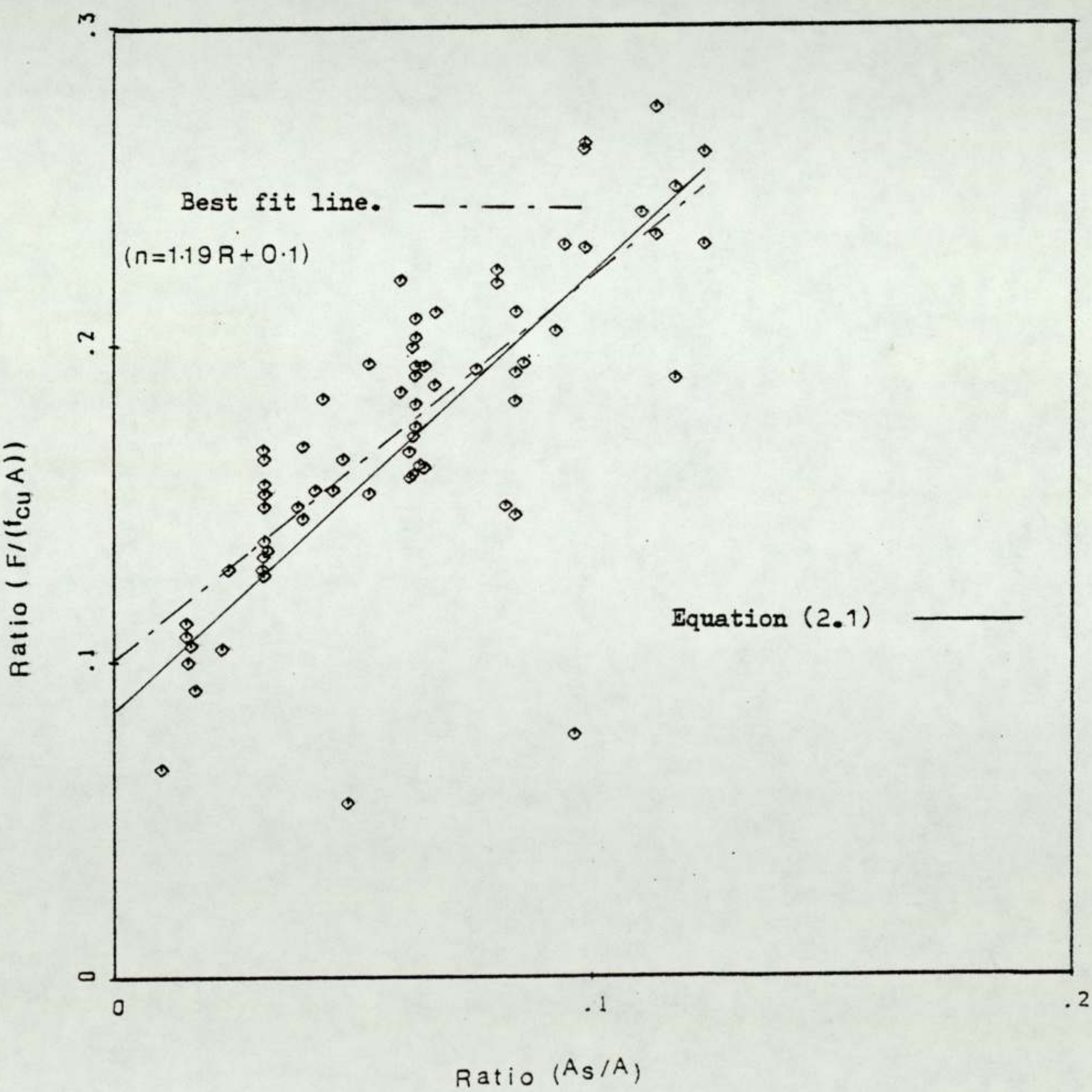

Fig. 2.3 Experimental results of previous researchers (Table A.1), central concentric loading for $A_s / A < 0.125$.

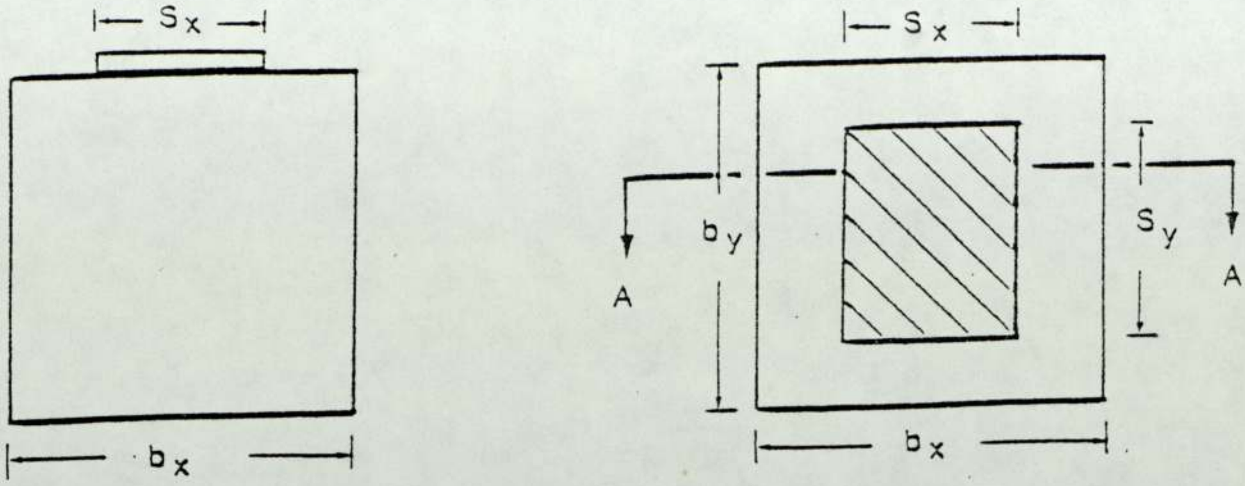

Section AA **Plan view**

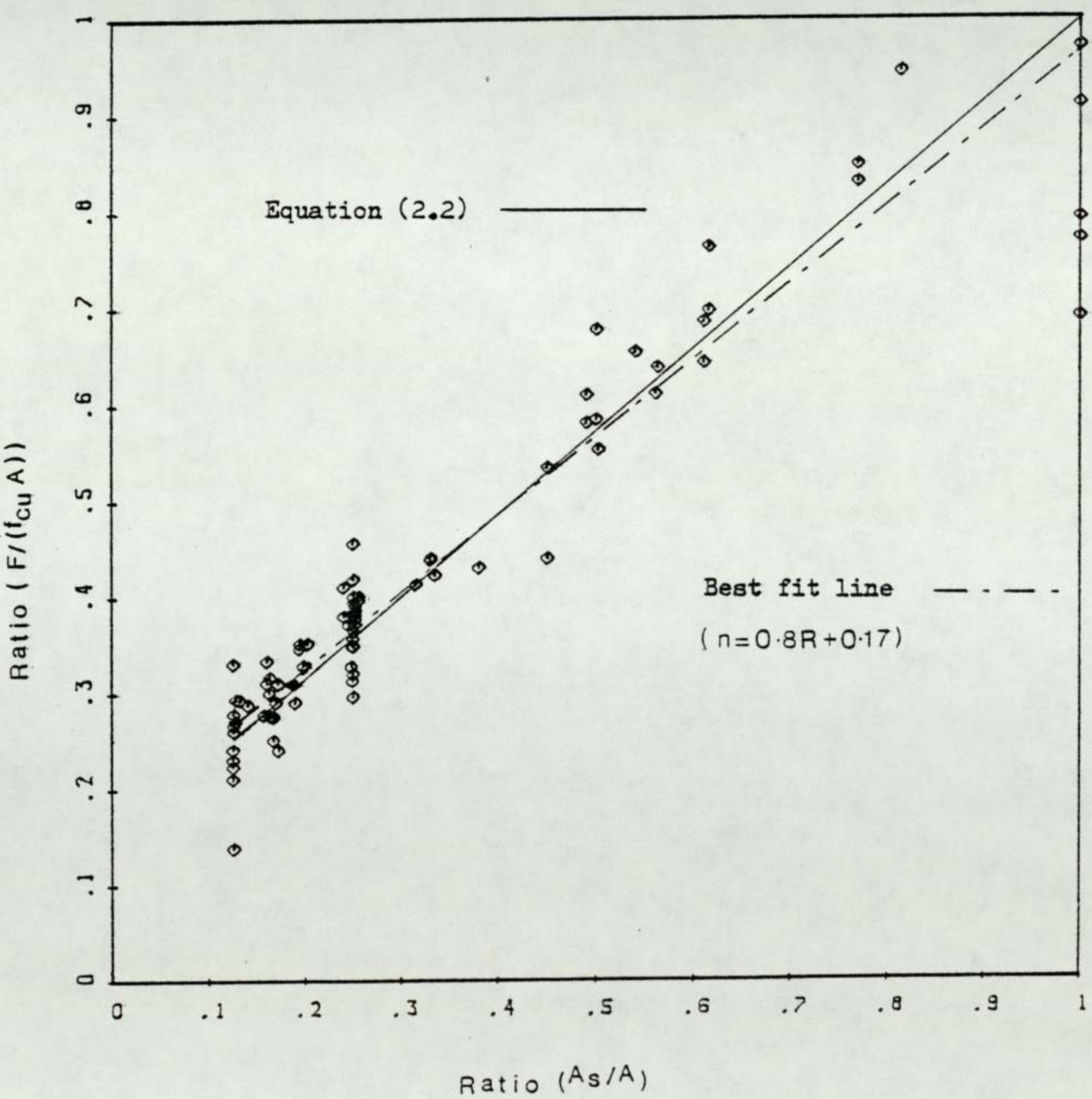

Fig. 2.4 Experimental results of previous researchers (Table A.1), central concentric loading for $A_s/A > 0.125$.

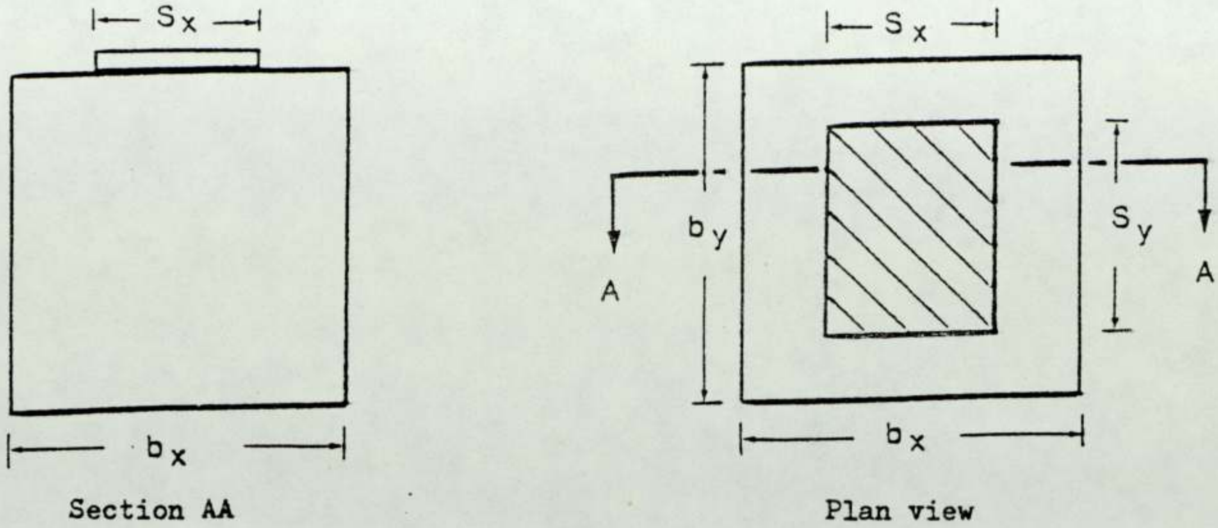

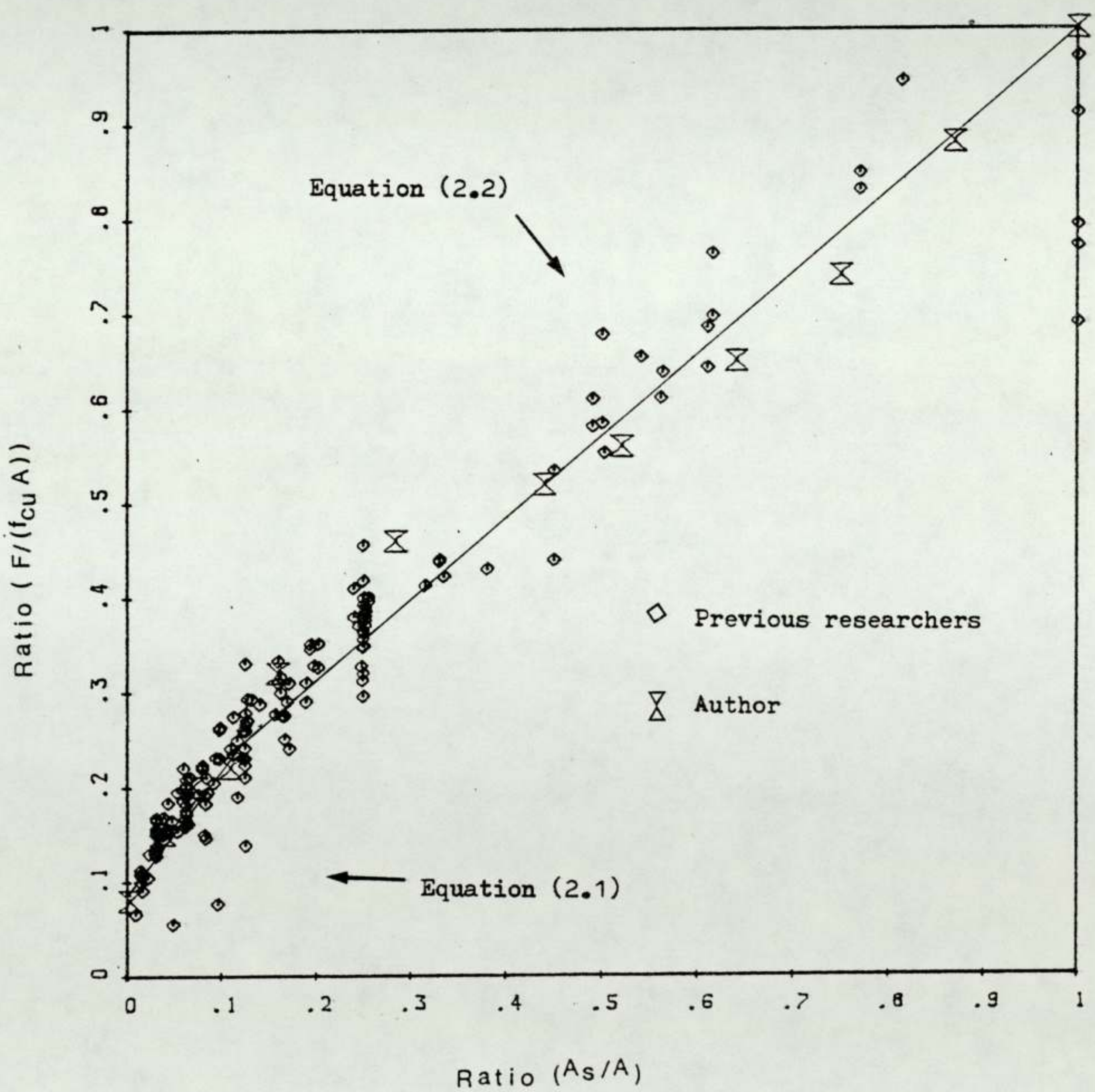

Fig. 2.5 Presented empirical theory, compared to test results of previous researchers and Author.

investigator.

The results of both previous and present tests are plotted in Figure 2.5. The correlation of the present test results and those of other researchers is good, bearing in mind that the tests were done in different locations under different standards of loading and with a wide range of concrete strengths. In some cases the concrete cube strengths were not given by the investigators and for these results concrete cylinder strength has been divided by a factor of 0.8.

2.9 Correlation of Equations (2.1),(2.2) and Tests Carried Out by Niyogi.

The two empirical Equations (2.1),(2.2) were used to predict the ultimate load of tests done by Niyogi (18) on 203mm cubes loaded concentrically through strip, rectangular and square bearings. Also for comparison, the theoretical Equations (5) and (7) proposed by Hawkins (10) for square and rectangular rigid bearing plates were used to calculate the ultimate failure load of the tests above. These results are shown in Tables 2.2, 2.3 and 2.4. The value of K in Hawkins' equations was taken from his Table 4.

Table 2.2 compares Niyogi's (18) test results for rectangular rigid plates with the results obtained using the Author's and Hawkins' equations. The standard deviation and the percentage difference of all tests with rectangular bearing plates are + 0.058, (6.0%) using the Author's equations and + 0.25, (26.0%) for Hawkins' theory. Table 2.3 shows Niyogi's (18) test results for square rigid plates. For this set of tests the standard deviation and the percentage difference for both the Author's and Hawkins' equations are + 0.074, (7.0%) and $\pm$ 0.12,

Type of Bearing	Concrete Strength	Size of Bearing		Ratio	Niyogi's Tests Measured	Present Investigation Theory	Present Investigation Theory	Hawkins' Investigation Theory	Hawkins' Investigation Theory	Ratio Measured/computed (Failure Load) Equations	Ratio Measured/computed (Failure Load) Equations
Bearing	f_{cu}	S_x	S_y	A_s/A	F	F Eq.(2.1)	F Eq.(2.2)	F Eq.(5)	F Eq.(7)	(2.1)OR(2.2)	5 OR 7
	N/mm^2	mm	mm	mm/mm	TONS	TONS	TONS	TONS	TONS	Author	Hawkins
1	2	3	4	5	6	7	8	9	10	11	12
	29.7	33	100	0.083	25.3	24.2			28.3	1.05	0.90
	29.7	34	152	0.125	28.4		31.97		31.1	0.89	0.91
	27.0	51	76	0.094	26.1		24.14		34.3	1.08	0.76
Rectangular	24.8	51	102	0.125	26.3		26.69		35.7	0.99	0.74
Rigid-Plate	27.6	51	127	0.156	32.0		32.76		40.8	0.98	0.78
	28.1	51	152	0.190	34.3		36.77		44.0	0.93	0.78
On 203mm	31.5	76	102	0.190	40.4		41.20		57.2	0.98	0.71
Cubes	30.2	102	152	0.370	54.9		56.77		82.1	0.97	0.67
	29.6	13	51	0.015	12.7	13.1			10.2	0.97	1.25
	29.5	13	76	0.023	15.6	14.4			10.8	1.08	1.45
									Mean ----->	(.992)	(0.895)
									Standard Deviation ----->	(±0.061)	(±0.255)
									% ----->	(6.10)	(28.49)

Table 2.2. Axially loaded cubes through rectangular rigid plates. Comparison of measured and computed load, for tests carried out by Niyogi (18). (CONTINUED)

Type of	Concrete Strength	Size of Bearing		Ratio	Niyogi's Tests Measured	Present Investigation Theory	Present Investigation Theory	Hawkins' Investigation Theory	Hawkins' Investigation Theory	Ratio Measured/computed (Failure Load) Equations	Ratio Measured/computed (Failure Load) Equations
Bearing	f_{cu}	S_x	S_y	A_s/A	F	F Eq.(2.1)	F Eq.(2.2)	F Eq.(5)	F Eq.(7)	(2.1)OR(2.2)	5 OR 7
	N/mm^2	mm	mm	mm/mm	TONS	TONS	TONS	TONS	TONS	Author	Hawkins
1	2	3	4	5	6	7	8	9	10	11	12
	31.8	13	102	0.030	17.5	16.80			11.8	1.04	1.40
	29.8	13	152	0.047	20.1	18.6			14.8	1.08	1.36
	29.6	25	51	0.030	16.3	15.64			18.6	1.04	0.88
	26.0	25	76	0.047	17.2	16.71			18.9	1.03	0.91
	29.6	25	102	0.063	20.9	21.22			21.7	0.99	0.96
	29.6	25	152	0.094	25.8	26.46			23.8	0.98	1.04
	28.5	34	51	0.042	18.2	16.70			22.8	1.09	0.80
	29.7	34	76	0.063	21.2	21.3			26.3	1.00	0.81
						FINAL RESULTS			Mean ---->	(1.009)	(0.950)
									Standard Deviation ---->	(±0.058)	(±0.25)
									% ---->	(6.00)	(26.00)

Table 2.2. Axially loaded cubes rectangular through rigid plates. Comparison of measured and computed load, for tests carried out by Niyogi (18).

Type of Bearing	Concrete Strength	Size of Bearing		Ratio	Niyogi's Tests Measured	Present Investigation Theory	Present Investigation Theory	Hawkins' Investigation Theory	Hawkins' Investigation Theory	Ratio Measured/computed (Failure Load) Equations	Ratio Measured/computed (Failure Load) Equations
Bearing	f_{cu}	S_x	S_y	A_s/A	F	F Eq.(2.1)	F Eq.(2.2)	F Eq.(5)	F Eq.(7)	(2.1)OR(2.2)	5 OR 7
	N/mm^2	mm	mm	mm/mm	TONS	TONS	TONS	TONS	TONS	Author	Hawkins
1	2	3	4	5	6	7	8	9	10	11	12
	28.1	25	25	0.015	13.1	12.44		13.3		1.05	0.98
Square	29.7	36	36	0.031	18.5	15.86		19.1		1.17	0.97
Rigid Plate	27.2	51	51	0.063	21.5	19.5		25.6		1.10	0.84
	27.7	72	72	0.125	30.1		29.82	36.1		1.00	0.83
On 203 mm	30.6	102	102	0.250	49.8		46.60	53.8		1.07	0.93
Cubes	31.4	152	152	0.570	81.0		83.70	80.5		0.97	1.00
	28.8	203	203	1.000	117.4		120.98			0.97	1.21
									Mean ----->	(1.047)	(0.97)
									Standard Deviation ----->	($\pm$0.074)	($\pm$0.12)
									% ----->	(7.00)	(13.0)

Table 2.3- Axially loaded cubes through square rigid plates. Comparison of measured and computed load, for tests carried out by Niyogi (18).

Type of Bearing	Concrete Strength	Size of Bearing		Ratio	Niyogi's Tests Measured	Present Investigation Theory	Present Investigation Theory	Hawkins' Investigation Theory	Hawkins' Investigation Theory	Ratio Measured/computed (Failure Load) Equations	Ratio Measured/computed (Failure Load) Equations
	f_{cu}	S_x	S_y	A_s/A	F	F Eq.(2.1)	F Eq.(2.2)	F Eq.(5)	F Eq.(7)	(2.1)OR(2.2)	5 OR 7
	N/mm^2	mm	mm	mm/mm	TONS	TONS	TONS	TONS	TONS	Author	Hawkins
1	2	3	4	5	6	7	8	9	10	11	12
	32.1	13	203	0.064	21.4	23.0			13.7	0.93	1.60
Strip	30.5	17	203	0.084	23.4	24.83			17.6	0.94	1.30
Rigid-Plate	31.3	25	203	0.123	30.8		33.70		26.5	0.91	1.16
	26.9	34	203	0.167	30.9		32.99		31.1	0.94	0.99
On 203mm	28.6	51	203	0.250	41.6		43.55		47.7	0.96	0.87
Cubes	31.1	64	203	0.310	53.4		54.00		62.6	0.99	0.85
	31.3	68	203	0.330	55.2		61.10		65.6	0.90	0.84
	32.0	102	203	0.500	73.1		77.30		95.6	0.95	0.76
	28.9	203	203	1.000	117.2.		121.40		151.5	0.97	0.74
									Mean ----->	(0.940)	(1.01)
									Standard Deviation ----->	(±0.028)	(±0.29)
									% ----->	(3.00)	(28.8)

Table 2.4. Axially loaded cubes through strip rigid plates. Comparison of measured and computed load, for tests carried out by Niyogi (18).

(13.0%) respectively. The results of the last set of tests, with strip rigid plates are shown in Table 2.4. The standard deviation and the percentage difference using the Author's and Hawkins' equations being $\pm$ 0.028, (3.0%) and $\pm$ 0.29, (28.8%) respectively.

It is clear from these results that the suggested simple formulae predict the failure load for all ratios of loaded area to concrete area (A_s/A) with a reasonably degree of accuracy.

2.10 Discussion of the Theoretical Equation Developed by Hawkins for Concentric Loading Through Rigid Plate.

In developing his theoretical Equation (5) for concrete prisms loaded through square rigid plates Hawkins (10) assumed that an inverted pyramid was formed underneath the loading plate, and the downward penetration of this pyramid would cause horizontal pressures distributed uniformly over the interface between the pyramid and the confining concrete.

Based on the dual failure criterion for concrete suggested by Cowan (11), Hawkins developed the following theoretical formula,

$$\frac{F}{A_s f_{cp}} = 1 + \frac{K}{\sqrt{f_{cp}}} \left(\sqrt{R_2} - 1 \right) \qquad (2.3)$$

Where $R_2 = \dfrac{A}{A_s}$

$$K = \frac{f_{sp}}{\sqrt{f_{cp}}} \operatorname{Cot}^2 \alpha \qquad \left(\alpha = 45^\circ - \frac{\phi}{2} \right)$$

By rearranging Equation (2.3) Hawkins presented the following expression (Equation (7) in his paper) for rectangular shape loading piece.

$$\frac{F}{A_s f_{cp}} = 1 + \frac{K}{2\sqrt{f_{cp}}} \left[\frac{b_x}{s_y} \left(3 - \frac{s_x}{s_y} - 1 \right) \right] \qquad (2.4)$$

This Equation (2.4), Hawkins argued was only applicable, provided the tensile strength of the concrete is developed through both restraining dimensions of the uppermost slice.

The theoretical Equation (2.3) implies that $F/A_s f_{cp}$ continues to increase without limit as the ratio of block area to contact area R_2 increases. It further implies that for the ratio of R_2 equal to unity $F/A_s f_{cp}$ will also be equal to unity. This in turn suggests that when the rigid base plate covers the whole surface of the concrete cube the ratio of F/A will be equal to the concrete cylinder strength. Neither of these suggestions can be confirmed by tests.

Hawkins claims that Equation (2.3) is also applicable to a cylinder specimen loaded through a circular plate. However, having applied his Equation (2.3) to the tests carried out by Meyerhof (2) on cylinder specimens loaded through circular loading pieces, Hawkins found that the correlation of the theory and the tests was reasonable only when the ratio of A/A_s was limited to a maximum of 40. The correlation of Hawkins' theory and Meyerhof's test results when ratio of A/A_s was limited to a maximum of 40 had a standard deviation and percentage difference of $\pm$ 0.238 (21%).

Both Hawkins' and the Author's equations are drawn in Fig.

- - - - - - -   Hawkins' theory, Equation (2.3)

————————   Author's Equations, (2.1), (2.2)

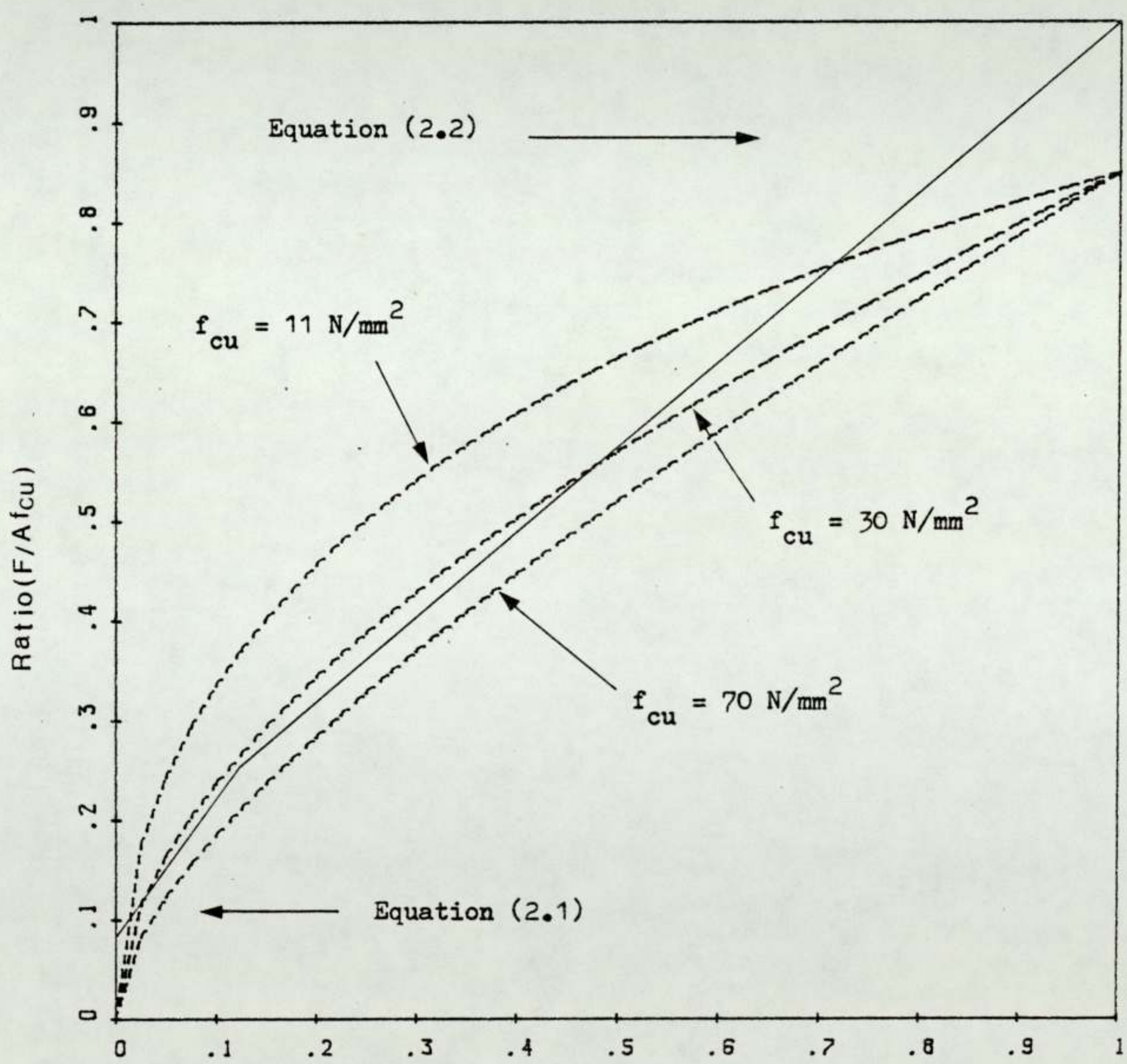

Fig. 2.6 Comparison of Hawkins' and Author's theories, for concentric loading through stiff bearing.

2.6. Hawkins' equation was drawn for three values of concrete cube strengths of 11, 30 and 70 N/mm^2 with value of K equal to 50. As can be seen from Fig. 2.6 for the value of $f_{cu} = 30\ N/mm^2$ and ratio of $0.03 < R < 0.05$ Hawkins' theory agrees quite well with the equations suggested by the Author.

As shown in Fig.2.6 Hawkins' theory suggests that as the value of f_{cu} decreases the ratio of $F/f_{cu}A$ increases and this increase is considerable for concrete cube strengths of 11 and 70 N/mm^2. However, tests carried out on concrete cubes loaded through square rigid plates by Niyogi (19) and Williams (21) with cube strengths of 11.4 and 70.9 N/mm^2 (shown in Table A.1 of Appendix A) do not agree with the trend suggested by Hawkins' theory.

CHAPTER THREE

EXPERIMENTAL WORK ON PLEXIBLE BEARING PLATES

3.1 Introduction

In the preceding chapter, empirical formulae were developed for calculating the ultimate load for concrete cubes loaded concentrically through rigid strip, rectangular and square steel plates. In this chapter the work is extended to applying the load through flexible base plates of different thicknesses.

Initial tests were carried out to establish the bending stress distribution in the base plates when loaded through a strip bearing piece. In the first series of main tests, 150 mm concrete cubes with varying cube strengths of 10 to 40N/mm^2 were loaded through a thin (4mm) steel base plate. In the second series, concrete cubes of cube strengths 40 and 32 N/mm^2 were loaded through different thicknesses of steel base plate (4 to 40mm). For both these series, knife-edge loading was applied and, in some tests, strain gauges were fixed to the concrete cubes in order to determine the axial strain distribution.

In the third series, tests were carried out on 250mm cubes where knife-edge loading was applied through 6 and 12mm thick steel base plates. In the fourth series of tests with 150mm cubes of strengths 30 and 37N/mm^2, 4mm thick base plates were used to which load was applied through rigid strip plates of progressively increasing width 10, 32 and 98mm. Finally, in the fifth series of the main tests , with 150mm cubes, concentric loading tests were carried out, for different sizes of rigid square and rectangular loading pieces. The sizes are tabulated in Table 3.1.

Series	Test	Concrete Properties			Steel Base Plate				Loading Piece		Failure Load
No	No	f_{cu}	f_{sp}	E_c	f_y	b_x	b_y	t	S_x	S_y	F
		N/mm^2	N/mm^2	KN/mm^2	KN/mm^2	mm	mm	mm	mm	mm	KN
(1)	S1	10.9	0.69	13.7	260	150	150	4.0	2.0	150	80.0
150 mm	S2	13.7	0.93	18.2	260	150	150	4.0	2.0	150	97.5
Cubes	S3	30.0	1.63	26.4	260	150	150	4.0	2.0	150	150.0
	S4	37.0	2.60	29.3	260	150	150	4.0	2.0	150	175.0
(2)	S5	40.0	2.61	31.0	265	150	150	4.0	2.0	150	190.0
	S6	40.0	2.61	31.0	265	150	150	6.0	2.0	150	260.0
150 mm	S7	40.0	2.61	31.0	265	150	150	8.0	2.0	150	290.0
Cubes	S8	40.0	2.61	31.0	265	150	150	10.0	2.0	150	330.0
	S9	37.0	2.60	29.2	265	150	150	11.7	2.0	150	320.0
	S10	32.0	2.44	28.3	260	150	150	22.5	2.0	150	529.74
	S11	32.0	2.44	28.3	260	150	150	30.0	2.0	150	647.46
	S12	32.0	2.44	28.3	260	150	150	40.0	2.0	150	721.0
(3)	S13	24.8	1.56	26.2	260	250	250	6.0	2.0	250	337.5
250 mm	S14	24.8	1.56	26.2	260	250	250	12.0	2.0	250	514.1
Cubes											

Table 3.1 Results of concentric loading via strip, square and rectangular loading pieces.

(CONTINUED)

Series	Test	Concrete Properties			Steel Base Plate				Loading Piece		Failure Load
No	No	f_{cu}	f_{sp}	E_c	f_y	b_x	b_y	t	S_x	S_y	F
		N/mm^2	N/mm^2	KN/mm^2	KN/mm^2	mm	mm	mm	mm	mm	KN
(4)	S15	30.0	1.70	27.0	265	150	150	4.0	10.0	150	205.0
150 mm	S16	37.5	2.93	29.0	265	150	150	4.0	32.0	150	382.6
Cubes	S17	37.5	2.93	29.0	265	150	150	4.0	98.0	150	651.3
	S18	37.5	2.93	29.0	265	150	150	5.9	32.0	150	392.2
(5)	P1	36.2	2.81	27.2	265	150	150	4.0	80	80	431.6
150 mm	P2	32.8	2.50	27.0	265	150	150	4.0	75	75	412.0
Cubes	P3	23.0	1.45	25.4	265	150	150	3.8	38	75	215.0
	P4	32.8	2.50	27.0	265	150	150	4.0	61	75	333.5

Table 3.1 Results of concentric loading via strip, square and rectangular loading pieces.

3.2 Concrete Specification

In manufacturing the concrete, the same materials and processes as explained in Chapter 2 were used. The crushing strength of the control specimens for the tests is given in Table 3.1. The values given for cube compressive strength (f_{cu}), tensile strength (f_{sp}) and modulus of elasticity (E_c) are the average values obtained from testing three control specimens. The methods used in obtaining the splitting tensile strength and the modulus of elasticity are explained in Chapter 2.

3.3 Test Procedure

All the specimens were placed in a central position on the machine at right-angles to the direction in which they were cast. Mild steel base plates were placed symmetrically on the upper face of the cube specimen, and the loading piece was placed on top of the plate so that the longitudinal axis of both the plate and the loading piece were colinear with an axis of the cube.

The upper platen of the testing machine was brought into contact with the upper surface of the loading piece (Photograph B.3), and the load was transmitted through the base plate to the concrete. The load was applied at a constant rate of one ton for every thirty seconds on average (except when gauge readings were taken). The specimens were loaded in this manner until failure occurred.

3.3.1 Initial Tests

In an attempt to understand the behaviour of steel base plates whilst under load a few tests were carried out with strain gauges fixed on the top and bottom surface of the base plates. In this way the bending strains on top and bottom surfaces of base plate were recorded.

3.3.1.1 An Investigation of the Distribution of Stress on the Top Surface of the Steel Base Plate

In one test with a 150mm cube of cube strength of 30N/mm^2, the knife-edge loading piece was applied concentrically through a 4mm thick steel base plate. Eleven electrical strain gauges of the type (PL.3) were fixed to the base plate at right-angles to the longitudinal axis of the knife edge load. The disposition of the gauges is shown in Fig .B.2 of Appendix B. When all the gauges had been fixed to the plate, a wire was soldered to each of the tags, two per gauge. The other ends of the leads were connected to the terminals of an extension box (type 23 u No 6718) which was connected to the Pieckel (type B 103U No. 6552). For all the gauges only one dummy was used, as it could be switched into each gauge circuit in turn.

Before loading commenced, the reading of each gauge was taken and then at each increment of load, until the stage when it became impossible to take readings due to fluctuations of the strains. The strain recorder was then disconnected from the extension box and the loading was continued until failure (load dropped off).

With the same concrete strength and size, two other tests were carried out in which loading pieces (10 x 150mm) were concentrically applied through a 4mm thick steel base plate. Strain gauges were fixed to the plate as before, but in the first test only two strain gauges were used. These were placed opposite to one another under a gap in the loading piece (9 x 4mm) and along the edge of the strip loading. In the second test, three strain gauges were placed along the edge of the strip loading and under the gaps, at distances of 45mm. The shape of both knife and strip loading pieces and the disposition of the strain gauges are shown in Photographs B.1 and B.2 (Appendix B).

3.3.1.2 Investigation of the Distribution of Stresses on the Top and Bottom Surfaces of the Steel Base Plate

A gap was made in the concrete, and strain gauges were fixed in the centre of the top and bottom surfaces of the 4mm thick base plate. The gap in the 150mm concrete cubes was made just deep enough (5mm) to take the electrical lead on the bottom face of the plate. The strain gauges were put in position and readings taken, as explained in Section 3.3.1.1.

3.3.2 Main Tests

These tests were divided into two groups of strip and square loadings. The positioning and reading of strain gauges in the main tests was the same as the methods explained in Section 3.3.1.1, and the loading configuration was the same as in Section 3.3.

3.3.2.1 Strip Loading

In all the tests in this group, which was comprised of four series, 150mm cubes were used except in series 3, where 250mm cubes were tested. In all of the tests with strip loading, only one strain gauge was fixed to the base plate, which was positioned at its centre and at right-angles to the longitudinal axis of the knife edge load.

3.3.2.1.1 Tests With Varying Concrete Strengths

In this series of tests, four different concrete cube strengths ranging from 10 to 37 N/mm^2 were used. Knife-edge loading was applied through a 4mm thick steel base plate. In three tests, with concrete strengths of 10.9, 13.7 and 37 N/mm^2, five electrical strain gauges were fixed to the surface of concrete specimen, parallel to the longitudinal axis of the loading piece. Gauges of the type (PL-60-11) were spaced as close together as possible in the region in which high compressive stresses were expected. The disposition of the gauges is shown in Photograph B.3 and Fig. B.5. Before loading commenced the reading of each gauge was taken and then at each increment of loading (every thirty seconds), until it became impossible to take any reading due to fluctuation of the strains. The results of these longitudinal strain measurements for tests with concrete strength of 13.7 and $37N/mm^2$ are tabulated in Tables 3.2 and 3.3. The test results with concrete strength of 10.9 N/mm^2 are tabulated in Table B.5. A discussion of this set of tests is presented in Section 3.6.

3.3.2.1.2 Tests With Varying Thickness of Steel Base Plate

Tests to failure were made on eight different thicknesses of steel base plate (4, 6, 8, 10, 11.6, 22.5, 30, 40mm). Load was applied through a knife-edge to 150mm cubes. In the first four tests the concrete cube strength was $40N/mm^2$ and in the last three it was $32N/mm^2$. The cube strength in the test with 11.6mm thick steel base plate was $37N/mm^2$. In two of the tests, with base plate thicknesses of

Load	Stress in concrete at five different positions N/mm^2				
KN	1	2	3	4	5
0.00	0.00	0.00	0.00	0.00	0.00
2.50	1.64	1.46	1.10	0.55	0.18
7.50	2.56	2.56	1.83	1.10	0.55
15.00	4.47	4.02	2.92	1.64	0.82
25.00	7.30	7.12	4.93	2.74	1.46
35.00	10.22	9.50	6.75	3.65	2.19
45.00	12.14	11.86	8.39	4.38	2.58
55.00	15.15	14.10	10.04	5.29	3.10
60.00	17.16	15.50	11.30	6.02	3.56
65.00	18.90	16.88	12.32	6.75	3.83
70.00	20.99	18.79	13.69	7.48	4.20
75.00	20.99	19.89	15.15	8.12	4.47
82.50	24.64	22.10	17.52	9.31	4.75
90.00	30.11	25.60	19.89	10.95	5.11
97.00	U S.*	U S.	U S.	U S.	U S.

Table 3.2. Concentric knife-edge loading through a 4mm steel base plate on a 150mm concrete cube (f_{cu} = 13.7N/mm^2).

* No reading could be taken due to fluctuations.

Load	Stress in concrete at five different positions N/mm^2				
KN	1	2	3	4	5
50.0	0.96	0.44	0.80	0.82	0.58
55.0	1.31	0.73	1.00	0.88	0.64
60.0	1.90	1.50	1.40	1.20	0.96
65.0	2.50	2.00	1.80	1.50	1.00
70.0	3.00	2.50	2.30	1.80	1.30
75.0	3.94	3.40	2.74	2.20	1.50
80.0	4.76	4.00	3.42	2.60	1.90
85.0	5.70	5.00	4.00	3.00	2.00
90.0	6.90	6.00	6.50	3.50	2.40
95.0	8.30	7.50	5.60	4.00	2.80
100.0	9.20	8.20	6.20	4.50	3.00
110.0	11.80	10.50	7.70	5.40	3.50
115.0	13.30	11.80	8.50	6.00	3.90
120.0	15.00	13.00	9.00	6.40	4.40
125.0	16.00	14.50	9.80	6.80	4.75
130.0	17.70	15.60	10.60	7.30	5.00
137.0	20.00	19.00	11.00	7.80	5.00
147.0	29.00	24.00	13.00	8.80	5.80
155.0	35.30	31.70	15.50	9.30	6.30
165.0	U S.	U S.	U S.	U S.	U S.
175.0	U S.	U S.	U S.	U S.	U S.

Table 3.3. Concentric knife-edge loading through a 4mm steel base plate on a 150mm concrete cube (f_{cu} = 37.0N/mm^2).

6.0 and 11.6mm, five strain gauges were fixed to the surface of concrete, in the same way as explained in section 3.3.2.1.1. The results of these longitudinal strain measurement for the test with plate thickness of 11.6 mm are tabulated in Table 3.4 and for the test with plate thickness of 6mm is tabulated in Table B.6.

Tests were also carried out on 250mm cubes with a cube crushing strength of 24.8N/mm^2. Knife-edge loading was applied through 6.0 and 12mm thick base plates, and the results of these tests are tabulated in Series 3 of Table 3.1.

3.3.2.1.3 <u>Tests With a Strip Loading Piece</u>

The results of this set of tests are tabulated in Series 4 of Table 3.1. Rectangular strip loading pieces were applied through 4.0 and 6.0mm thick base plates to the 150mm cubes. A concrete strength of 30N/mm^2 was used for the 150 x 10mm strip loading. The cube strength of the concrete for 150 x 32mm and 150 x 98mm strip loadings was 37.5N/mm^2. For this series, no strain gauges were fixed to the base plates.

3.3.2.2 <u>Tests with Square and Rectangular Loading Plates</u>

Series 5 of the tests was carried out on 150mm cubes which were loaded through rectangular and square loading pieces. The load was applied through 4mm thick steel base plates. It was not necessary to perform a large number of tests, as this had been done by other researchers (4,13,20). The purpose of this limited series of tests was to establish a clear pattern of failure and to compare the results with previous reports. The results of this series are given in Series

Load KN	Stress in concrete at five different positions N/mm^2 1	2	3	4	5
80.0	0.35	0.58	0.44	0.29	0.00
90.0	1.00	1.00	0.73	0.59	0.15
100.0	1.50	1.80	0.73	0.93	0.44
110.0	2.30	2.20	1.70	1.20	0.73
120.0	3.00	3.00	2.40	1.90	1.30
130.0	3.70	3.80	3.10	2.30	1.50
140.0	5.30	5.00	4.00	3.10	2.00
150.0	6.60	6.20	5.00	4.00	2.60
160.0	7.00	7.30	5.80	4.70	3.10
180.0	10.00	9.00	7.70	6.00	4.10
190.0	12.40	11.60	9.30	7.30	5.00
200.0	14.60	13.70	10.90	8.50	5.90
210.0	16.60	15.50	12.40	9.90	6.60
220.0	19.00	17.50	17.70	10.80	7.40
230.0	23.30	21.30	16.60	12.80	8.60
250.0	33.60	28.20	20.70	15.50	9.80
270.0	45.0	36.20	25.40	17.50	10.70
300.0	U S.	U S.	U S.	U S.	U S.
320.0	U S.	U S.	U S.	U S.	U S.

Table 3.4 Concentric knife-edge loading through a 11.70 mm steel base plate on a 150mm concrete cube (f_{cu}=37.0N/mm^2).

5 of Table 3.1.

3.4 Discussion of the Initial Test Results

Table B.1 gives the results of the tests in which the concrete cube was loaded concentrically through a 4mm thick base plate with a knife-edge loading piece. This table shows eleven values of stress for every increment of loading, which correspond to the eleven strain gauges fixed to the base plate at right-angles to the direction of the load applied. The disposition of the gauges is shown in Photograph. B.2 and Fig. B.1. The table also shows the average of the readings corresponding to the gauges fixed on the same line, parallel to the direction of the load applied. The letters C and F in the load column of the table refer to the load at which a crack first appeared and the failure load, respectively.

Graphs of stress plotted against distance from the centre line for every increment of loading are plotted in Fig. 3.1. The number on a graph indicates the load in KN. The dotted lines drawn are based on the assumed symmetrical conditions of loading. It can be seen from Fig. 3.1 that for large load values, plastic hinges occur in the steel base plate close to the knife edge load. As a result of this mechanism and the formation of the hinges, the plate was deformed into a shallow V-shape.

The results of the second series of initial tests with strip loading pieces (150 x 10mm) are tabulated in Tables B.2 and B.3. It can be seen that the readings from corresponding gauges are approximately the same value.

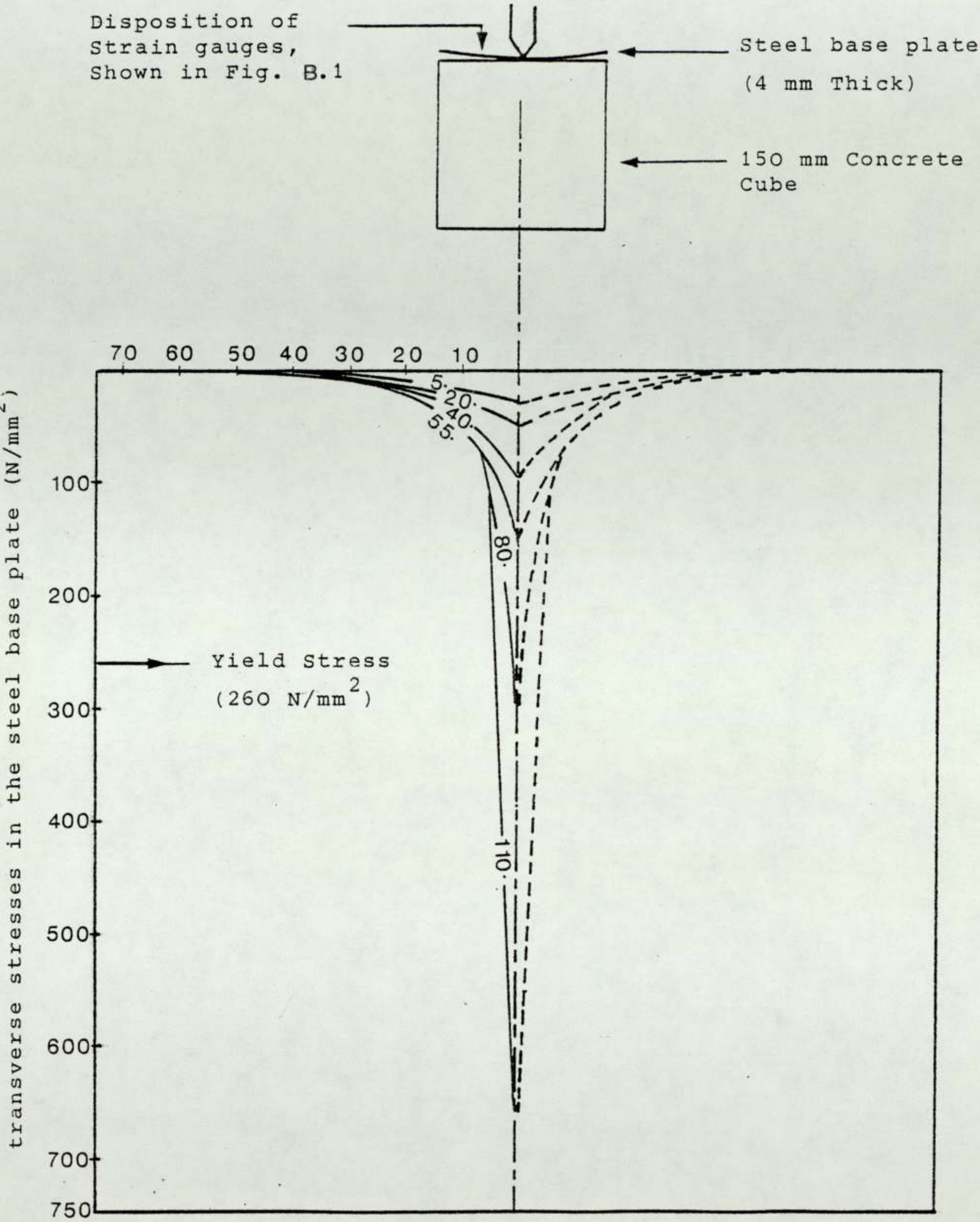

Fig 3.1 Distribution of bending stresses in the steel base plate.

The results of the final series of initial tests, in which the stresses on both sides of the plate were measured, are tabulated in Table B.4. The results indicate that the stresses (tensile and compressive) directly underneath the loading piece are almost identical and there is little friction resistance between the steel plate and concrete.

3.5 General Observations and Modes of Failure

In the tests with different thicknesses of base plate (4.0 to 40mm), it was observed that for a knife edge loading and the thin plates (4 to 8mm), parallel crack lines, some distance apart were formed in the concrete along the direction of the applied load, as shown in Photograph B.4. A vertical crack also started from the apex of the wedge formed underneath the loading piece, which propagated downwards and inwards, suggesting a splitting and sliding mode of failure.

A similar pattern of failure was reported in Chapter 2 for small ratios of R with concrete loaded through rigid strip loading piece (Photograph 2.1). The sharp parallel crack lines along the edges of the rigid strip plates are noted in Photograph 2.1 in comparison to the jagged cracks in the concrete loaded through an 8mm thick base plate. Also, the wedge formed under the base plate is already crushed in comparison to the uncrushed wedges formed by rigid loading. However, the general patterns of failure are the same for rigid and flexible plates.

The horizontal distance between the top of the two surface cracks increased as the thickness of the base plates increased, until the maximum distance was reached. (This distance in a test with 12m thick base plate and 150mm concrete cube of cube strength of 37N/mm^2 was approximately 80mm.) Once this distance had been attained, the pattern of failure changed from that detailed above to one of crushing, in which the failure occurred with the punching out of an inverted cone, accompanied by the formation of debris, similar to cube crushing tests.

In all the tests with flexible base plates, the plate lifted at its free ends as loading increased, and when failure had occurred it was observed that the plates had been bent permanently into a shallow V-shape. The reading of srain gauges fixed at the centre of the steel base plates also showed a permanent deformation.

3.6 Presentation and Discussion of the Main Test Results

The results of the five series of concentric loading tests are shown in Table 3.1. The properties of the concrete used, together with plate dimensions, the dimensions of the loading piece and failure load are given for all tests. From the results of the first series of tests with one thickness of base plate (4mm) and increasing concrete strength, it was found that as concrete strength increased the failure load increased. However, this increase was not linear, and for one thickness of base plate the rate of increase in failure load decreased with the increase in cube strength. In the second series of tests with eight different thicknesses of steel base plate ranging from 4 to 40mm, it was found that in all the tests except with 40mm thick base plate the plates were permanently deformed into a shallow V-shape. As a result of this deformation plastic hinges were formed in the steel base plates.

In tests (S1,S2,S4,S6,S8 and S9), strain gauges were fixed to the surface of the concrete parallel to the direction of the load applied. The purpose of these tests was to find the distribution of the longitudinal stresses in the concrete under different thicknesses of base plate. Graphs of longitudinal stress plotted against distance from the centre line of the cube for every increment of loading are plotted in Figs. 3.2, 3.3 and 3.4 for the three tests S2, S4 and S9. The number on a graph indicates the load in KN. The dotted lines indicate the distribution of the longitudinal stress on the other half of the concrete, based on the symmetrical condition of loading.

It is clear from Figs. 3.2, 3.3 and 3.4 that the distribution of the stresses is not uniform within the contact area. In fact the rate of increase in the stresses for an increased load is quite higher at the centre line than at the edges of the contact area.

For the higher concrete strength of $37N/mm^2$, a considerable load was applied before any measurable reading could be taken from the strain gauges. These were 80 and 130 KN. for tests with 4 and 11.7mm base plates. Comparing the two Figs 3.2 and 3.3 (which refer to the same plate thickness of 4mm and two different concrete strengths of 13.7 and $37N/mm^2$), it should be noted that with higher concrete strength the steel base plate experiences larger bending deformation, therefore stresses are concentrated within a smaller contact area. On the other hand, for the same concrete strength ($37N/mm^2$) and increasing plate thicknesses from 4 to 11.7mm in tests S4 and S9, it can be seen from Figs. 3.3 and 3.4 that as the plate thickness increases, the gradient of the curves becomes less, and the stresses

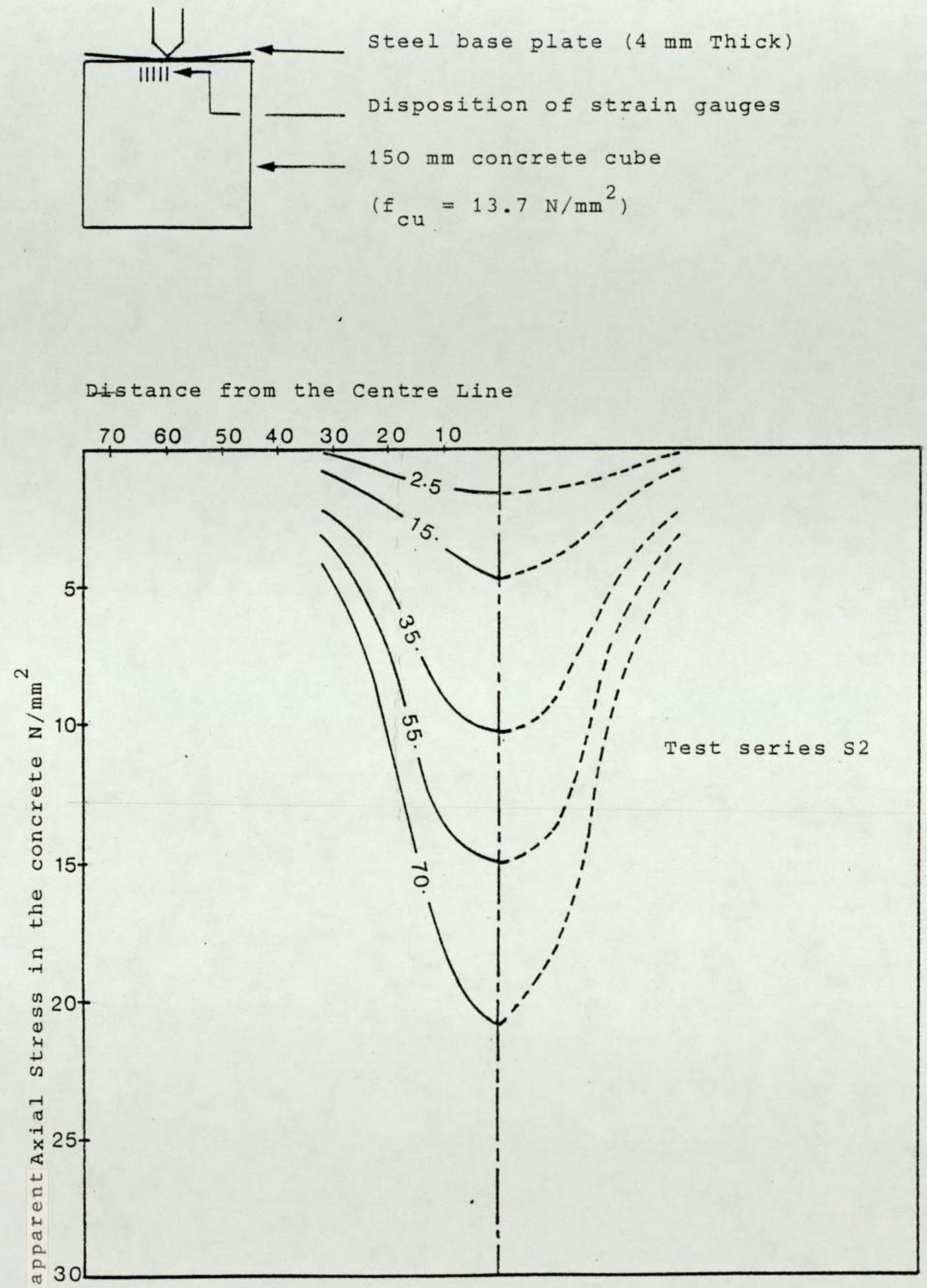

Fig 3.2. Distribution of axial stresses in the concrete cube, for test series S2.

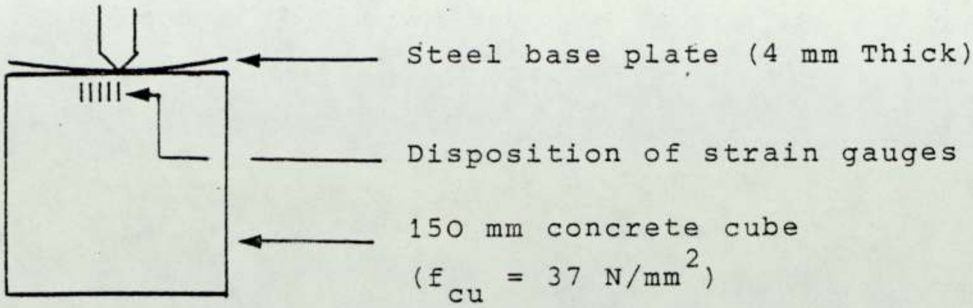

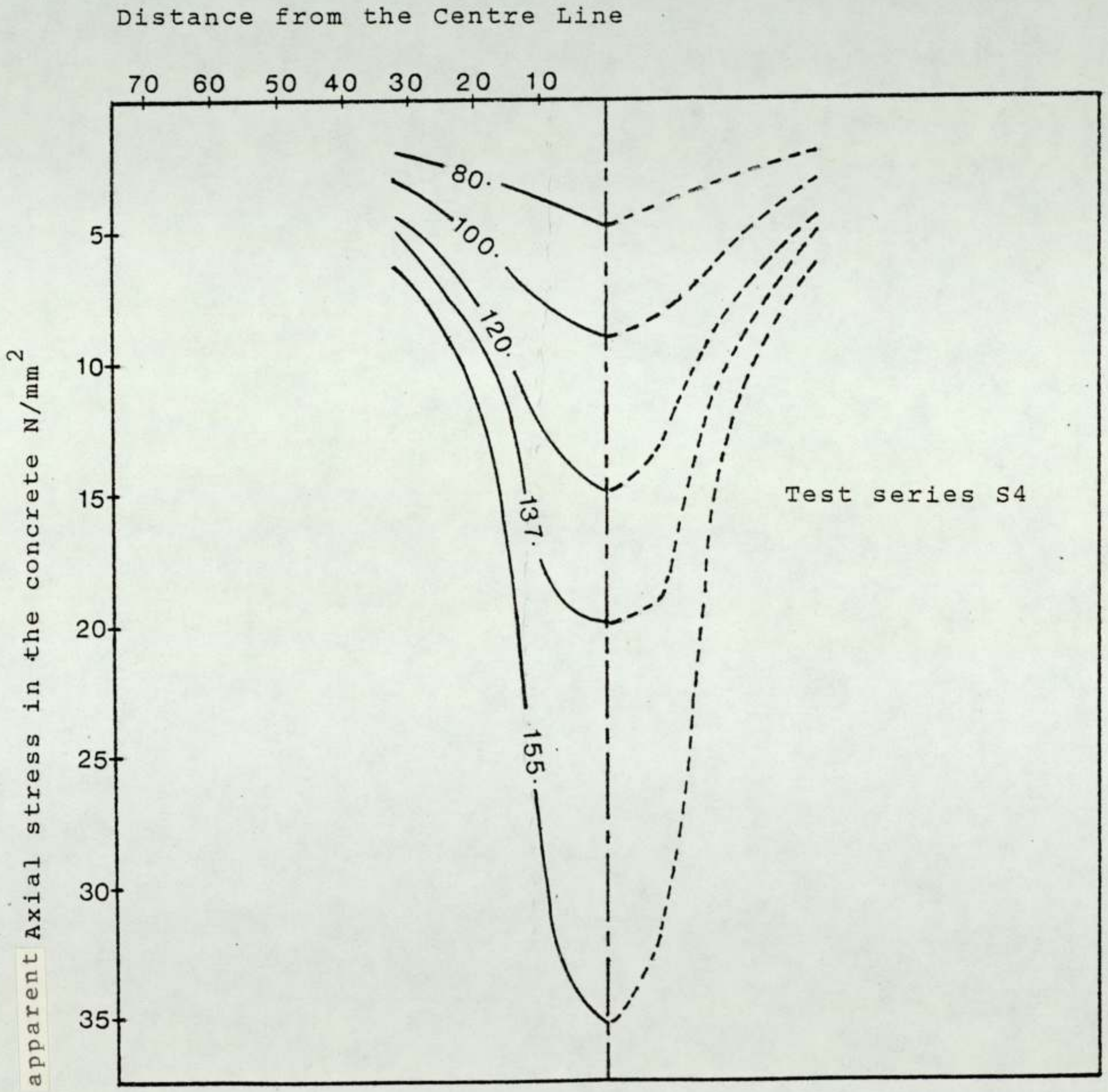

Fig. 3.3 Distribution of axial stresses in the concrete cube,
<u>for test series S4</u>.

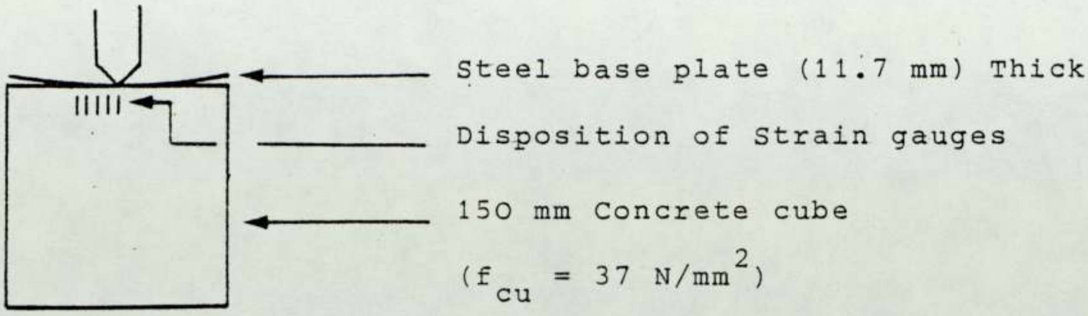

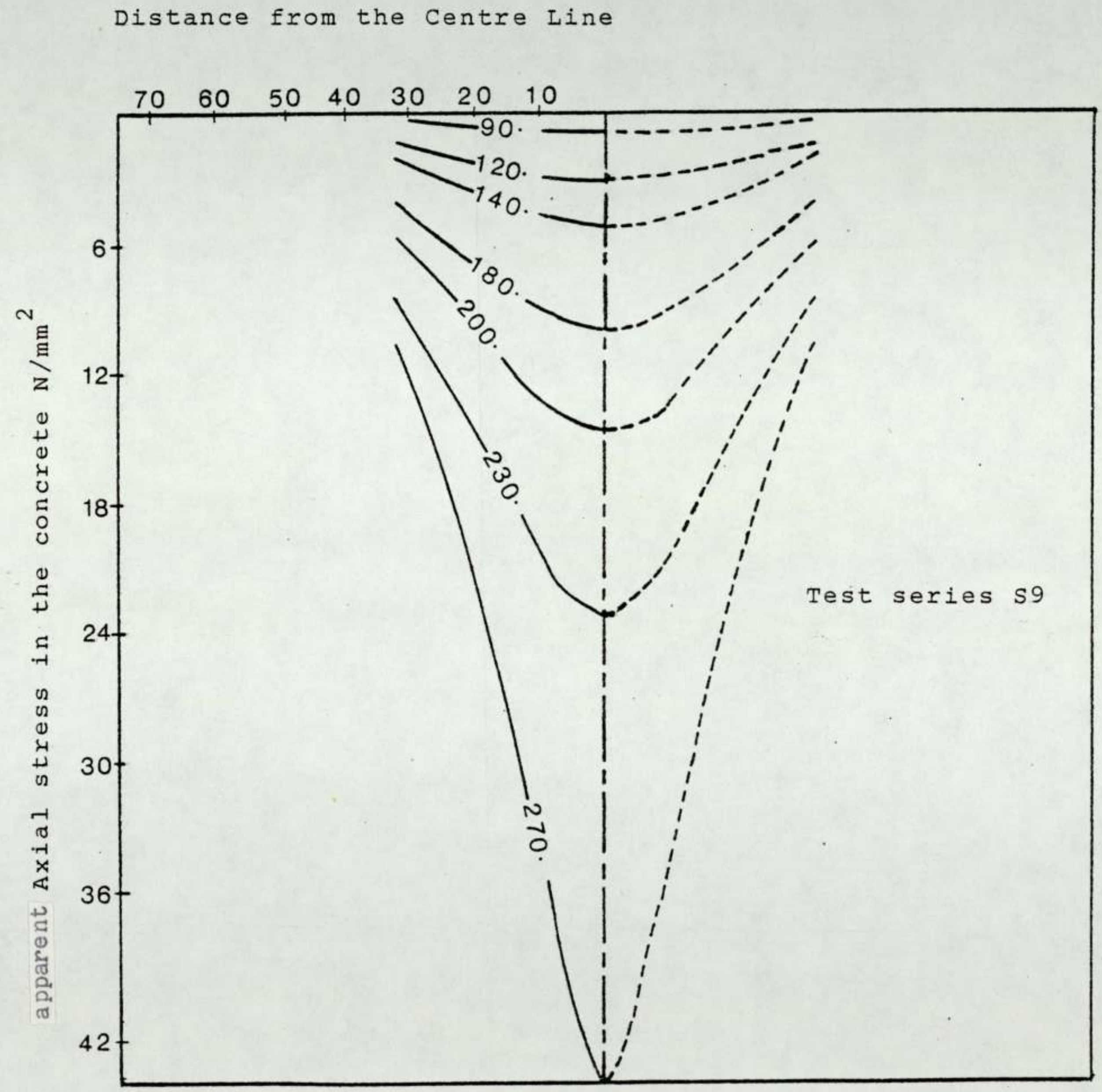

Fig. 3.4 Distribution of axial stresses in the concrete cube,

for test series S9

are distributed over a larger contact length.

In the future it may well be decided that the real contact length is an important factor in finding the bearing capacity of the concrete under such a loading configuration. However, for simple analysis it was decided to assume a rectangular pattern of stress distribution, whose width corresponds to the contact length of an equivalent stiff bearing at failure.

CHAPTER FOUR

THEORETICAL WORK FOR AXIALLY LOADED CUBES

4.1 Introduction

In Chapter 2 empirical formulae were presented for concrete cubes loaded through rigid base plates. In the preceding chapter the work was extended to loading through flexible and rigid plates (4 to 40 mm thick). A series of test results were presented in which strip knife-edge, square and rectangular loading pieces were used. Modes of failure and the distribution of stresses on both the concrete and the base plates were discussed. In this chapter the empirical formulae based on stiff bearing area are extended for cases of loading through different thicknesses of base plate and varying cross sections of loading piece.

4.2 Square and Rectangular Loading

Consider a cube loaded with a force F through a loading piece and flexible base plate, as shown in Fig. 4.1.

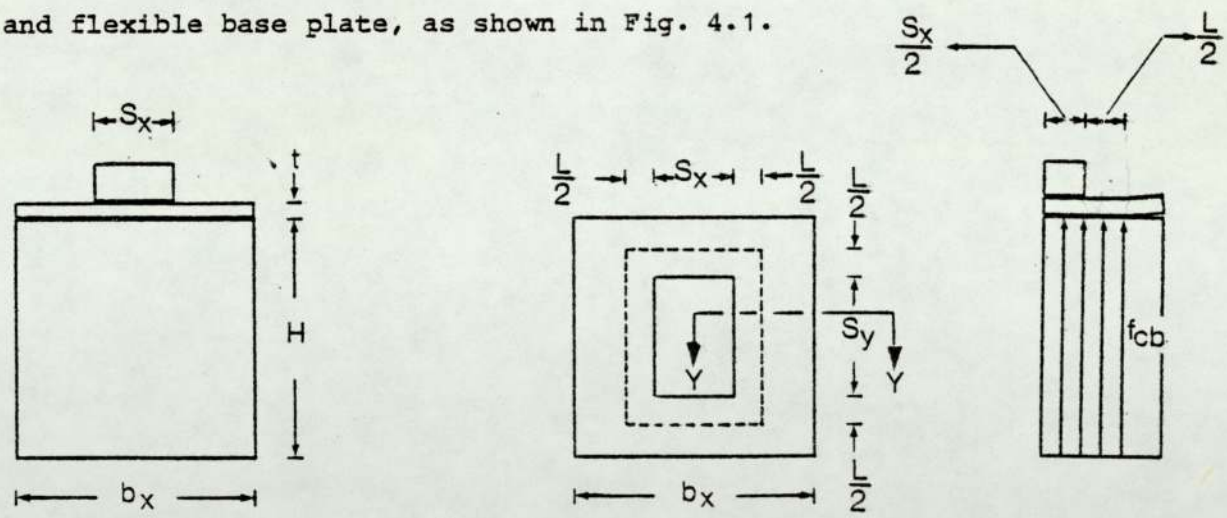

(a) Elevation (b) Plan (c) Section YY

Fig. 4.1 Configuration of loading through a steel base plate with a thichness t.

The loading piece dimensions are S_x by S_y, but the "equivalent stiff bearing area" has dimensions which are greater , i.e. $(S_x + L)$ by $(S_y + L)$ where L is the length of the steel base plate that is in contact with the cube as shown in Fig.4.1b.

Resolving forces vertically,

$$F = (S_x+L)(S_y+L)f_{cb} \tag{4.1}$$

Where f_{cb} is the bearing strength of concrete.

The second equation can be derived by considering Fig. 4.1 Assuming a uniform stress distribution and that the projection of the flexible plate beyond the edge of the loading piece acts as a cantilever beam, the bending moment on a cantilever of length L/2 for a unit width is,

$$M = f_{cb} \left(\frac{L}{2} \right) \left(\frac{L}{4} \right)$$

Rearranging the above equation,

$$M = f_{cb} \left(\frac{L^2}{8} \right) \tag{4.2}$$

From the theory of bending, for unit width of steel base plate,

$$M = Z_p f_y$$

where $Z_p = t^2/4$ is the plastic section modulus of a steel base plate of thickness t. Therefore,

$$M = \frac{t^2}{4} f_y \tag{4.3}$$

Equating equations (4.2) and (4.3),

$$f_{cb} \left(\frac{L^2}{8} \right) = \frac{t^2}{4} f_y$$

therefore

$$f_{cb} = 2f_y \frac{t^2}{L^2} \tag{4.4}$$

Substitute for fcb in equation (4.1)

$$F = (S_x+L)(S_y+L)\left(2f_y \frac{t^2}{L^2}\right) \tag{4.5}$$

Depending on the value of A_s/A (area of concrete in contact with specimen)/(area of specimen), being less or greater than 0.125 two empirical Equations (2.1) and (2.2) were developed in Chapter Two.

4.2.1 For Ratio of R< 0.125

From Chapter Two Equation (2.1) was developed for ratios of R<0.125.

$$\frac{F}{f_{cu}A} = 1.36\left(\frac{A_{se}}{A} \right)+0.085 \tag{4.6}$$

$A_{se} = (S_x+L)(S_y+L)$

Substituting for A_{se} in (4.6)

$$F = 1.36f_{cu}(S_x+L)(S_y+L)+0.085Af_{cu} \qquad (4.7)$$

Substituting for F in (4.5)

$$1.36f_{cu}(S_x+L)(S_y+L)+0.085Af_{cu} = (S_x+L)(S_y+L)(2f_y \frac{t^2}{L^2})$$

Dividing both sides of the above equation by $(S_x+L)(S_y+L)f_{cu}$

$$1.36 + \frac{0.085\ A}{(S_x+L)(S_y+L)} = \frac{2f_y}{f_{cu}} \times \frac{t^2}{L^2} \qquad (4.8)$$

Multiplying both sides of the above equation by L^2 and expressing the equation in terms of L

$$\frac{16}{t^2}(L^4) + \frac{16}{t^2}(S_x+S_y)(L^3) + \left(\frac{A}{t^2} + \frac{16A_s}{t^2} - 23.53\frac{f_y}{f_{cu}}\right)(L^2)$$

$$- \frac{23.53f_y}{f_{cu}}(S_x+S_y)(L) - 23.53\frac{f_y}{f_{cu}}A_s = 0.0 \qquad (4.9)$$

4.2.2 <u>For Ratio of R> 0.125</u>

From Chapter Two Equation (2.2) was developed for ratios of R> 0.125.

$$\frac{F}{f_{cu}A} = 0.85\left(\frac{A_{se}}{A}\right)+0.15 \qquad (4.10)$$

As in Section 4.2.1, substituting for F in Equation (4.10) the following expression can be developed,

$$0.85 + \frac{0.15\,A}{(S_x+L)(S_y+L)} = \frac{2f_y}{f_{cu}} \times \frac{t^2}{L^2} \qquad (4.11)$$

Following the same procedure as that for ratio of As/A <0.125 the final formula in term of L is as follows:

$$\frac{5.7}{t^2}(L^4) + \frac{5.7}{t^2}(S_x+S_y)(L^3) + \left(\frac{A}{t^2} + \frac{5.7A_s}{t^2} - 13.33\frac{f_y}{f_{cu}}\right)(L^2)$$

$$- \frac{13.33f_y}{f_{cu}}(S_x+S_y)(L) - 13.13\frac{f_y}{f_{cu}}A_s = 0.0 \qquad (4.12)$$

4.3 Strip Loading Piece

In this case of strip loading one side of the loading piece is equal to one side of the specimen.

$$S_y = b_y$$

Therefore, resolving forces vertically,

$$F = (S_x+L)(b_y)f_{cb} \qquad (4.13)$$

Using Equation (4.4) and substituting for f_{cb} it can be written :

$$F = (S_x+L)(b_y)\left(\frac{2f_y t^2}{L^2} \right) \tag{4.14}$$

4.3.1. For Ratio of R < 0.125

Following exactly the same procedure as in Section 4.2.1 by combining Equations (4.6) and (4.14), an expression in terms of L can be written as follows,

$$\frac{16}{t^2}(L^3) + \left(\frac{b_x}{t^2} + \frac{16}{t^2} \right)(L^2) - 23.5\,\frac{f_y}{f_{cu}}(L)$$

$$- 23.5\,(S_x)\,\frac{f_y}{f_{cu}} = 0.0 \tag{4.15}$$

4.3.2 For Ratio of R > 0.125

In the same way as in Section 4.2.2 by combining Equations (4.10) and (4.14), an expression in term of L can be developed as follows,

$$\frac{5.7}{t^2}(L^3) + \left(\frac{b_x}{t^2} + \frac{5.7}{t^2} \right)(L^2) - 13.3\,\frac{f_y}{f_{cu}}(L)$$

$$- 13.3\,(S_x)\,\frac{f_y}{f_{cu}} = 0.0 \tag{4.16}$$

4.4 Correlation of the Theory and Test Results

The results of the tests described in Chapter 3 are tabulated in Table 4.1 and the theoretical failure load and ratio of measured to calculated failure load are also shown. To further support the proposed method, the test results of Hawkins(12) and De-Wolf(20) are also given for comparison, as shown in Tables 4.2, 4.3. To make a clearer comparison between the present theory and that of Hawkins, the formula proposed by Hawkins was also applied to De-Wolf's test results and tabulated in Table 4.3.

In calculating the failure load in De-Wolf's tests, the Author's method produced a mean of 1.12 with a percentage difference of 7.5%. Hawkins' method gave a mean of 1.09 with a percentage difference of 13.0.

It should also be emphasised here that the present formula has been applied for different shapes of loading piece i.e. strip, knife-edge, rectangular and square. Although Hawkins(13) developed a formula for strip loading, the equation has several limitations, one of which is that the depth of the block should be 1.5 times its width, and therefore the method cannot be applied to cubic blocks. When Hawkins(13) applied his equation for strip loading to a series of tests conducted at Sydney University, he decided that the equation did not realistically predict the observed effects of changes in concrete compressive strength, and the correlation between measured and calculated bearing capacities was poor. In the case of rectangular loading plates, Hawkins' (10,12) formula showed a poor correlation when compared with his own tests. Hawkins pointed out that his formula for rectangular loading pieces was not sufficiently accurate. Hawkins'

Series	Test	Concrete Strength	Steel Base Plate		Contact Length	Ratio	Failure Load Theory	Failure Load Measured	Ratio of Measured/Computed (Failure Load)
No	No	f_{cu}	f_y	t	L Eq.(4.9) OR Eq.(4.12)	A_{se}/A	F Eq.(4.6) Or Eq.(4.10)	F	By Author
		N/mm^2	KN/mm^2	mm	mm	mm/mm	KN	KN	Dimensionless
(1)	S1	10.9	260	4.0	20.4	0.15	68.0	80.0	1.18
150 mm	S2	13.7	260	4.0	17.6	0.13	80.5	97.5	1.20
Cubes	S3	30.0	260	4.0	10.9	0.09	136.3	150.0	1.10
	S4	37.0	260	4.0	9.6	0.08	158.3	175.0	1.10
(2)	S5	40.0	265	4.0	9.2	0.07	167.9	190.0	1.13
150 mm	S6	40.0	265	6.0	15.1	0.11	216.0	260 0	1.20
Cubes	S7	40.0	265	8.0	22.0	0.16	257.4	290.0	1.14
	S8	40.0	265	10.0	29.2	0.21	294.1	330.0	1.12
	S9	37.0	265	11.6	36.8	0.26	307.9	320.0	1.04
	S10	32.0	260	22.5	86.4	0.59	468.7	529.7	1.13
	S11	32.0	260	30.0	118.8	0.81	600.9	647.5	1.08
	S12	32.0	260	40.0	148.0	1.00	718.4	721.0	1.00
(3)	S13	24.8	260	6.0	17.8	0.08	298.7	337.5	1.13
250 mm	S14	24.8	260	12.0	42.4	0.18	466.5	514.1	1.10
Cubes									

Table 4.1 Comparison of results predicted by the Author's theory to those obtained through his tests on concentric loading.

(CONTINUED)

Series	Test	Concrete Strength	Steel Base Plate		Contact Length	Ratio	Failure Load Theory	Failure Load Measured	Ratio of Measured/Computed (Failure Load)
No	No	f_{cu}	f_y	t	L Eq.(4.9) OR Eq.(4.12)	A_{se}/A	F Eq.(4.6) Or Eq.(4.10)	F	By Author
		N/mm^2	KN/mm^2	mm	mm	mm/mm	KN	KN	Dimensionless
(4)	S15	30.0	265	4.0	12.4	0.15	186.9	198.0	1.05
150 mm	S16	37.5	265	4.0	13.2	0.30	342.7	382.6	1.10
Cubes	S17	37.5	265	4.0	14.8	0.75	665.9	651.3	0.91
	S18	37.5	265	5.9	19.6	0.34	373.3	392.2	1.05
								Mean ------>	(1.10)
								Standard Deviation ------>	($\pm$0.06)
								% ------>	(5.10)

Table 4.1 Comparison of results predicted by the Author's theory to those obtained through his tests on concentric loading.

Test Series	Hawkins' Investigation Test Results						Author's Empirical Theory			
	Concrete Strength	Size of Specimen	Square Punch Side Length	Steel Base Plate		Failure Load	Contact Length	Ratio	Failure Load	Ratio of Measured/Computed (Failure Load)
	f_{cu}		$S_x = S_y$	f_y	t	F	L Eq.(4.9) OR Eq.(4.12)	A_{se}/A	F Eq.(4.6) OR Eq.(4.10)	
	N/mm^2		mm	KN/mm^2	mm	KN	mm	mm/mm	KN	Dimensionless
A1	23.7	150 mm cubes	100	338	1.5	178.5	6.0	0.16	156.6	1.14
A2	23.7		100	276	3.0	185.4	11.25	0.18	169.7	1.09
A3	23.7		100	262	6.35	258.0	25.0	0.27	210.9	1.22
A4	23.7		100	283	8.90	276.6	38.3	0.37	258.0	1.07
B1	38.7	150 mm cubes	100	345	0.76	267.8	2.5	0.15	255.1	1.05
B2	38.7		100	338	1.50	285.5	4.75	0.17	261.9	1.09
B3	38.7		100	276	3.0	303.1	9.0	0.19	280.6	1.08
B4	38.7		100	262	6.35	388.5	19.25	0.25	329.6	1.18
B5	38.7		100	282	8.90	421.8	29.25	0.32	384.6	1.10
B6	38.7		100	276	25.4	569.0	44.0	0.45	476.8	1.19
C1	51.9	150 mm cubes	100	345	0.76	303.1	2.25	0.15	337.5	0.90
C2	51.9		100	338	1.50	306.1	4.25	0.16	348.3	0.90
C3	51.9		100	276	3.0	363.0	7.75	0.18	367.9	1.00

Table 4.2 Comparison of Hawkins' test results to the empirical theory proposed by the Author.

(CONTINUED)

Test Series	Hawkins' Investigation Test Results						Author's Empirical Theory			
	Concrete Strength	Size of Specimen	Square Punch Side Length	Steel Base Plate		Failure Load	Contact Length	Ratio	Failure Load	Ratio of Measured/Computed (Failure Load)
	f_{cu}		$S_x = S_y$	f_y	t	F	L Eq.(4.9) OR Eq.(4.12)	A_{se}/A	F Eq.(4.6) OR Eq.(4.10)	
	N/mm^2		mm	KN/mm^2	mm	KN	mm	mm/mm	KN	Dimensionless
C4	51.9		100	262	6.35	460.1	16.5	0.24	422.8	1.10
C5	51.9		100	282	8.90	529.7	24.75	0.29	481.7	1.10
C6	51.9		100	276	25.40	683.8	44.0	0.45	638.6	1.07
D1	36.1	150 mm cubes	97.5	317	8.9	346.3	31.5	0.30	337.5	1.03
D2	36.1		97.5	317	8.9	353.2	32.8	0.36	381.6	0.93
D3	36.1		97.5	276	12.4	382.6	42.75	0.38	396.3	0.97
D4	36.1		97.5	276	12.4	425.8	40.75	0.42	427.7	1.00
D5	36.1		97.5	262	15.7	427.7	40.75	0.42	427.7	1.00
E1	36.1	250 mm cubes	147.5	517	12.6	692.6	52.3	0.19	728.9	0.95
E2	36.1		147.5	262	18.5	703.4	54.8	0.20	747.5	0.94
F1	26.0	200x200x300 prisms	150.0	620	6.35	352.2	34.5	0.21	353.2	1.00
F2	26.0		147.5	276	8.9	375.7	31.75	0.20	343.4	1.08

Table 4.2 Comparison of Hawkins' test results to the empirical theory proposed by the Author.

(CONTINUED)

	Hawkins' Investigation Test Results						Author's Empirical Theory			
Test Series	Concrete Strength	Size of Specimen	Square Punch Side Length	Steel Base Plate		Failure Load	Contact Length	Ratio	Failure Load	Ratio of Measured/Computed (Failure Load)
	f_{cu}		$S_x = S_y$	f_y	t	F	L Eq.(4.9) OR Eq.(4.12)	A_{se}/A	F Eq.(4.6) OR Eq.(4.10)	
	N/mm^2		mm	KN/mm^2	mm	KN	mm	mm/mm	KN	Dimensionless
F3	26.0		147.5	517	12.6	468.9	71.22	0.41	537.6	0.87
F4	26.0		147.5	289	15.7	478.7	65.25	0.37	503.3	0.95
F5	26.0		147.5	262	18.5	530.7	74.75	0.43	562.1	0.95
F6	26.0		147.5	262	50.0	703.4	90.75	0.55	657.3	1.07
G1	36.1	200x200x300	147.5	620	6.35	431.6	28.5	0.18	456.2	0.95
G2	36.1	prisms	147.5	276	8.89	440.5	26.25	0.17	444.4	1.00
G3	36.1		147.5	289	15.7	536.6	53.5	0.31	612.1	0.88
G4	36.1		147.5	289	50.0	881.9	90.75	0.55	915.3	0.96
									Mean ------>	(1.04)
									Standard Deviation ------>	(± 0.09)
									% ------>	(8.8)

Table 4.2 Comparison of Hawkins' test results to the empirical theory proposed by the Author.

Test No	De-Wolf's Investigation Test Results						Measured Failure		Ratio of Measured/Computed (Failure Load)	
	Concrete Strength	Size of Specimen	Squre Punch Side Length	Steel Base Plate		Failure Load	Author	Hawkins		
	f_{cu}		$S_x = S_y$	f_y	t		F Eq.(4.6) OR Eq.(4.10)	F Eq.(5) OR Eq.(5),(9)	Author	Hawkins
	N/mm^2	mm^3	mm	KN/mm^2	mm	KN	KN		Dimensionless	
1	23.5	333	53	189	28.6	890.8	796.1	852.0	1.12	1.05
2	25.9	333	53	189	28.6	1024.2	843.7	842.7	1.20	1.22
3	25.4	333	53	260	25.4	932.9	860.3	932.9	1.08	1.00
4	25.8	333	53	258	19.1	779.9	779.9	740.7	1.00	1.05
5	25.6	248	39	258	22.2	619.0	519.9	676.6	1.19	0.90
6	25.4	248	39	227	19.1	557.2	475.8	477.7	1.17	1.17
7	25.8	248	39	258	15.9	478.7	405.2	418.9	1.18	1.14
8	25.6	279	53	242	31.8	1202.7	1157.6	1199.8	1.04	1.00
9	25.4	279	53	305	25.4	846.6	806.4	822.1	1.05	1.03
10	25.8	279	53	260	19.1	668.1	619.0	646.5	1.08	1.03
11	25.9	210	37	258	25.4	656.3	616.1	675.9	1.07	0.97

Table 4.3 Comparison of De-Wolf's test results to the theories proposed by the Author and Hawkins.

(CONTINUED)

Test No	De-Wolf's Investigation Test Results						Measured Failure		Ratio of Measured/Computed (Failure Load)	
	Concrete Strength	Size of Specimen	Squre Punch Side Length	Steel Base Plate		Failure Load	Author	Hawkins		
	f_{cu}		$S_x = S_y$	f_y	t		F Eq.(4.6) OR Eq.(4.10)	F Eq.(5) OR Eq.(5),(9)	Author	Hawkins
	N/mm^2	mm^3	mm	KN/mm^2	mm	KN	KN		Dimensionless	
12	25.4	210	37	243	19.1	489.5	449.3	424.8	1.09	1.16
13	25.8	210	37	258	15.9	467.9	366.9	366.9	1.28	1.28
14	27.6	235	53	242	31.7	1321.4	1152.7	1219.4	1.15	1.08
15	26.1	235	53	305	25.4	798.5	777.9	756.5	1.03	1.06
16	25.8	235	53	260	19.1	712.2	560.2	1101.0	1.27	1.43
17	30.4	175	39	258	25.4	603.3	621.0	741.6	0.97	0.81
18	26.1	175	39	258	19.1	476.8	423.1	404.0	1.13	1.18
19	25.8	175	39	258	19.1	500.3	418.9	404.9	1.19	1.24
								Mean ------>	(1.12)	(1.09)
							Standard Deviation	------>	($\pm$0.086)	($\pm$0.14)
								% ------>	(7.50)	(13.0)

Table 4.3 Comparison of De-Wolf's test results to the theories proposed by the Author and Hawkins.

formula for a square loading piece is also restricted to ratios of A/A_{se} less than 40.

CHAPTER FIVE

EXPERIMENTAL WORK USING UNIVERSAL COLUMNS

5.1 Introduction.

The tests of previous researchers, and those carried out in this work so far, were on prisms or cubes of concrete where the load was transferred through strip, rectangular, and square loading pieces of different sizes. In practice however, Universal Columns (H and I sections) are often used to transfer the load to the foundation via base plates of different thicknesses. It was therefore decided to carry out a series of tests using Universal Column sections as loading pieces.

Four series of tests were carried out using 150 and 250 mm cubes. In the first series 150 mm cubes were loaded through Universal Columns of various flange width from 10 to 76 mm. In this series of tests 4 mm thick base plate was used. In the next three series 250 mm cubes were tested using plate thicknesses of 4, 8, and 12 mm. Details of both the concrete and the loading sections used in each series are given in Table 5.1.

5.2 Concrete Specification

In manufacturing the concrete, the same materials and mix design as explained in Chapter 2 were used. The strengths of the control specimens in each series of tests are given in Table 5.1. The values given are the average obtained from three control specimens.

5.3 Manufacture of Specimens

5.3.1 Mould

Steel moulds were used to cast the first series of tests involving 150 mm cubes similar to the tests performed in Chapter 2.

For Series 2, 3, and 4 timber moulds 20 mm thick consisting of four wall sections and a base, were used. The interior of the first set of moulds had no special surfacing and as a result their shape was rapidly lost and the timber surface deteriorated. Therefore it was decided to line the walls and the base of these moulds with formica sheets on the inner face. This increased the useful life of the moulds and produced a smoother surface to the concrete.

5.3.2 Casting and Curing

Before casting commmenced the moulds were assembled and checked for squareness and then oiled. The materials were mixed in a 'Linear Cumflow 1A' mixer of 0.25 m^3 capacity and cast on a vibrating table. Each mix included cylinder and cubes required for the control test specimens. The specimens were cast in layers. The first layer in the mould was vibrated until air bubbles on the surface disappeared and the same process was repeated for each layer. The concrete control specimens were also cast and vibrated in layers as the work progressed. The top surfaces of all specimens were trowelled smooth and level with the top of the mould. After one day the specimens were stripped down and stored in the laboratory in the open. The reason for storing these specimens in the open was to be consistent with the tests previously performed in this research. As before, specimens were stored on wooden racks to ensure that the air could circulate freely over all surfaces.

5.4 Test Procedure

The bearing specimens were placed in a central position on the machine at right angles to the direction in which they were cast. Mild steel base plates machined down to the required thickness (4,8,12mm) were placed symmetrically on the upper surface of the cube. The upper and lower edges of the Universal Columns were accurately machined true and parallel to each other in order to facilitate symmetrical loading of the cube when pressure was applied uniformly on the upper edges. To provide a wide range of ratios of (flange width)/(depth of section), varying from 0.1 to 1.0, flanges were machined uniformly and parallel to each other in each test series.

The Universal Columns were positioned centrally on the base plate so that the longitudinal axes of both the plate and the column were colinear with an axis of the cube.

The upper platen of the testing machine was in contact with the entire area of the bearing plate. Load was then applied at an average rate of one ton for every thirty seconds. The specimens were loaded until failure occured i.e. the load dropped off. For each specimen the load at first crack, the progress of cracking, the mode of failure and maximum load were recorded.

5.4.1 Test Series One

In this series 150mm cubes of cube strength 28.0 N/mm^2 with a standard deviation of 2.6% were loaded through I-sections (76 x 76 x 12.65Kg) for ratios of (flange width)/(depth of section) ranging from 0.132 to 1.0. Four millimeter thick steel base plates of yield strength 260 N/mm^2 were used in this series and the thickness of the web of the I-section was 5.5mm. A micrometer was used to measure the thickness of the flange at several points and the average of these readings is shown in Table 5.1. In the same table the ratio of flange width to depth of section, cube strength of the concrete specimen and the ratio of the failure load to f_{cu} are tabulated for every test.

5.4.2 Test Series Two

In this series, which consisted of 8 tests, 250mm cubes were loaded through a 152 x 152 x 23Kg UC via a 4mm thick base plates of yield strength 250 N/mm^2. In four tests with concrete cube strength of 34 N/mm^2 (standard deviation of 4.4%), ratios of flange width to depth of section were 0.07, 0.46, 0.6 and 0.86. The remaining four tests were on concrete with cube strength of 30 N/mm^2 (standard deviation of 5.0%) in which the ratios of flange width to depth of section were 0.2, 0.33, 0.73 and 1.0. The results of this series of tests are presented in Table 5.1.

5.4.3 Test Series Three

The load in this series of tests was applied through a 152 x 152 x 37Kg UC via 8mm thick base plates (yield strength 250 N/mm^2) on 250mm cubes. Seven tests were carried out with concrete of cube strengths 34.4 and 26 N/mm^2 , and standard deviations of 4.5% and 3.4% respectively. Ratios of flange width to depth of section varied from 0.06 to 0.93. In all the tests flange and web thickness were 8.1 and 11.5mm respectively.

Test Series	Test NO	Concrete Strength	Cube Size	Loading Section Dimension			Ratio	Ratio	Ratio	Ratio	Failure Load
							B/D	F/Af_{cu}	A_I/A_{Rec}	BD/t^2	
		f_{cu}		B	t_w	t_f					F
		N/mm^2	mm^3	mm	mm	mm	Dimensionless				KN
(I)	I1	27.90	150	10	5.5	10.0	0.132	0.25	0.88	47.5	157.0
t=4mm	I2	27.90	150	22	5.5	11.0	0.290	0.266	0.76	104.5	167.0
f_y=260	I3	27.90	150	36	5.5	11.0	0.470	0.331	0.70	171.0	207.9
	I4	27.90	150	61	5.5	8.0	0.800	0.406	0.61	289.8	255.0
KN/mm^2	I5	27.90	150	76	5.5	7.5	1.000	0.422	0.59	361.0	264.9
	II1	34.00	250	10	6.5	10.0	0.070	0.182	0.85	94.8	385.5
(II)	II2	30.00	250	30	6.5	7.5	0.200	0.190	0.55	245.0	353.2
	II3	30.00	250	50	6.5	7.0	0.330	0.218	0.42	509.4	404.2
t=4mm	II4	34.00	250	70	6.5	7.0	0.460	0.194	0.39	546.0	412.0
	II5	34.00	250	90	6.5	7.0	0.600	0.249	0.34	849.4	529.7
f_y=250	II6	30.00	250	110	6.5	7.0	0.730	0.245	0.34	1038.1	455.2
	II7	34.00	250	130	6.5	7.5	0.860	0.329	0.33	1112.8	697.7
KN/mm^2	II8	30.00	250	151	6.5	7.0	1.000	0.378	0.33	1292.6	701.4
	III1	34.40	250	10	8.1	11.5	0.060	0.202	0.95	25.3	431.6
(III)	III2	26.00	250	50	8.1	11.5	0.310	0.338	0.67	126.6	549.4
	III3	26.00	250	70	8.1	11.5	0.430	0.374	0.63	177.2	608.2

Table 5.1- Results of concentric loading on different thickness of base columns.

(CONTINUED)

Test Series	Test NO	Concrete Strength	Cube Size	Loading Section Dimension			Ratio B/D	Ratio F/Af_{cu}	Ratio A_I/A_{Rec}	Ratio BD/t^2	Failure Load
		f_{cu}		B	t_w	t_f		n			F
		N/mm^2	mm^3	mm	mm	mm	Dimensionless				KN
t=8mm	III4	34.40	250	90	8.1	11.5	0.560	0.351	0.55	227.8	755.4
f_y=250	III5	34.40	250	110	8.1	11.5	0.680	0.397	0.53	278.4	853.5
	III6	26.00	250	130	8.1	11.5	0.800	0.519	0.56	329.0	843.7
KN/mm^2	III7	26.00	250	150	8.1	11.5	0.930	0.561	0.56	379.7	912.3
(IV)	IV1	26.00	250	50	8.1	11.5	0.310	0.447	0.80	56.3	725.9
	IV2	26.00	250	70	8.1	11.5	0.430	0.459	0.76	78.0	745.6
t=12mm	IV3	26.00	250	90	8.1	11.5	0.555	0.561	0.74	101.3	912.2
f_y=259	IV4	26.00	250	110	8.1	11.5	0.680	0.610	0.72	123.0	990.8
	IV5	26.00	250	130	8.1	11.5	0.800	0.694	0.71	146.3	1128.2
KN/mm^2	IV6	26.00	250	150	8.1	11.5	0.930	0.712	0.70	168.8	1157.6

Table 5.1- Results of concentric loading on different thickness of base columns.

5.4.4 Test Series Four

The same sizes of concrete specimen and Universal Column as those of series three were used in these tests. A total of 6 tests were carried out with base plates of 12mm thickness and yield strength of 259 N/mm^2. The specimens had a cube strength of 26 N/mm^2 with standard deviation of 2.2% and the ratios of flange width to depth of section varied from 0.31 to 0.93.

5.5 Mode of Failure.

A typical pattern of cracks and mode of failure is shown in Photograph 5.1. for two tests with 250mm cubes and ratios of B/D=1 and 0.2. The thickness of the base plate was 4mm. As the specimen was progressively loaded cracks formed on the top of the specimen around the edges of the Universal Column. As loading increased and failure approached, major inclined cracks usually developed in the corners of the block.

After a test was completed and the load dropped off, when the plate was removed a tracing of the shape of the I-section loading piece was left on the face of the plate which had been in contact with the concrete. Photograph 5.2 shows a typical pattern left on the plate for the ratio of B/D = 0.6. The shape of this pattern includes the area of the column web, flanges and the equivalent stiff bearing. Lines were drawn round these tracings on all the plates in order to provide a clearer photographic image.

For three of the tests in series two with 250mm cubes and 4mm thick base plates Photographs 5.3, 5.4 and 5.5 were taken for three

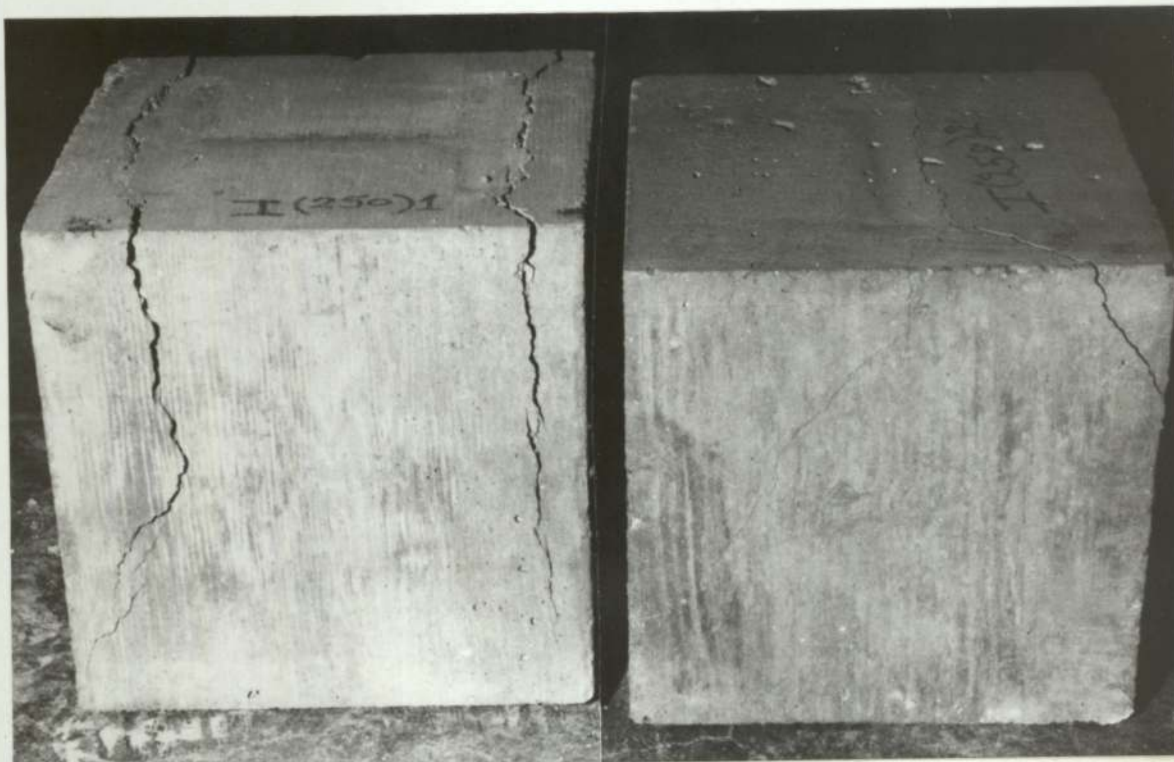

(a) (b)

Plate 5.1 Typical crack formation at failure under a column base.

(a) 4mm thick base column loaded through column of B/D = 1.0

(b) 4mm thick base column loaded through column of B/D = 0.2

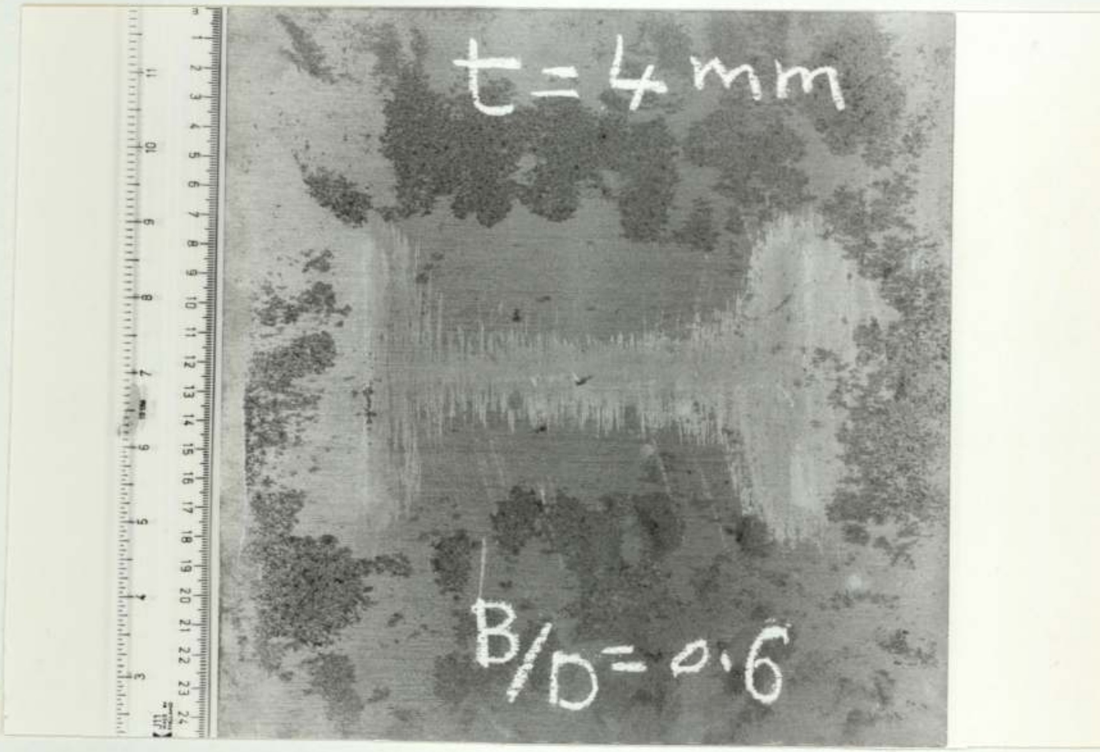

Plate 5.2 A typical tracing of contact area on a plate after testing.

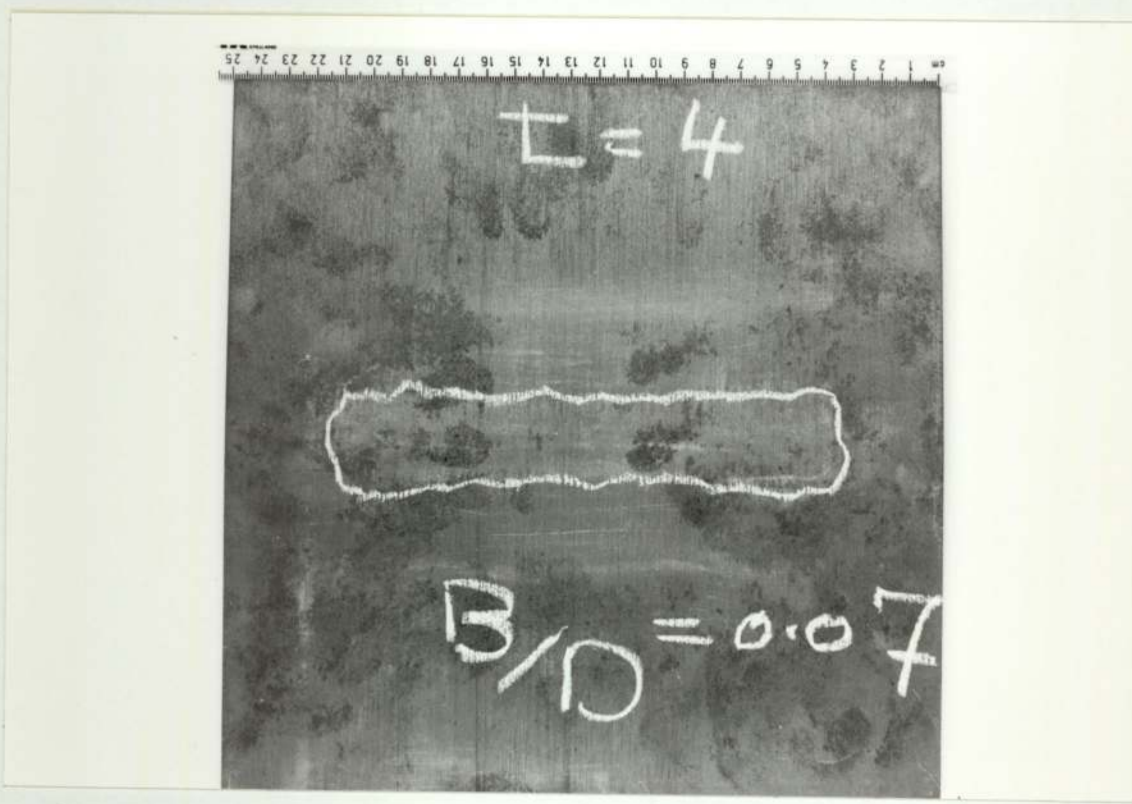

Plate 5.3 Tracing of contact area on a 4mm thick column base for ratio of B/D = 0.07.

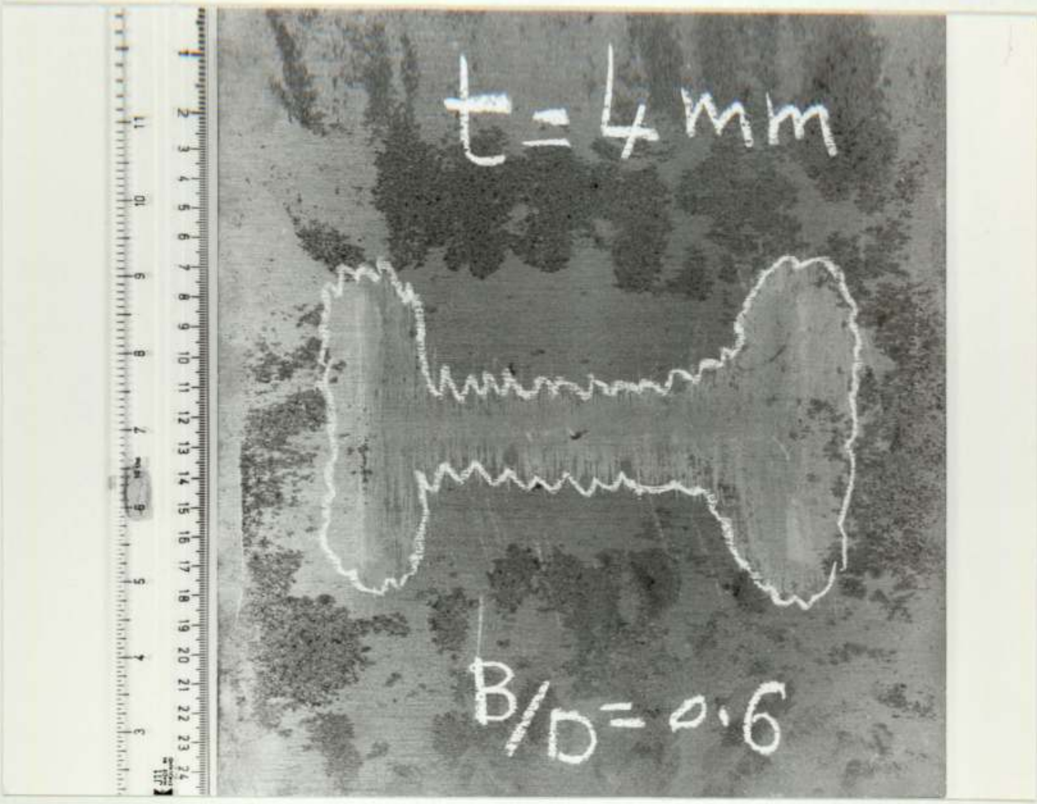

Plate 5.4 Tracing of contact area on a 4mm thick column base for ratio of B/D = 0.6.

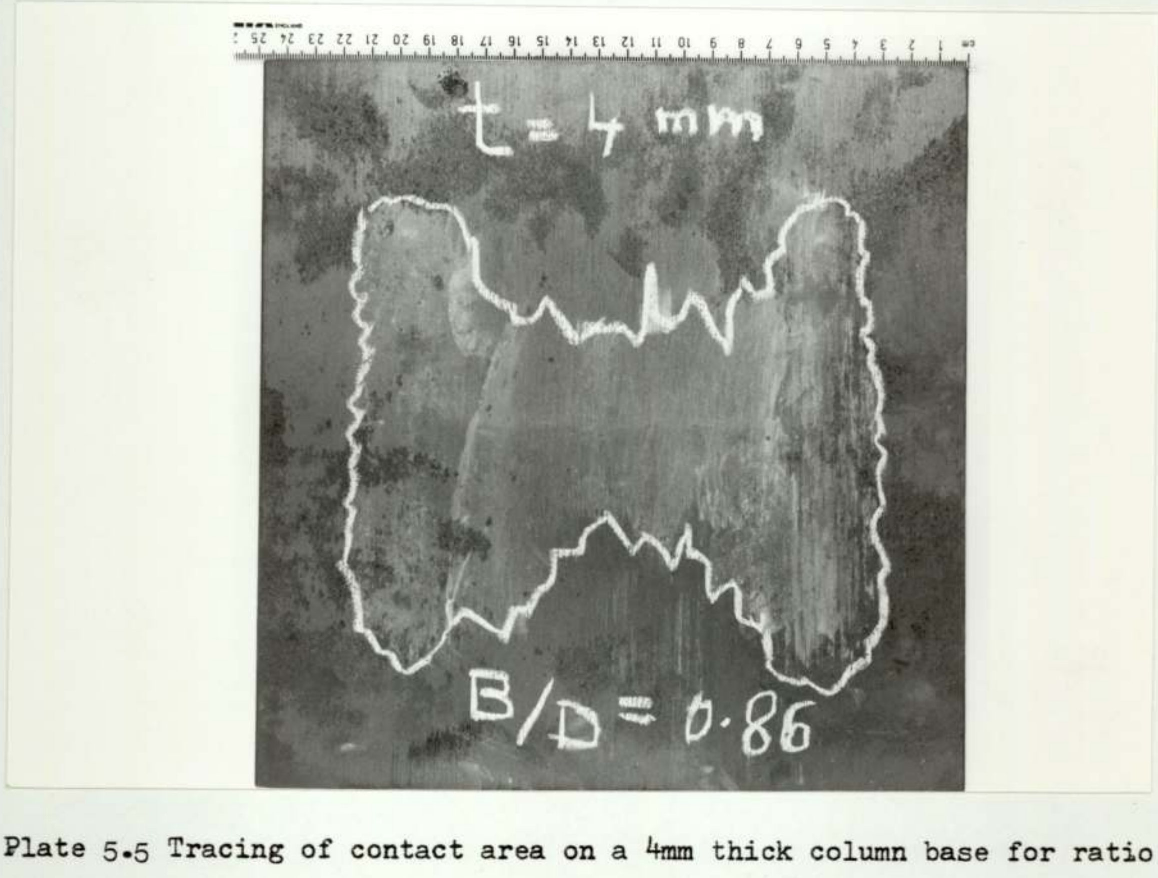

Plate 5.5 Tracing of contact area on a 4mm thick column base for ratio of B/D = 0.86.

ratios of B/D = 0.07, 0.6 and 0.86 respectively. For the ratio of B/D = 0.07 the shape of the pattern on the plate is very close to a rectangle, whilst Photograph 5.4 for ratio of B/D =0.6 shows the outline of an I-shape. However, for the ratio of B/D = 0.86 it seems that the pattern is somewhere between these two, suggesting a transition from an I-shape to a rectangle.

With an 8mm thick base plate in series three, for ratios of B/D = 0.31 and 0.93, Photographs 5.6 and 5.7 were taken respectively. For a small ratio of B/D = 0.31 the pattern of tracing on the plate is very close to a rectangle, as compared with a large ratio of B/D = 0.93 where the outline is again somewhere between the rectangle and the I-shape.

Photograph 5.8 shows a typical pattern of contact area on a 12mm base plate in series four for the ratio of B/D = 0.93. The jagged line drawn around the tracing in Photograph 5.8 is unsymmetrical about the web and could be the result of both the non-homogeneity of concrete material and the effect of slightly unsymmetrical loading. However, the shape of the tracing is a transitional one (somewhere between rectangular and I-shape), though closer to a rectangle than an I-shape. With 4mm thick base plate and 150mm cube in series one, the patterns on the plates with B/D = 0.27 and 0.8 are shown in Photographs 5.9 and 5.10.

From the representative photographs showing the shape of patterns left on the plates it can be concluded that for one thickness of base plate the shape of the effective bearing area in contact with the concrete changes for different ratios of B/D.

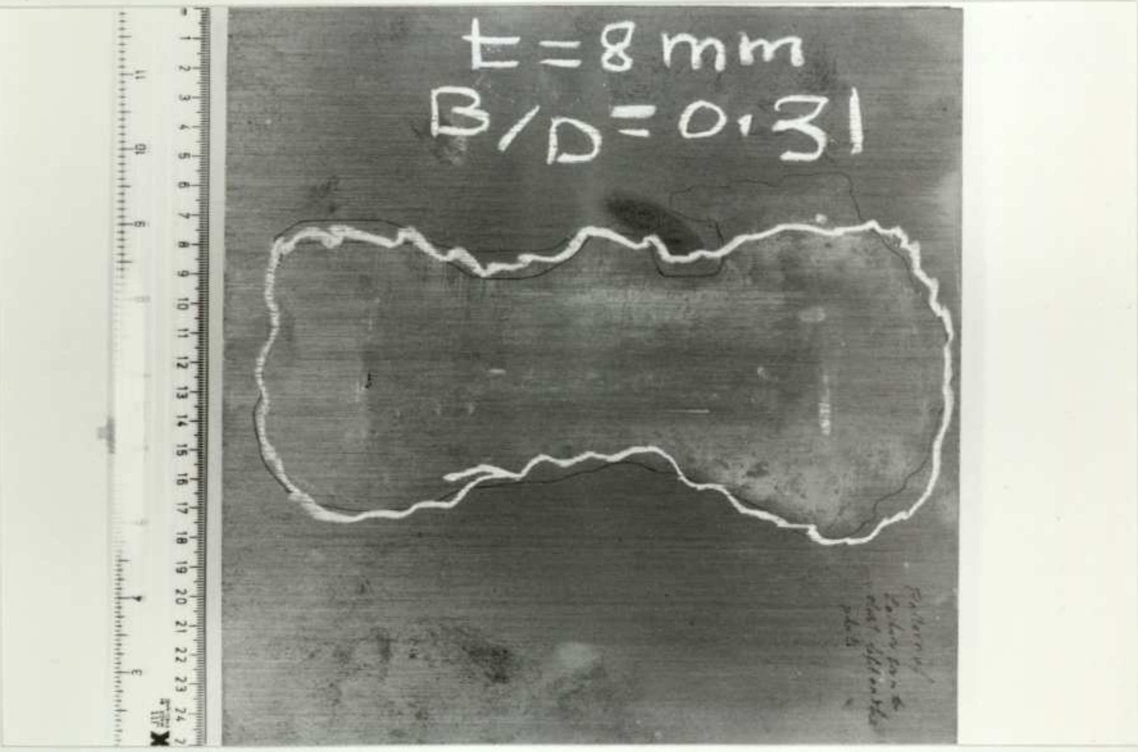

Plate 5.6 Tracing of contact area on an 8mm thick column base for ratio of B/D = 0.31.

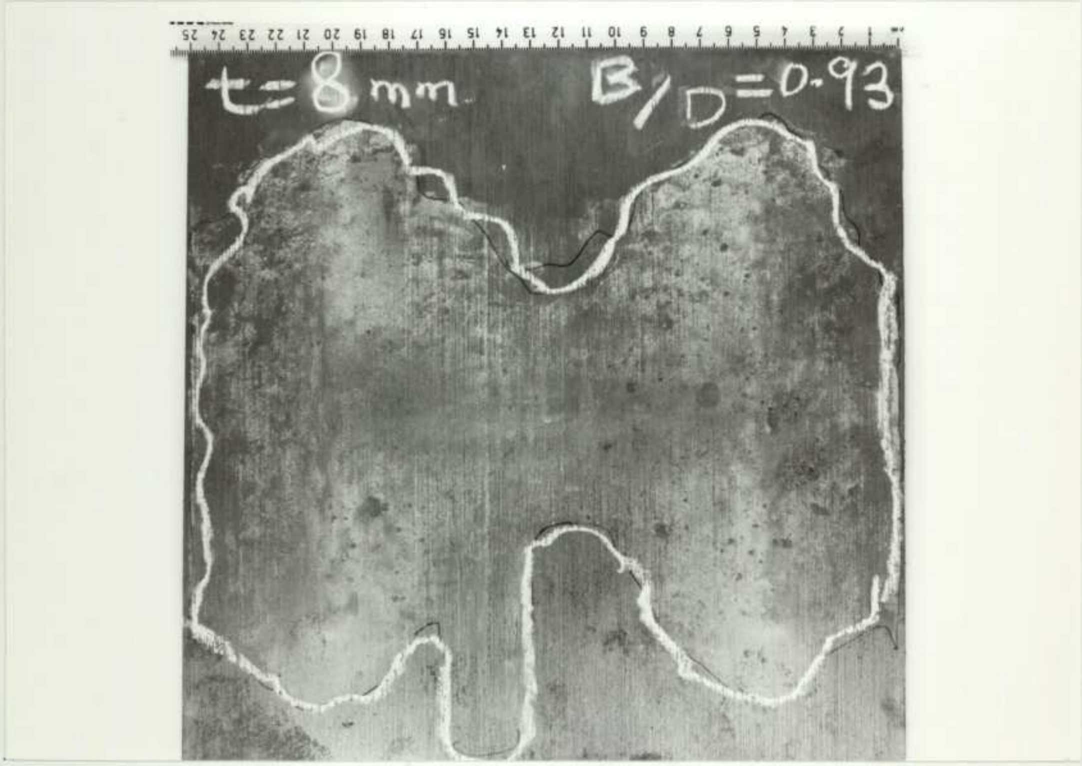

Plate 5.7 Tracing of contact area on an 8mm thick column base for ratio of B/D = 0.93.

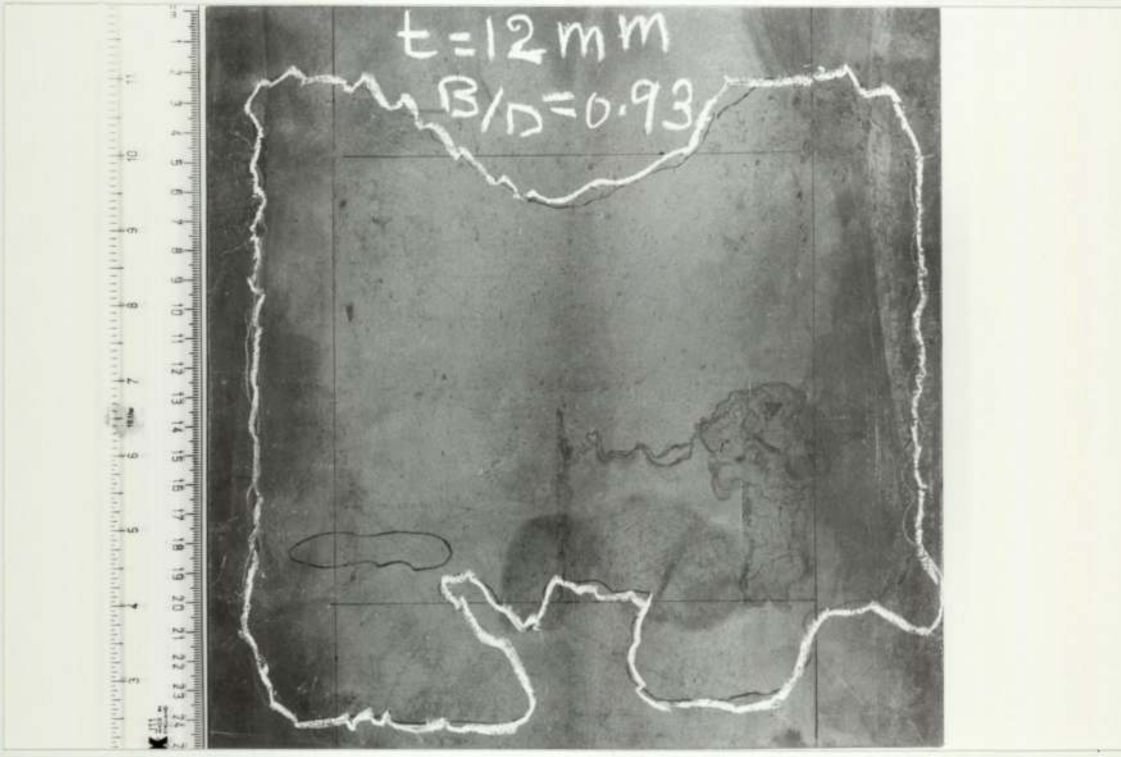

Plate 5.8 Tracing of contact area on a 12mm thick column base for ratio of B/D = 0.93.

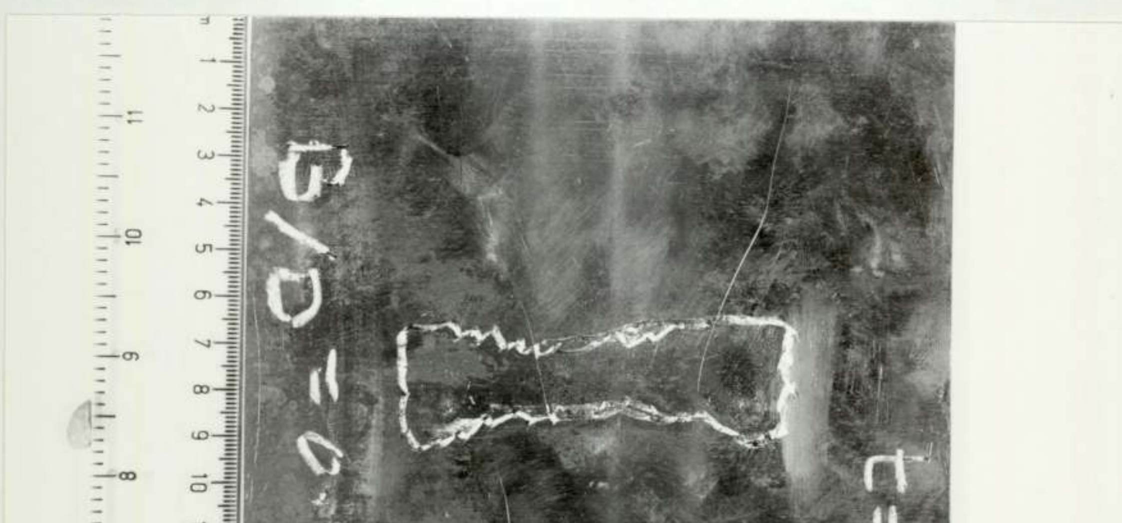

Plate 5.9 Tracing of contact area on a 4mm thick column base for ratio of B/D = 0.27.

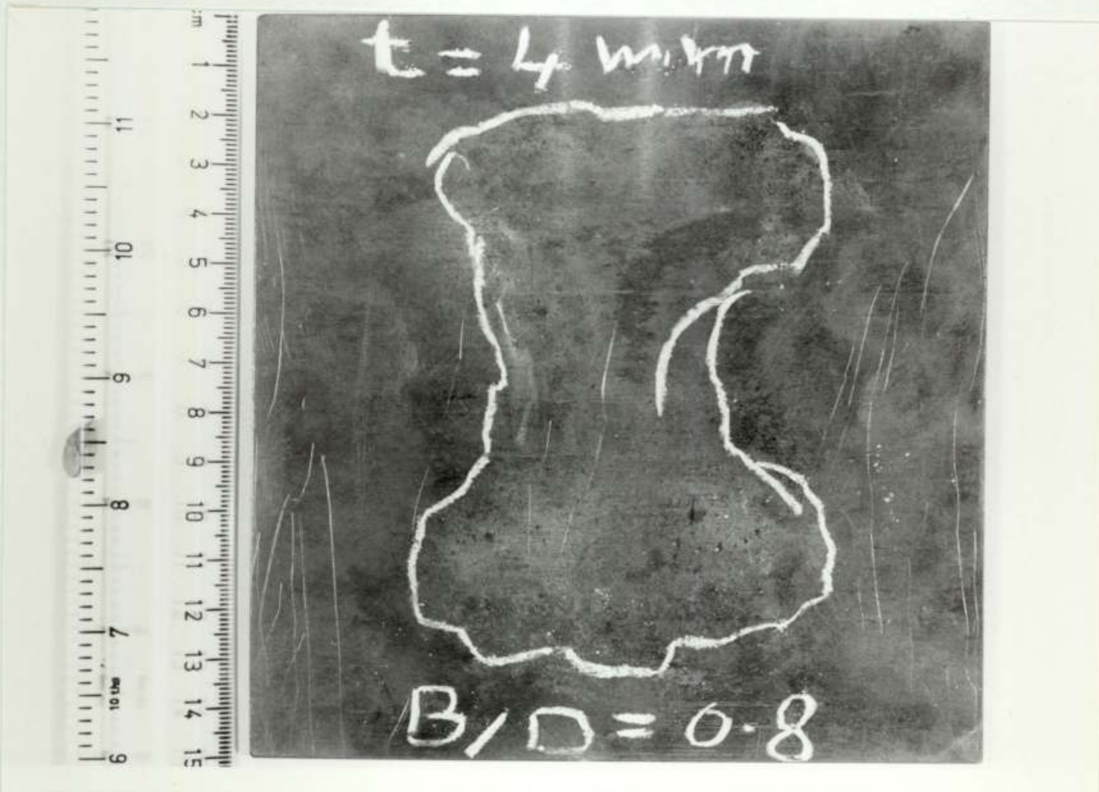

Plate 5.10 Tracing of contact area on a 4mm thick column base for ratio of B/D = 0.8.

5.6 Theory.

The current method of design procedure of column base plates recommended by AISC (29) assumes that the column load is uniformly distributed over the base plate within a rectangle whose dimensions are 0.95 of the column depth and 0.8 of the flange width. The AISC method also assumes that the plate projections beyond the critical sections act as cantilever beams. However, there is no available explanation as to why these values of 0.95 and 0.8 are assumed. As was shown experimentally in Section 5.5, the crack line pattern changed for various ratios of B/D and it would not therefore be reasonable to assume a rectangular distribution of load for every ratio of flange width to depth of section.

In this research, in order to extend the empirical formula developed in chapter 4, two shapes of bearing areas are assumed as shown in Fig 5.1. An I-shape bearing area (A'B'Q P M N D'C' H G F K) and a rectangular one (A'B'D'C'). From Fig 5.1 the areas for the rectangle and I-shape bearing can be evaluated as follows :

For a rectangular shape loading piece the effective area of bearing is,

$$A_{Rec} = A_{se} = (B+L)(D+L) \qquad (5.1)$$

Where A_{Rec} is the area of the rectangular shape bearing.

For an I-Shape loading piece the effective area of bearing is,

$$A_I = A_{se} = 2(t_f+L)(B+L)+(D-2t_f-L)(t_w+L)$$

Where A_I is the area of the I-shape bearing.

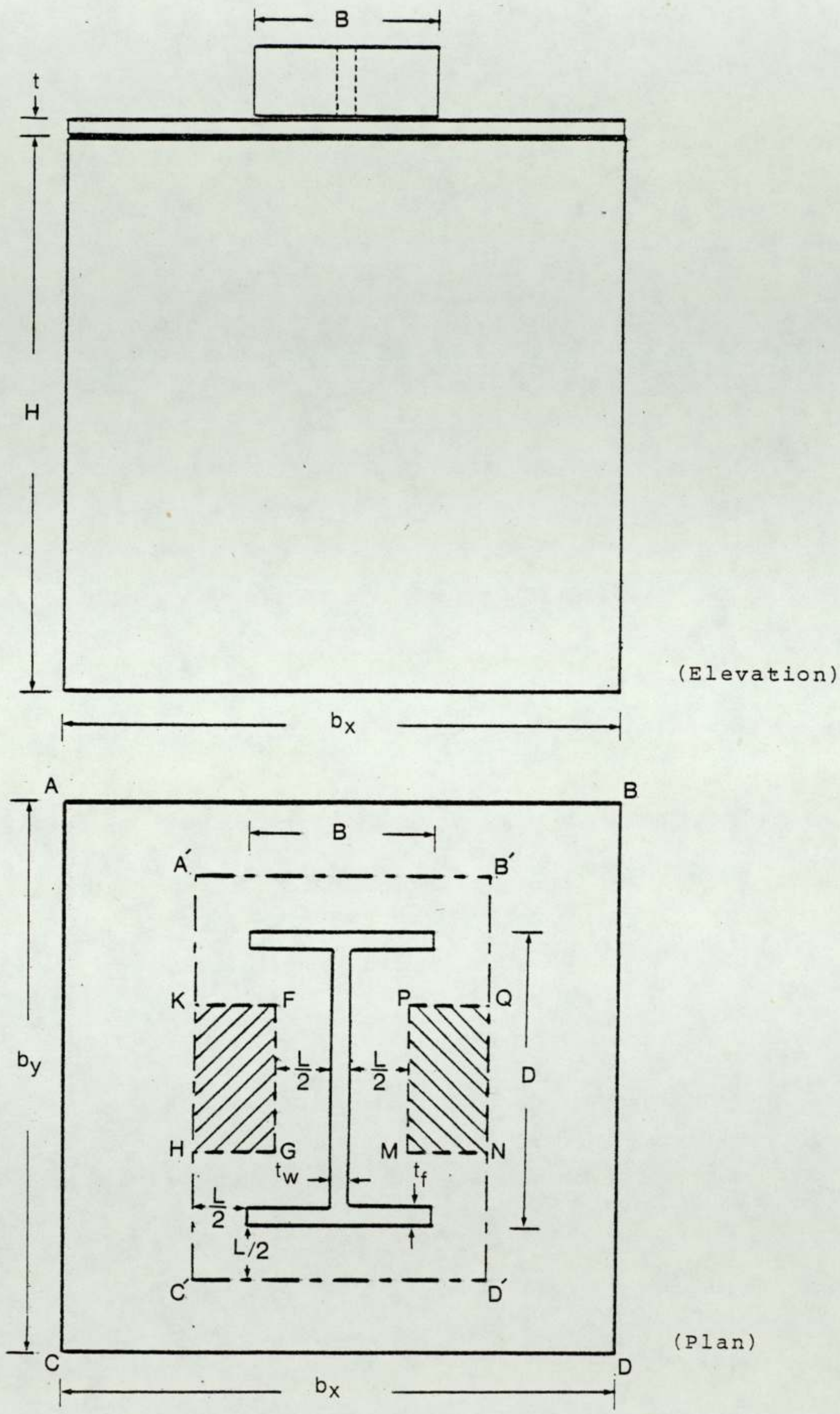

Fig. 5.1 Rectangular and I-shape bearing for an I-section column.

Simplifying the above equation,

$$A_I = A_{se} = L^2+L(2B-t_w+D)+2t_fB+t_wD-2t_ft_w \qquad (5.2)$$

5.6.1 Ratio of R <0.125

Using the formulae developed in Chapter 4, Equation (4.8),

$$1.36 + \frac{0.085\ A}{A_{se}} = \frac{2f_y}{f_{cu}} \times \frac{t^2}{L^2}$$

Rearranging the above equation,

$$\left(\frac{f_{cu}}{2f_y}\right)\left(\frac{L^2}{t^2}\right)\left(0.085\ \frac{A}{A_{se}}+1.36\right)-1= 0.0 \qquad (5.3)$$

5.6.2 Ratio of R >0.125

Equation (4.11) developed in Chapter 4 can be used for ratios of A_s/A >0.125,

$$0.85 + \frac{0.15\ A}{A_{se}} = \frac{2f_y}{f_{cu}} \times \frac{t^2}{L^2}$$

Rearranging the above equation,

$$\left(\frac{f_{cu}}{2f_y}\right)\left(\frac{L^2}{t^2}\right)\left(0.15\ \frac{A}{A_{se}}+0.85\right) - 1 = 0.0 \qquad (5.4)$$

In Equations (5.3) and (5.4) the corresponding expressions for A_{se} as obtained for rectangular and I-shape bearing areas and expressed in Equations (5.1) and (5.2) should be used whenever required.

5.7 Presentation of Test Results.

The results of the four series of tests including control tests are tabulated in Table 5.1.

In Figs 5.2 to 5.7 the values of n (ratio of failure load to (area of specimen x cube crushing strength)) for different ratios of B/D are plotted. The broken and unbroken lines in these figures are from Equations (5.1) and (5.2). The broken line assumes an I-shape and the unbroken line a rectangular bearing stress area. It should, however be pointed out that the value of contact length L in Equation (5.1) and (5.2) was found using Equations (5.3) and (5.4). These equations were used for values of R less than 0.125 and greater than 0.125 respectively.

From Fig 5.2 for test series one with 150mm cube it can be seen that the correlation of test results to empirical theory for a rectangular shape bearing is good, especially for the ratios of B/D between 0.2 and 0.8. The mean, standard deviation and the percentage difference for the results in this range of B/D are 1.04 ± 0.04 (3.8%) respectively.

Figs 5.3 and 5.4 show the test results plotted for series two, with 250mm cubes of cube strengths 34 and 30 N/mm^2 loaded through 4mm thick steel base plates. Both figures indicate that in

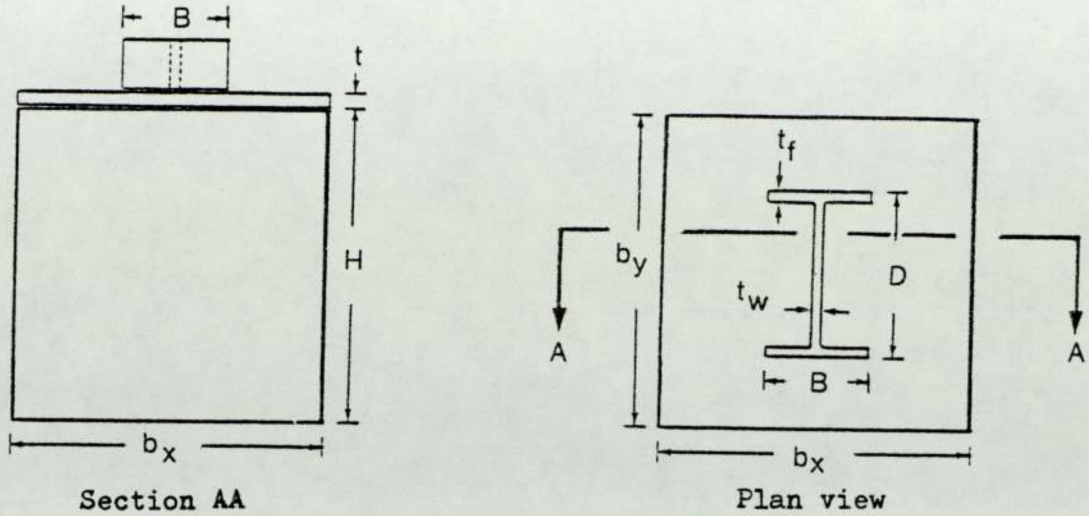

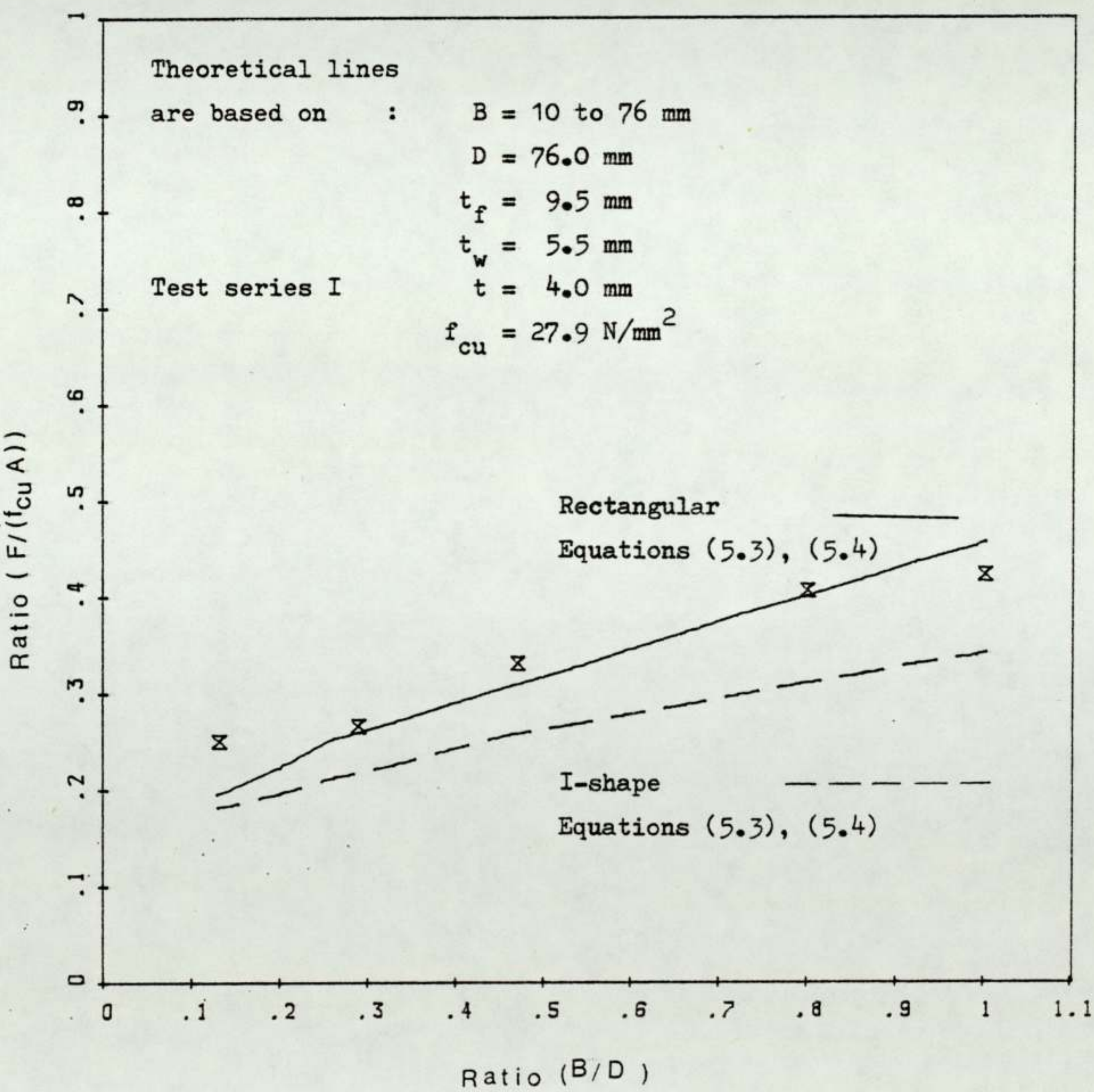

Fig. 5.2 Experimental results of author, for axial loading via a steel I-section on 150 mm cubes.

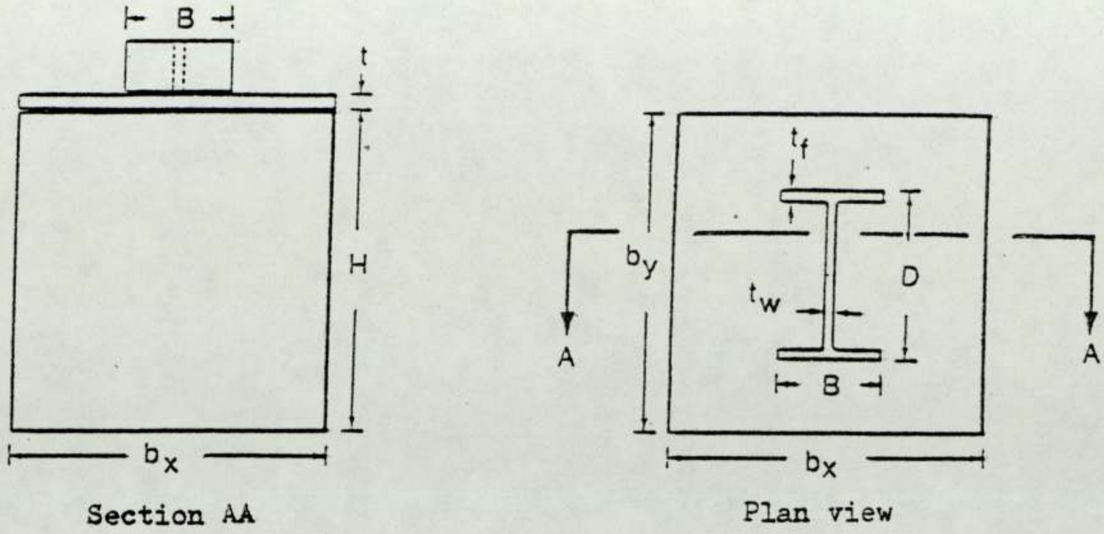

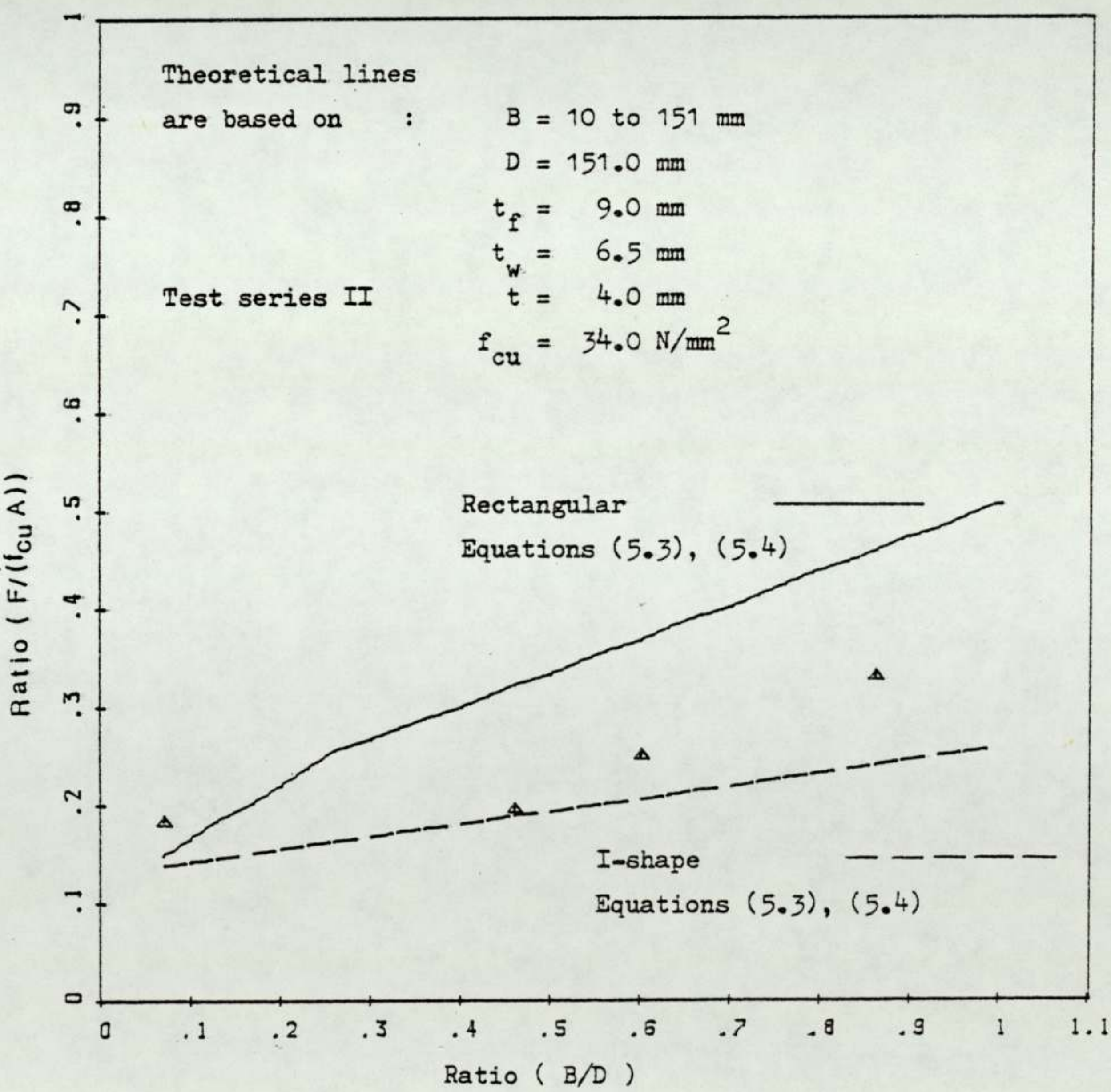

Fig. 5.3 Experimental results of Author, for axial loading via a steel I-section on 250 mm cubes (t = 4.0 mm, f_{cu} = 34 N/mm^2).

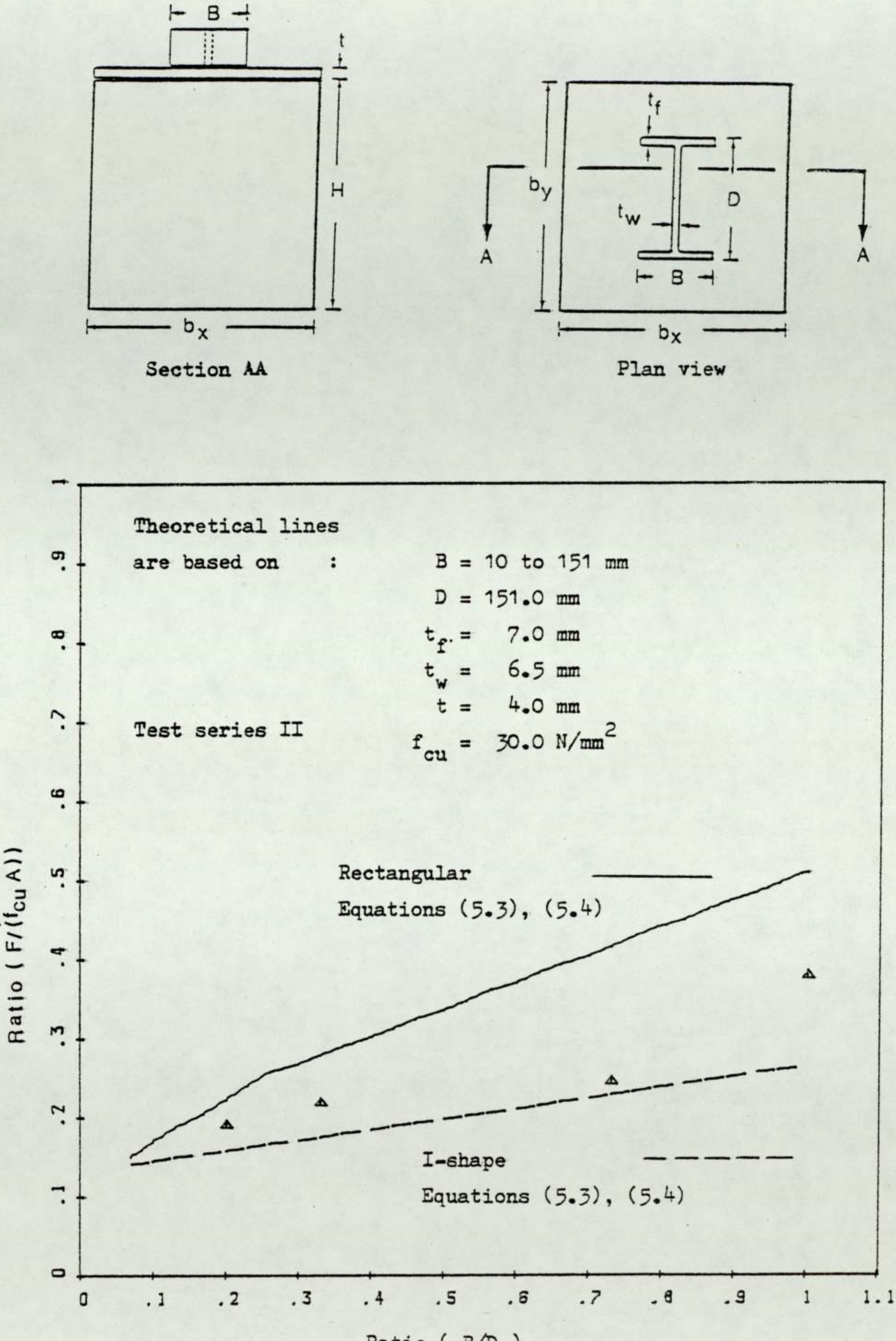

Fig 5.4 Experimental results of Author, for axial loading via a steel I-section on 250 mm cubes (t = 4.0 mm, f_{cu} = 30 N/mm^2).

contrast to series one, some test results are within the two theoretical lines and the others correlate quite well with the I-shape bearing area theory. From Fig 5.3 with concrete strength of 34 N/mm^2, it seems that as the ratio of B/D increases (above 0.6) the shape of the bearing area changes from an I-shape to a rectangular one. However, for this thickness of base plate in this series none of the test results correlate with the theoretical line based on rectangular shape bearing area. Fig 5.4 shows that for small ratios of B/D the test results are between the theoretical lines and as this ratio increases, the test result is very close to the dotted line based on an I-shape loading area. However, for ratios of B/D around unity the test result is between the two lines. The reason for the change in shape of the bearing area from rectangular to I-shape is given in the discussion section of this chapter.

The results for series three with 8mm thick base plate and 250mm concrete cubes of cube strength 34.4 and 26 N/mm^2 are plotted in Figs 5.5 and 5.6. Although not all of the test results are on the theoretical line for rectangular bearing area, nevertheless the results are either within the two lines or very close to the theoretical solid line. Comparing Figs 5.3 and 5.4 for 4mm thick base plate to Figs 5.5 and 5.6 for 8mm thick base plate, it seems that as the thickness of the base plate increases the shape of the bearing area changes from an I-shape to a rectangular one. Fig 5.7 shows the test results from series four, with 250mm cubes of cube strength 26 N/mm^2 and 12mm thick steel base plates. There is a good correlation between test results and theory for a rectangular shape bearing area.

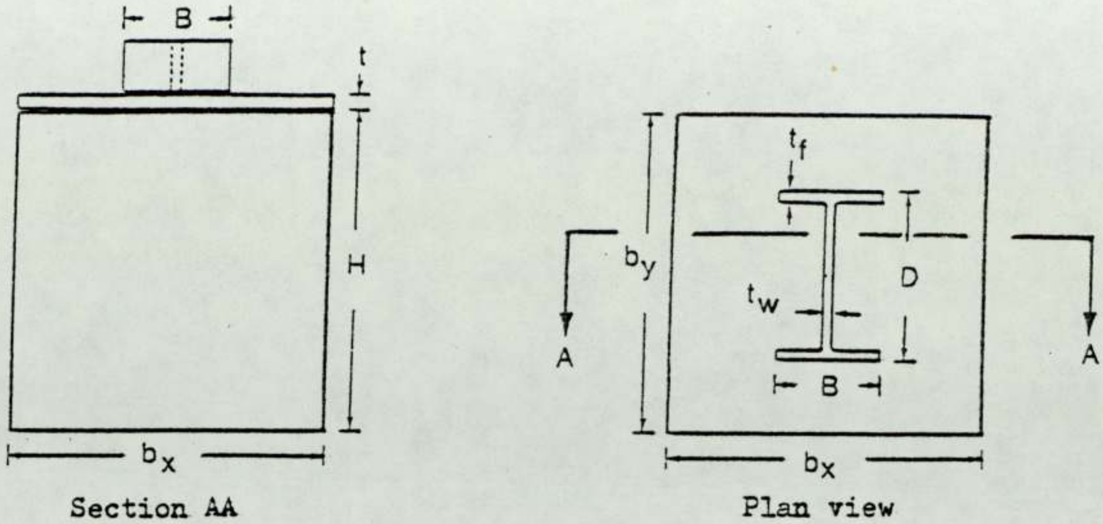

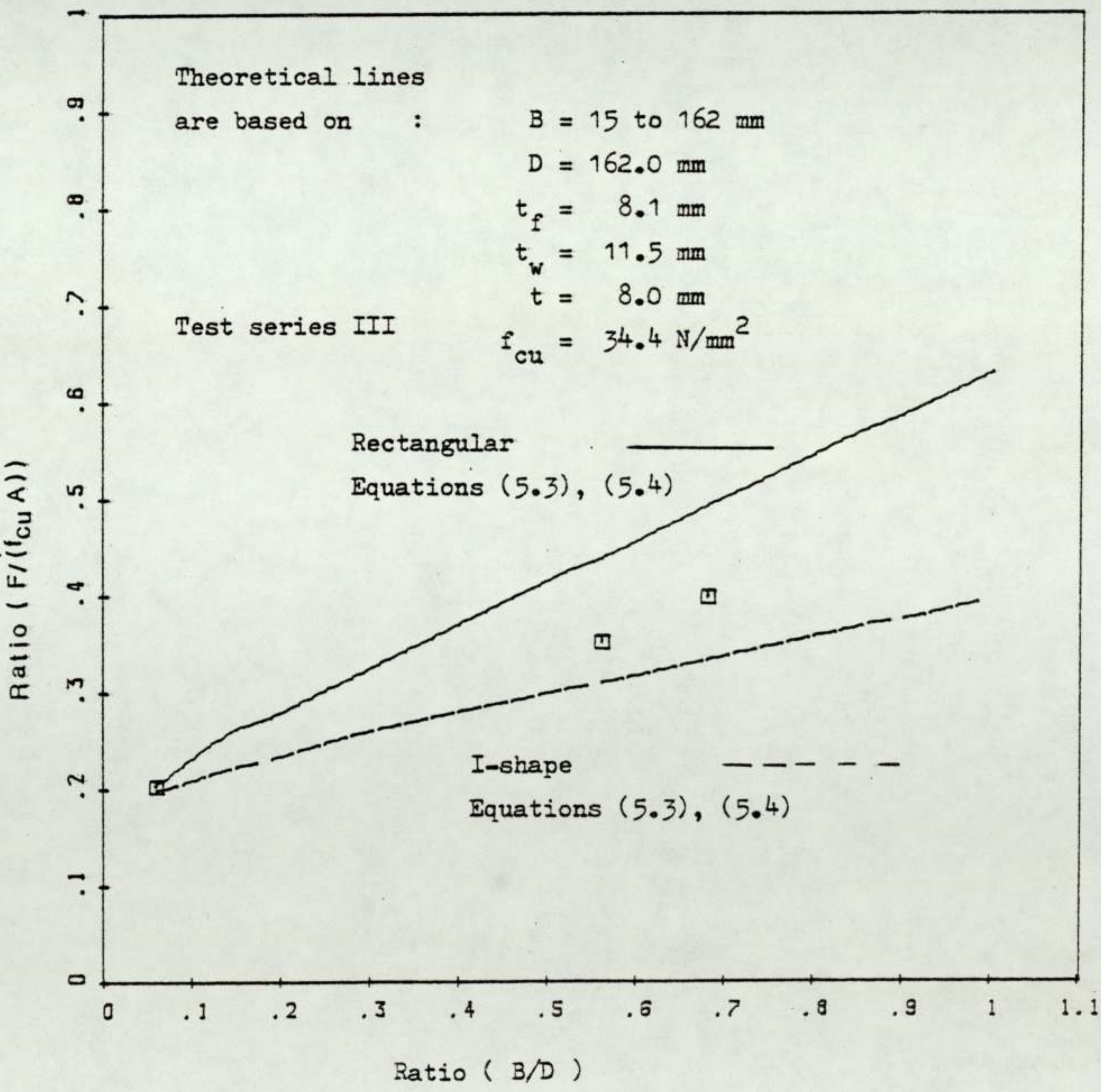

Fig. 5.5 Experimental results of Author, for axial loading via a steel I-section on 250 mm cubes (t = 8.0 mm, f_{cu} = 34.4 N/mm^2).

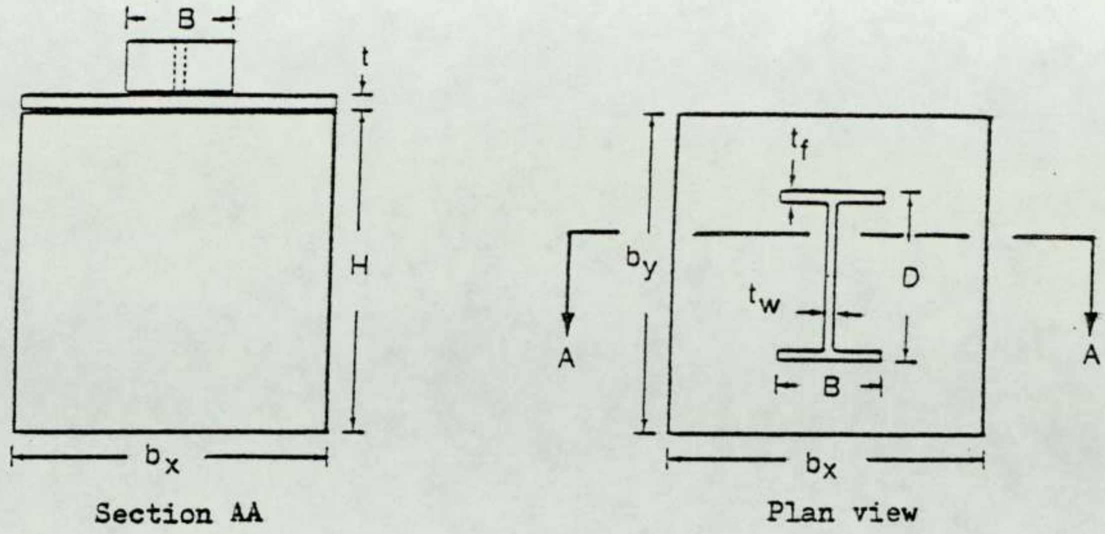

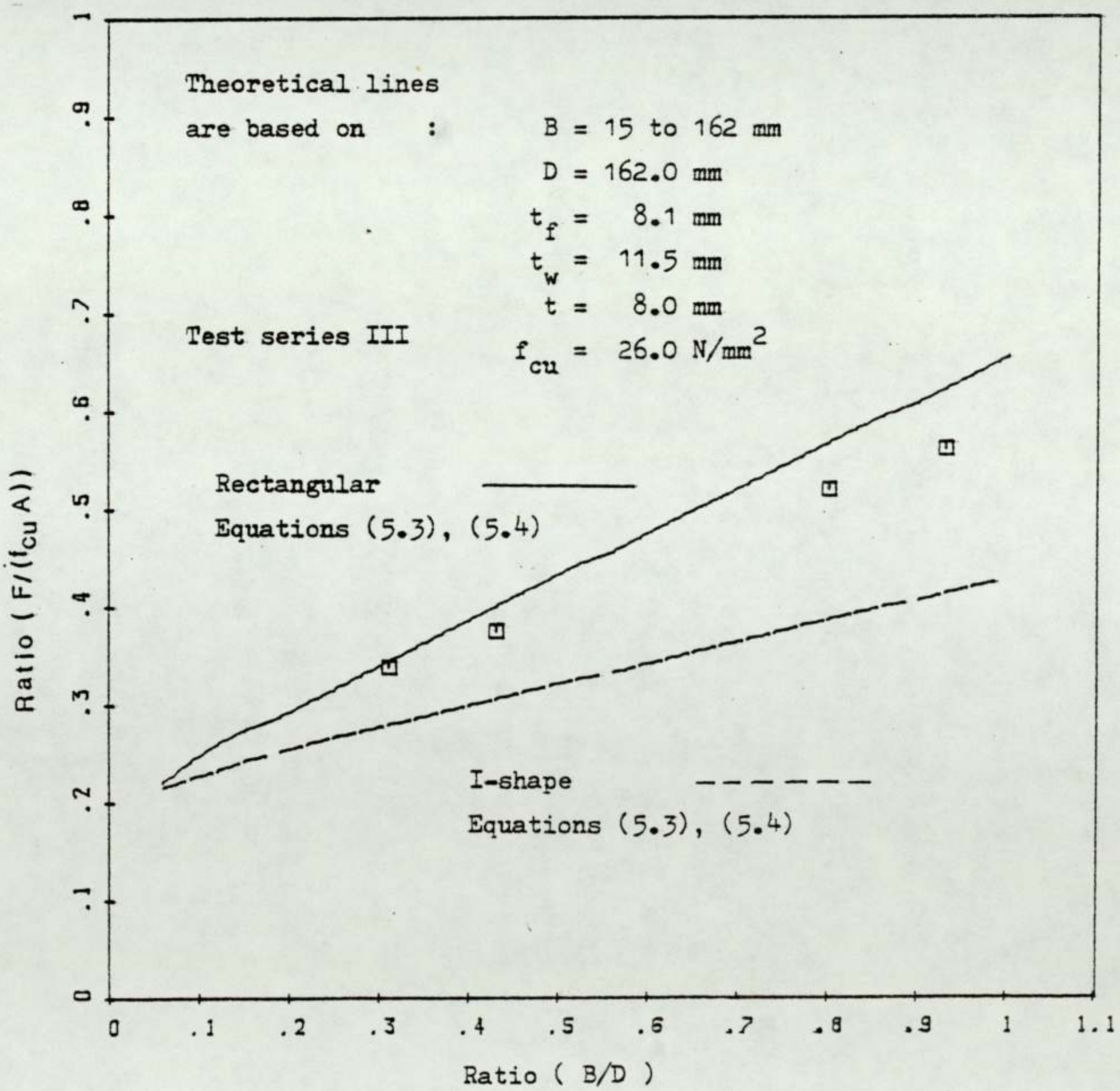

Fig. 5.6 Experimental results of Author, for axial loading via a steel I-section on 250 mm cubes (t = 8.0 mm, f_{cu} = 26 N/mm^2).

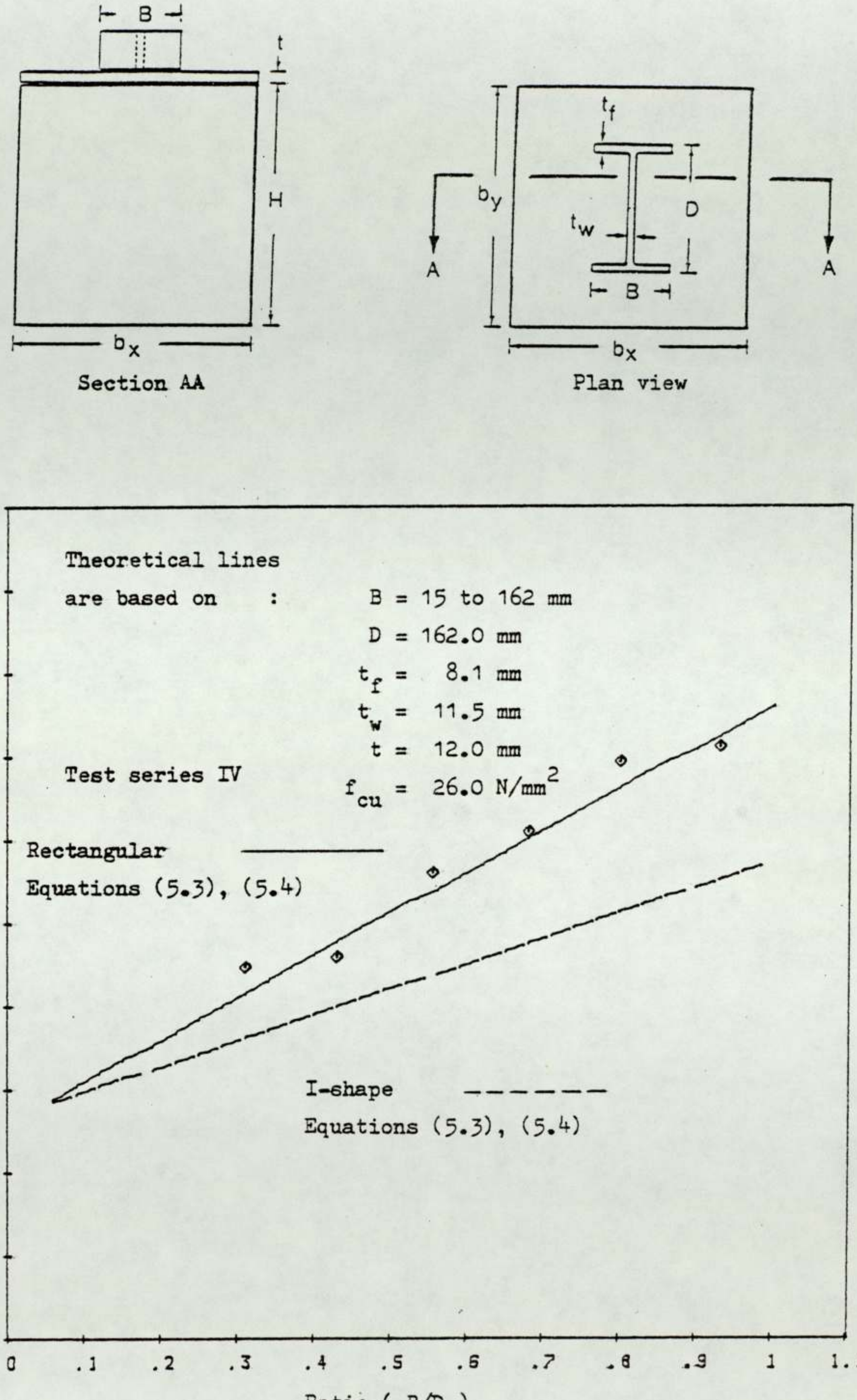

Fig. 5.7 Experimental results of Author, for axial loading via a steel I-section on 250 mm cubes (t = 12.0 mm, f_{cu} = 26 N/mm^2).

In order to be able to study the results obtained from these series they are all plotted in Fig 5.8. In this figure the results are plotted with a dimensionless ratio of A_I/A_{Rec} (calculated areas of I to rectangular shape bearing), as the ordinate, and the ratio of B/D (flange width to depth of section) as the abscissa. The numbers in the circle indicate to which series the results belong. The letters I, R and T shown next to each test result indicate whether that particular test result could be best predicted by the empirical theory for I, for rectangular bearing area or if it was on the transitional lines somewhere between the two.

From Fig 5.8. it can be seen that for values of B/D greater than 0.85 and also for values of $0.4 < A_I/A_{Rec} < 0.6$, almost none of the test results could be predicted by either theory. The shaded sections are referred to in this research as 'transitional areas'. For values of $A_I/A_{Rec} > 0.6$ the test results were predicted with a reasonable degree of accuracy using a rectangular shape bearing area. For values of $A_I/A_{Rec} < 0.4$ the I-shape bearing area theory is more accurate.

5.8 Discussion

It is of considerable interest to note that in most cases for the same thickness of base plate and concrete strength the shape of the bearing area changes from rectangular to I-shape as the ratios of B/D increase. However, for some values of B/D the bearing area assumes a transitional shape between the two. This can be clearly seen from the results plotted for series two in Fig 5.8, where for values of B/D less than 0.16 the test result is on the theoretical line assuming a

Series No	Cube Size	Plate Thickness	Ratio of B/D
1	150	4	0.13-1.0
2	250	4	0.07-1.0
3	250	8	0.06-0.93
4	250	12	0.31-0.93

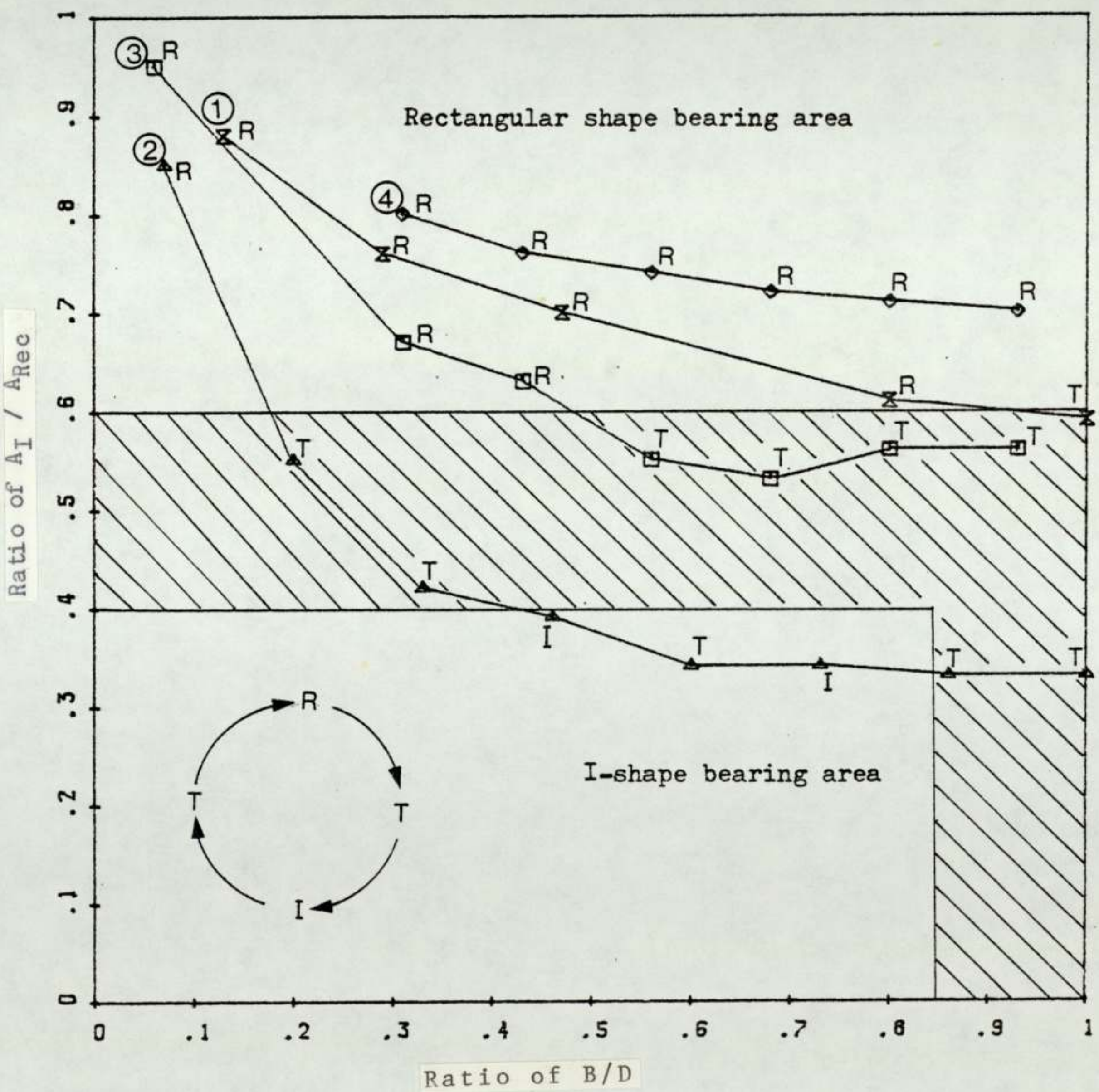

Fig. 5.8 Test results plotted from 4 series with 150 and 250 mm concrete cubes, using I-sections of various ratios of B/D.

rectangular bearing area. As the ratio of B/D increases to B/D = 0.4 the test results lie between the two theoretical lines. For ratios of B/D = 0.4 to 0.85 the results obtained from the tests were very closely predicted assuming an I-shape bearing area. However, for ratios of B/D greater than 0.85 the test results again lie between the two theoretical lines. Therefore it can be concluded that the shape of the bearing area goes through cyclic changes, namely rectangular, transitional, I-shape, and then rectangular, as shown in Fig 5.8.

The only test result not compatible with the described cyclic pattern in series two is the point with B/D = 0.6. This test result is on the transitional area, as shown in Fig 5.3. Nevertheless, as the ratio of B/D increases (above 0.6), the test results lie on the I-shape theoretical line, i.e. B/D = 0.73; for ratios of B/D > 0.73 there are two test results which are on the transitional lines. This is in agreement with the comments made concerning the cyclic change in the shape of the bearing area.

With the 8 and 12mm thick base plates of series three and four, it seems that in order to have a complete cycle of change, test results are required for ratios of B/D greater than unity. In series three, with an 8mm thick base plate and ratios of B/D < 0.47 the rectangular shape theory closely predicts the failure load, and for ratios of 0.47 < B/D < 1.0 the results lie on the transitional lines. With a thicker base plate (12mm) in series four however, test results can be quite accurately predicted using the empirical theory based on the rectangular bearing area.

The physical interpretation of this change in the shape of bearing area can be explained with reference to Fig 5.1. The main factor in determining whether the bearing area assumes an I-shape pattern (A'B'QPMND'C'HGFK), rectangular-shape (A'B'D'C'), or transitional one, depends on the contact length between the base plate and the cube. For small values of contact length the difference between the rectangular area A_{Rec} and I-shape area A_I (shaded areas shown in Fig 5.1, NGFk and MNQP) is considerable and there will be no overlap between the two shapes. In this situation the bearing area assumes an I-shape pattern. However, as the contact length increases the difference between the A_{Rec} and A_I decreases and for certain values of contact length this difference in the areas of bearing will be small enough, so that there will be an overlap. Consequently for this value of contact length, the shape of bearing area will be a rectangular one. Clearly a transitional shape is formed when the contact length is not large enough to cause an overlap nor the contact length is quite small in order for bearing area to have an I shape. In this case the assumed bearing area is some where between the rectangular and the I shape, which is called transitional shape.

In series one (with 4mm thick base plate and a 150mm cube), although for ratios of $0.13 < B/D < 0.9$ the contact length is small in comparison to series four, nevertheless the difference between the I- and rectangular shape area is minimal. Therefore there is an overlap between the two shapes. However, for ratios of B/D above 0.9 the difference between the two assumed shapes gets larger and therefore there is a transitional area instead of the overlap.

Finally it can be concluded that as ratios of B/D increases the bearing area assumes any one of the three shapes of rectangular, I or transitional pattern. In series four with a thick base plate and for the range $B/D < 1$ the pattern assumed a rectangular shape. In tests using a thinner base plate, as in series two, the full cyclic pattern was observed - namely, rectangular, transitional, I, and then transitional shape.

5.9 <u>An Alternative Method of Presenting the Test Results.</u>

The four series of test results are plotted in Figs 5.9 and 5.10. In both figures values of n (ratio of failure load to (area of specimen x concrete cube strength) are plotted for different ratios of R (the area of the steel base plate in contact with the concrete / area of concrete).

In Fig 5.9 values of R for each test result are obtained by assuming that the loading piece is of the dimensions B by D (width and depth of section). For this Equation (5.1) is used. In Fig 5.10, however, values of R are obtained by using Equation (5.2) for an I-shape loading piece. Tables 5.2 and 5.3 show the results plotted in Figs. 5.9 and 5.10 respectively.

In both Figs 5.9 and 5.10 two straight lines are drawn for values of R less than and greater than 0.125. These lines are drawn from Equations (2.1) and (2.2) obtained in Chapter Two for loading through rigid plates of various sizes.

In Fig 5.9 the test results are either on or below the lines for stiff bearing plates. This implies that, assuming a rectangular loading piece instead of the actual I-shape loading section, the calculated results would either be very close to or above the actual experimental values. On the other hand, the results drawn in Fig 5.10

Series No	Symbol	Cube Size	Plate Thickness
I	⧖	150	4
II	△	250	4
III	□	250	8
IV	◇	250	12

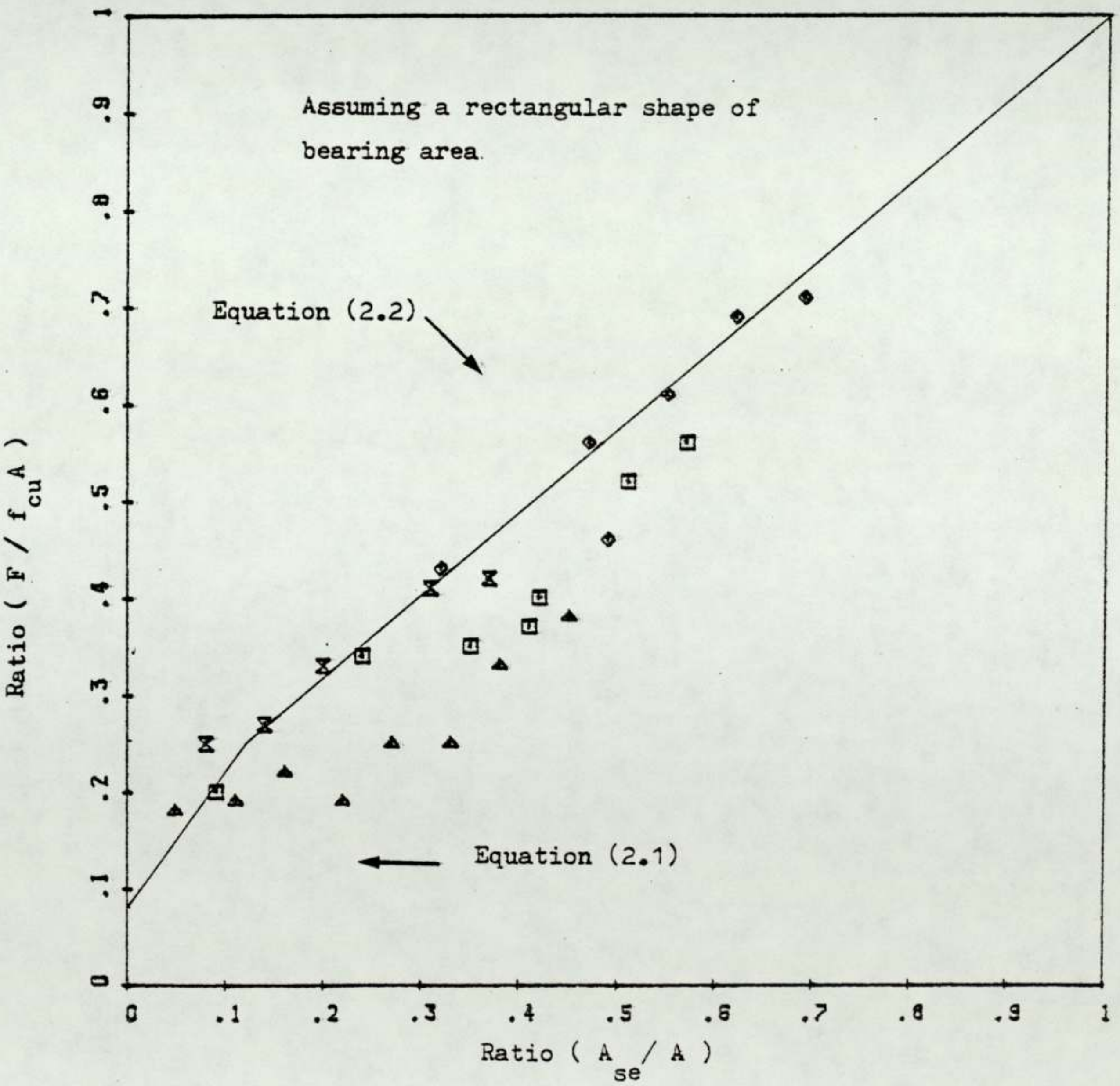

Fig. 5.9 Relationship between $F/(f_{cu}A)$ and A_{se}/A for experiments by Author, assuming a rectangular shape of bearing area.

Series No	Symbol	Cube Size	Plate Thickness
I	⧖	150	4
II	△	250	4
III	□	250	8
IV	◇	250	12

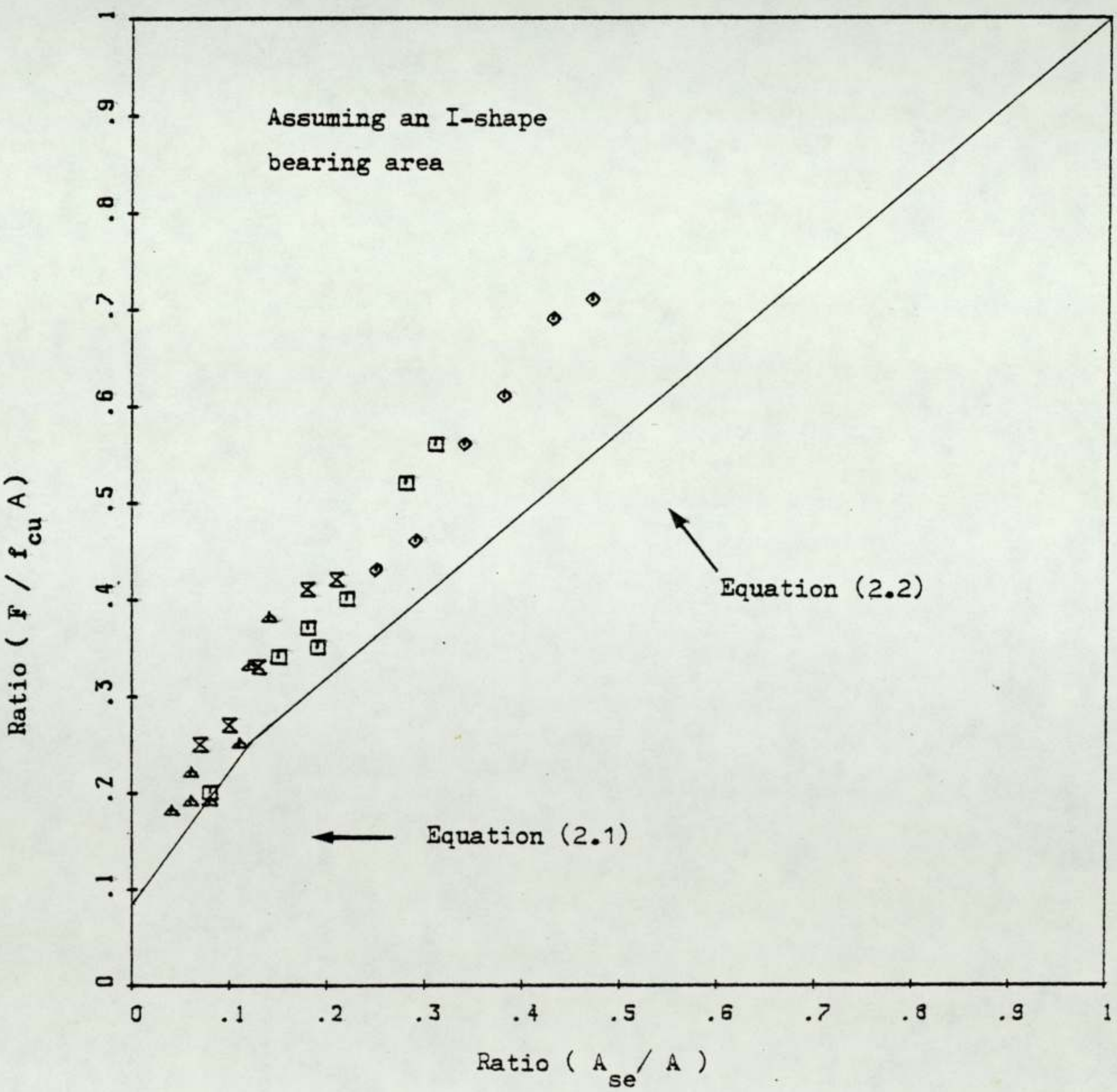

Fig. 5.10 Relationship between $F/(f_{cu}A)$ and A_{se}/A for experiments by Author, assuming an I-shape of bearing area.

Test Series	Test No	Experimental Failure Load	Loading Section		Ratio of	Empirical Theory for I-Shape Section Eq.(5.2) Contact Length	Failure Load	Ratio of	Ratio of	Ratio of Experimental/Computed (Failure Load)
		F	B	D	BD/t^2	L	F	A_I/A	F/Af_{cu}	
		KN	mm	mm	mm/mm	mm	KN			Dimensionless
(I)	I1	157.0	10	76	47.5	10.9	114.6	0.07	0.183	1.370
on 150mm	I2	167.0	22	76	104.5	11.7	138.9	0.10	0.221	1.203
cubes	I3	207.9	36	76	171.0	12.3	165.1	0.13	0.263	1.260
t=4mm	I4	255.0	61	76	289.8	13.4	190.6	0.18	0.304	1.340
	I5	264.9	76	76	361.0	13.9	207.1	0.21	0.330	1.280
(II)	II1	385.5	10	151	94.8	8.3	295.1	0.04	0.139	1.310
on 250mm	II2	353.2	30	151	245.0	10.6	303.5	0.06	0.163	1.160
cubes	II3	404.2	50	151	509.4	9.7	321.5	0.06	0.173	1.260
t=4mm	II4	412.0	70	151	546.0	10.9	415.8	0.08	0.196	0.990
	II5	529.7	90	151	849.4	11.0	519.4	0.10	0.200	1.020
	II6	455.2	110	151	1038.1	11.2	486.4	0.11	0.230	1.070
	II7	697.7	130	151	1112.8	11.2	527.2	0.12	0.248	1.320
	II8	701.4	151	151	1292.6	12.5	499.1	0.14	0.269	1.410
(III)	III1	431.6	10	162	25.3	20.3	425.6	0.08	0.198	1.014
on 250mm	III2	549.4	50	162	126.6	26.0	454.9	0.15	0.280	1.208
cubes	III3	608.2	70	162	177.2	27.2	497.2	0.18	0.306	1.223
t=8mm	III4	755.4	90	162	227.8	23.8	664.9	0.19	0.309	1.136

Table 5.2 Correlation of the Author's test results to his theory assuming an I-shape loading piece.

(CONTINUED)

Test Series	Test No	Experimental Failure Load	Loading Section		Ratio of	Empirical Theory for I-Shape Section Eq.(5.2)				Ratio of Experimental/Computed (Failure Load)
						Contact Length	Failure Load	Ratio of	Ratio of	
		F	B	D	BD/t^2	L	F	A_I/A	F/Af_{cu}	
		KN	mm	mm	mm/mm	mm	KN			Dimensionless
	III5	853.5	110	162	278.4	24.6	716.0	0.22	0.333	1.192
	III6	843.7	130	162	329.0	29.8	626.9	0.28	0.386	1.346
	III7	912.3	150	162	379.7	30.4	670.3	0.31	0.412	1.360
(IV)	IV1	725.9	50	162	56.3	44.5	587.5	0.25	0.362	1.236
on 250mm	IV2	745.6	70	162	78.0	46.0	649.8	0.29	0.400	1.147
cubes	IV3	912.2	90	162	101.3	47.1	711.0	0.34	0.438	1.283
t=12mm	IV4	990.8	110	162	123.0	48.1	773.1	0.38	0.476	1.282
	IV5	1128.2	130	162	146.3	48.9	834.9	0.43	0.514	1.351
	IV6	1157.6	150	162	168.8	49.6	896.8	0.47	0.552	1.290

Table 5.2 Correlation of the Author's test results to his theory assuming an I-shape loading piece.

Test Series	Test No	Experimental Failure Load	Loading Section		Ratio of	Empirical Theory for Rectangular Section Eq.(5.1) Contact Length	Failure Load	Ratio of	Ratio of	Ratio of Experimental/Computed (Failure Load)
		F	B	D	BD/t^2	L	F	A_{Rec}/A	F/Af_{cu}	
		KN	mm	mm	mm/mm	mm	KN			Dimensionless
(I)	I1	157.0	10	76	47.5	11.2	123.6	0.08	0.197	1.270
on 150mm	I2	167.0	22	76	104.5	12.4	166.3	0.14	0.265	1.000
cubes	I3	207.9	36	76	171.0	13.7	199.9	0.20	0.318	1.040
t=4mm	I4	255.0	61	76	289.8	15.0	258.2	0.31	0.411	0.988
	I5	264.9	76	76	361.0	15.5	292.7	0.37	0.470	0.905
(II)	II1	385.5	10	151	94.8					
on 250mm	II2	353.2	30	151	245.0	12.1	435.2	0.11	0.234	0.811
cubes	II3	404.2	50	151	509.4	11.9	533.0	0.16	0.287	0.758
t=4mm	II4	412.0	70	151	546.0	13.7	716.7	0.22	0.337	0.575
	II5	529.7	90	151	849.4	13.0	806.5	0.27	0.438	0.657
	II6	455.2	110	151	1038.1	14.4	797.9	0.33	0.430	0.570
	II7	697.7	130	151	1112.8	14.5	1009.3	0.38	0.470	0.691
	II8	701.4	151	151	1292.6	15.9	981.7	0.45	0.529	0.715
(III)	III1	431.6	10	162	25.3	20.0	438.5	0.09	0.204	0.984
on 250mm	III2	549.4	50	162	126.6	29.0	577.2	0.24	0.355	0.952
cubes	III3	608.2	70	162	177.2	30.4	670.7	0.31	0.413	0.907
t=8mm	III4	755.4	90	162	227.8	27.1	969.9	0.35	0.451	0.779

Table 5.3 Correlation of the Author's test results to his theory assuming a rectangular shape loading piece.
(CONTINUED)

Test Series	Test No	Experimental Failure Load	Loading Section		Ratio of	Empirical Theory for Rectangular Section Eq.(5.1)				Ratio of Experimental/Computed (Failure Load)
						Contact Length	Failure Load	Ratio of	Ratio of	
		F	B	D	BD/t^2	L	F	A_{Rec}/A	F/Af_{cu}	
		KN	mm	mm	mm/mm	mm	KN			Dimensionless
	III5	853.5	110	162	278.4	27.8	1087.3	0.42	0.506	0.785
	III6	843.7	130	162	329.0	32.8	944.6	0.51	0.581	0.893
	III7	912.3	150	162	379.7	33.3	1034.9	0.57	0.637	0.882
(IV)	IV1	725.9	50	162	56.3	46.8	690.4	0.32	0.425	1.051
on 250mm	IV2	745.6	70	162	78.0	48.4	794.3	0.40	0.489	0.939
cubes	IV3	912.2	90	162	101.3	49.6	896.6	0.47	0.552	1.018
t=12mm	IV4	990.8	110	162	123.0	50.6	998.3	0.55	0.614	0.992
	IV5	1128.2	130	162	146.3	51.3	1098.4	0.62	0.676	1.027
	IV6	1157.6	150	162	168.8	51.9	1198.8	0.69	0.737	0.966

Table 5.3 Correlation of the Author's test results to his theory assuming a rectangular shape loading piece.

are all above the lines for stiff bearing apart from a few with 4mm thick base plates and 250mm cubes. Therefore, the assumption of an I-shape stiff bearing would generally underestimate the experimental results.

This finding is in agreement with the results plotted in Fig 5.8. This figure shows that only three of the tests carried out in this research are within the area where an I-shape bearing area may be assumed. Of course, the trend of the results plotted in Fig 5.8 indicates that for the assumption of an I-shape bearing area to be true, a steel base plate thinner than 4mm should be used with a 250mm cube.

Figure 5.11 is plotted with n1 (experimental / calculated failure load) as the ordinate and the ratio of BD/t^2 as the abscissa. In Fig 5.11 failure load was calculated based on a rectangular loading piece of dimensions B by D as in Fig 5.9. As can be seen from this figure, for ratios of BD/t^2 equal to approximately 200 and less, the assumption of a rectangular loading piece instead of the actual I-section is reasonable. However, as this ratio of BD/t^2 increases from 200 to 500, the ratio of n1 decreases. This indicates that for these ratios of BD/t^2 (200-500) a rectangular bearing area increasingly overestimates the test results. For values of BD/t^2 above 500 the plotting shows that there is a little change in the ratio of n1, and this ratio is very close to 0.65.

Although there is a change in the ratio of n1 for increasing ratios of BD/t^2 above 200, nevertheless in practice we are generally concerned with designs where the ratios of BD/t^2 are approximately 200 or less. For example, if in a design of a column base the required

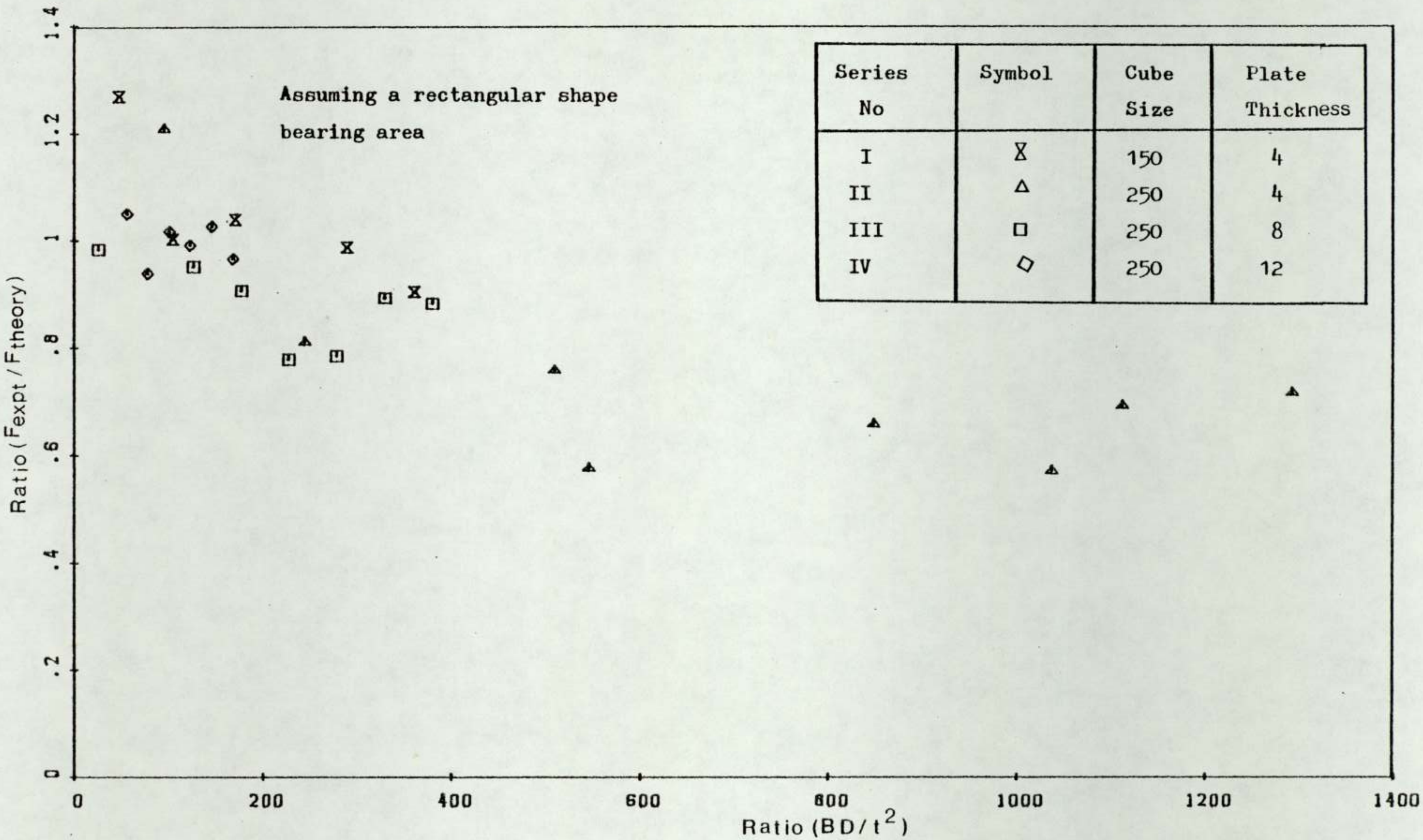

Fig. 5.11 Relationship between F_{expt}/F_{theory} and BD/t^2 for Author's 4 series of test results.

column section is 356 x 406 x 235Kg UC. and the thickness of base plate is 25mm, then the ratio of BD/t^2 will be 240 and for this ratio a rectangular shape bearing area yields a reasonably accurate prediction of failure load.

5.10 Discussion of Theories for Design of Base Column Presented by AISC , Draft of Steel Code and BS 449 .

For a thickness of base plate t and the effective cantilever lengths a_e and b_e as shown in Fig 5.12, AISC (29) includes formula for working design load as follows :

Assuming the uniform distribution of bearing stress, from the simple theory of elastic bending for a strip of steel base plate of unit width,

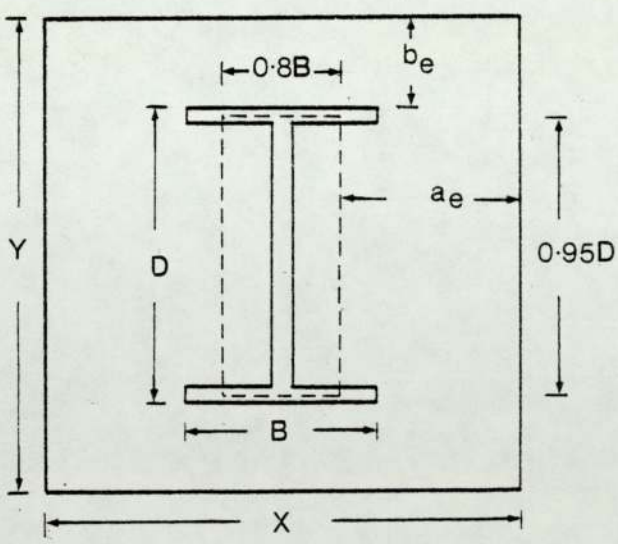

Fig. 5.12 Loading configuration for AISC method.

$$f_b \frac{t^2}{6} = f_p \frac{a_e^2}{2} \qquad \text{OR} \qquad f_b \frac{t^2}{6} = f_p \frac{a_e^2}{2}$$

Rearranging the above formulae,

$$t = \sqrt{\frac{3f_p \, a_e^2}{f_b}} \qquad \text{OR} \qquad t = \sqrt{\frac{3f_p \, b_e^2}{f_b}}$$

Where,

f_p is allowable bearing pressure ($f_p = 0.25\ f_{cp}$)

f_b is allowable bearing stress in steel base plate

($f_b = 0.75\ f_y$)

Rearranging the formulae for t in terms of a_e and b_e,

$$a_e = t\sqrt{\frac{f_b}{3f_p}} \qquad b_e = t\sqrt{\frac{f_b}{3f_p}}$$

Inserting the allowable design stresses for concrete $f_p = 0.25f_{cp}$ and steel $f_b = 0.75f_y$,

$$a_e = t\sqrt{\frac{0.75f_y}{3 \times 0.25f_{cp}}}, \qquad b_e = t\sqrt{\frac{0.75f_y}{0.75f_{cp}}}$$

Simplifying the above equations,

$$a_e = t\sqrt{\frac{f_y}{f_{cp}}} \tag{5.5}$$

$$b_e = t\sqrt{\frac{f_y}{f_{cp}}} \quad (5.6)$$

From Fig 5.12 the steel base column has dimensions,

$$X = 2a_e + 0.8B \quad (5.7)$$

$$Y = 2b_e + 0.95D \quad (5.8)$$

The Design Working Load (F_w) is

$$F_w = 0.25f_{cp}\ X\ Y \quad (5.9)$$

In a similar manner, the Draft of Steel Code(30) developed a formula for Ultimate Design Load, based on the simple theory of bending,

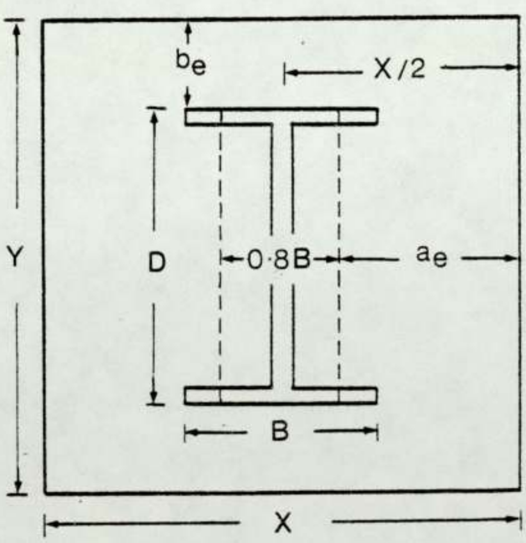

Fig. 5.13 Loading configuration based on the information in the Draft of Steel Code.

$$f_N \frac{t^2}{6} = f_p \frac{b_e^2}{2}$$

Rearranging this formula,

$$b_e = \sqrt{\frac{f_N\ t^2}{3f_p}}$$

Where,

f_N is the design bending strength of a steel base plate taken as 267 N/mm^2.

f_p is the allowable bearing pressure ($f_p = 0.4f_{cu}$)

Therefore,

$$b_e = \sqrt{\frac{267t^2}{3 \times 0.4f_{cu}}}$$

Simplifying the above equation,

$$b_e = \frac{14.93t}{\sqrt{f_{cu}}} \qquad (5.10)$$

However, the effective value of a_e is defined by Draft of Steel Code as follows,

$$a_e = X - 0.4B \quad \text{but} \quad < a_{min} \qquad (5.11)$$

Where

$$a_{min} = 0.8X > 0.35(D-b_e)$$

From Fig 5.13 the steel base column has dimensions,

$$X = 0.8B + 2a_e \qquad (5.12)$$

$$Y = D + 2b_e \qquad (5.13)$$

Therefore, the Ultimate Design Load (F_u) can be calculated as follows,

$$F_u = 0.4f_{cu}\ X\ Y \qquad (5.14)$$

A similar design of column base is recommended by the BS 449 (31), based on the simple theory of bending.

Assuming a uniform distribution of bearing stress for strip of steel base plate of unit width,

$$f_b \frac{t^2}{6} = f_p \frac{{b_e}^2}{2} \qquad \text{OR} \qquad f_b \frac{t^2}{6} = f_p \frac{{a_e}^2}{2}$$

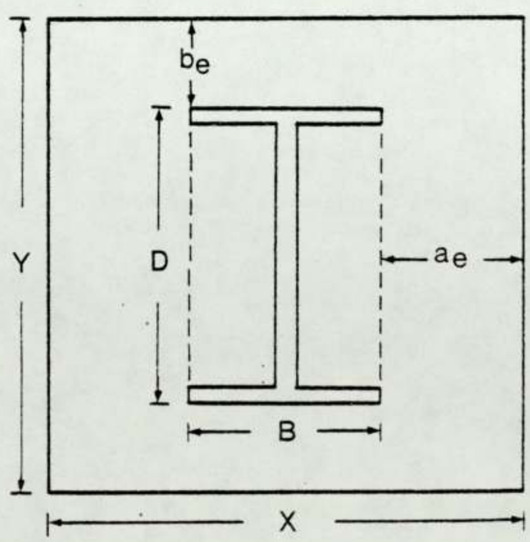

Fig 5.14 Loading configuration for BS 449 method.

Rearranging the above formulae,

$$t = \sqrt{\frac{3f_p\, a_e^{\,2}}{f_b}} \qquad \text{OR} \qquad t = \sqrt{\frac{3f_p\, b_e^{\,2}}{f_b}}$$

Where,

f_p is allowable bearing pressure (f_p = 0.25 f_{cu})

f_b is allowable bearing stress in steel base plate

(f_b = 185 N/mm^2)

Rearranging the formulae for t in terms of a_e and b_e,

$$a_e = t\sqrt{\frac{f_b}{3f_p}} \qquad b_e = t\sqrt{\frac{f_b}{3f_p}}$$

Inserting the allowable design stresses for concrete $f_b = 0.25f_{cu}$ and for steel f_b = 185 N/mm^2,

$$a_e = t\sqrt{\frac{185}{3 \times 0.25f_{cu}}}, \qquad b_e = t\sqrt{\frac{185}{3 \times 0.25f_{cu}}}$$

Simplifying the above equations,

$$a_e = t \quad \frac{15.71\ t}{\sqrt{f_{cu}}} \qquad (5.15)$$

$$b_e = t \quad \frac{15.71\ t}{\sqrt{f_{cu}}} \qquad (5.16)$$

From Fig 5.14 the steel base column has dimensions,

$$X = 2a_e + B \tag{5.17}$$

$$Y = 2b_e + D \tag{5.18}$$

The Design Working Load (F_w) is

$$F_w = 0.25 f_{cu} X Y \tag{5.19}$$

5.11 Correlation and Discussion of Allowable Design Load Recommended by AISC , DSC and BS 449 to THE Tests Carried Out by the Author.

The equations of AISC (29), Draft of Steel Code (30) and BS 449 (31) for column base were applied to the four series of tests carried out by the Author and the results of the comparison between the equations and the tests are tabulated in Table 5.4, 5.5 and 5.6. Details of the calculation are presented in the subsiduary Tables C.1,C.2 and C.3 of Appendix C.

As can be seen from Tables 5.4, 5.5 and 5.6 for test Series I, II and III as the ratios of B/D increase both the ratios of F/F_u and F/F_w decrease.

In Series II with a 4mm thick steel base plate and 250mm cubes there is a wide range in the ratio of measured to calculated failure load for increasing ratios of B/D, between 0.066 to 1.0. These ranges are 5.37 to 1.55 (F/F_u) for Draft of Steel Code (30). For AISC(29) and BS 449(31) the ratio of F/F_w ranges between 10.13 to 4.48 and 8.31 to 3.09 respectively. As the thickness of the steel base plate increases, as in test series III with 8mm thick steel base plate, this difference in the ratio of measured to calculated failure load decreases. For this series of tests with increasing ratio of B/D from 0.062 to 0.93 the ratio of F/F_u ranges from 3.18 to 1.94, the ratio of F/F_w for the AISC and the BS 449 ranges from 5.37 to 4.57 and 4.64 to 3.33 respectively. In Series IV, however, with a 12mm thick steel base plate and 250mm cubes, as the ratio of B/D increases from 0.31 to 0.93 there is little change in the ratios of F/F_u and F/F_w. These ratios for the Draft of steel code vary between F/F_u = 2.13 to 2.42; for the AISC and the BS 449 vary between 4.14 to 4.65 and 3.82 to 3.37 respectively.

The reason for this wide range in ratios of measured to computed failure load (especially for a thiner steel base column) is because of the assumption made by the AISC, the Draft of Steel Code and BS 449. This assumption is that for all thicknesses of steel base plate the column acts as a solid rectangle. The dimensions of this rectangle is assumed by the AISC, the Draft of Steel Code and BS 449 to be 0.95D by 0.8B, D by 0.8B and D by B respectively. This assumption, as pointed out in Section 5.9 of this chapter, was reasonable only when thick steel base plates were considered.

These results indicate that neither the AISC or the Draft of Steel Code or the BS 449 give a reliable prediction of the failure load when applied to a thin steel base plate. Nevertheless in practice these methods are safe with a high percentage of coefficient of variation as shown in Tables 5.4 to 5.6.

Test Series	Test No	Author's Test Results: Concrete Strength f_{cu} N/mm^2	Ratio of B/D mm/mm	Failure Load F KN	AISC Design Load F_w Eq.(5.9) KN	Ratio of Measured/Computed (Failure Load) Dimensionless
(I)	I1	27.9	0.13	157	20.2	7.78
on 150mm	I2	27.9	0.29	167	25.3	6.50
cubes	I3	27.9	0.47	207.9	32.4	6.40
t=4	I4	27.9	0.80	255	44.1	5.79
	I5	27.9	1.00	264.9	51.1	5.19
(II)	II1	34.0	0.07	385.5	38.0	10.13
on 250mm	II2	30.0	0.20	353.2	52.7	6.70
cubes	II3	30.0	0.33	404.2	69.9	5.80
t=4	II4	34.0	0.46	412	96.0	4.30
	II5	34.0	0.60	429.7	115.0	4.60
	II6	30.0	0.73	455.2	121.4	3.80
	II7	34.0	0.86	697.7	153.9	4.50
	II8	30.0	1.00	701.4	156.7	4.50
(III)	III1	34.4	0.06	431.6	80.4	5.37
on 250mm	III2	26.0	0.31	549.4	106.7	5.10
cubes	III3	26.0	0.43	608.2	126.6	4.83
t=8	III4	34.4	0.56	755.4	174.3	4.33

Table 5.4 Correlation of tests carried out by the Author to the design load recommended by the AISC. (CONTINUED)

Test Series	Test No	Author's Test Results Concrete Strength f_{cu} N/mm^2	 Ratio of B/D mm/mm	 Failure Load F KN	AISC Design Load F_w Eq.(5.9 KN	Ratio of Measured/Computed (Failure Load) Dimensionless
	III5	34.4	0.68	853.5	197.7	4.32
	III6	26.0	0.80	843.7	181.1	4.66
	III7	26.0	0.93	912.3	199.5	4.57
(IV)	IV1	26.0	0.31	725.9	159.3	4.56
on 250mm	IV2	26.0	0.43	745.6	180.2	4.14
cubes	IV3	26.0	0.55	912.2	201.1	4.54
t=12	IV4	26.0	0.68	990.8	221.9	4.50
	IV5	26.0	0.80	1128.2	242.8	4.65
	IV6	26.0	0.93	1157.6	263.7	4.40
				Mean	------>	(5.24)
				Standard Deviation	------>	(±1.36)
				%	------>	(26.00)

Table 5.4 Correlation of tests carried out by the Author to the design load recommended by the AISC.

Test Series	Test No	Author's Test Results: Concrete Strength f_{cu} N/mm^2	Ratio of B/D mm/mm	Failure Load F KN	DSC Design Load F_u Eq.(5.14) KN	Ratio of Measured/Computed (Failure Load) Dimensionless
(I)	I1	27.9	0.13	157	35.7	4.39
on 150mm	I2	27.9	0.29	167	54.8	3.05
cubes	I3	27.9	0.47	207.9	79.9	2.70
t=4	I4	27.9	0.80	255	103.5	2.50
	I5	27.9	1.00	264.9	116.7	2.27
(II)	II1	34.0	0.07	385.5	71.8	5.37
on 250mm	II2	30.0	0.20	353.2	125.7	2.80
cubes	II3	30.0	0.33	404.2	185.4	2.18
t=4	II4	34.0	0.46	412	273.3	1.51
	II5	34.0	0.60	429.7	340.6	1.56
	II6	30.0	0.73	455.2	364.6	1.25
	II7	34.0	0.86	697.7	472.3	1.48
	II8	30.0	1.00	701.4	453.8	1.55
(III)	III1	34.4	0.06	431.6	135.8	3.18
on 250mm	III2	26.0	0.31	549.4	237.7	2.31
cubes	III3	26.0	0.43	608.2	300.2	2.03
t=8	III4	34.4	0.56	755.4	452.3	1.67

Table 5.5 Correlation of tests carried out by the Author to the design load recommended by the Draft of Steel Code. (CONTINUED)

Test Series	Test No	Author's Test Results: Concrete Strength f_{cu} N/mm^2	Ratio of B/D mm/mm	Failure Load F KN	DSC Design Load F_u Eq.(5.14) KN	Ratio of Measured/Computed (Failure Load) Dimensionless
	III5	34.4	0.68	853.5	522.0	1.63
	III6	26.0	0.80	843.7	436.5	1.93
	III7	26.0	0.93	912.3	471.3	1.94
(IV)	IV1	26.0	0.31	725.9	309.6	2.35
on 250mm	IV2	26.0	0.43	745.6	349.8	2.13
cubes	IV3	26.0	0.55	912.2	388.4	2.35
t=12	IV4	26.0	0.68	990.8	427.1	2.32
	IV5	26.0	0.80	1128.2	465.7	2.42
	IV6	26.0	0.93	1157.6	504.3	2.30
					Mean ------>	(2.35)
					Standard Deviation ------>	($\pm$.90)
					% ------>	(38.30)

Table 5.5 Correlation of tests carried out by the Author to the design load recommended by the Draft of Steel Code.

Test Series	Test No	Author's Test Results: Concrete Strength f_{cu} N/mm^2	Ratio of B/D mm/mm	Failure Load F KN	BS449 Design Load F_w Eq.(5.19) KN	Ratio of Measured/Computed (Failure Load) Dimensionless
(I)	I1	27.9	0.13	157	23.5	6.68
on 150mm	I2	27.9	0.29	167	31.9	5.24
cubes	I3	27.9	0.47	207.9	41.6	5.00
t=4	I4	27.9	0.80	255	59.0	4.32
	I5	27.9	1.00	264.9	69.5	3.81
(II)	II1	34.0	0.07	385.5	46.4	8.31
on 250mm	II2	30.0	0.20	353.2	69.2	5.10
cubes	II3	30.0	0.33	404.2	95.3	4.24
t=4	II4	34.0	0.46	412	134.4	3.07
	II5	34.0	0.60	429.7	163.7	2.62
	II6	30.0	0.73	455.2	173.6	2.62
	II7	34.0	0.86	697.7	222.4	3.14
	II8	30.0	1.00	701.4	227.1	3.09
(III)	III1	34.4	0.06	431.6	93.0	4.64
on 250mm	III2	26.0	0.31	549.4	136.6	4.02
cubes	III3	26.0	0.43	608.2	164.1	3.71
t=8	III4	34.4	0.56	755.4	233.9	3.23

Table 5.6 Correlation of tests carried out by the Author to the design load recommended by the BS 449. (CONTINUED)

Test Series	Test No	Author's Test Results: Concrete Strength f_{cu} (N/mm^2)	Author's Test Results: Ratio of B/D (mm/mm)	Author's Test Results: Failure Load F (KN)	BS449 Design Load F_w Eq.(5.19) (KN)	Ratio of Measured/Computed (Failure Load) Dimensionless
	III5	34.4	0.68	853.5	269.1	3.17
	III6	26.0	0.80	843.7	246.5	3.42
	III7	26.0	0.93	912.3	274.0	3.33
(IV)	IV1	26.0	0.31	725.9	190.2	3.82
on 250mm	IV2	26.0	0.43	745.6	220.9	3.38
cubes	IV3	26.0	0.55	912.2	251.6	3.63
t=12	IV4	26.0	0.68	990.8	282.2	3.51
	IV5	26.0	0.80	1128.2	312.9	3.61
	IV6	26.0	0.93	1157.6	343.6	3.37
					Mean ------>	(4.00)
					Standard Deviation ------>	($\pm$1.26)
					% ------>	(31.5)

Table 5.6 Correlation of tests carried out by the Author to the design load recommended by the BS 449.

CHAPTER SIX

EXPERIMENTAL WORK ON UNIAXIAL ECCENTRIC LOADING

6.1 Introduction

The test results presented in the preceding chapters were all based on concentric loading. In this chapter, however, concrete cubes loaded eccentrically through stiff bearing plates of various sizes are considered. The purpose of carrying out such tests was both to standardise the experimental results and also to fill the gap which existed in the tests performed by other researchers.

Three series of tests were carried out in which eccentricities of 10, 40 and 50mm were considered. The results of the three test series using 150mm cubes are tabulated in Table 6.1.

6.2 Specification and Manufacture of Concrete Specimens.

The same materials, mix design, manufacturing process and curing as explained in Chapter 2 were implemented for the specimens tested in this chapter. The values of control tests given in Table 6.1 are the average values obtained from testing three control specimens.

6.3 Test Procedure.

The specimens were placed in a central position on the machine, at right-angles to the direction in which they were cast, and loaded eccentrically through square mild steel bearing plates 20mm thick. Bearing plates machined down to the required size were placed uniaxially on top of the concrete specimens so that the four sides of the bearing plate were parallel to the four sides of the cube. The thick upper platen of the testing machine was in contact with the entire area of the bearing plate. Load was then applied at an average

Test	Concrete Strength	Loading Plate		Eccentricity	Failure Load	Ratio of	
No	f_{cu}	b_x	b_y	e	F_e	F_e/Af_{cu}	A_s/A
	N/mm^2	mm	mm	mm	KN	Dimensionless	
E1	31.4	10	10	10	54.0	0.076	0.0044
E2	31.4	40	40	10	127.5	0.180	0.0710
E3	31.4	60	60	10	191.3	0.270	0.1600
E4	31.4	70	70	10	235.4	0.330	0.2200
E5	31.4	90	90	10	313.9	0.440	0.3600
E6	31.4	100	100	10	363.0	0.510	0.4400
E7	31.7	20	20	40	48.1	0.067	0.0180
E8	31.7	40	40	40	89.0	0.125	0.0710
E9	31.7	60	60	40	140.4	0.197	0.1600
E10	31.7	20	20	50	39.5	0.055	0.0180

Table 6.1 Author's test results for uniaxial eccentric loading for 150mm concrete cubes.

rate of one ton for every thirty seconds until failure occurred i.e. the load dropped off. For each specimen the load at first crack, the progress of cracking, the mode of failure and maximum load were recorded.

6.3.1 Eccentricity.

To achieve greater eccentricity whilst still keeping the bearing plate within the top surface of the specimen, a smaller bearing plate must of necessity be used. With this in mind, tests were carried out on 150mm cubes in which eccentricities of 10, 40 and 50mm were considered. With an eccentricity of 10mm tests were carried out for ranges of R (loaded area/concrete area) 0.004 to 0.44. For these tests the cube strength of the concrete was 31.4N/mm^2 with standard deviation of 0.6%. With 40mm eccentricity three ratios of R = 0.018, 0.07 and 0.16 were considered. For 50mm eccentricity only one ratio of R = 0.018 could be evaluated since larger bearing plates would have extended beyond the edge of the specimen. In the tests with 40 and 50mm eccentricity the concrete cube strength was 31.7N/mm^2 with standard deviation of 2%.

6.4 Mode of Failure.

Photographs 6.1 to 6.4 show a typical pattern of cracks and mode of failure for four different sizes of stiff bearing : 20, 40, 70 and 100mm^2.

A distinct difference in the mode of failure between eccentric loading and concentric loading is that in the former the first visible crack always appeared on the side of the specimen

Plate 6.1 Typical crack formation at failure under square eccentric loading condition. (e = 50mm , A_s = 20mm^2)

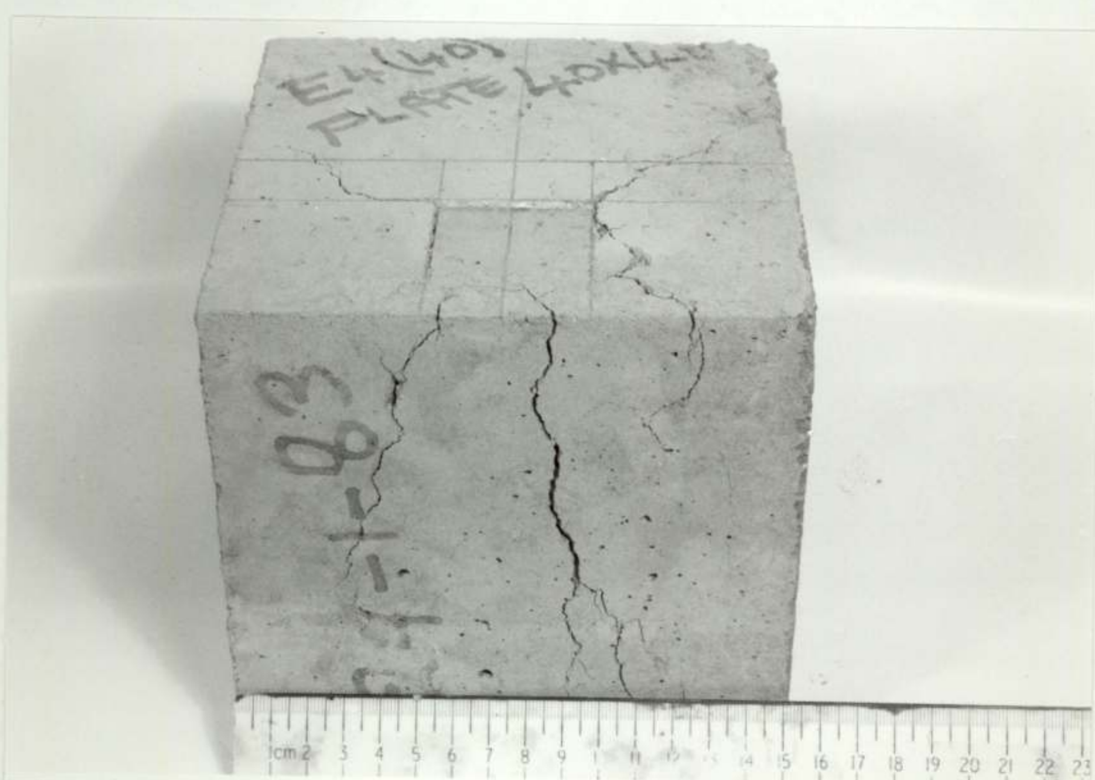

Plate 6.2 Typical crack formation at failure under square eccentric loading condition. (e = 40mm , A_s = 40mm^2)

Plate 6.3 Typical crack formation at failure under square eccentric loading condition. (e = 10mm , A_s = 70mm^2)

Plate 6.4 Typical crack formation at failure under square eccentric loading condition. (e = 10mm , A_s = 100mm^2)

nearest to the bearing plate. This could be due to the less confining pressure from the side of the concrete nearest to the bearing plate. In concentric loading, however, the cracks generally originated from near the loaded surface. For large values of eccentricity, as shown in Photograph 6.1 (50mm eccentricity and 20mm^2 stiff bearing), no crack developed on the side of the specimen furthest from the stiff bearing. With 70mm^2 stiff bearing and eccentricity of 10mm, as shown in Photograph 6.3, somewhat smaller cracks developed on the side of the specimen furthest from the stiff bearing plate. The same form of crack can also be seen in Photographs 6.2 and 6.4 with 40 and 100mm^2 stiff bearings. With small ratios of loaded area to concrete area (R), as in the case with concentric loading, failure occurred with the punching out of an inverted cone, and for large values of R failure changed from that above to one of crushing, similar to a cube crushing test.

6.5 Presentation of Test Results.

The results of tests carried out are tabulated in Table 6.1. In Fig. 6.1 test results plotted with dimensionless ratio of failure load divided by concrete surface area, F_e/A to concrete cube strength (f_{cu}) as the ordinate and the ratio of loaded area to concrete surface area (A_s/A) as the abscissa. Three sets of test results with eccentricities of 10, 40 and 50mm are plotted as explained above. The solid drawn in Fig. 6.1 is based on the empirical formulae Equations (2.1) and (2.2) developed in Chapter 2 for concentric loading i.e. zero eccentricity. It is clear from the plotted results that the bearing strength decreases with increasing eccentricity for a constant ratio of R. As can be expected for the small eccentricity of 10mm the results are very close to the empirical line for zero eccentricity,

Test No	Symbol	Square plate size	Eccentricity
E1-E6	⧖	10-100	10
E7-E9	△	20-60	40
E10	□	20	50

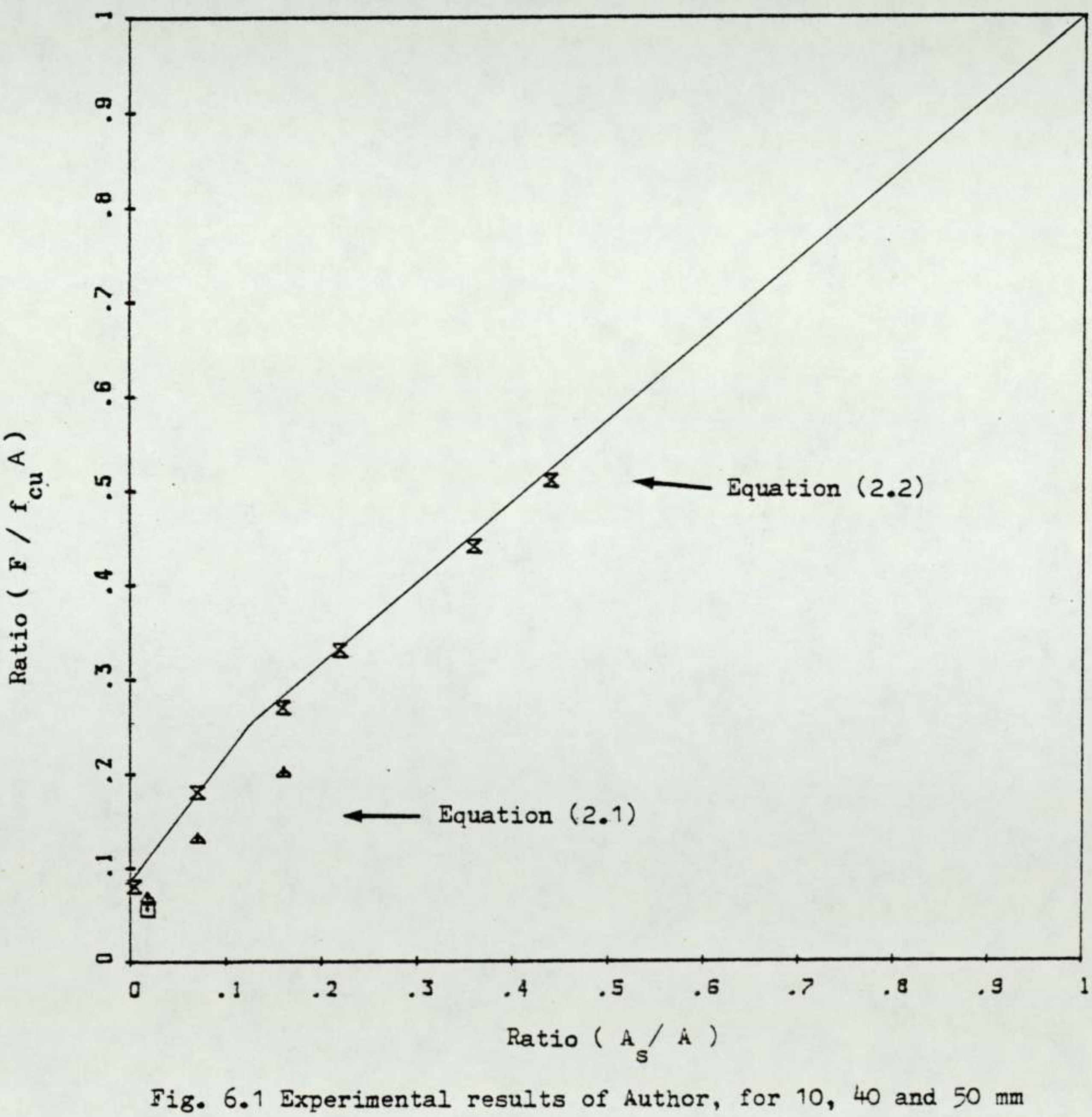

Fig. 6.1 Experimental results of Author, for 10, 40 and 50 mm eccentric loading via rigid loading piece on 150 mm cubes.

yet they are all below the zero eccentricity line.

6.6 Theory.

Based on the following assumptions an empirical theory is developed for the bearing capacity of concrete under various eccentricities.

a)Bearing strength decreases with increasing eccentricity for a constant ratio of R,

b) For the same value of eccentricity e1 the bearing capacity decreases for increasing ratios of R,

Based on the above statements it is therefore possible to draw two lines for zero and e1 eccentricity, as shown in Fig. 6.2.

6.6.1 Ratios of R<0.125.

From Chapter 2 for zero eccentricity and R<0.125 the following equation was developed.

$$n = 1.36\ R + 0.085 \qquad (6.1)$$

For an eccentricity of e1 Equation 6.1 can be written as follows

$$n_{e1} = R_{e1}\ (1.3\ R + 0.085) \qquad (6.2)$$

where R_{e1} is defined as a reduction factor for eccentricity of e1.

n_{e1} is defined as $\dfrac{F_{e1}}{Af_{cu}}$ (F_{e1} is the failure load for eccentricity of e1)

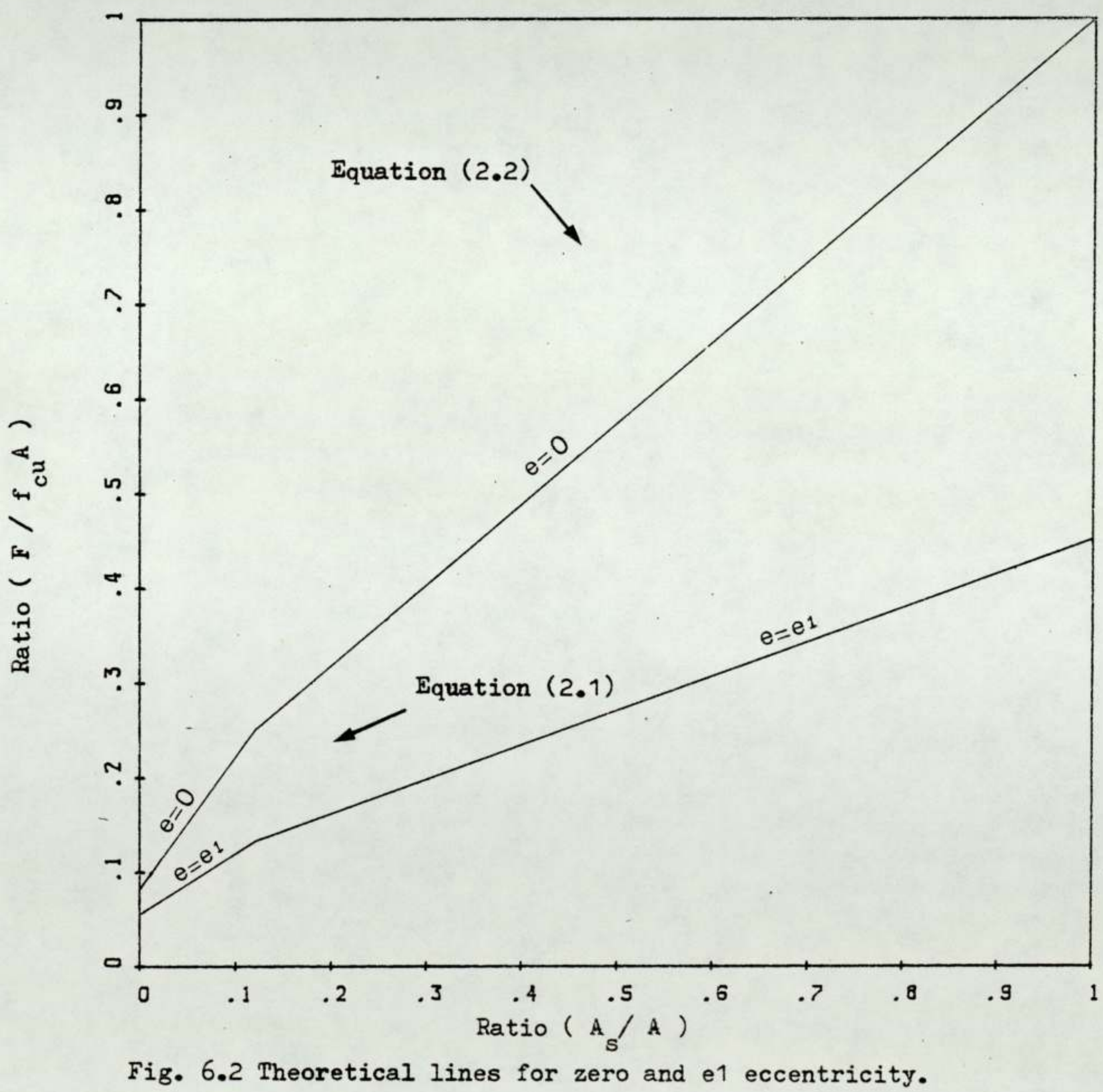

Fig. 6.2 Theoretical lines for zero and e1 eccentricity.

Dividing the two Equations 6.1 and 6.2,

$$\frac{n}{n_{e1}} = \frac{(1.36\ R + 0.085)}{(1.36\ R + 0.085)R_{e1}}$$

Therefore

$$n_{e1} = n\ R_{e1} \qquad (6.3)$$

where n can be calculated using Equation 6.1.

An expression for R_{e1} is developed in Section 6.6.3.

6.6.2 Ratios of R>0.125.

Following exactly the same procedure as in Section 6.6.1 and using the empirical equation developed in Chapter 2 (Equation 2.2), for ratios of $R > 0.125$, a similar expression for reduction factor with an eccentricity of e1 can be found as follows,

$$n_{e1} = n\ R_{e1} \qquad (6.4)$$

where

$$n = 0.85 + 0.15\ R \qquad (6.5)$$

6.6.3 Evaluation of Reduction Factor for Various Eccentricities of e1.

The relationship obtained for reduction factor, Equations 6.3 and 6.4 can be simplified as follows,

$$R_{e1} = \frac{F_{e1}}{F} \qquad (6.6)$$

The above Equation 6.6 indicates that the reduction factor for an eccentricity of e1 is the ratio of the ultimate load for eccentricity of e1 to the ultimate load for concentric loading i.e. zero eccentricity.

In order to evaluate the reduction factor R_{e1} test results obtained in this research for eccentricities of 10, 40 and 50mm and those carried out by Niyogi (18) for eccentricities of 25, 38 and 51mm are used. From these test results the average values of F_e/F for various ratios of e/b_x are obtained as shown in Table 6.2. The best fit obtained using least-square curve fit method for the test results is an exponential function with the index of determination equal to 0.97. The equation of this function is of the following form,

$$1 - \frac{F_e}{F} = 0.0235 \text{ (EXP) } 9.275 \frac{e}{b_x} \qquad (6.7)$$

This equation does not, however, satisfy the boundary condition for zero eccentricity. Therefore, the following steps are taken to find an equation which both satisfies the boundary condition and yet is close to the best fit Equation 6.7.

Assuming that the equation which satisfies the boundary condition is of the form,

$$1 - \frac{F_e}{F} = 0.0235 \text{ (EXP) } 9.275 \frac{e}{b_x} + C1 \qquad (6.8)$$

where C1 is a constant.

Researcher	Cube Size	Ratio of	Failure Load	Ratio of	Ratio of	Average of
	mm^3	A_s/A mm/mm	F_e KN	e/b_x mm/mm	F_e/F^*	$1-F_e/F$
	150	0.0044	54.0	0.067	0.84	
	150	0.0710	127.5	0.067	0.99	
	150	0.1600	191.3	0.067	0.95	
Author	150	0.2200	235.4	0.067	0.99	0.05
	150	0.3600	313.9	0.067	0.96	
	150	0.4400	363.0	0.067	0.98	
	150	0.0180	48.1	0.270	0.62	
Author	150	0.0710	89.0	0.270	0.69	0.33
	150	0.1600	140.4	0.270	0.69	
Author	150	0.0180	39.5	0.330	0.51	0.49
	203	0.0160	121.0	0.125	0.91	
	203	0.0310	145.7	0.125	0.96	0.06
Niyogi	203	0.0630	193.6	0.125	0.94	
	203	0.2520	431.7	0.125	0.94	
	203	0.0310	139.4	0.188	0.92	
Niyogi	203	0.0630	186.1	0.188	0.91	0.10
	203	0.2520	389.2	0.188	0.87	
	203	0.0160	87.3	0.250	0.66	
Niyogi	203	0.0310	120.3	0.250	0.79	0.25
	203	0.0630	164.2	0.250	0.81	

Table 6.2 Results of tests carried out by the Author and Niyogi for uniaxial eccentric loading.

* F (the ultimate load), is obtained using the Equations(2.1) and (2.2) of of Chapter 2.

When $e = 0$ then $F_e = F$ and substituting for e and F_e in Equation 6.7 we will find C1 as,

$$1 - \frac{F}{F} = 0.0235\ (EXP)\ 9.275 \left(\frac{0}{b_x} \right) + C1$$

$$1 - 1 = 0.0235 + C1$$

Therefore,

$$C1 = -0.0235$$

Substituting back for C1 in Equation 6.8,

$$1 - \frac{F_e}{F} = 0.0235\ (EXP)\ 9.275 \frac{e}{b_x} - 0.0235$$

$$\frac{F_e}{F} = 1.0235 - 0.0235\ (EXP)\ 9.275 \frac{e}{b_x}$$

But F_e/F was defined as the reduction factor R_e.

Therefore,

$$R_e = 1.0235 - 0.0235\ (EXP)\ 9.275 \frac{e}{b_x} \qquad (6.9)$$

To summarise,

$$n_e = R_e\ n \qquad (6.10)$$

where,

$$n = 1.36\ R + 0.085 \qquad \text{for } R < 0.125$$

$$n = 0.85\ R + 0.15 \qquad \text{for } R > 0.125$$

and R_e can be found from Equation 6.9

6.7 Theory Developed by Niyogi for Eccentric Loading of Concrete Cubes.

Niyogi (18) developed an empirical equation for eccentric loading on square plates which is of the form,

$$n_e = n\ R_e$$

Although the overall pattern of Niyogi's equation is similar to Equation 6.10 presented in this research, however, Niyogi's expressions for n and R_e are very different to those developed here. The following expressions were developed by Niyogi for n and R_e,

$$n = 0.84\ \ R\ - 0.23 \qquad (6.11)$$

$$R_e = 2.36\ \ (0.83 - (\frac{e}{b_x})^2) - 0.94\frac{e}{b_x} - 1.15 \qquad (6.12)$$

Therefore,

$$n_e = (0.84\ \ R\ - 0.23R)(2.36\ \ 0.83 - (\frac{e}{b_x})^2 - 0.94\frac{e}{b_x} - 1.15) \qquad (6.13)$$

6.8 Application of the Author's and Niyogi's Theories to the Available Test Results.

Both Equation 6.10 developed by the Author and Equation 6.13 produced by Niyogi (18) were used to predict the ultimate load of tests carried out in this research, (Table 6.3), and tests carried out

Test	Eccen-tricity	Concrete Strength	Square Loading Plate	Ratio of	Ratio of	Experimental Failure Load	Theoretical Results Failure Load	Failure Load	Ratio of Measured/Computed (Failure Load)	
No	e	f_{cu}	S_x	A_s/A	e/b_x	F_e	F_e Author Eq.(6.9)	F_e Niyogi Eq.(6.12)	Author	Niyogi
	mm	N/mm^2	mm	mm/mm	mm/mm	KN	KN	KN	Dimensionless	
E1	10	31.4	10	0.0044	0.067	54.0	63.0	36.0	0.857	1.500
E2	10	31.4	40	0.0710	0.067	127.5	125.7	136.5	1.015	0.934
E3	10	31.4	60	0.1600	0.067	191.3	198.0	196.9	0.966	0.972
E4	10	31.4	70	0.2200	0.067	235.4	233.3	225.9	1.009	1.042
E5	10	31.4	90	0.3600	0.067	313.9	315.6	277.1	0.994	1.133
E6	10	31.4	100	0.4400	0.067	363.0	362.7	300.0	1.000	1.210
E7	40	31.7	20	0.0170	0.270	48.1	56.8	48.9	0.847	0.983
E8	40	31.7	40	0.0710	0.270	89.0	95.3	96.2	0.934	0.926
E9	40	31.7	60	0.1600	0.270	140.4	150.1	138.6	0.935	1.013
E10	50	31.7	20	0.0170	0.330	39.5	40.3	41.0	0.981	0.964
							Mean	----->	(0.954)	(1.068)
							Standard Deviation	----->	(±0.0605)	(±0.1760)
							%	----->	(6.3)	(16.5)

Table 6.3 Comparison of the Author's and Niyogi's empirical theories to the Author's tests on uniaxial eccentric loading on 150mm cubes via rigid loading pieces.

Test	Eccen-tricity	Concrete Strength	Square Loading Plate	Ratio of	Ratio of	Experimental Failure Load	Theoretical Results Failure Load	Failure Load	Ratio of Measured/Computed (Failure Load)	
No	e	f_{cu}	S_x	A_s/A	e/b_x	F_e	F_e Author Eq.(6.9)	F_e Niyogi Eq.(6.12)	Author	Niyogi
	mm	N/mm^2	mm	mm/mm	mm/mm	KN	KN	KN	Dimensionless	
1	13	29.2	36	0.031	0.063	157.7	150.2	158.5	1.050	0.995
2	13	33.0	51	0.063	0.063	239.4	227.8	248.8	1.051	0.958
3	13	27.0	102	0.252	0.063	410.4	397.6	378.7	1.032	1.098
4	25	30.1	25	0.016	0.125	121.0	125.6	109.7	0.963	1.103
5	25	28.8	36	0.031	0.125	145.7	143.2	147.6	1.018	0.987
6	25	29.2	51	0.063	0.125	193.6	194.9	204.4	0.994	0.947
7	25	30.9	102	0.252	0.125	431.7	434.0	399.3	0.981	1.081
8	38	29.2	36	0.031	0.188	139.4	136.1	131.8	1.025	1.057
9	38	28.8	51	0.063	0.188	186.1	180.1	181.0	1.033	1.028
10	38	29.2	102	0.252	0.188	389.2	389.6	340.1	0.999	1.144
11	51	30.1	25	0.016	0.250	87.3	103.9	86.8	0.840	1.010
12	51	29.2	36	0.031	0.250	120.3	120.1	115.6	1.000	1.041
13	51	29.2	102	0.063	0.250	164.2	161.2	161.2	1.018	1.018
								Mean ----->	(1.000)	(1.036)
								Standard Deviation ----->	(±0.0547)	(±0.059)
								% ----->	(5.5)	(5.7)

Table 6.4 Comparison of the Author's and Niyogi's empirical theories to the Niyogi's tests on uniaxial eccentric loading on 203mm cubes via rigid loading pieces.

by Niyogi (Table 6.4). As shown in Table 6.3, applying Niyogi's theory to the tests carried out in this research produces a mean of 1.068 which is an acceptable result. However, the values for standard deviation and the percentage difference are + 0.176 and 16.5%. The empirical theory developed in this research produces a mean of 0.954 with a standard deviation of + 0.0605 and percentage difference of 6.3%.

To further support the proposed method developed in this research both Equations 6.10 and 6.13 were also applied to the tests carried out by Niyogi. As is shown in Table 6.4 the proposed empirical formulae in this research, Equation 6.10, give a more accurate prediction of failure load than Niyogi's Equation 6.13.

6.9 Comparison and Discussion of the Two Empirical Equations Recommended by Author and Niyogi for Uniaxial Eccentric Loading

The equations developed by the Author and Niyogi were both of the form $n_e = n\ R_e$. However, it should be pointed out that despite the overall similarity in the form of the two equations, the expression for n and R_e are very different. To compare this difference, the expressions developed for reduction factor (R_e) both in this research, Equation 6.9, and Niyogi's Equation 6.12 were drawn for different ratios of e/b_x in Fig. 6.3.

Equations 2.1 and 2.2 for zero eccentrcity from this research and 6.11 from Niyogi's are also plotted in Fig. 6.4. As can be seen, the expression presented by Niyogi for n is of a parabolic form. The shape of this curve suggests that for the ratio of $A_s/A = 1$, when the

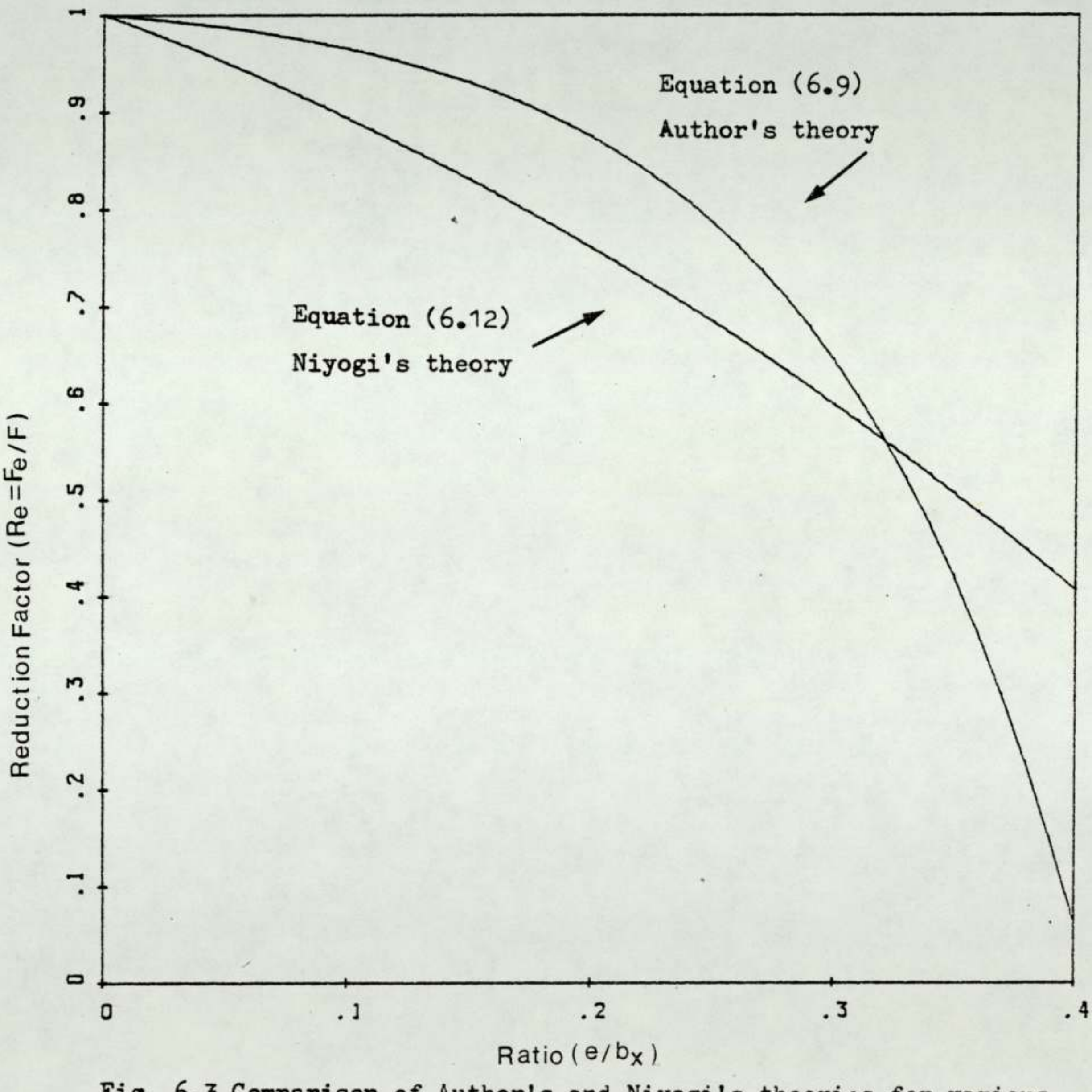

Fig. 6.3 Comparison of Author's and Niyogi's theories for various eccentricities loaded via a rigid loading piece.

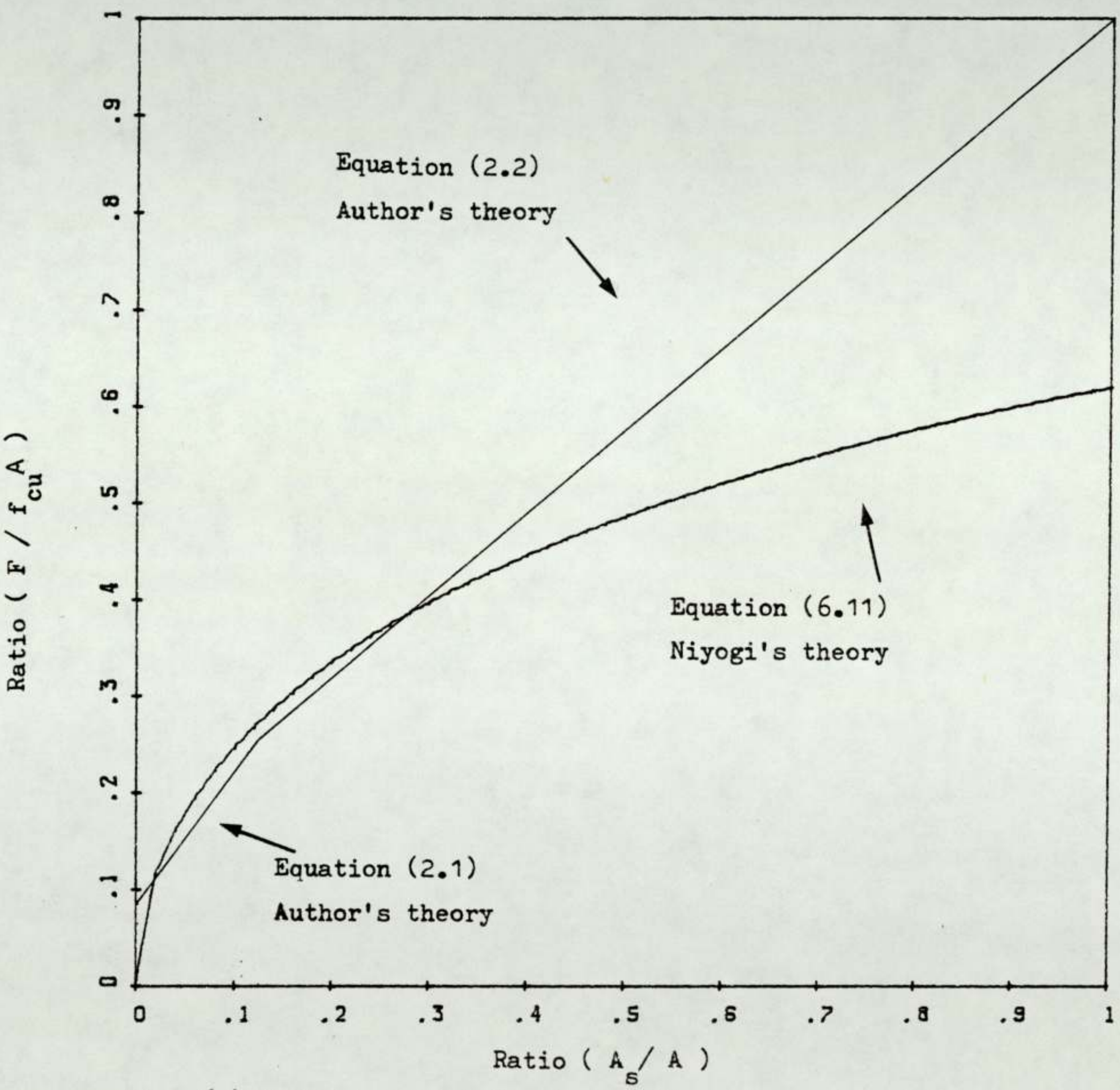

Fig. 6.4 Comparison of Author's and Niyogi's empirical formulae for concrete cubes loaded via a rigid loading piece.

rigid base plate covers the whole surface of the concrete, the value of F/Af_{cu} is equal to 0.61. This is not a reasonable result since, for the ratio of $A_s/A = 1$, the ratio of F/Af_{cu} should be equal to unity. The equation presented by Niyogi also suggests that for the ratio of $A_s/A = 0$ the value of $F/Af_{cu} = 0$. This in turn implies that the cohesive stress of the concrete equals zero, which is not true.

CHAPTER SEVEN

REVIEW OF THEORETICAL ANALYSIS OF THE BEHAVIOUR of CONCENTRICALLY LOADED CONCRETE PRISMS

7.1 Introduction

7.2 Historical Review

7.3 Comparison and Discussion of Reviewed Work

7.1 Introduction

The analysis of the distribution of stresses of a foundation loaded through a rigid steel base plate using various linear theoretical methods utilising the continuum method of stress analysis has been extensively investigated (33-44). Other researchers (32,33) have reviewed much of the theoretical work concerning a concentrated load acting on a small area on the free end surface of a prism made of a elastic material. Therefore, it is not intended here to analyse all the existing methods but, in order that this work may be put into its historical perspective, a discussion of the more relevant theoretical attempts at solving the stresses in foundations loaded through rigid base plates is necessary.

7.2 Historical Review

The strength of material approach is perhaps one of the first methods used for calculating the stresses in blocks loaded concentrically on a small upper surface area. Morsch (34), Bortsch (35) and Magnel (36) are among a few who have presented theoretical formulae using the above approach, in which the block was generally considered as a deep beam.

In 1924 Morsch was one of the first to develop a rather simple expression for calculating stresses in blocks subjected to concentrated loads. His work was based on some tests that were carried out mainly on stone blocks although a few were made on plain and reinforced concrete. Morsch assumed that the stresses produced by a concentrated load applied on one face of prism are distributed uniformly at a distance from the face equal to the width of the prism. Morsch's second assumption was that the curvature of the compressive and tensile stress trajectories caused the tensile stresses, these tensile stresses were distributed according to a second order parabolic law. It should be pointed out that the assumptions made by Morsch was also made by Bortsch(35) and Magnel(36) and many others until the 1970s. In order to have some agreement between the calculated and measured values of tensile stress Morsch recommended a correction for the depth of the block.

A more advanced approach was made by Bortsch(35) in 1935 to the problem of bearing capacity as well as stress distribution in a block under a partial concentric load. Bortsch assumed a distributed load on the contact area as a cosine function and developed expressions for transverse, longitudinal and shear stresses.

Magnel(36) in 1949 was the first researcher concerned with stress concentration, in particular the anchorages of prestressed concrete beams. Magnel's theory was based on the assumption that the transverse stress diagram at any plane parallel to the central axis of the beam was that of a cubic parabola. He developed an expression for transverse stress and by considering the equilibrium condition for an infinitesimal element Magnel produced an expression for the shear stress in the block.

Guyon (37) in 1951 took a different approach in his paper on the stresses in prismatic bodies loaded on their surface. Applying the continuum approach, Guyon assumed a semi-infinite prism of unit thickness loaded by forces of any magnitude and inclination to the top surface (the longitudinal axis being vertical). In order to describe the stress system required to keep the prism in equilibrium under the action of the applied load Guyon considered a method employing Fourier series, a technique also used by Timoshenko (38). By developing a Fourier series Guyon developed an approximate solution for the two-dimensional case of plane-stress analysis. He then extended his theory to a three dimensional loading of small areas on prisms by modifying the coefficients. Guyon's theory has been used with some success in the design of end-blocks of prestressed concrete beams.

In 1960 Rowe and Zielinski (32) published a research report concerning the stress distribution in the anchorage zone of post-tensioned prestressed concrete members. They compared Guyon's theory with the results of photo-elastic tests performed by Christodulides (39-40) and also with the results of their own tests on concrete prisms. Their comparison showed that Guyon's theory considerably underestimated the maximum tensile stress developed in the block by, in some cases, as much as fifty percent. It should be pointed out here that Guyon's theory was primarily developed for the two-dimensional case of plane-stress and the model used by Rowe and Zielinski for their experiments, i.e. prisms loaded through square rigid plates (three dimensional loading) was different from the model used by Guyon. Hence good agreement between the results of the two different models could not be expected. Bleich (41) also developed a two dimensional solution by making use of an Airy stress function.

Ban, Muguruma and Ogaki (42) reported a reasonable agreement between predicted strains by Bleich and strains measured in their tests with electrical resistance gauges across a longitudinal axis. The work by Bleich(41) was extended theoretically to three dimensions by Sievers (43) using a modification of Bleich's two dimensional approach. Good agreement was reported by Muguruma et al. between surface strains measured on the outside of a concrete block and those predicted theoretically along the internal central axis, but no justification was given for this wholly irrelevant comparison.

An exact theory for end-block analysis for two and three dimensional loading, satisfying all the equations of elasticity and the boundary conditions within the elastic limit has been given by Iyengar (33). The theoretical values calculated by Iyengar's exact solution were checked against experimental results obtained by Muguruma et al. (9). In these tests prisms and cubes were loaded through strip loading pieces of increasing width. Three ratios of block depth to width (H/bx) were considered (2, 1, 0.6). The comparison showed that there was a good correlation for large values of strip loading width with H/bx of 2 and 1.

Muguruma et al. argued that the assumption made by Iyengar that the initial crack took place when the calculated maximum tensile splitting stress on the central axis of the concrete block exceeded the tensile strength of concrete was not strictly true. Muguruma et al's experiments indicated that the initial crack did not always appear along the central axis of the block and plastic deformation took place by reason of higher tensile stress in some critical part of the block just before reaching the initial cracking level. However, as was pointed out by Muguruma et al. for all practical purposes the assumption made by Iyengar for approximate elastic solution was reasonable.

7.3 Comparison and Discussion of Reviewed Work

The theoretical solution presented, in common with most other theories, assumes concrete to be a homogeneous, isotropic, elastic material. In the theories discussed here, failure of the material is governed by some form of limiting tensile stress or strain criterion. There is no doubt that the assumption that this material behaves as a linearly elastic homogeneous solid is a serious one; without making this assumption any attempt at a completely theoretical solution of the state of stress of a prism under concentrated loading becomes totally intractable. In particular, as was shown in the previous chapters, the manner in which a member is loaded can affect the behaviour of the material and therefore the values of the limiting stresses and strains which occur when the member is loaded to failure. Perhaps one of the very serious implications of such an assumption is that the values of the elastic moduli of concrete in compression and tension are equal and remain constant throughout the entire loading range. Some authorities such as Chen (44) have argued that concrete loaded in uniaxial compression, as shown in Fig.7.1, indicate characteristic differences in behaviour through three distinct stages of loading :

(i) in the first stage, the action is nearly linearly elastic;

(ii) in the second stage, an appreciable part of the nonlinear deformation is irreversible or plastic;

(iii) in the third stage, which begins at approximately 75 to 85 percent of the ultimate load, a general breakdown of the internal continuity of the material develops, and the unstable strain-softening portion of the stress-strain curve gradually develops for increasing deformation.

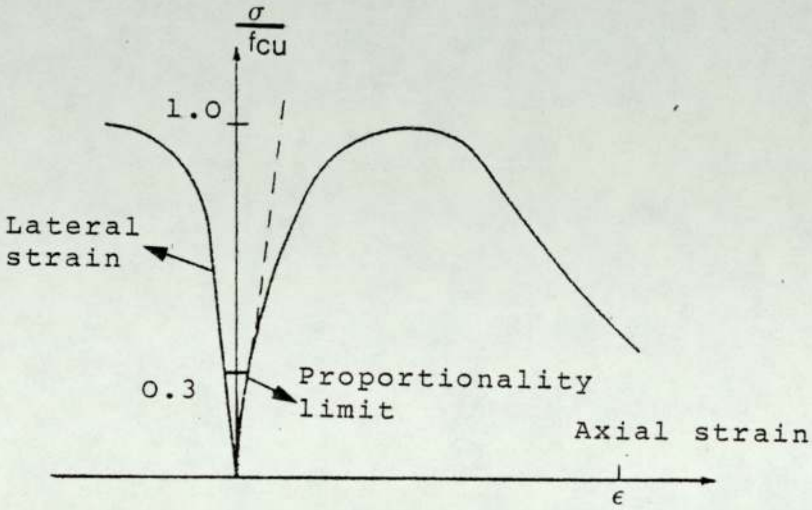

Fig. 7.1 Typical plot of compressive stress Vs. axial and lateral srain.

In his discussion of the modulus of elasticity Guyon (45) claims that for stress values up to 0.1fcu there is an instantaneous or immediate modulus of elasticity. It then decreases as the stress increases.

The distribution of transverse stresses on the prism's central lines as obtained through various theories and experiments, has been presented by Zielinski et al. (32) and here is shown in Figs. 7.2a to 7.5a. These results are predicted by normal symmetrical loading for four ratios of S_x/b_x (width of loading piece to that of concrete specimen), 0.31, 0.43, 0.53 and 0.67. Although the value of

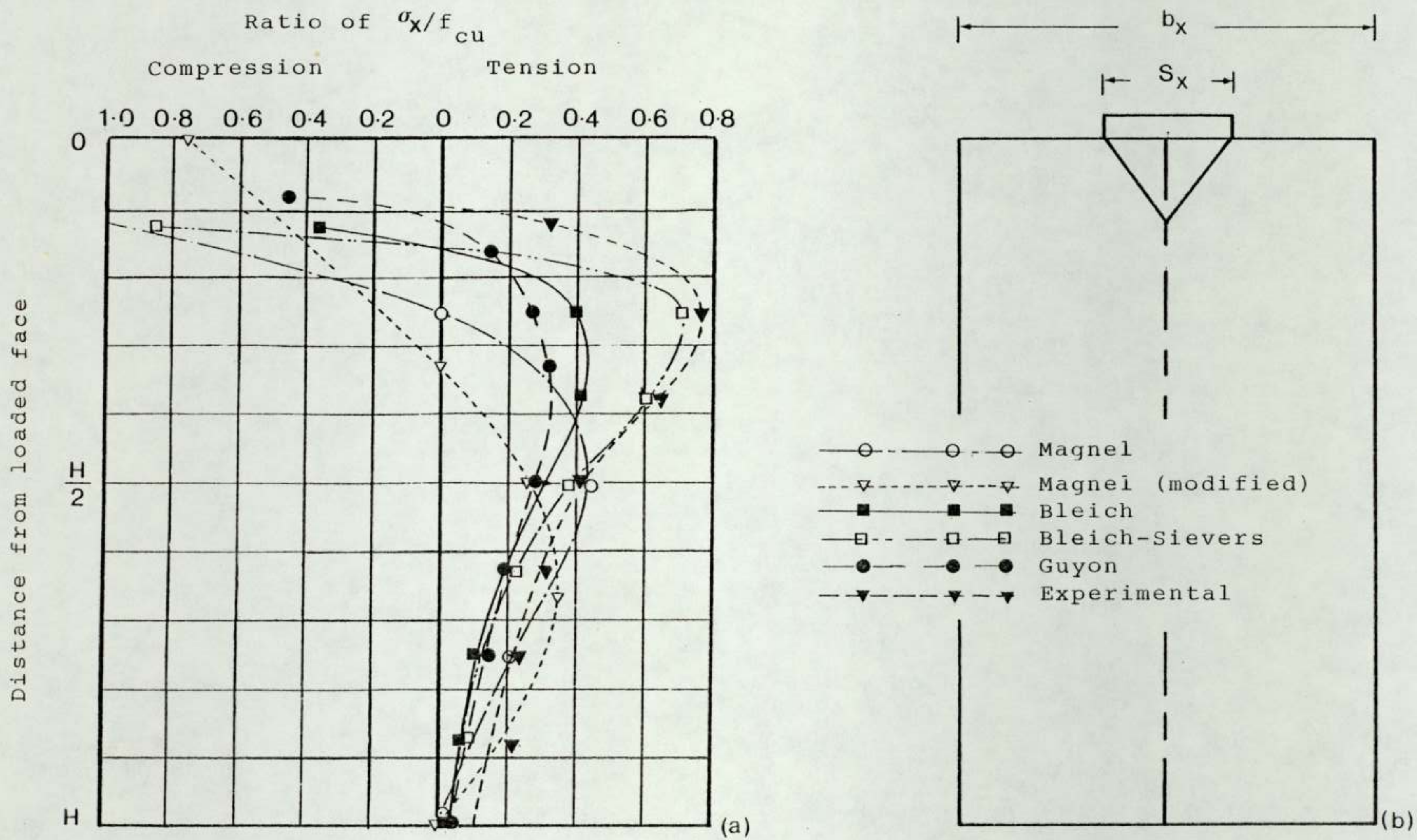

Fig 7.2 Theoretical and experimental transverse stresses for ratio of $S_x/b_x = 0.31$ as function of uniform compression.

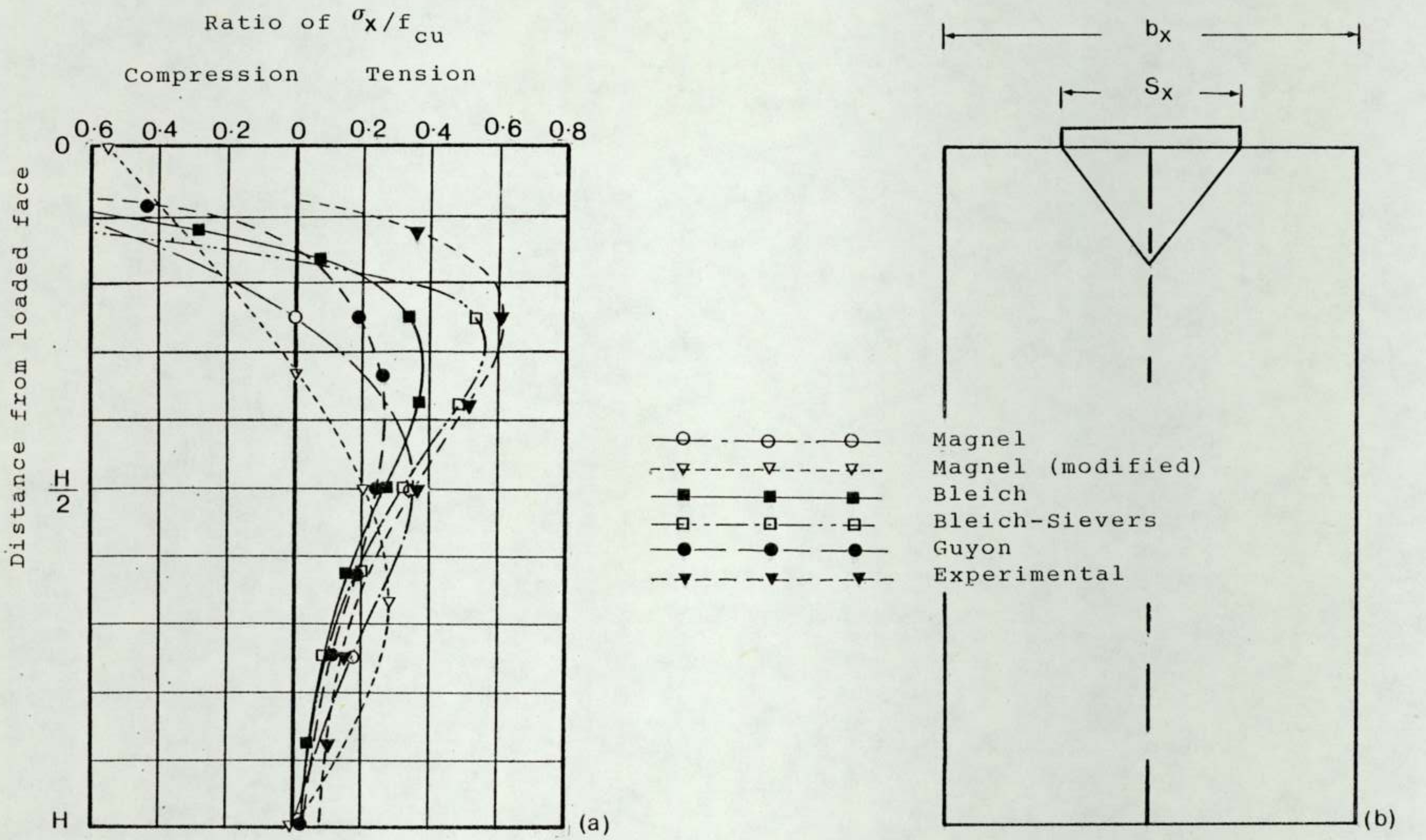

Fig. 7.3 Theoretical and experimental transverse stresses for ratio of $S_x/b_x = 0.43$ as function of uniform compression.

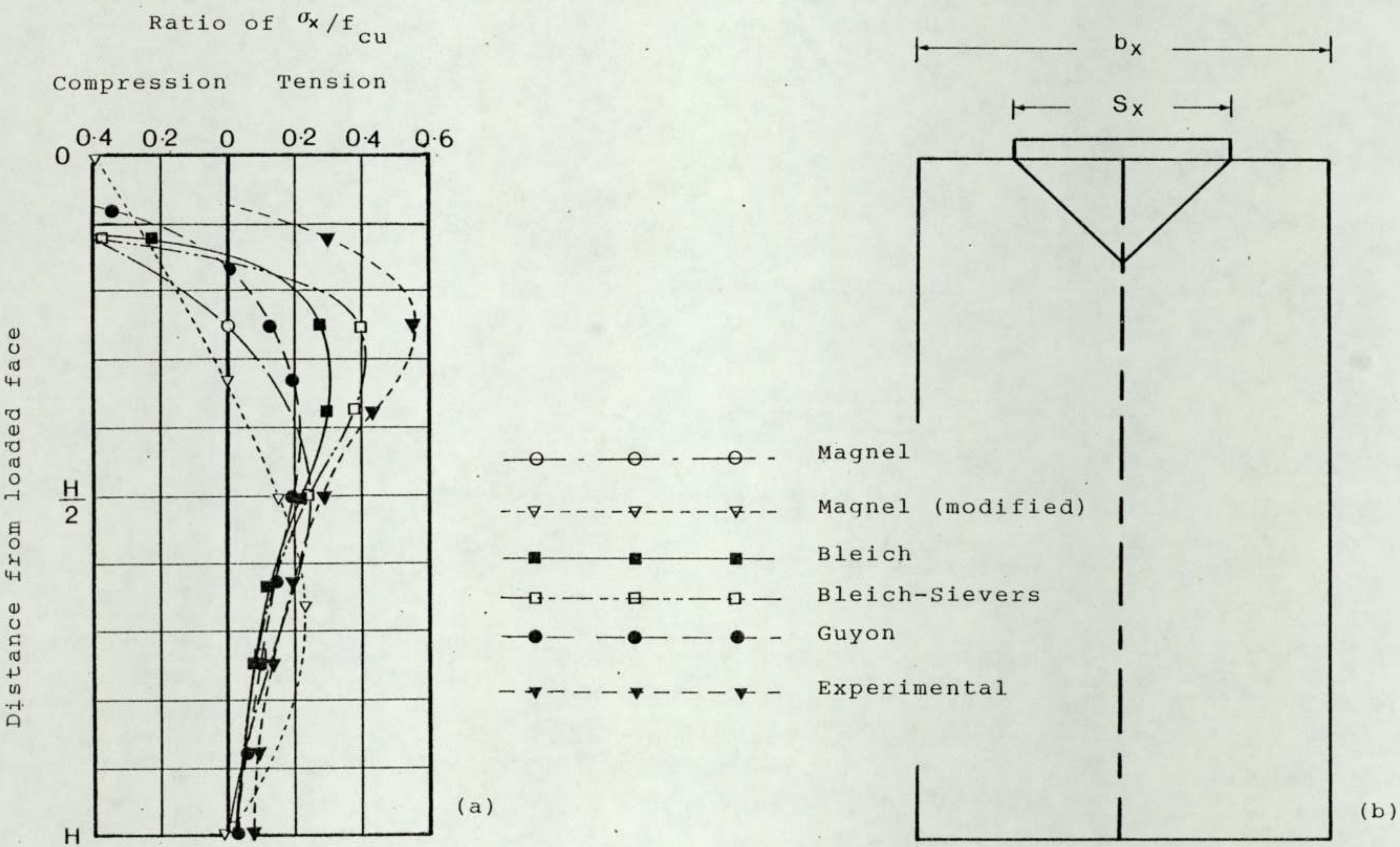

Fig. 7.4 Theoretical and experimental transverse stresses for ratio of $S_x/b_x = 0.53$ as function of uniform compression

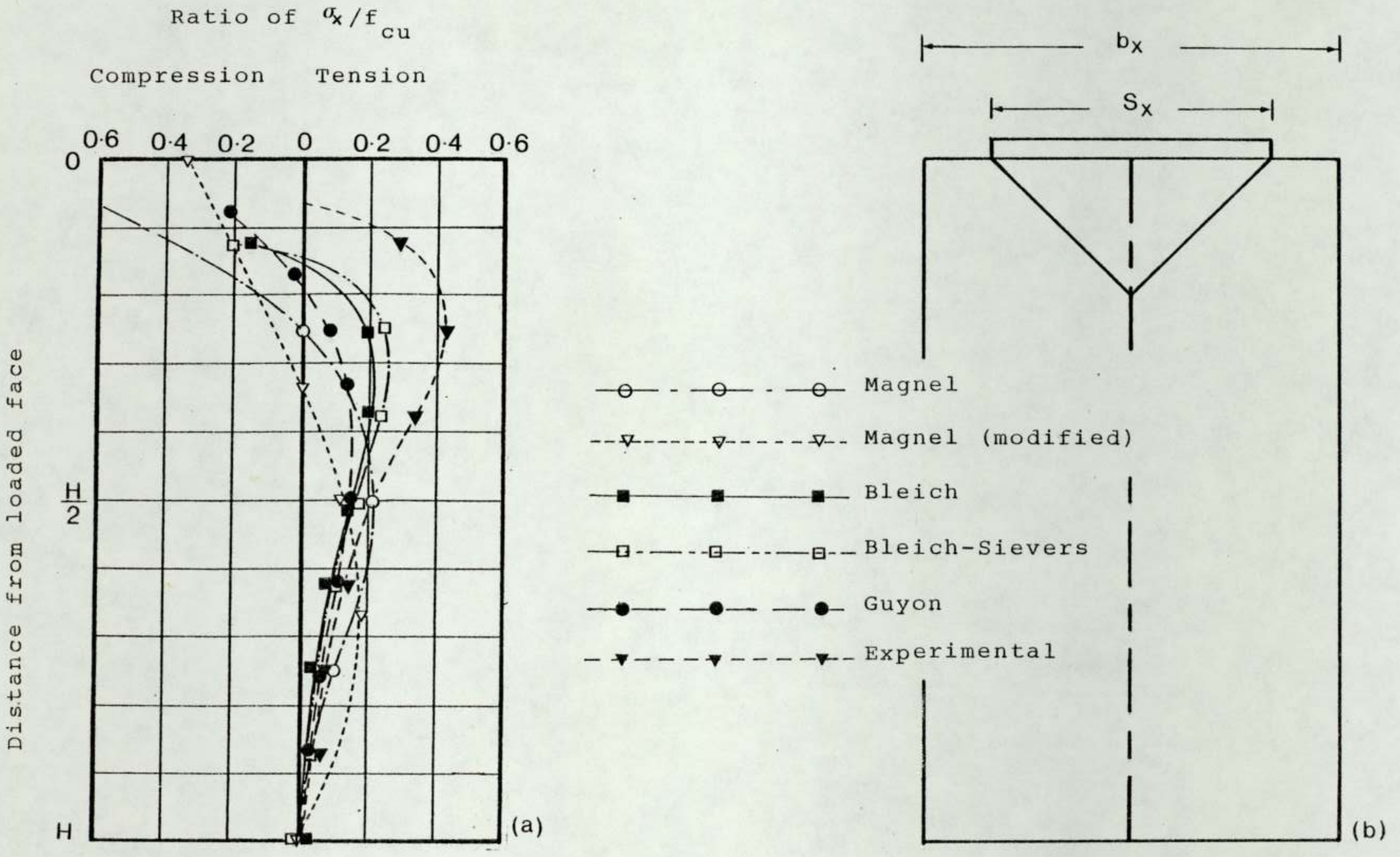

Fig. 7.5 Theoretical and experimental transverse stresses for ratio of $S_x/b_x = 0.67$ as function of uniform compression.

the maximum tensile stress, its distance from the top of the prism and the point of zero stress all differ for various theories, nevertheless the general pattern of the stress distribution presented by all the researchers is the same. This pattern of transverse stress distribution can be explained as follows :

Owing to the different stiffness characteristics of the steel plate and concrete, the bearing plate restrains the lateral expansion of the concrete, thus inducing complex triaxial compressive stresses in the concrete below the plate. The increase in bearing strength as the ratio of S_x/b_x increases (as was noticed in previous chapters) is in fact due to an increase of the load-carrying capacity of the material in the region beneath the loaded surface, which is in a state of high compressive stress.

From the plotted results it can also be concluded that for concrete prisms ($H > 2b_x$) loaded concentrically through various ratios of stiff bearing to concrete surface area, failure generally initiates along the boundary of a cone at points of maximum shear stress. Once the shear resistance along the surface of the cone is overcome, the cone is forced into the concrete block, creating a wedging action and setting up high tensile stresses perpendicular to the load. The propagation of tensile cracks in the complex compression-tension stress field, caused by the wedging action of the cone, appears to govern the failure of the prism under such loading. The experimental results of the tests carried out by Zielinski et al. (32), Fig. 7.2a to 7.5a, indicates that the position of the maximum tensile stress is nearly the same for different ratios of S_x/b_x but the actual value of the tensile stress decreases for increasing ratios

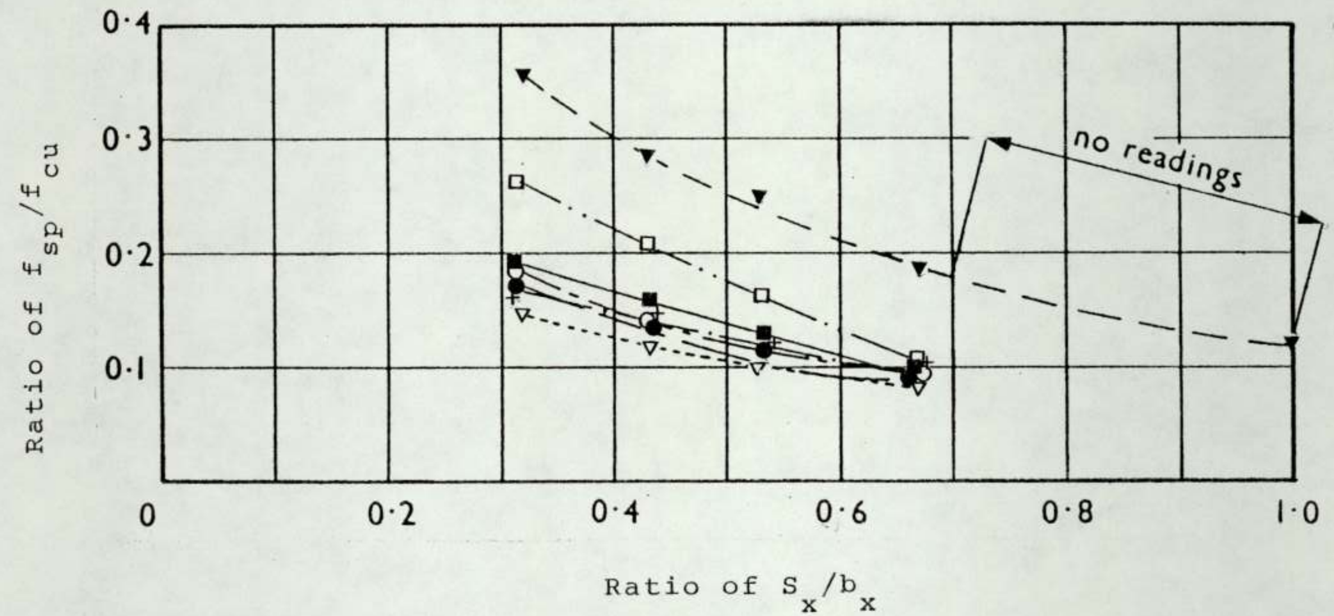

Fig. 7.6 - Relation between tensile stress (f_{sp}) and increasing ratios of S_x/b_x for various theoretical and experimental results.

Magnel

Magnel (modified)

Bleich

Guyon

Experimental

Bleich-Sievers

Morsch

of S_x/b_x. Fig. 7.6 shows the theoretical and experimental ratios of tensile to compressive force as a function of S_x/b_x. The fact that the maximum tensile stress occurs at approximately the same distance from the loading force for varying ratios of S_x/b_x can be attributed to the specimen's height being twice its width, which results in there being little or no influence from the frictional force between the concrete and the lower platen of the machine. On the other hand, as the ratio of S_x/b_x increases the compressive stresses extend overa greater depth of the block which in effect reduces the amount of tensile stress as shown in Fig. 7.6.

Consequently mode of failure proposed by Author for each of the tests with different ratios of S_x/b_x are those shown in Figs. 7.2b to 7.5b. This pattern of failure is similar to that presented for narrow strip loading (Photograph 7.1). As can be seen from the photograph, when cubes are loaded through a narrow strip loading, failure occurs with the formation of a wedge and is accompanied by sharp splitting. However, as the area of the loading piece increases there forms a double cone and multiple vertical cracks.

Of course it is noted that in all the tests carried out by the Author loading was on a cubic specimen, which is more susceptible to the frictional force between the concrete and the lower platen. It should also be remarked that, as shown in Photograph 7.1, the depth of the wedge increases for greater width of loading piece. Although it was not possible to obtain the exact angles of failure, nevertheless Photograph 7.1 clearly shows that this angle increases with wider loading pieces.

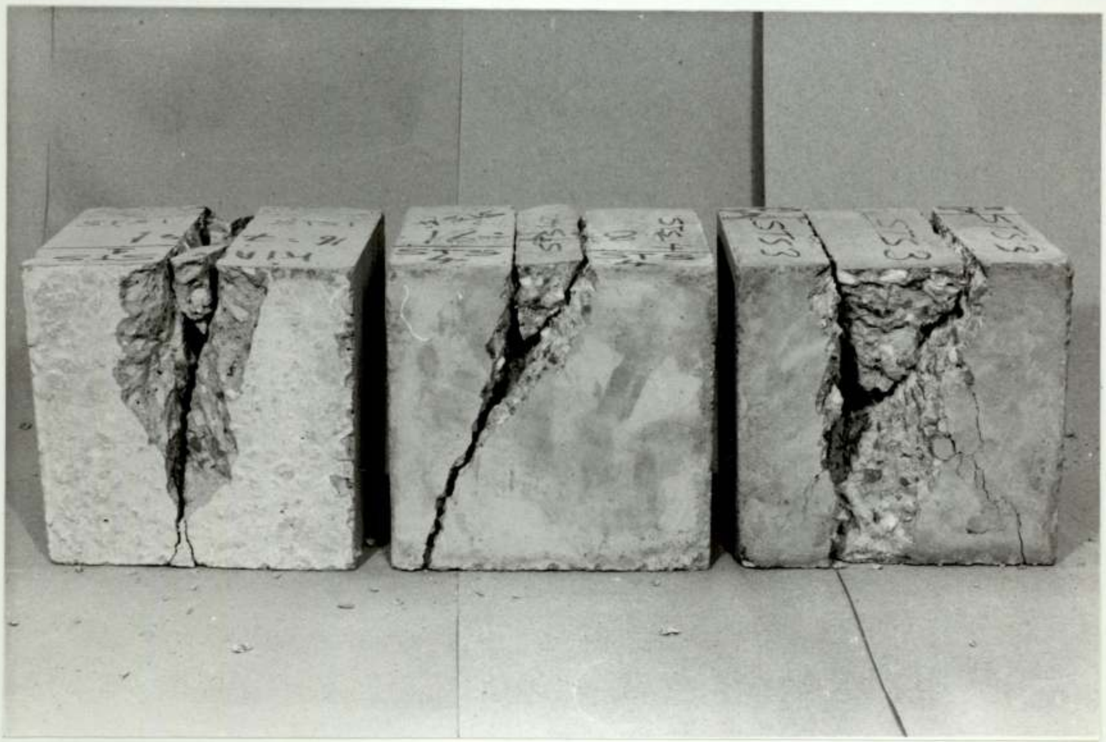

Plate 7.1 Comparison of crack formation for increasing ratio of S_x/b_x on 150 mm cubes.

(Scale 1:3.95)

CHAPTER EIGHT

FINITE ELEMENT ANALYSIS OF THE BEHAVIOUR OF CONCRETE CUBES LOADED CONCENTRICALLY THROUGH FLEXIBLE STEEL BASE PLATES

8.1 Introduction

Up to Chapter Six inclusive in this work, empirical formulae were developed for calculating the ultimate load of a foundation loaded through rigid and flexible steel base plates. In tests with flexible steel base plates it was observed that as load increased, except with a very thick steel base plate(40 mm) the plates lifted up at their free ends. At failure plates were permanently deformed into a shallow V-shape and plastic hinges occured in the steel plate close to the knife edge load. The development of the empirical formulae was based on the assumption of a rectangular block pattern of stress distribution, whose width corresponded to the contact length of an non-flexible bearing at failure. It was pointed out that the real contact length was an important factor in finding the bearing capacity of the concrete under such a loading configuration.

As a result of such findings it was felt desirable to make some theoretical determination of the stress distribution which resulted from the type of loading described above.

The theories discussed in Chapter Seven were concerned with the distribution of stress when the load had been applied through a rigid steel base plate; however, no fundamental approach to the problem of investigating the distribution of stress in a foundation loaded through a flexible base plate using a linear method had been attempted until the work reported in this thesis.

In this chapter an attempt has been made to use a plane-stress finite element method with the available knowledge of the experimental results presented in previous chapters in order to bridge the gap in the existing work.

8.2 Theory

In recent years the finite element method has become widely accepted by the engineering profession as an extremely valuable method of analysis. The reason for this development is that a variety of problems with different boundary conditions can be dealt with automatically by means of the electronic digital computer, once a suitable analysis program has been written. Through such an analytical method it is possible to obtain an estimate of the stress and the strain throughout the element, and typically at the centre, on a two-dimensional grid which represents the elastic stress plane.

Plane elasticity problems may be separated into two classes, namely plane-stress and plane-strain problems. In plane-stress problems the continuum is usually thin relative to other dimensions, and stresses normal to plane are absent In plane-strain problems, however, the strain normal to the plane of loading is assumed to be zero. In this thesis it was decided to use a rectangular element in plane-stress as this was most suitable for the type of loading considered. The method of solving plane-stress problems through the derivation of the element stiffness matrix of a 4 node rectangular element having two degree of freedom per node has been investigated by many researchers, and a clear description of the element has been given by Rocky et al. (46).

8.3 Finite Element Characteristics and Computer Program

The program that was used in this work has been developed at the University of Aston, notably by Bray (47). This program was suitable for running on the ICL 1900 and has now been extended in this research to use the GINO graphical library for plotting the output data.

The displacement functions in the X and Y directions were assumed to take the form

$$u = a_1 + a_2X + a_3Y + a_4XY$$

$$v = a_5 + a_6X + a_7Y + a_8XY$$

respectively, implying that the strain take a linear form of

$$\frac{du}{dX} = a_2 + a_4Y$$

$$\frac{dv}{dY} = a_7 + a_8X$$

$$\frac{du}{dY} + \frac{dv}{dX} = a_2 + a_4Y + a_7 + a_8X$$

8.4 Subdivision of Structure

In finite element analysis it is assumed that elements are only interconnected at their nodes. This assumption by itself means that continuity requirements are generally only satisfied at the nodal points. In general, therefore, the accuracy of the solution increases with the number of elements taken. On the other hand, the increase in the number of elements results in an increase in the required

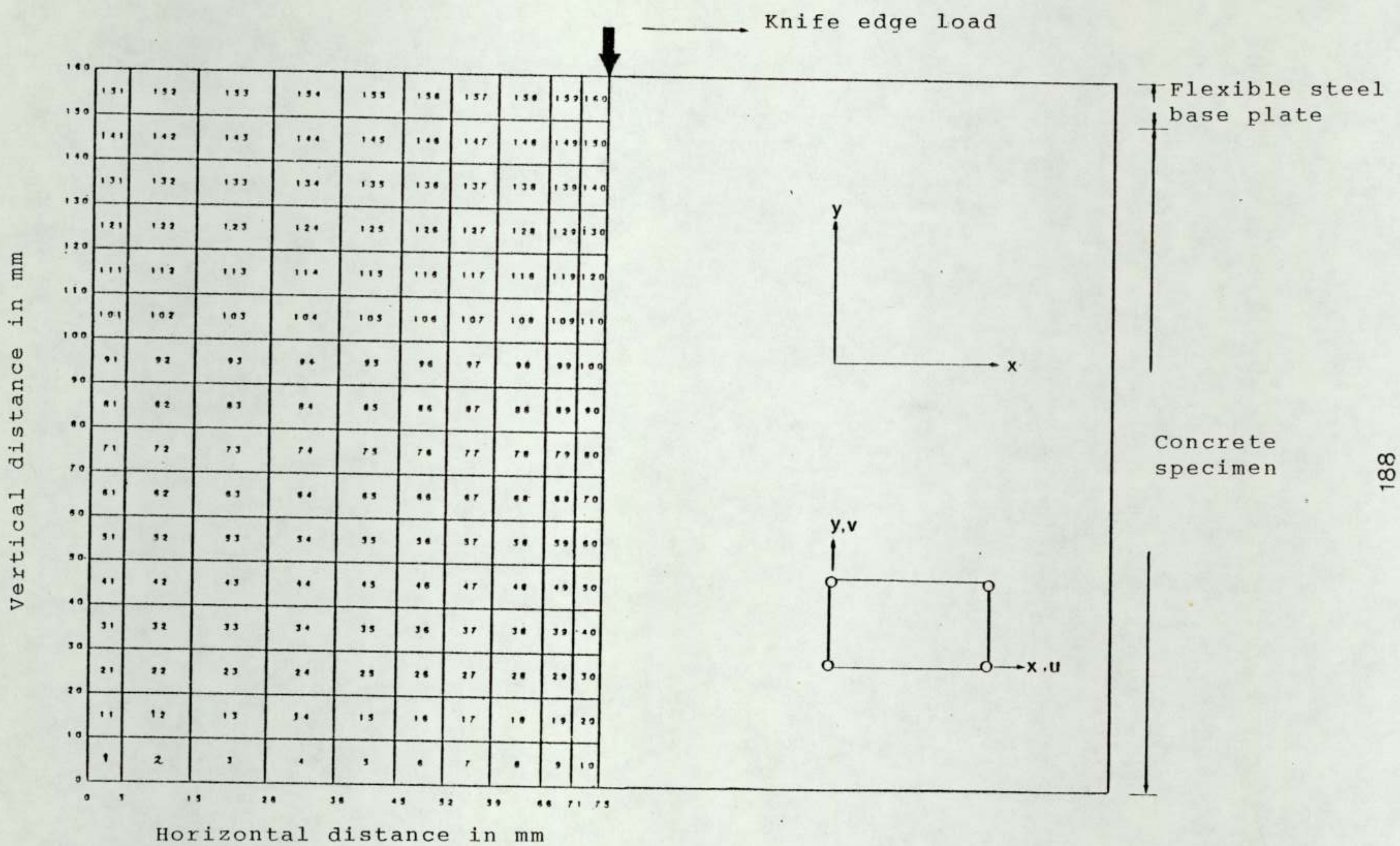

Fig 8.1 - The subdivision of concrete cube and flexible steel base plate considered in the finite element analysis.

computation time, which in effect increases the cost of obtaining a solution.

The model chosen in this work was to resemble the tests presented in Table 3.1 of Chapter 3. These tests (S5 to S12) were on 150mm concrete cubes, in which a knife-edge load was applied symmetrically through plates of increasing thicknesses (4 to 40mm). A mesh of 320 rectangular elements with a 4 node having two degrees of freedom per node (Fig. 8.1a) was considered in this investigation. The top row of the elements belong to the steel base plate and the rows below to the concrete cube.

A plate of dimensions 150x150mm and of thickness 150mm was used to simulate the concrete cube. A plate of 150x150mm and of various thicknesses (4, 22.5, 40mm) was used to simulate the flexible steel base plate which was placed on the top surface of the cube. As a result of the loading being symmetrical about the vertical centre line it was only necessary to analyse half the plate; the nodes on the centre line being given horizontal restraint. The plate was regarded as being fixed at its base by giving two degrees of fixity to the nodes along the base. This condition in effect implied that friction between the cube and the lower platen of the machine does not allow the cube to expand freely. This assumption was made in the light of the tests carried out by both the Author and Zielinski et al. (48). These tests showed that in general there did not appear to be any visible cracking near the base of the concrete cube until 90% of the ultimate load. This is considered to be due to the existence of friction which does not allow the cube to expand freely. In this situation straining can take place without the disintegration of the cube. It must be pointed out here that although the tests showed no visible cracking at the base of the concrete until approximately 90% of ultimate load, this does not mean that micro-cracking which is the main factor for nonlinear behaviour of concrete did not occur.

The value of Poisson's ratio recommended by many authorities (44, 50, 51) for concrete under uniaxial compressive loading ranges from 0.15 to 0.22. Nevertheless, Chen (44) claims that under uniaxial loading Poisson's ratio remains constant until approximately 80% of cylinder strength, at which stress the apparent Poisson's ratio begins to increase. This ratio is believed to be around 0.5 for the unstable crushing phase. However, for the analysis carried out in this work, Poisson's ratio of the concrete and the steel base plates were taken to be 0.2 and 0.35 respectively for the first set of results.

The load applied at the position corresponding to the centre of the upper face of the steel base plate is shown in Fig. 8.1. The magnitude of this load and values of modulus of elasticity for different thicknesses of base plate correspond to the measured ultimate load and measured values of Young's Modulus, as presented in Table 3.1 of Chapter 3.

8.5 Theoretical Results

8.5.1 Initial Results

In order to analyse the theoretical axial and lateral stress distribution in both the flexible steel base plate and the concrete under knife-edge loading, three of the tests presented in Chapter 3 with 4, 22.5 and 40 mm thick steel base plates were considered. In

Table 3.1 of Chapter 3 the three tests considered are presented under the test numbers S5, S10 and S12 and the properties of both the steel base plate and the concrete are also given. The ultimate loads for these tests are shown in the same table. The results of the computer analysis are shown in Tables 8.1, 8.2 and 8.3, in which both axial (toprow) and transverse stresses (bottom row) at the centre of each element are given, the negative sign indicating compresive stress. The Poisson's ratios used in this analysis were 0.2 and 0.35 for the concrete and steel base plate respectively.

The results of axial stresses for the three rows of concrete elements parallel to the loaded surface (121-150) are plotted for the three tests in Figs. 8.2, 8.3 and 8.4. The axial stress for each row of elements is drawn with respect to the top face elements in that paricular row. The plotted results for 4mm thick base plate show that only the elements within the vicinity of the applied load are under noticeable stress.

In fact, the stress distribution predicted by the plane-stress analysis indicates that in the planes some distance below the top surface, the stresses are more uniformly distributed than in the cross-sections just below the loaded surface. This pattern of distribution can be very clearly seen in Fig. 8.2 with the 4mm thick base plate. The elements 141 to 146 experience no axial stress but there is a rapid increase in axial stress from elements 147 to 150. With the thicker steel base plates, as shown in Figs. 8.3 and 8.4, the axial stresses are more uniformly distributed along the cross-sections parallel to the loading surface.

It should be pointed out here that some of the elements of

KEY

Element No
Lateral
Axial

151 .9507E -1 .7298E -1	152 .7457E 0 .6861E -1	153 .1435E 1 -.9542E -2	154 .1027E 1 -.8317E -2	155 -.1389E 1 .6002E -1	156 -.5745E 1 .1508E 0	157 -.1450E 2 .3393E 0	158 -.3438E 2 -.7553E 1	159 -.6294E 2 -.3731E 1	160 -.1059E 3 -.1411E 3
141 -.3808E -3 .5078E 0	142 -.1369E 0 .1131E 0	143 -.5418E 0 -.3568E 0	144 -.1321E 1 -.6954E 0	145 -.2586E 1 -.1085E 1	146 -.4534E 1 -.2074E 1	147 -.6880E 1 -.5730E 1	148 -.8371E 1 -.1806E 2	149 -.6675E 1 -.4055E 2	150 .7047E 1 -.6087E 2
131 -.4235E -1 .8431E 0	132 -.3318E 0 -.1160E 0	133 -.1014E 1 -.1120E 1	134 -.2044E 1 -.2125E 1	135 -.3266E 1 -.3702E 1	136 -.4230E 1 -.6560E 1	137 -.4093E 1 -.1203E 2	138 -.1278E 1 -.2197E 2	139 .3999E 1 -.3084E 2	140 .5835E 1 -.3389E 2
121 -.3058E -1 .6230E 0	122 -.3184E 0 -.6770E 0	123 -.9400E 0 -.2181E 1	124 -.1650E 1 -.3848E 1	125 -.2049E 1 -.6241E 1	126 -.1742E 1 -.9594E 1	127 -.3986E 0 -.1408E 2	128 .2071E 1 -.1932E 2	129 .3891E 1 -.2292E 2	130 .4626E 1 -.2424E 2
111 -.2084E -1 -.1542E 0	112 -.2042E 0 -.1548E 1	113 -.5528E 0 -.3336E 1	114 -.7813E 0 -.5358E 1	115 -.5583E 0 -.7881E 1	116 .1979E 0 -.1074E 2	117 .1380E 1 -.1372E 2	118 .2741E 1 -.1663E 2	119 .3709E 1 -.1849E 2	120 .4046E 1 -.1911E 2
101 -.7112E -2 -.1302E 1	102 -.6722E -1 -.2593E 1	103 -.1303E 0 -.4397E 1	104 .1604E -2 -.6427E 1	105 .4801E 0 -.8673E 1	106 .1213E 1 -.1086E 2	107 .2040E 1 -.1284E 2	108 .2876E 1 -.1460E 2	109 .3410E 1 -.1566E 2	110 .3592E 1 -.1600E 2
91 .3136E -2 -.2588E 1	92 .3860E -1 -.3664E 1	93 .1754E 0 -.5285E 1	94 .4983E 0 -.7105E 1	95 .1024E 1 -.8957E 1	96 .1628E 1 -.1060E 2	97 .2210E 1 -.1195E 2	98 .2742E 1 -.1308E 2	99 .3067E 1 -.1374E 2	100 .3174E 1 -.1395E 2
81 .8715E -2 -.3823E 1	82 .9714E -1 -.4654E 1	83 .3353E 0 -.6000E 1	84 .7252E 0 -.7522E 1	85 .1214E 1 -.8995E 1	86 .1695E 1 -.1022E 2	87 .2111E 1 -.1118E 2	88 .2469E 1 -.1195E 2	89 .2680E 1 -.1238E 2	90 .2748E 1 -.1252E 2
71 .1044E -1 -.4898E 1	72 .1158E 0 -.5512E 1	73 .3790E 0 -.6572E 1	74 .7596E 0 -.7788E 1	75 .1180E 1 -.8931E 1	76 .1555E 1 -.9847E 1	77 .1860E 1 -.1054E 2	78 .2110E 1 -.1108E 2	79 .2253E 1 -.1138E 2	80 .2299E 1 -.1147E 2
61 .9670E -2 -.5775E 1	62 .1080E 0 -.6224E 1	63 .3460E 0 -.7035E 1	64 .6716E 0 -.7972E 1	65 .1009E 1 -.8838E 1	66 .1294E 1 -.9517E 1	67 .1517E 1 -.1002E 2	68 .1695E 1 -.1040E 2	69 .1796E 1 -.1061E 2	70 .1827E 1 -.1066E 2
51 .7884E -2 -.6466E 1	52 .8349E -1 -.6805E 1	53 .2640E 0 -.7415E 1	54 .5059E 0 -.8112E 1	55 .7523E 0 -.8746E 1	56 .9584E 0 -.9237E 1	57 .1117E 1 -.9596E 1	58 .1243E 1 -.9870E 1	59 .1313E 1 -.1002E 2	60 .1335E 1 -.1007E 2
41 .3525E -2 -.7011E 1	42 .4631E -1 -.7289E 1	43 .1429E 0 -.7738E 1	44 .2808E 0 -.8222E 1	45 .4330E 0 -.8658E 1	46 .5686E 0 -.8998E 1	47 .6763E 0 -.9248E 1	48 .7628E 0 -.9440E 1	49 .8116E 0 -.9546E 1	50 .8270E 0 -.9578E 1
31 .4589E -2 -.7478E 1	32 -.1146E -1 -.7723E 1	33 -.2699E -1 -.8023E 1	34 -.1280E -1 -.8301E 1	35 .5320E -1 -.8561E 1	36 .1327E 0 -.8780E 1	37 .2025E 0 -.8947E 1	38 .2607E 0 -.9079E 1	39 .2942E 0 -.9153E 1	40 .3047E 0 -.9175E 1
21 -.2470E -1 -.7971E 1	22 -.9800E -1 -.8172E 1	23 -.3067E 0 -.8268E 1	24 -.4011E 0 -.8316E 1	25 -.3885E 0 -.8435E 1	26 -.3435E 0 -.8565E 1	27 -.2983E 0 -.8675E 1	28 -.2591E 0 -.8765E 1	29 -.2362E 0 -.8816E 1	30 -.2289E 0 -.8832E 1
11 .7330E -1 -.8685E 1	12 -.4441E 0 -.8735E 1	13 -.7847E 0 -.8373E 1	14 -.8800E 0 -.8234E 1	15 -.8745E 0 -.8267E 1	16 -.8457E 0 -.8344E 1	17 -.8169E 0 -.8418E 1	18 -.7922E 0 -.8481E 1	19 -.7778E 0 -.8517E 1	20 -.7732E 0 -.8529E 1
1 -.1092E 1 -.1054E 2	2 -.1268E 1 -.9020E 1	3 -.1358E 1 -.8269E 1	4 -.1368E 1 -.8077E 1	5 -.1360E 1 -.8073E 1	6 -.1351E 1 -.8119E 1	7 -.1344E 1 -.8170E 1	8 -.1339E 1 -.8215E 1	9 -.1336E 1 -.8242E 1	10 -.1336E 1 -.8250E 1

Table 8.1 - Axial and lateral stress (N/mm^2) at the centre of each element for the cube loaded through a knife-edge load via 4 mm thick steel base plate.

KEY

Element No

Lateral

Axial

151 -.3166E 0 .2640E 1	152 -.9337E 0 -.4009E 0	153 -.2709E 1 -.3938E 1	154 -.5875E 1 -.7097E 1	155 -.1027E 2 -.1055E 2	156 -.1521E 2 -.1456E 2	157 -.2047E 2 -.2042E 2	158 -.2645E 2 -.3759E 2	159 -.3134E 2 -.7831E 2	160 -.3403E 2 -.1717E 3
141 .4956E 0 .5087E 1	142 -.6375E 0 -.2338E 1	143 -.2295E 1 -.9534E 1	144 -.3467E 1 -.1583E 2	145 -.3512E 1 -.2245E 2	146 -.2360E 1 -.2959E 2	147 .1003E 0 -.3787E 2	148 .4642E 1 -.4847E 2	149 .1041E 2 -.5665E 2	150 .1622E 2 -.5304E 2
131 -.2791E -1 .2444E 0	132 .5347E -1 -.5101E 1	133 -.3114E 0 -.1199E 2	134 -.4145E 0 -.1842E 2	135 .3752E 0 -.2476E 2	136 .2050E 1 -.3091E 2	137 .4513E 1 -.3691E 2	138 .7734E 1 -.4241E 2	139 .9910E 1 -.4477E 2	140 .8874E 1 -.4573E 2
121 .3645E -1 -.4436E 1	122 .2282E 0 -.8420E 1	123 .6849E 0 -.1418E 2	124 .1431E 1 -.2005E 2	125 .2680E 1 -.2559E 2	126 .4292E 1 -.3041E 2	127 .6018E 1 -.3439E 2	128 .7564E 1 -.3756E 2	129 .8270E 1 -.3945E 2	130 .8864E 1 -.4002E 2
111 .3193E -1 -.8702E 1	112 .3663E 0 -.1157E 2	113 .1150E 1 -.1613E 2	114 .2290E 1 -.2104E 2	115 .3649E 1 -.2556E 2	116 .4994E 1 -.2923E 2	117 .6163E 1 -.3202E 2	118 .7149E 1 -.3426E 2	119 .7780E 1 -.3550E 2	120 .7916E 1 -.3589E 2
101 .3755E -1 -.1233E 2	102 .4064E 0 -.1432E 2	103 .1294E 1 -.1776E 2	104 .2508E 1 -.2166E 2	105 .3787E 1 -.2522E 2	106 .4898E 1 -.2801E 2	107 .5783E 1 -.3008E 2	108 .6508E 1 -.3168E 2	109 .6908E 1 -.3257E 2	110 .7050E 1 -.3284E 2
91 .3406E -1 -.1526E 2	92 .3868E 0 -.1658E 2	93 .1235E 1 -.1910E 2	94 .2365E 1 -.2208E 2	95 .3488E 1 -.2483E 2	96 .4407E 1 -.2696E 2	97 .5104E 1 -.2850E 2	98 .5650E 1 -.2968E 2	99 .5958E 1 -.3033E 2	100 .6051E 1 -.3053E 2
81 .2910E -1 -.1751E 2	82 .3341E 0 -.1837E 2	83 .1070E 1 -.2018E 2	84 .2037E 1 -.2241E 2	85 .2974E 1 -.2449E 2	86 .3718E 1 -.2609E 2	87 .4267E 1 -.2725E 2	88 .4690E 1 -.2813E 2	89 .4923E 1 -.2861E 2	90 .4996E 1 -.2875E 2
71 .2310E -1 -.1917E 2	72 .2673E 0 -.1975E 2	73 .8569E 0 -.2105E 2	74 .1627E 1 -.2269E 2	75 .2363E 1 -.2423E 2	76 .2941E 1 -.2542E 2	77 .3362E 1 -.2628E 2	78 .3683E 1 -.2692E 2	79 .3859E 1 -.2727E 2	80 .3913E 1 -.2738E 2
61 .1685E -1 -.2037E 2	62 .1954E 0 -.2080E 2	63 .6229E 0 -.2175E 2	64 .1179E 1 -.2294E 2	65 .1709E 1 -.2405E 2	66 .2125E 1 -.2490E 2	67 .2428E 1 -.2552E 2	68 .2660E 1 -.2598E 2	69 .2786E 1 -.2623E 2	70 .2826E 1 -.2631E 2
51 .1152E -1 -.2123E 2	52 .1186E 0 -.2161E 2	53 .3709E 0 -.2233E 2	54 .6982E 0 -.2316E 2	55 .1019E 1 -.2392E 2	56 .1280E 1 -.2450E 2	57 .1475E 1 -.2492E 2	58 .1627E 1 -.2523E 2	59 .1711E 1 -.2541E 2	60 .1737E 1 -.2546E 2
41 .1124E -2 -.2187E 2	42 .3008E -1 -.2228E 2	43 .7750E -1 -.2283E 2	44 .1567E 0 -.2336E 2	45 .2687E 0 -.2381E 2	46 .3872E 0 -.2416E 2	47 .4898E 0 -.2441E 2	48 .5758E 0 -.2461E 2	49 .6255E 0 -.2472E 2	50 .6412E 0 -.2475E 2
31 .6823E -2 -.2247E 2	32 -.1017E 0 -.2293E 2	33 -.3139E 0 -.2331E 2	34 -.5196E 0 -.2351E 2	35 -.5917E 0 -.2366E 2	36 -.5810E 0 -.2382E 2	37 -.5448E 0 -.2395E 2	38 -.5053E 0 -.2406E 2	39 -.4797E 0 -.2412E 2	40 -.4713E 0 -.2414E 2
21 -.6998E -1 -.2326E 2	22 -.3022E 0 -.2373E 2	23 -.9879E 0 -.2376E 2	24 -.1436E 1 -.2351E 2	25 -.1602E 1 -.2342E 2	26 -.1640E 1 -.2343E 2	27 -.1635E 1 -.2348E 2	28 -.1619E 1 -.2353E 2	29 -.1606E 1 -.2356E 2	30 -.1602E 1 -.2357E 2
11 .2124E 0 -.2470E 2	12 -.1203E 1 -.2493E 2	13 -.2221E 1 -.2389E 2	14 -.2620E 1 -.2327E 2	15 -.2741E 1 -.2305E 2	16 -.2767E 1 -.2299E 2	17 -.2763E 1 -.2300E 2	18 -.2752E 1 -.2301E 2	19 -.2744E 1 -.2303E 2	20 -.2741E 1 -.2303E 2
1 -.2987E 1 -.2923E 2	2 -.3518E 1 -.2546E 2	3 -.3824E 1 -.2350E 2	4 -.3894E 1 -.2283E 2	5 -.3902E 1 -.2259E 2	6 -.3898E 1 -.2252E 2	7 -.3891E 1 -.2250E 2	8 -.3885E 1 -.2250E 2	9 -.3882E 1 -.2250E 2	10 -.3881E 1 -.2251E 2

Table 8.2 - Axial and lateral stress (N/mm^2) at the centre of each element for cube loaded through a knife-edge load via a 22.5 mm thick steel base plate.

KEY
Element No
Lateral
Axial

151 -.3432E -2 -.5170E 1	152 -.4156E 0 -.7,51E 1	153 -.1623E 1 -.1037E 2	154 -.3552E 1 -.1388E 2	155 -.5890E 1 -.1806E 2	156 -.8226E 1 -.2378E 2	157 -.1043E 2 -.3378E 2	158 -.1261E 2 -.5773E 2	159 -.1410E 2 -.9716E 2	160 -.1469E 2 -.1543E 3
141 -.3475E 0 -.8224E 1	142 -.1164E 1 -.1518E 2	143 -.1837E 1 -.2208E 2	144 -.1737E 1 -.2804E 2	145 -.7397E 0 -.3380E 2	146 .9609E 0 -.3938E 2	147 .3346E 1 -.4500E 2	148 .6886E 1 -.5040E 2	149 .1064E 2 -.5204E 2	150 .1375E 2 -.4494E 2
131 .1360E 0 -.1304E 2	132 .2674E 0 -.1793E 2	133 .3708E 0 -.2406E 2	134 .9123E 0 -.2959E 2	135 .2126E 1 -.3462E 2	136 .3811E 1 -.3899E 2	137 .5769E 1 -.4256E 2	138 .7715E 1 -.4478E 2	139 .8428E 1 -.4467E 2	140 .6969E 1 -.4469E 2
121 .4065E -1 -.1757E 2	122 .4439E 0 -.2079E 2	123 .1200E 1 -.2560E 2	124 .2200E 1 -.3036E 2	125 .3461E 1 -.3449E 2	126 .4775E 1 -.3771E 2	127 .5901E 1 -.3994E 2	128 .6625E 1 -.4133E 2	129 .6762E 1 -.4205E 2	130 .7109E 1 -.4221E 2
111 .4579E -1 -.2129E 2	112 .4590E 0 -.2339E 2	113 .1377E 1 -.2693E 2	114 .2538E 1 -.3071E 2	115 .3709E 1 -.3398E 2	116 .4695E 1 -.3638E 2	117 .5411E 1 -.3801E 2	118 .5920E 1 -.3918E 2	119 .6234E 1 -.3978E 2	120 .6258E 1 -.3996E 2
101 .3776E -1 -.2419E 2	102 .4178E 0 -.2553E 2	103 .1290E 1 -.2805E 2	104 .2387E 1 -.3093E 2	105 .3414E 1 -.3345E 2	106 .4206E 1 -.3530E 2	107 .4768E 1 -.3657E 2	108 .5187E 1 -.3750E 2	109 .5398E 1 -.3799E 2	110 .5476E 1 -.3814E 2
91 .3088E -1 -.2635E 2	92 .3490E 0 -.2720E 2	93 .1095E 1 -.2897E 2	94 .2036E 1 -.3111E 2	95 .2900E 1 -.3303E 2	96 .3551E 1 -.3446E 2	97 .4010E 1 -.3545E 2	98 .4347E 1 -.3618E 2	99 .4531E 1 -.3657E 2	100 .4584E 1 -.3669E 2
81 .2375E -1 -.2790E 2	82 .2741E 0 -.2846E 2	83 .8678E 0 -.2972E 2	84 .1619E 1 -.3130E 2	85 .2308E 1 -.3274E 2	86 .2826E 1 -.3383E 2	87 .3190E 1 -.3459E 2	88 .3459E 1 -.3515E 2	89 .3603E 1 -.3546E 2	90 .3647E 1 -.3555E 2
71 .1749E -1 -.2896E 2	72 .2012E 0 -.2938E 2	73 .6371E 0 -.3032E 2	74 .1188E 1 -.3149E 2	75 .1694E 1 -.3256E 2	76 .2074E 1 -.3337E 2	77 .2342E 1 -.3394E 2	78 .2541E 1 -.3436E 2	79 .2648E 1 -.3458E 2	80 .2681E 1 -.3465E 2
61 .1152E -1 -.2967E 2	62 .1307E 0 -.3006E 2	63 .4055E 0 -.3081E 2	64 .7480E 0 -.3168E 2	65 .1062E 1 -.3245E 2	66 .1300E 1 -.3303E 2	67 .1470E 1 -.3343E 2	68 .1598E 1 -.3373E 2	69 .1668E 1 -.3389E 2	70 .1689E 1 -.3394E 2
51 .6936E -2 -.3015E 2	52 .5600E -1 -.3058E 2	53 .1565E 0 -.3124E 2	54 .2727E 0 -.3187E 2	55 .3848E 0 -.3239E 2	56 .4795E 0 -.3275E 2	57 .5536E 0 -.3301E 2	58 .6133E 0 -.3320E 2	59 .6479E 0 -.3331E 2	60 .6587E 0 -.3334E 2
41 -.4564E -2 -.3052E 2	42 -.3534E -1 -.3107E 2	43 -.1509E 0 -.3166E 2	44 -.2931E 0 -.3206E 2	45 -.3911E 0 -.3232E 2	46 -.4310E 0 -.3250E 2	47 -.4405E 0 -.3263E 2	48 -.4381E 0 -.3273E 2	49 -.4326E 0 -.3278E 2	50 -.4305E 0 -.3280E 2
31 5366E -2 - 3096E 2	32 -.1863E 0 -.3164E 2	33 -.5970E 0 -.3210E 2	34 -.1056E 1 -.3219E 2	35 -.1341E 1 -.3218E 2	36 -.1479E 1 -.3220E 2	37 -.1543E 1 -.3222E 2	38 -.1577E 1 -.3225E 2	39 -.1590E 1 -.3227E 2	40 -.1593E 1 -.3228E 2
21 .9516E -1 -.3174E 2	22 -.4308E 0 -.3248E 2	23 -.1431E 1 -.3256E 2	24 -.2163E 1 -.3215E 2	25 -.2524E 1 -.3191E 2	26 -.2687E 1 -.3180E 2	27 -.2764E 1 -.3176E 2	28 -.2806E 1 -.3174E 2	29 -.2823E 1 -.3174E 2	30 -.2828E 1 -.3174E 2
11 .2880E 0 -.3344E 2	12 -.1615E 1 -.3391E 2	13 -.3037E 1 -.3265E 2	14 -.3663E 1 -.3181E 2	15 -.3917E 1 -.3145E 2	16 -.4024E 1 -.3129E 2	17 -.4073E 1 -.3122E 2	18 -.4098E 1 -.3119E 2	19 -.4109E 1 -.3117E 2	20 -.4112E 1 -.3117E 2
1 -.3999E 1 -.3928E 2	2 -.4745E 1 -.3450E 2	3 -.5201E 1 -.3207E 2	4 -.5338E 1 -.3121E 2	5 -.5383E 1 -.3086E 2	6 -.5400E 1 -.3071E 2	7 -.5406E 1 -.3065E 2	8 -.5410E 1 -.3061E 2	9 -.5411E 1 -.3059E 2	10 -.5411E 1 -.3059E 2

Table 8.3.- Axial and lateral stress (Nmm^{2}) at the centre of each element for the cube loaded through a knif-edge load via a 40. mm thick steel base plate.

Elements 1-150 represent concrete block

Elements 151-160 represent steel base plate

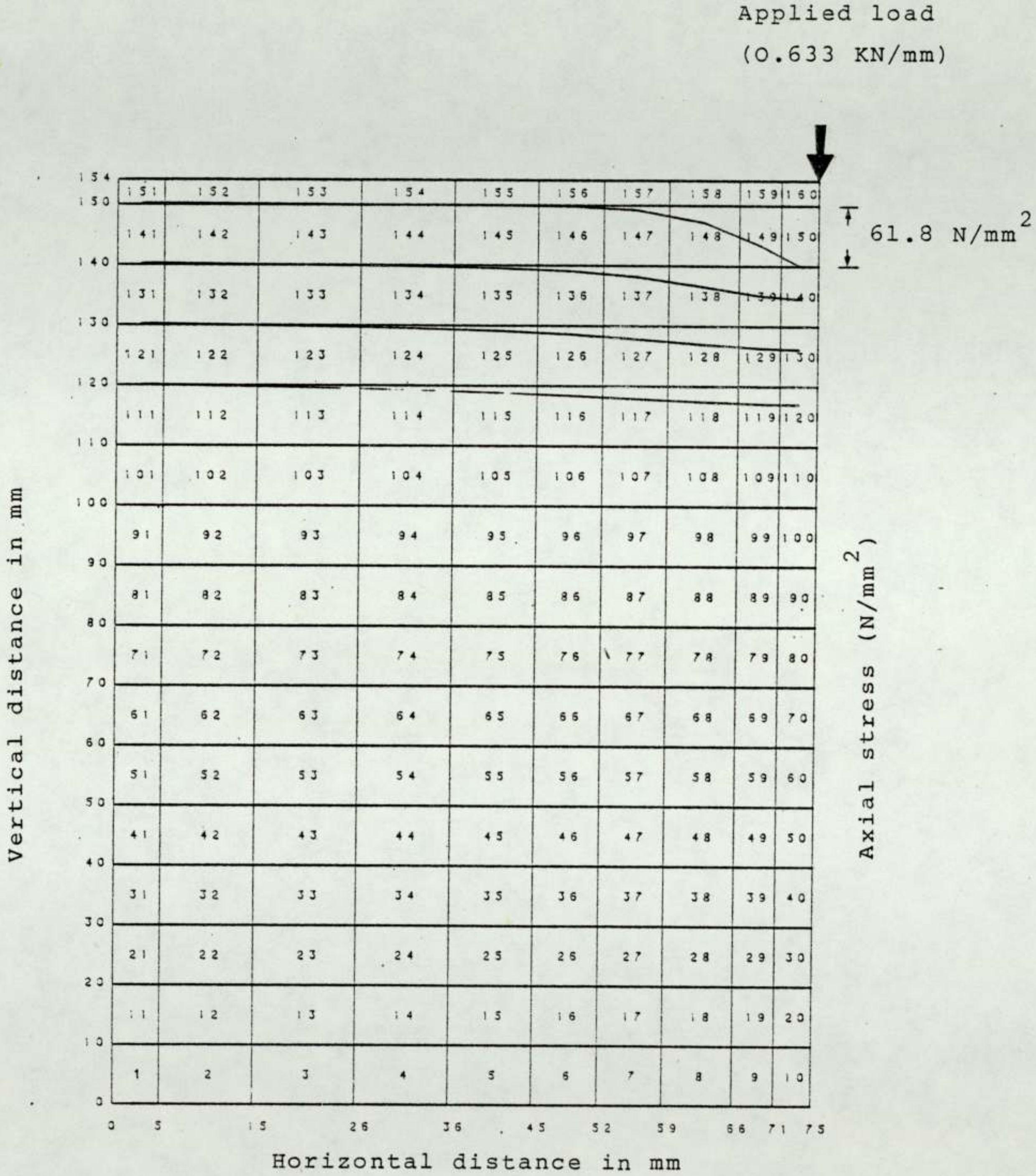

Fig. 8.2 - Axial stress profile at the centre of each element (t=4mm) for the three top row of the concrete specimen, stress lines are drawn with respect to the top of each element.

Elements 1-150 represent concrete block

Elements 151-160 represent steel base plate

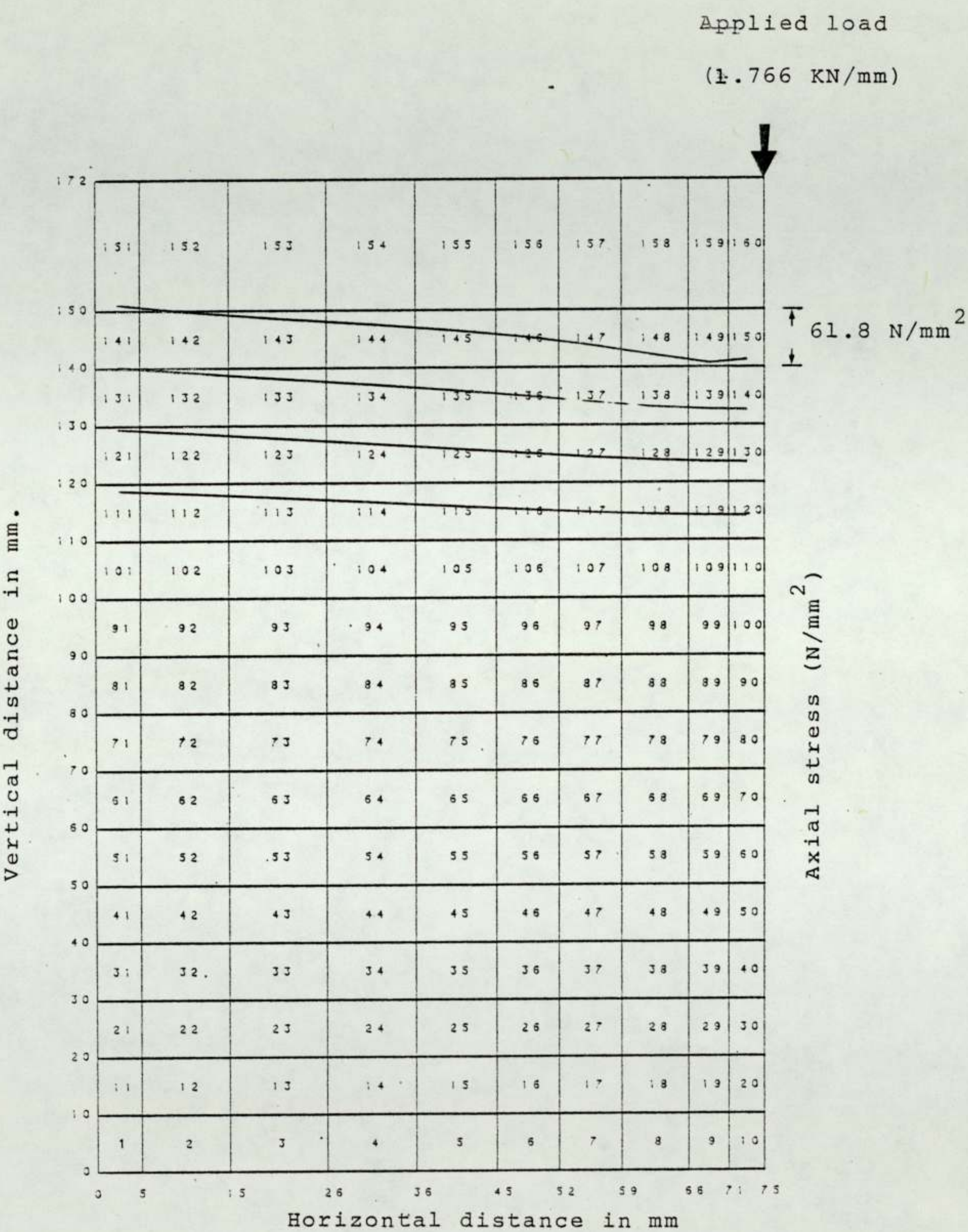

Fig. 8.3 - Axial stress profile at the centre of each element (t=22.5mm) for the three top row of the concrete specimen stress lines are drawn with respect to the top of each element.

Elements 1-150 represent concrete block

Elements 151-160 represent steel base plate

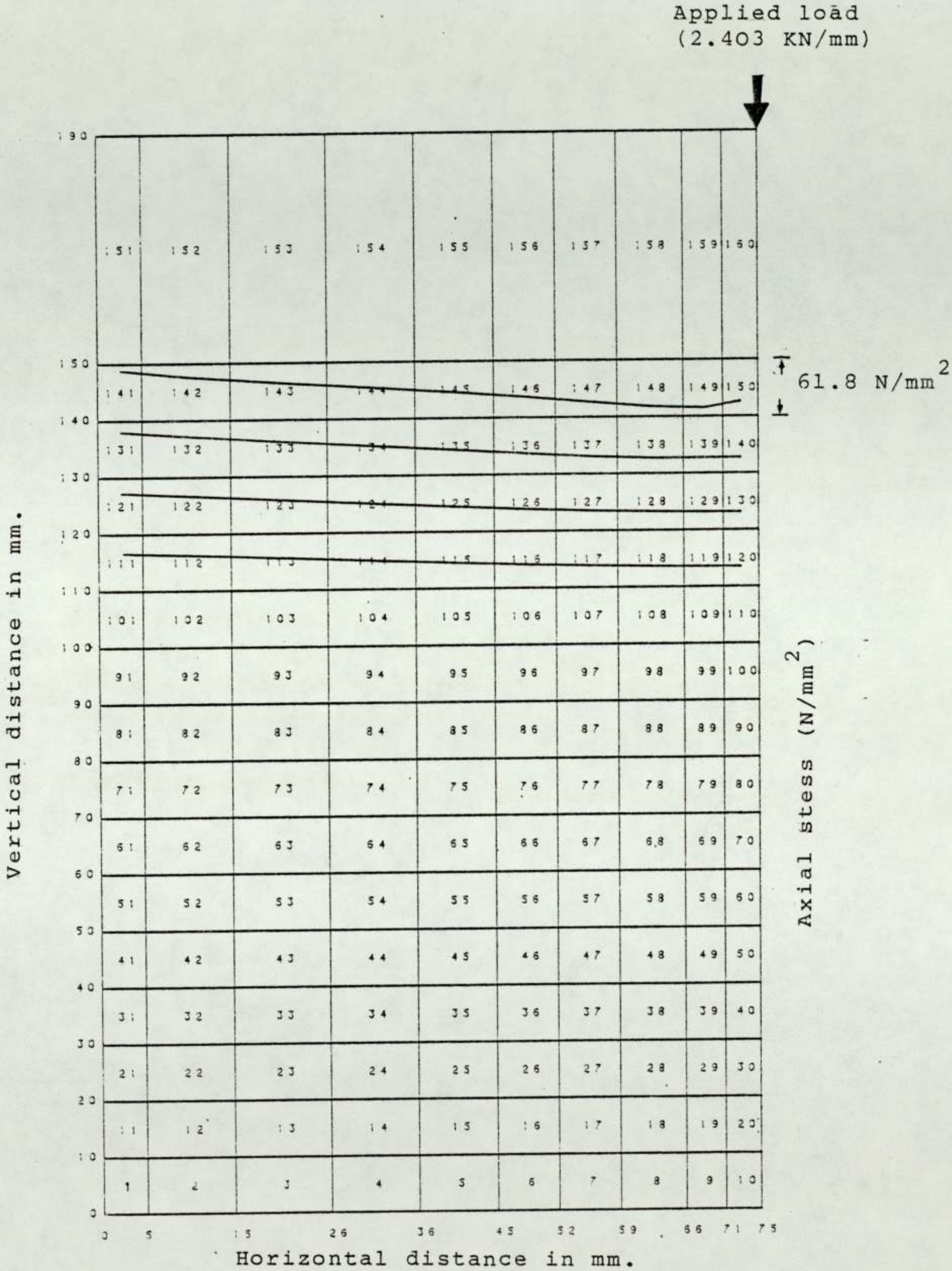

Fig. 8.4 - Axial stress profile at the centre of each element (t=40mm) for the three top rows of the concrete specimen, stress lines are drawn with respect to the top of each element.

the 4 and 22.5mm thick steel base plates near the edge are predicted by the plane-stress analysis to be in tension, as shown in Tables 8.1 and 8.2. This indicates that the plates have lifted up at their free ends. However, with 40mm thick steel base plate the stresses are all compressive, indicating that there is no lifting. Although the actual occurrence of lifting at the free end of the thin base plates and non-lifting of the thick base plates is in agreement with the experimental results obtained in Chapter 3, nevertheless the extent of lifting at failure observed experimentally was much greater than that predicted by the plane-stress analysis.

To show the stress distribution between the steel base plate and the concrete, the deformed shape of the steel plate was drawn over its original outline, for the 4, 22.5 and 40mm thick plates in Figs. 8.5, 8.6 and 8.7. As can be seen from Fig. 8.5 for a thickness of 4mm the plate goes into compression half way between elements 142 and 152; with a 22.5mm thick base plate the boundary between the two materials is in compression from the edge of elements 142 and 152. This large difference in the calculated and measured lifting up in the steel base plate can possibly be explained in the following manner.

The theoretical plane-stress analysis assumes the material to be homogeneous, isotropic and elastic. The modulus of elasticity for both concrete and steel used in the above analysis was that found in the control tests. The general stress-strain curves presented by CP110 (22) for concrete and steel are shown in Figs. 8.8 and 8.9. The moduli used here are the initial tangent moduli which are within the elastic range. However, it is clear that at failure the moduli are more likely to be the tangents BC in the stress-strain diagrams. In other words,

Elements 1-150 represent concrete block

Elements 151-160 represent steel base plate

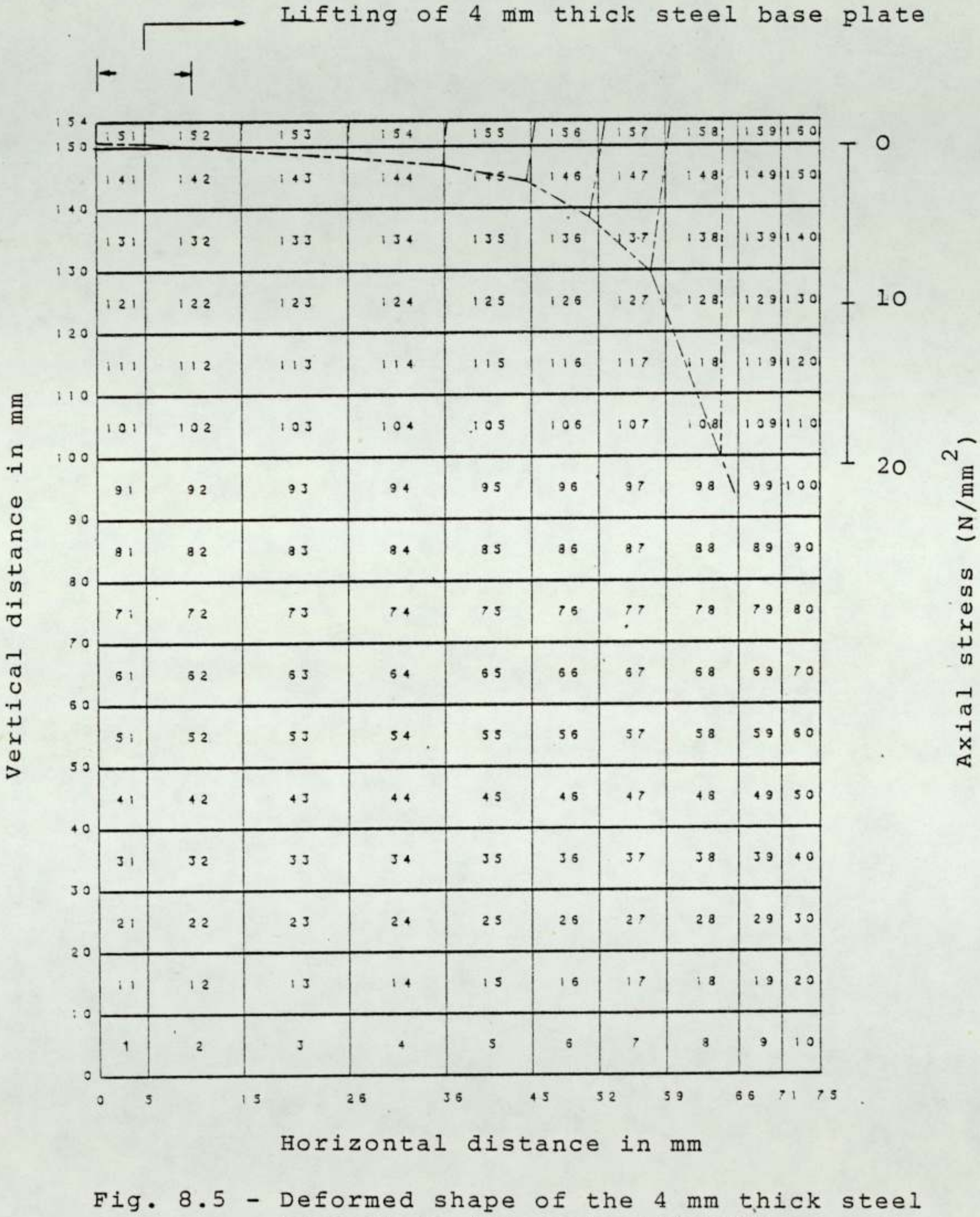

Fig. 8.5 - Deformed shape of the 4 mm thick steel base plate (elements 151-158) over its original outline of zero stress.

Elements 1-150 represent concrete block

Elements 151-160 represent steel base plate

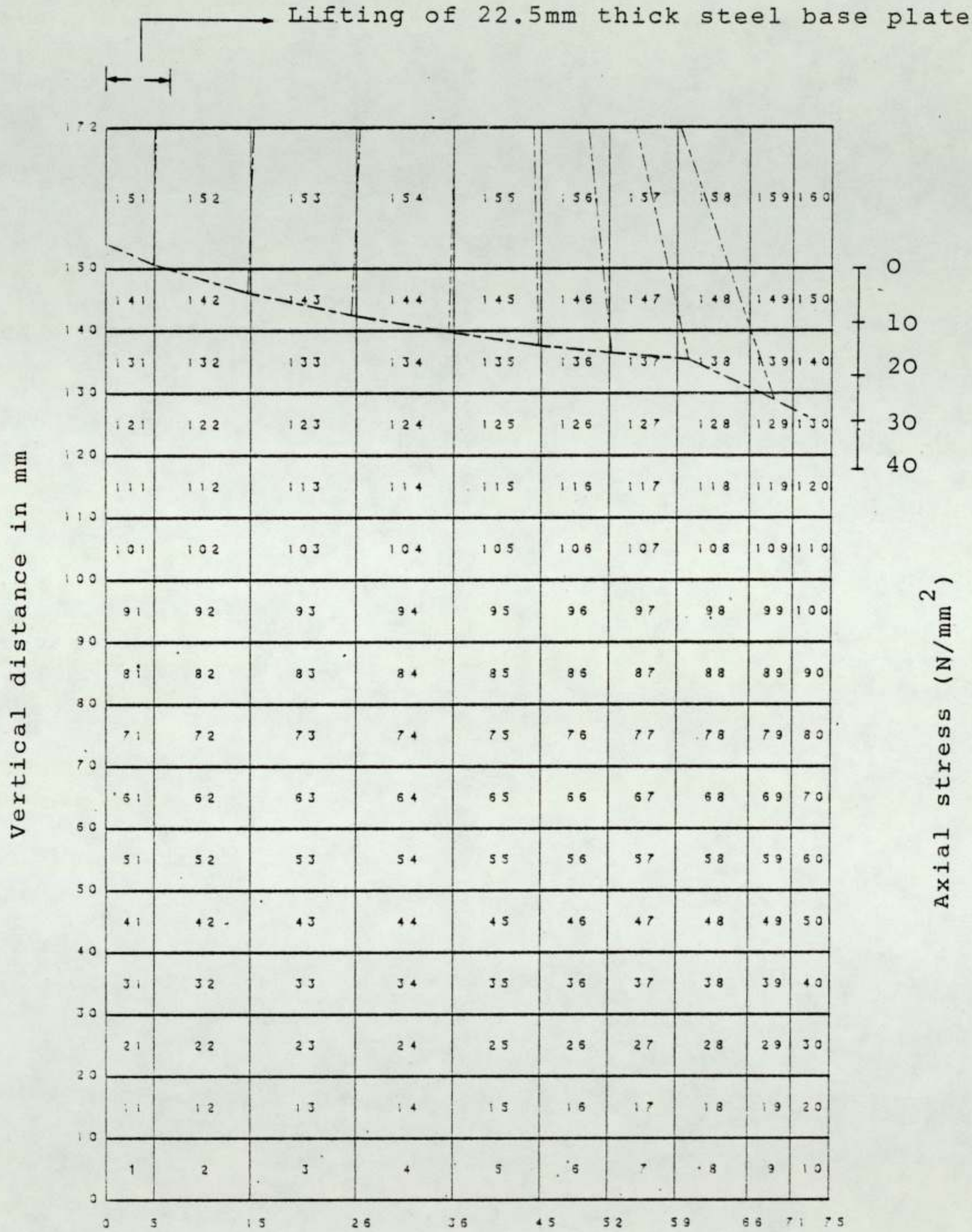

Fig. 8.6 - Deformed shape of the 22.5 thick steel base plate (elements 151-158) over its original outline of zero stress.

Elements 1-150 represent concrete block

Elements 151-160 represent steel base plate

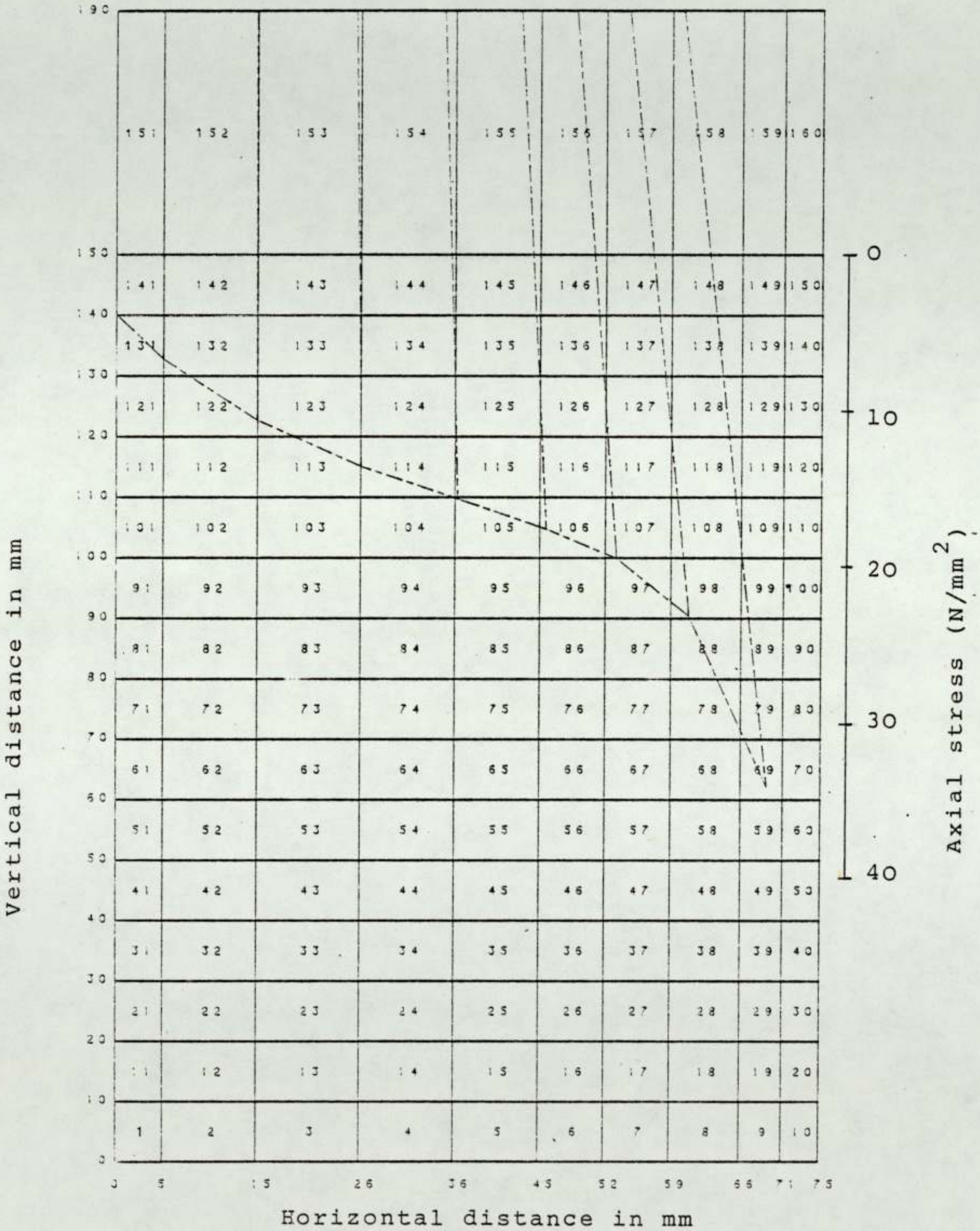

Fig. 8.7 - Deformed shape of the 40mm thick steel base plate (elements 151-158) over its original outline of zero stress.

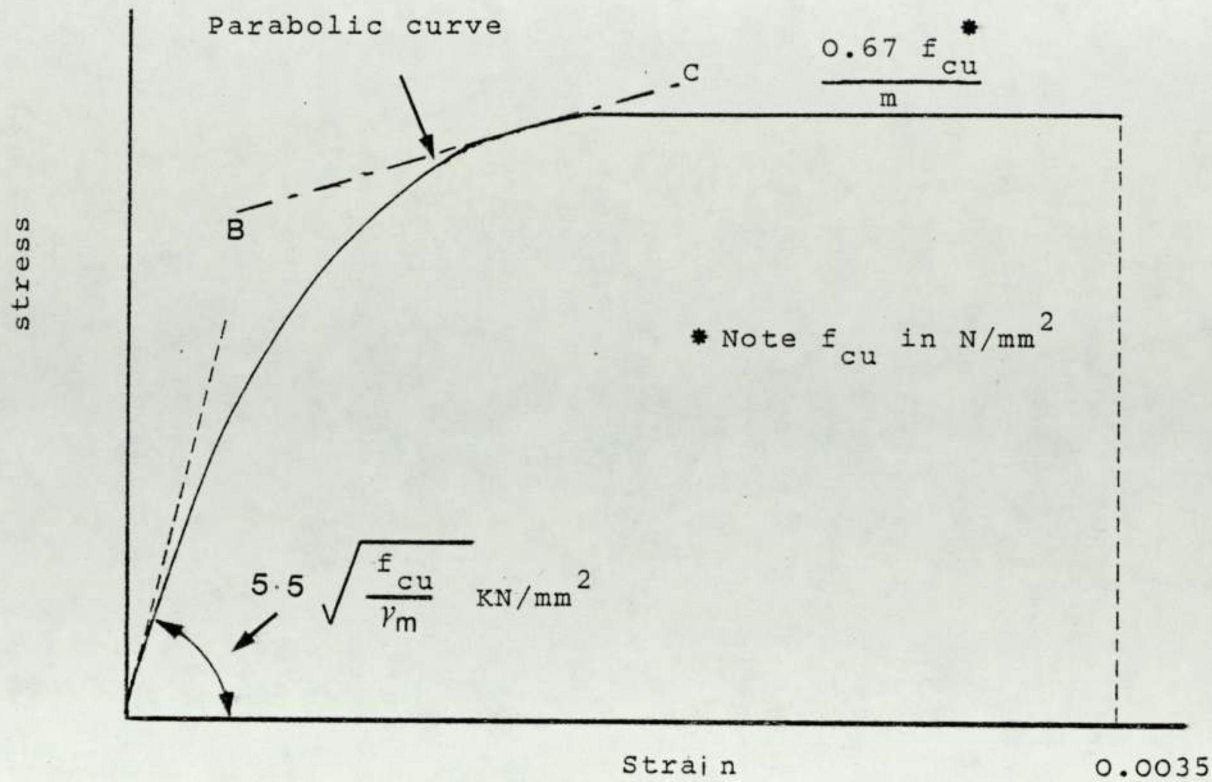

Fig. 8.8 Short term design stress-strain curve for normal weight concrete

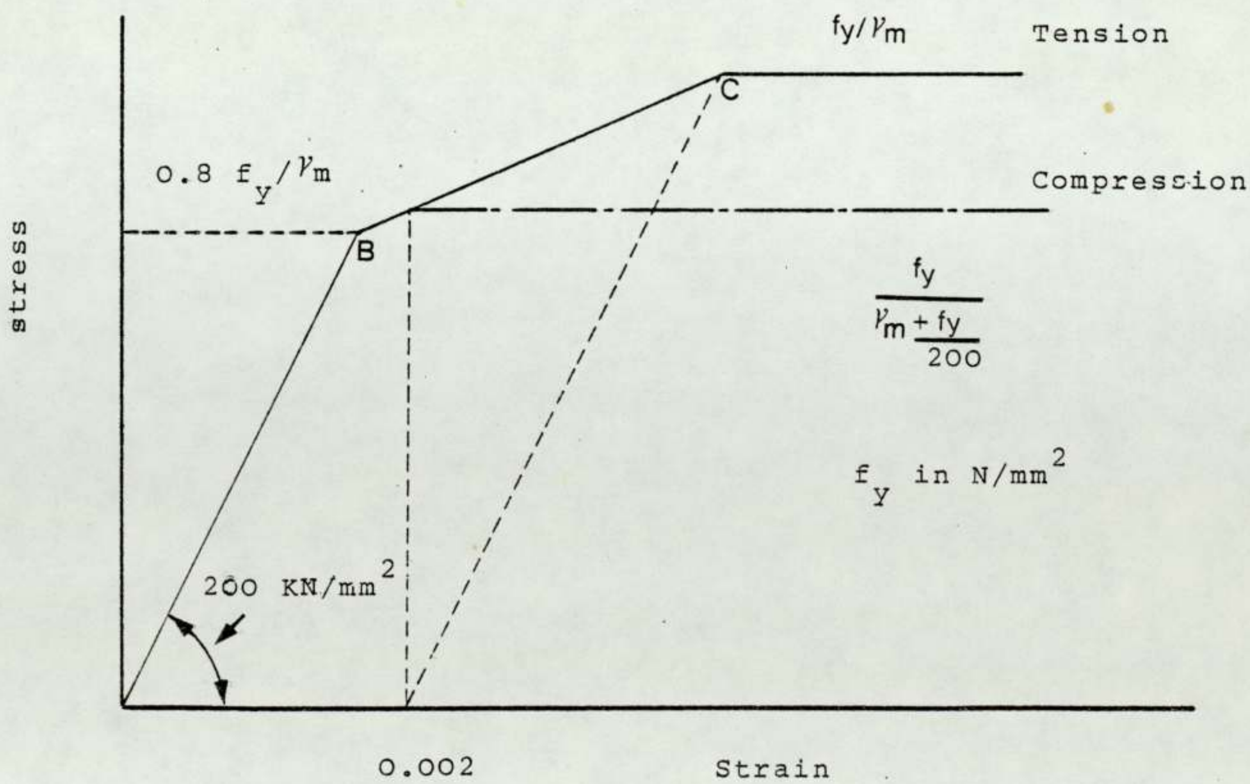

Fig. 8.9 Short term design stress-strain curve for reinforcement.

the actual values of moduli at or just before failure are much less than those used in plane-stress analysis. Therefore it would be more realistic to apply a small value of the moduli with larger Poisson's ratio for elements which were under greater concentrations of stress.

8.5.2 Secondary Results with Reduced Moduli of Elasticity

In the second series of analysis the results of tests on 4 and 22.5mm thick steel base plates were reconsidered with the following modifications. The modulus of elasticity was reduced for some elements and Poisson's ratio increased. As was discussed in section 8.5.1, the elements within the vicinity of the loaded area were under much higher stresses than the other elements. In fact, with a 4mm thick base plate, as shown in Table 8.1, elements 150 and 149 showed axial compressive stresses of 60.8 and 40 N/mm^2. The remainder of the elements were under much lower stresses. The results of the analysis with a 22.5mm thick base plate shown in Table 8.2 show that elements 150, 149 and 148 have higher values of axial stress in comparison to the other elements. Also, as was shown in Chapter 3, in the tests with flexible base plates loaded through a knife-edge loading piece, it was observed that the plate bent along the edges of the loading piece and became permanently deformed. In other words, at failure the modulus of elasticity of the plate must also have been reduced.

Consequently, for the tests with 4mm thick base plate it was decided to reduce the moduli of elasticity of elements 150, 149 of the concrete and 160 of the steel base plate to 30, 5,000 and 100 N/mm^2 respectively. The Poisson's ratios of these elements were increased to

0.25, 0.3 and 0.35. Similarly, for the test with 22.5mm thick base plate the elements 148, 149 and 150 were given elastic moduli of 15,000, 1,000 and 30 N/mm^2. The values of Poisson's ratio for these elements were taken as 0.25, 0.3 and 0.35 for elements 148, 149 and 150 respectively. In the same way, elements 160 and 159 of the steel base plate were given reduced values of moduli of elasticity and Poisson's ratio. The former became 100 and 10,000 N/mm^2 and the latter 0.35 and 0.4 respectively.

The result of plane-stress analysis for 4mm thick base plate with reduced values of Young's Modulus is shown in Table 8.4. It is of considerable interest to note that, as a result of the new values of modulus of elasticity, elements 151 to 153 at the free end of the steel plate show tensile stress. In other words, a much greater lifting up of the plate is recorded. The results of tests with 22.5mm thick base plate and reduced values of elastic modulus are shown in Table 8.5. This result also indicates an increase in the lifting up of the base plate as compared to the first series of tests under similar loading conditions. Figs. 8.10 and 8.11 show the pattern of the deformed shapes of the steel base plates (elements 151 to 158) drawn over their original positions, demonstrating clearly the lifting of the plates at their free ends.

8.6 Discussion and Conclusion

It is not claimed here that by using an elastic theory of plane-stress analysis it is possible to find the exact values of stresses and consequently the precise amount of lifting up of the steel base plate as measured experimentally. Nevertheless, the

KEY
Element No
Lateral
Axial

151 .1864E 0 -.3618E -1	152 .2016E 1 .1396E 0	153 .6041E 1 .4356E -1	154 .1140E 2 .8508E -1	155 .1750E 2 .7616E 0	156 .2457E 2 .2097E 1	157 .2940E 2 .6480E 1	158 .2091E 2 -.2152E 2	159 -.1516E 2 .1480E 2	160 -.5319E 2 -.1519E 3
141 .3740E -1 .1003E 1	142 .4299E -1 .7852E 0	143 -.1815E 0 .3436E 0	144 -.9089E 0 .3451E 0	145 -.2701E 1 .1204E 1	146 -.6730E 1 .2388E 1	147 -.1414E 2 -.1626E 1	148 -.2375E 2 -.4341E 2	149 -.1902E 2 -.5094E 2	150 -.8583E 1 -.2861E 2
131 -.6661E -1 .2492E 1	132 -.4786E 0 .1344E 1	133 -.1545E 1 .3156E 0	134 -.3541E 1 -.3224E 0	135 -.6718E 1 -.1316E 1	136 -.1049E 2 -.4649E 1	137 -.1253E 2 -.1540E 2	138 -.7238E 1 -.3145E 2	139 -.1328E 1 -.3788E 2	140 .5162E 1 -.2515E 2
121 -.5575E -1 .3211E 1	122 -.5944E 0 .1383E 1	123 -.1862E 1 -.4649E 0	124 -.3623E 1 -.2289E 1	125 -.5212E 1 -.5283E 1	126 -.5463E 1 -.1046E 2	127 -.3134E 1 -.1745E 2	128 .1568E 0 -.2354E 2	129 .1663E 1 -.2506E 2	130 -.1306E 1 -.2565E 2
111 -.4603E -1 .2916E 1	112 -.4663E 0 .7769E 0	113 -.1362E 1 -.1711E 1	114 -.2246E 1 -.4389E 1	115 -.2403E 1 -.7919E 1	116 -.1511E 1 -.1203E 2	117 -.7736E -1 -.1598E 2	118 .1173E 1 -.1915E 2	119 .1523E 1 -.2110E 2	120 .2276E 1 -.2170E 2
101 -.2300E -1 .1800E 1	102 -.2383E 0 -.2970E 0	103 -.6302E 0 -.2995E 1	104 -.8071E 0 -.5876E 1	105 -.4247E 0 -.9026E 1	106 .3667E 0 -.1202E 2	107 .1249E 1 -.1458E 2	108 .2051E 1 -.1674E 2	109 .2644E 1 -.1797E 2	110 .2704E 1 -.1836E 2
91 -.3473E -2 .2386E 0	92 -.3854E -1 -.1575E 1	93 -.4526E -1 -.4099E 1	94 .1658E 0 -.6761E 1	95 .6776E 0 -.9373E 1	96 .1326E 1 -.1162E 2	97 .1952E 1 -.1342E 2	98 .2524E 1 -.1488E 2	99 .2847E 1 -.1571E 2	100 .2978E 1 -.1597E 2
81 .8198E -2 -.1417E 1	82 .8375E -1 -.2855E 1	83 .2963E 0 -.5002E 1	84 .6825E 0 -.7277E 1	85 .1208E 1 -.9388E 1	86 .1742E 1 -.1110E 2	87 .2210E 1 -.1240E 2	88 .2606E 1 -.1343E 2	89 .2846E 1 -.1401E 2	90 .2917E 1 -.1419E 2
71 .1286E -1 -.2942E 1	72 .1361E 0 -.4021E 1	73 .4378E 0 -.5740E 1	74 .8752E 0 -.7593E 1	75 .1364E 1 -.9268E 1	76 .1804E 1 -.1058E 2	77 .2161E 1 -.1155E 2	78 .2453E 1 -.1229E 2	79 .2622E 1 -.1271E 2	80 .2676E 1 -.1284E 2
61 .1309E -1 -.4236E 1	62 .1418E 0 -.5026E 1	63 .4470E 0 -.6351E 1	64 .8584E 0 -.7807E 1	65 .1280E 1 -.9108E 1	66 .1637E 1 -.1011E 2	67 .1912E 1 -.1083E 2	68 .2132E 1 -.1138E 2	69 .2257E 1 -.1169E 2	70 .2296E 1 -.1178E 2
51 .1129E -1 -.5284E 1	52 .1193E 0 -.5866E 1	53 .3736E 0 -.6864E 1	54 .7090E 0 -.7968E 1	55 .1044E 1 -.8952E 1	56 .1321E 1 -.9701E 1	57 .1532E 1 -.1024E 2	58 .1697E 1 -.1065E 2	59 .1790E 1 -.1087E 2	60 .1819E 1 -.1094E 2
41 .6359E -2 -.6125E 1	42 .7755E -1 -.6569E 1	43 .2413E 0 -.7302E 1	44 .4666E 0 -.8098E 1	45 .7030E 0 -.8808E 1	46 .9051E 0 -.9353E 1	47 .1061E 1 -.9749E 1	48 .1185E 1 -.1005E 2	49 .1254E 1 -.1021E 2	50 .1276E 1 -.1027E 2
31 .6512E -2 -.6832E 1	32 .1077E -1 -.7187E 1	33 .4754E -1 -.7682E 1	34 .1353E 0 -.8190E 1	35 .2753E 0 -.8663E 1	36 .4140E 0 -.9045E 1	37 .5269E 0 -.9330E 1	38 .6179E 0 -.9550E 1	39 .6694E 0 -.9671E 1	40 .6856E 0 -.9709E 1
21 -.2419E -1 -.7528E 1	22 -.8887E -1 -.7789E 1	23 -.2646E 0 -.8003E 1	24 -.3011E 0 -.8212E 1	25 -.2277E 0 -.8495E 1	26 -.1341E 0 -.8755E 1	27 -.5370E -1 -.8961E 1	28 .1203E -1 -.9123E 1	29 .4935E 1 -.9214E 1	30 .6133E 1 -.9242E 1
11 .6946E -1 -.8434E 1	12 -.4554E 0 -.8479E 1	13 -.7731E 0 -.8159E 1	14 -.8260E 0 -.8131E 1	15 -.7787E 0 -.8292E 1	16 -.7179E 0 -.8474E 1	17 -.6665E 0 -.8626E 1	18 -.6251E 0 -.8749E 1	19 -.6013E 0 -.8818E 1	20 -.5939E 0 -.8840E 1
1 -.1104E 1 -.1050E 2	2 -.1267E 1 -.8857E 1	3 -.1342E 1 -.8089E 1	4 -.1340E 1 -.7974E 1	5 -.1326E 1 -.8069E 1	6 -.1314E 1 -.8199E 1	7 -.1306E 1 -.8312E 1	8 -.1300E 1 -.8406E 1	9 -.1296E 1 -.8460E 1	10 -.1295E 1 -.8476E 1

Table 8.4 - Axial and lateral stress (N/mm^2) at the centre of each element for the cube loaded through a knife-edge load via a 4 mm thick steel base plate with the reduced moduli of elasticity.

KEY
Element No
Lateral
Axial

151 -.6825E 0 .9816F 1	152 -.1051E 1 .5610F 1	153 -.2201E 1 .1027E 1	154 -.4885E 1 -.2896E 1	155 -.9664E 1 -.8081E 1	156 -.1614E 2 -.1653E 2	157 -.2441E 2 -.3495F 2	158 -.3408E 2 -.9104E 2	159 -.3946E 2 -.7235E 2	160 -.4681E 2 -.1030E 3
141 .1453E 1 .2031E 2	142 -.7065F 0 .9742E 1	143 -.5068E 1 -.1784E 0	144 -.1039E 2 -.8729E 1	145 -.1544E 2 -.1927E 2	146 -.1940E 2 -.3410E 2	147 -.2108E 2 -.5827E 2	148 -.1979E 2 -.1199E 3	149 -.2257E 2 -.4111E 2	150 .2729F 1 .7119E 1
131 -.2718E 0 .1471E 2	132 -.7250E 0 .6364E 1	133 -.2840E 1 -.4155E 1	134 -.5263E 1 -.1446F 2	135 -.6071E 1 -.2650E 2	136 -.3991E 1 -.4107E 2	137 .2421E 1 -.5988E 2	138 .1619E 2 -.6712E 2	139 .3570E 2 -.4178E 2	140 .2934E 2 -.1908E 2
121 .1130E -1 .8241E 1	122 -.2424E 0 .1251E 1	123 -.4750E 0 -.8403E 1	124 .2275E -1 -.1878E 2	125 .2511E 1 -.2992E 2	126 .7301E 1 -.4076E 2	127 .1390E 2 -.4798E 2	128 .1767E 2 -.4547E 2	129 .1229E 2 -.3842E 2	130 .1026E 2 -.3378E 2
111 .2474F -1 .1322E 1	112 .3578E 0 -.4001E 1	113 .1328E 1 -.1212E 2	114 .3323E 1 -.2106E 2	115 .6455E 1 -.2959E 2	116 .9908E 1 -.3591E 2	117 .1207E 2 -.3866F 2	118 .1184E 2 -.3839E 2	119 .1136E 2 -.3703E 2	120 .1059F 2 -.3646F 2
101 .6335E -1 -.5043E 1	102 .6615E 0 -.8736E 1	103 .2184E 1 -.1496E 2	104 .4478E 1 -.2187E 2	105 .7023E 1 -.2791E 2	106 .8983E 1 -.3194E 2	107 .9959E 1 -.3400E 2	108 .1029E 2 -.3479E 2	109 .1012E 2 -.3490E 2	110 .1012E 2 -.3485F 2
91 .6523E -1 -.1030E 2	92 .7178E 0 -.1265E 2	93 .2278E 1 -.1706E 2	94 .4345E 1 -.2212E 2	95 .6286E 1 -.2644E 2	96 .7649E 1 -.2937E 2	97 .8434E 1 -.3109E 2	98 .8832E 1 -.3211E 2	99 .8994E 1 -.3256E 2	100 .9003E 1 -.3267E 2
81 .5652F -1 -.1432F 2	82 .6311E 0 -.1570E 2	83 .1983E 1 -.1868E 2	84 .3688E 1 -.2227E 2	85 .5213E 1 -.2541E 2	86 .6286E 1 -.2761E 2	87 .6954E 1 -.2902E 2	88 .7386E 1 -.2997E 2	89 .7587E 1 -.3045E 2	90 .7647E 1 -.3058E 2
71 .4326E -1 -.1723E 2	72 .4952E 0 -.1801E 2	73 .1562E 1 -.1996E 2	74 .2897E 1 -.2246E 2	75 .4088E 1 -.2472E 2	76 .4942E 1 -.2637E 2	77 .5505E 1 -.2748E 2	78 .5896E 1 -.2826E 2	79 .6096E 1 -.2867E 2	80 .6154E 1 -.2879E 2
61 .3056E -1 -.1927E 2	62 .3570E 0 -.1972E 2	63 .1133E -1 -.2099E 2	64 .2112E 1 -.2270E 2	65 .2999E 1 -.2429E 2	66 .3650E 1 -.2548E 2	67 .4095E 1 -.2630E 2	68 .4416E 1 -.2690E 2	69 .4584E 1 -.2722E 2	70 .4635E 1 -.2732E 2
51 .2044F -1 -.2068E 2	52 .2278E 0 -.2099E 2	53 .7247E 0 -.2183E 2	54 .1361E 1 -.2295E 2	55 .1955E 1 -.2401E 2	56 .2408E 1 -.2482E 2	57 .2730E 1 -.2540E 2	58 .2969E 1 -.2583E 2	59 .3097E 1 -.2606E 2	60 .3136E 1 -.2613E 2
41 .6526E -2 -.2169E 2	42 .1002E 0 -.2198E 2	43 .3117E 0 -.2253E 2	44 .6084E 0 -.2319E 2	45 .9232E 0 -.2381E 2	46 .1192E 1 -.2431E 2	47 .1399E 1 -.2467E 2	48 .1561E 1 -.2495E 2	49 .1649E 1 -.2511E 2	50 .1677E 1 -.2516E 2
31 .1003E -1 -.2253E 2	32 -.6139E -1 -.2286E 2	33 -.1713E 0 -.2316E 2	34 -.2316E 0 -.2338E 2	35 -.1588E 0 -.2362E 2	36 -.3507E -1 -.2385E 2	37 .8213E -1 -.2405E 2	38 .1822E 0 -.2422E 2	39 .2393E 0 -.2431E 2	40 .2575E 0 -.2434E 2
21 -.7029E -1 -.2349E 2	22 -.2858E 0 -.2382E 2	23 -.9189E 0 -.2371E 2	24 -.1275E 1 -.2341E 2	25 -.1340E 1 -.2334E 2	26 -.1298E 1 -.2339E 2	27 -.1233E 1 -.2347E 2	28 -.1172E 1 -.2356E 2	29 -.1135F 1 -.2361E 2	30 -.1123E 1 -.2362E 2
11 .2165F 0 -.2507E 2	12 -.7218E 1 -.2513E 2	13 -.2212E 1 -.2391E 2	14 -.2551E 1 -.2319E 2	15 -.2606E 1 -.2295E 2	16 -.2579E 1 -.2289E 2	17 -.2536E 1 -.2291E 2	18 -.2496E 1 -.2294E 2	19 -.2472E 1 -.2297E 2	20 -.2464F 1 -.2297E 2
1 -.3050E 1 -.2979E 2	2 -.3566F 1 -.2573E 2	3 -.3838E 1 -.2355E 2	4 -.3870E 1 -.2275E 2	5 -.3847E 1 -.2247E 2	6 -.3820F 1 -.2237E 2	7 -.3799E 1 -.2235E 2	8 -.3782E 1 -.2236E 2	9 -.3772E 1 -.2237E 2	10 -.3770E 1 -.2237E 2

Table 8.5 - Axial and lateral stress (N/mm^2) at the centre of each element for the cube loaded through a knife-edge load via a 22.5 mm thick steel base plate with the reduced moduli of elasticity.

~~Elements~~ Elements 1-150 represent concrete block

Elements 151-160 represent steel base plate

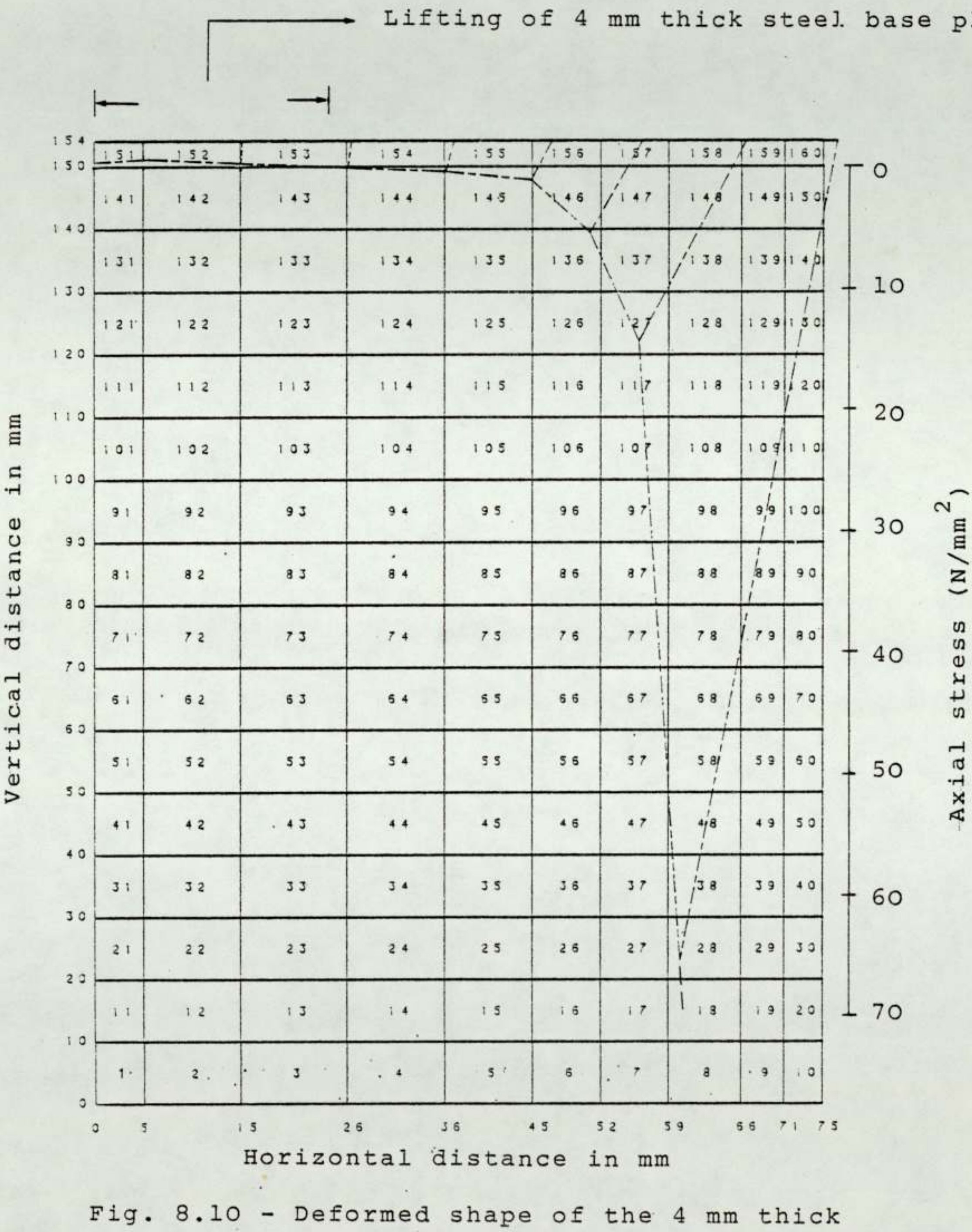

Fig. 8.10 - Deformed shape of the 4 mm thick steel base plate with reduced values of moduli of elasticity over its original outline of zero stress, (elements 151-158)

Elements 1-150 represent concrete block

Elements 151-160 represent steel base plate

Lifting of 22.5 mm thick steel base plate

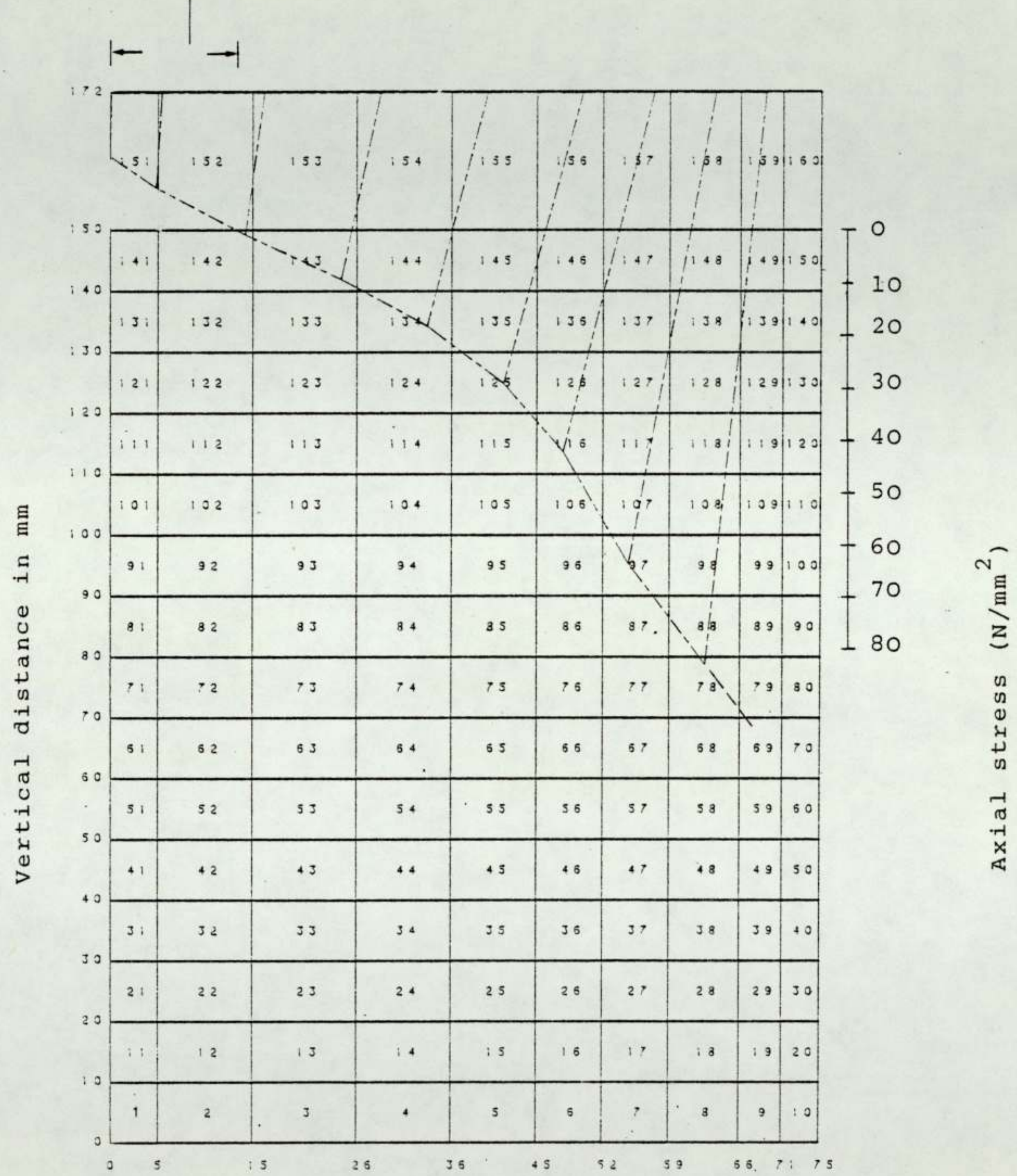

Fig. 8.11 - Deformed shape of the 22.5 mm thick steel base plate with reduced values of moduli of elasticity over its outline of zero stress, (elements 151-158)

nonlinear behaviour of the concrete and the steel base plate becomes more pronounced with increasing stresses. These higher stress concentrations result in a reduction of the modulus of elasticity of the material in these regions. In this investigation, by using lesser but admittedly not exact values of elastic moduli it was possible to simulate more closely the actual pattern of stress distribution and consequently predict more accurately the lifting up of the steel base plate.

The reduced values of elastic moduli were initially estimated and the general pattern of lifting up with lower Young's Moduli emerged. Of course, to arrive at the exact values of stress in the elements under ultimate load would have required exhaustive running of the program with incremental changes in elastic moduli and Poisson's ratio. This was beyond the scope of this research for financial and practical reasons. Nevertheless, a more refined iterative approach such as the Modified Newton-Raphson method or the incremental methods recommended by Zienkiewicz (51) would yield results closer to those found in the experiments i.e. a greater lifting of the steel base plate at failure.

Similarly, it would be possible to achieve a more accurate result by increasing the number of elements in the mesh. However, this too would require much more computer time.

Nevertheless, the assumption made in this research (that reducing the elastic moduli of the elements under high compressive stress provides a closer prediction of the lifting up of the base plate at ultimate load) has been conclusively proved. The pattern of stress distribution at ultimate load is thereby considerably improved and therefore produces a more accurate picture of actual behaviour under such a loading configuration.

CHAPTER NINE

CONCLUSIONS

9.1 General Conclusions

The following conclusions were reached as a result of the work carried out for these investigations.

1) There are two distinct modes of failure for concrete cubes loaded through stiff steel bearings. A single cone and splitting occurs for ratios of loaded area to concrete surface area (R) less than or equal to 0.125. As the ratio of R increases from the value of 0.125 the mode of failure changes from a single to a double cone which is accompanied by crushing.

2) The ultimate load for unreinforced concrete cubes subjected to concentric stiff bearing for ratios of R less than 0.125 can be predicted from the following empirical equation with a reasonable degree of accuracy.

$$\frac{F}{Af_{cu}} = 0.085 + 1.36 \frac{A_s}{A} \qquad (2.1)$$

3) The ultimate load for unreinforced concrete cubes subjected to concentric stiff bearing for ratios of $0.125 < R < 1$ can be predicted from the following empirical equation with a reasonable degree of accuracy.

$$\frac{F}{Af_{cu}} = 0.15 + 0.85 \frac{A_s}{A} \qquad (2.2)$$

4) When concrete cubes are loaded through flexible plates, the plate

lifts up at its free end and plastic hinges form close to the loading piece at ultimate load.

5) The same modes of failure, i.e. the formation of single and double cones, were observed when loading through flexible steel base plates. The single cone formed with a thin plate and as the thickness of plate increased a double cone failure was observed.

6) Vertical stresses in concrete cubes loaded through flexible plates are not uniform within the contact area. The stresses are greater at the centre line than at the edge of the contact area.

7) With the same thickness of flexible steel base plate, as the concrete cube strength increases the steel base plate is subjected to greater bending deformation. As a result of this mechanism the contact length at ultimate load decreases for increasing cube strength.

8) With the same concrete strength, as the thicknesses of flexible steel base plate increases the plate is subjected to less bending deformation and the contact length increases.

9) When load is applied through flexible steel plates of various thicknesses, the contact length is an important factor in determining the bearing capacity of the concrete.

10) For concrete cubes loaded through universal columns of various ratios of column width to depth (B/D) via different thichnesses of steel base plate, it was found that:

a) in most cases for the same thickness of base plate and increasing ratio of B/D (0.06 to 1.0) the bearing area changes from rectangular to I-shape

b) in most cases for the same ratio of B/D and increasing thicknesses of steel base plate (4 to 12mm) the bearing area changes from I to rectangular shape.

11) For the purpose of designing a steel base plate for an I-section column for ratios of BD/t^2 greater and equal to 200, the assumption of a rectangular shape bearing area is reasonably accurate.

12) The present methods of design for column bases, i.e. AISC(29), the Draft of Steel Code (30) and BS 449(31), do not give a reliable prediction of the failure load when applied to a thin steel base plate. Nevertheless in practice these methods are safe although inaccurate.

13) A distinct difference in the mode of failure between eccentric and concentric loading is that in the former the first visible crack in the concrete cube always appears on the side of the specimen nearest to the bearing plate.

14) For a constant ratio of loaded area to concrete surface area the bearing strength of concrete cubes deceases with increasing eccentricity of the applied load.

15) From tests with an increasing ratio of loaded area to concrete surface area it was found that the bearing capacity of smaller loaded

areas was more susceptible to the effects of eccectricity than larger ones.

16) In the plane-stress analysis it was found that under a given load the elements within the vicinity of the loaded area were subjected to much higher compressive and tensile stresses than those found in the cube crushing and split cylinder tests. Since these high stresses reflect a non- linear behaviour of concrete, the material under these high stress concentrations therefore has a reduced modulus of elasticity.

17) Using a plane-stress analysis it was found that a good prediction of the contact length and therefore bearing strength was possible only when the analysis made allowances for the reduction of Young's Modulus in the area of high stress and the restraint occuring between the cube and the lower platten.

A large discrepancy exists between various stress analysis methods and experimental results. This suggests the inadequacy of the assumptions made in the theories of failure. Due to the complex behaviour of stresses in concrete cubes or prisms under partial loading configurations, before any valid theoretical attempt can be made to determine the ultimate strength of a foundation it is of paramount importance to have a better understanding of the mode of failure of concrete under different loading situations. The Author consequently advocates an empirical design of steel bearing plates until such time as theoretical approaches can be considered to reflect more accurately the precise mode of failure.

9.2 Recommendations for Further Work

Further tests using other types of loading pieces commonly used in practice, such as hollow sections, will extend the work that has been carried out.

In the tests performed in this investigation none of the loading pieces were welded to the steel base plate. Different sizes of weld should be considered, and it is predicted by the Author that welding will increase the contact length.

It would be of considerable interest to develop a purely theoretical formula for predicting the bearing capacity of concrete loaded through flexible plates. This work should be carried out based on the assumption of single and double cone mode of failure as described in this thesis. Although some theoretical formulae have been developed which assume a single cone mode of failure, none of these satisy the boundary conditions for different ratios of R.

This work can also be extended to consider real column foundations such as steel slabs and built-up base plates which are subjected to axial load and bending moments.

A further development should also be made in the work of finite element analysis. A more refined iterative approach such as the Modified Newton-Raphson method or the Incremental methods recommended by Zienkiewicz (51) could be used in order to investigate more accurately the distribution of stresses in a concrete specimen loaded through various sizes of bearing.

APPENDIX A TO CHAPTER TWO

Table A.1 Results for concentric loading through stiff bearing plates of various sizes

Author	Test No	Concrete Strength f_{cu} N/mm^2	Concrete Cube Dimension $b_x=b_y=H$ mm	Loading Plate Dimension S_x mm	S_y mm	Ratio F/f_{cu} n (Dimensionless)	Ratio A_s/A R (Dimensionless)	No of Tests
University of Illinoi's (8)	1	27.4	152	44	44	0.191	0.084	3
	2	27.4	152	52	52	0.249	0.117	3
	3	27.4	152	63	63	0.309	0.172	3
	4	27.4	152	76	76	0.379	0.250	3
	5	27.4	152	102	102	0.534	0.450	3
	6	32.6	229	63	63	0.192	0.076	2
	7	32.6	229	76	76	0.241	0.111	2
	8	32.6	229	102	102	0.328	0.198	2
	9	65.6	152	44	44	0.146	0.084	3
	10	65.6	152	52	52	0.189	0.117	2
	11	65.6	152	63	63	0.240	0.172	3
	12	65.6	152	76	76	0.296	0.250	3
	13	65.6	152	102	102	0.439	0.450	3
	14	33.1	152	51	51	0.274	0.113	3
	15	33.1	152	76	76	0.418	0.250	3
	16	33.1	152	152	152	0.770	1.000	3
	17	43.7	152	51	51	0.234	0.113	3
	18	43.7	152	76	76	0.319	0.250	3
	19	43.7	152	152	152	0.689	1.000	3

(CONTINUED)

Author	Test No	Concrete Strength	Concrete Cube Dimension	Loading Plate Dimension		Ratio F/f_{cu}	Ratio A_s/A	No of Tests
		f_{cu}	$b_x=b_y=H$	S_x	S_y	n	R	
		N/mm^2	mm	mm	mm	Dimensionless		
Muguruma and Okamoto (9)	1	51.4	200	20	20	0.066	0.010	3
	2	51.4	200	25	25	0.066	0.016	3
	3	51.4	200	30	30	0.104	0.023	3
	4	51.4	200	50	50	0.159	0.063	6
	5	51.4	200	75	75	0.287	0.141	5
	6	51.4	200	150	150	0.638	0.563	5
	7	51.4	200	100	100	0.362	0.250	4
	8	51.4	200	200	200	0.792	1.000	3
Niyogi (18)	1	19.3	203	25	25	0.112	0.015	4
	2	17.3	203	36	36	0.153	0.031	4
	3	19.3	203	51	51	0.208	0.063	4
	4	15.0	203	72	72	0.266	0.126	4
	5	14.8	203	102	102	0.386	0.252	4
Niyogi (19)	1	59.0	203	36	36	0.127	0.031	3
	2	59.0	203	51	51	0.174	0.063	3
	3	59.0	203	102	102	0.370	0.252	2
	4	43.5	203	36	36	0.138	0.031	3
	5	43.5	203	51	51	0.181	0.063	3

(CONTINUED)

Author	Test No	Concrete Strength	Concrete Cube Dimension	Loading Plate Dimension		Ratio F/f_{cu}	Ratio A_s/A	No of Tests
		f_{cu}	$b_x=b_y=H$	S_x	S_y	n	R	
		N/mm^2	mm	mm	mm	Dimensionless		
	6	43.5	203	102	102	0.381	0.252	3
	7	29.7	203	36	36	0.149	0.031	3
Niyogi	8	27.2	203	51	51	0.190	0.063	3
	9	30.6	203	102	102	0.390	0.252	3
(19)	10	21.2	203	36	36	0.156	0.031	3
	11	20.9	203	51	51	0.193	0.063	3
	12	21.2	203	102	102	0.385	0.252	3
	13	11.4	203	36	36	0.164	0.031	3
	14	11.4	203	51	51	0.202	0.063	3
	15	11.4	203	102	102	0.376	0.252	3
	1	32.1	102	18	18	0.167	0.031	4
	2	31.5	152	27	27	0.153	0.032	4
	3	29.7	203	36	36	0.149	0.031	6
	4	32.6	305	54	54	0.133	0.031	3
Niyogi	5	31.2	102	25	25	0.220	0.060	3
	6	31.6	152	36	36	0.119	0.063	3
(19)	7	27.2	203	51	51	0.190	0.063	3
	8	32.3	305	76	76	0.158	0.062	3
	9	32.3	102	36	36	0.330	0.125	3

(CONTINUED)

Author	Test No	Concrete Strength	Concrete Cube Dimension	Loading Plate Dimension		Ratio F/f_{cu}	Ratio A_s/A	No of Tests
		f_{cu}	$b_x=b_y=H$	S_x	S_y	n	R	
		N/mm^2	mm	mm	mm	Dimensionless		
	10	30.5	152	54	54	0.278	0.126	3
	11	27.7	203	72	72	0.259	0.126	6
	12	32.2	305	108	108	0.223	0.125	3
	13	31.6	102	51	51	0.456	0.250	4
	14	32.6	152	76	76	0.393	0.250	4
	15	30.6	203	102	102	0.390	0.252	5
	16	30.9	305	152	152	0.327	0.248	3
	17	28.2	203	25	25	0.108	0.015	6
	18	29.7	203	36	36	0.149	0.031	6
	19	27.2	203	51	51	0.190	0.063	5
	20	27.7	203	72	72	0.138	0.126	6
	21	30.6	203	102	102	0.390	0.252	5
	22	31.4	203	152	152	0.611	0.561	4
	23	28.8	203	203	203	0.969	1.000	4
	1	34.8	102	10	10	0.077	0.096	3
Williams	2	33.2	102	20	20	0.149	0.038	3
	3	33.2	102	25	25	0.185	0.060	3
(21)	4	34.8	102	32	32	0.261	0.098	3
	5	33.2	102	51	51	0.356	0.250	3

(CONTINUED)

Author	Test No	Concrete Strength	Concrete Cube Dimension	Loading Plate Dimension		Ratio F/f_{cu}	Ratio A_s/A	No of Tests
		f_{cu}	$b_x=b_y=H$	S_x	S_y	n	R	
		N/mm^2	mm	mm	mm	Dimensionless		
Williams (21)	6	33.2	102	75	75	0.654	0.540	3
	7	34.8	102	92	92	0.944	0.814	3
	8	33.2	102	102	102	0.910	1.000	3
	9	20.9	102	102	102	1.090	1.000	3
	10	30.3	153	32	32	0.183	0.044	3
	11	33.4	153	75	75	0.410	0.240	3
	12	30.3	153	120	120	0.763	0.615	3
	13	70.9	153	20	20	0.091	0.017	3
	14	70.9	153	75	75	0.379	0.240	3
	15	70.9	153	120	120	0.697	0.615	3
Niyogi (18)	1	32.1	203	13	203	0.162	0.064	3
	2	30.5	203	17	203	0.182	0.084	3
	3	31.3	203	25	203	0.231	0.123	3
	4	26.9	203	34	203	0.275	0.167	4
	5	28.6	203	151	203	0.348	0.251	3
	6	31.1	203	64	203	0.413	0.315	3
	7	31.3	203	68	203	0.422	0.335	3
	8	31.6	203	102	203	0.553	0.502	4
	9	28.8	203	203	203	0.970	1.000	4

(CONTINUED)

Author	Test No	Concrete Strength	Concrete Cube Dimension	Loading Plate Dimension		Ratio F/f_{cu}	Ratio A_s/A	No of Tests
		f_{cu}	$b_x=b_y=H$	S_x	S_y	n	R	
		N/mm^2	mm	mm	mm	Dimensionless		
	10	29.6	203	13	51	0.105	0.016	3
	11	29.5	203	13	76	0.129	0.024	4
	12	31.8	203	13	102	0.135	0.032	3
	13	29.8	203	13	152	0.164	0.048	3
	14	29.6	203	25	51	0.129	0.031	3
	15	26.0	203	25	76	0.154	0.046	3
	16	29.6	203	25	102	0.166	0.062	3
	17	29.6	203	25	152	0.204	0.092	3
	18	28.5	203	34	51	0.154	0.042	3
	19	29.7	203	34	76	0.171	0.063	3
	20	29.7	203	34	102	0.210	0.084	3
	21	29.7	203	34	152	0.230	0.125	3
	22	27.0	203	51	76	0.231	0.094	3
	23	24.8	203	51	102	0.260	0.126	3
	24	27.6	203	51	127	0.277	0.157	3
	25	28.1	203	51	152	0.290	0.190	3
	26	31.5	203	76	102	0.310	0.190	3
	27	30.2	203	102	152	0.430	0.380	3

(CONTINUED)

Author	Test No	Concrete Strength	Concrete Cube Dimension	Loading Plate Dimension		Ratio F/f_{cu}	Ratio A_s/A	No of Tests
		f_{cu}	$b_x=b_y=H$	S_x	S_y	n	R	
		N/mm^2	mm	mm	mm	Dimensionless		
Niyogi (19)	1	14.6	203	25	203	0.260	0.123	2
	2	14.6	203	51	203	0.400	0.250	2
	3	14.6	203	10	203	0.055	0.049	2
	4	29.8	152	152	13	0.194	0.086	3
	5	30.5	203	203	17	0.182	0.084	3
	6	28.9	305	305	25	0.149	0.082	3
	7	29.8	102	102	13	0.270	0.127	3
	8	30.4	152	152	19	0.241	0.125	3
	9	31.3	203	203	25	0.231	0.123	3
	10	30.3	305	305	38	0.210	0.125	3
	11	29.8	102	102	17	0.290	0.170	3
	12	30.4	152	152	25	0.276	0.164	3
	13	26.9	203	203	34	0.275	0.167	4
	14	28.9	305	305	51	0.251	0.167	2
	15	30.7	102	102	25	0.370	0.245	3
	16	30.4	152	152	38	0.365	0.250	3
	17	28.6	203	203	51	0.348	0.249	3
	18	30.1	305	305	76	0.312	0.249	3
	19	30.7	102	102	51	0.678	0.500	3
	20	30.4	152	152	76	0.584	0.500	3
	21	31.6	203	203	102	0.553	0.502	4

(CONTINUED)

Author	Test No	Concrete Strength	Concrete Cube Dimension	Loading Plate Dimension		Ratio F/f_{cu}	Ratio A_s/A	No of Tests
		f_{cu}	$b_x=b_y=H$	S_x	S_y	n	R	
		N/mm^2	mm	mm	mm	Dimensionless		
	1	35.2	153	153	10	0.193	0.065	3
	2	37.2	153	153	25	0.316	0.163	3
	3	35.2	153	153	31	0.351	0.203	3
	4	37.2	153	153	50	0.440	0.330	3
	5	35.2	153	153	75	0.610	0.490	3
	6	37.2	153	153	93	0.686	0.610	3
Williams	7	37.2	153	153	118	0.830	0.770	3
	8	69.2	153	153	10	0.161	0.065	3
(21)	9	68.3	153	153	25	0.299	0.163	3
	10	68.3	153	153	31	0.326	0.203	3
	11	69.2	153	153	50	0.438	0.330	3
	12	68.3	153	153	75	0.581	0.490	3
	13	69.2	153	153	93	0.643	0.610	3
	14	69.2	153	153	118	0.848	0.770	3
	15	36.9	153	120	25	0.293	0.128	3
	16	35.2	153	92	25	0.263	0.098	3
	17	36.9	153	75	25	0.219	0.080	3
	18	35.2	153	63	25	0.210	0.067	3
	19	36.9	153	50	25	0.194	0.053	3
	20	36.2	153	37	25	0.168	0.040	3

(CONTINUED)

Author	Test No	Concrete Strength	Concrete Cube Dimension	Loading Plate Dimension		Ratio F/f_{cu}	Ratio A_s/A	No of Tests
		f_{cu}	$b_x=b_y=H$	S_x	S_y	n	R	
		N/mm^2	mm	mm	mm	Dimensionless		
	21	68.0	153	120	25	0.270	0.128	3
	22	69.2	153	75	25	0.223	0.080	3
	23	68.0	153	63	25	0.187	0.067	3
	24	69.2	153	50	25	0.153	0.053	3
	25	68.0	153	37	25	0.145	0.040	3
	26	36.2	153	120	50	0.400	0.256	3
	27	36.2	153	91	50	0.346	0.194	3
	28	34.4	153	75	50	0.333	0.160	3
	29	36.2	153	62	50	0.292	0.132	3
	30	70.6	153	120	50	0.396	0.256	3
	31	69.2	153	91	50	0.351	0.194	3
	32	67.7	153	75	50	0.310	0.160	3
	33	70.6	153	62	50	0.280	0.132	3

Table A.1. Results for concentric loading through stiff bearing plates of various sizes.

APPENDIX B TO CHAPTER THREE

Load	Stress in steel base plate corresponding to eleven strain gauges fixed to the plate. N/mm^2											Average			
KN	1	2	3	4	5	6	7	8	9	10	11	2,3	4,5	7,8	10,11
000.00	000.00	00.00	00.00	00.00	00.00	00.00	00.00	00.00	00.00	00.00	00.00	00.00	00.00	00.00	00.00
2.50	28.42	18.27	22.33	8.12	18.27	16.24	2.03	6.09	30.45	-2.03	00.00	20.3	13.20	4.00	-1.00
5.00	30.45	20.30	22.33	8.12	16.24	6.09	0.00	6.09	30.45	-2.03	00.00	21.3	12.18	3.00	-1.00
10.00	38.57	24.36	26.39	10.15	20.30	8.12	2.03	6.09	28.42	-2.03	00.00	25.40	15.24	4.10	-1.00
20.00	50.75	30.45	38.57	14.21	26.39	12.18	8.12	12.18	30.45	00.00	2.03	34.50	20.30	10.15	1.00
30.00	69.02	38.57	52.78	20.30	26.39	16.24	10.15	14.21	30.45	-2.03	2.03	45.70	23.34	12.18	00.00
40.00	95.41	52.78	69.02	26.39	20.30	22.33	14.21	14.21	32.48	00.00	00.00	60.90	23.34	14.21	00.00
50.00	148.19	69.02	75.11	30.45	12.18	26.39	16.24	20.30	32.48	00.00	2.03	72.10	21.32	18.27	1.00
55.00	152.25	75.11	75.11	30.45	8.12	26.39	18.27	12.18	32.48	00.00	2.03	75.11	19.29	15.20	1.00
60.00	196.91	81.20	73.08	28.42	4.06	26.39	18.27	12.18	36.54	00.00	00.00	77.14	16.24	15.20	00.00
65.00	219.24	85.26	66.99	28.42	2.03	26.39	16.24	12.18	40.60	-2.03	00.00	76.13	15.20	15.20	-1.00
70.00	235.48	89.32	66.99	26.39	00.00	28.42	18.27	12.18	46.69	00.00	00.00	78.20	13.20	15.20	00.00
80.00	284.20	93.38	62.93	26.39	-2.03	30.45	18.27	12.18	48.72	00.00	00.00	78.20	12.20	15.20	00.00
85.00	314.60	93.38	62.93	24.36	-4.06	32.48	18.27	14.21	50.75	00.00	00.00	78.20	10.15	16.20	00.00
90.00	363.37	89.32	60.90	24.36	-6.09	30.45	18.27	14.21	48.72	00.00	00.00	75.11	9.20	16.20	00.00
100.00	513.59	83.23	60.90	22.33	-2.03	32.48	18.27	14.21	48.72	-2.03	00.00	72.10	10.20	16.20	-1.00
110.00	672.93	79.17	60.90	20.30	-2.03	40.60	22.33	16.24	50.75	00.00	00.00	70.00	9.14	19.28	00.00
120.00	830.27	77.14	62.93	16.24	-2.03	46.69	24.36	18.27	54.81	00.00	2.03	70.00	7.10	21.30	1.00
130.00	1199.73	75.11	69.02	12.18	00.00	50.75	24.36	20.30	56.48	00.00	4.06	72.00	6.10	22.33	2.00
140.00	U S	69.00	79.17	6.09	4.06	58.87	28.42	26.39	58.57	2.03	6.09	74.00	5.10	27.40	4.00
150.00	U S	54.81	97.44	-6.09	16.24	73.08	32.48	38.57	66.99	4.06	8.12	76.00	5.00	35.50	6.00
Release	800.00	3.00	3.50	00.00	00.00	2.00	00.00	00.00	1.00	00.00	00.00	3.00	1.50	00.00	00.00

Table B.1 Concentric knife-edge loading through 4mm thick base plate on 150 mm cube.

F : Ultimate Load U S : Unsteady Reading

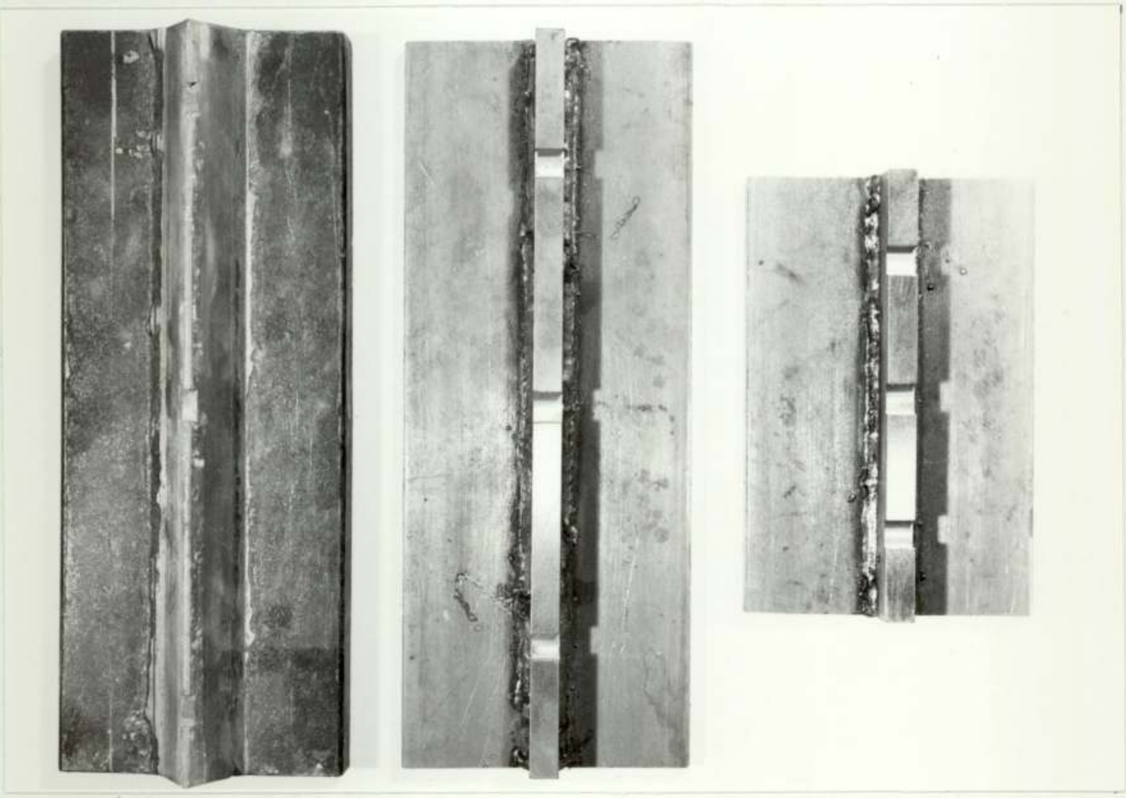

Plate B.1 Different loading pieces used in the main test series.

Scale 1 : 1.85

(a) (b)

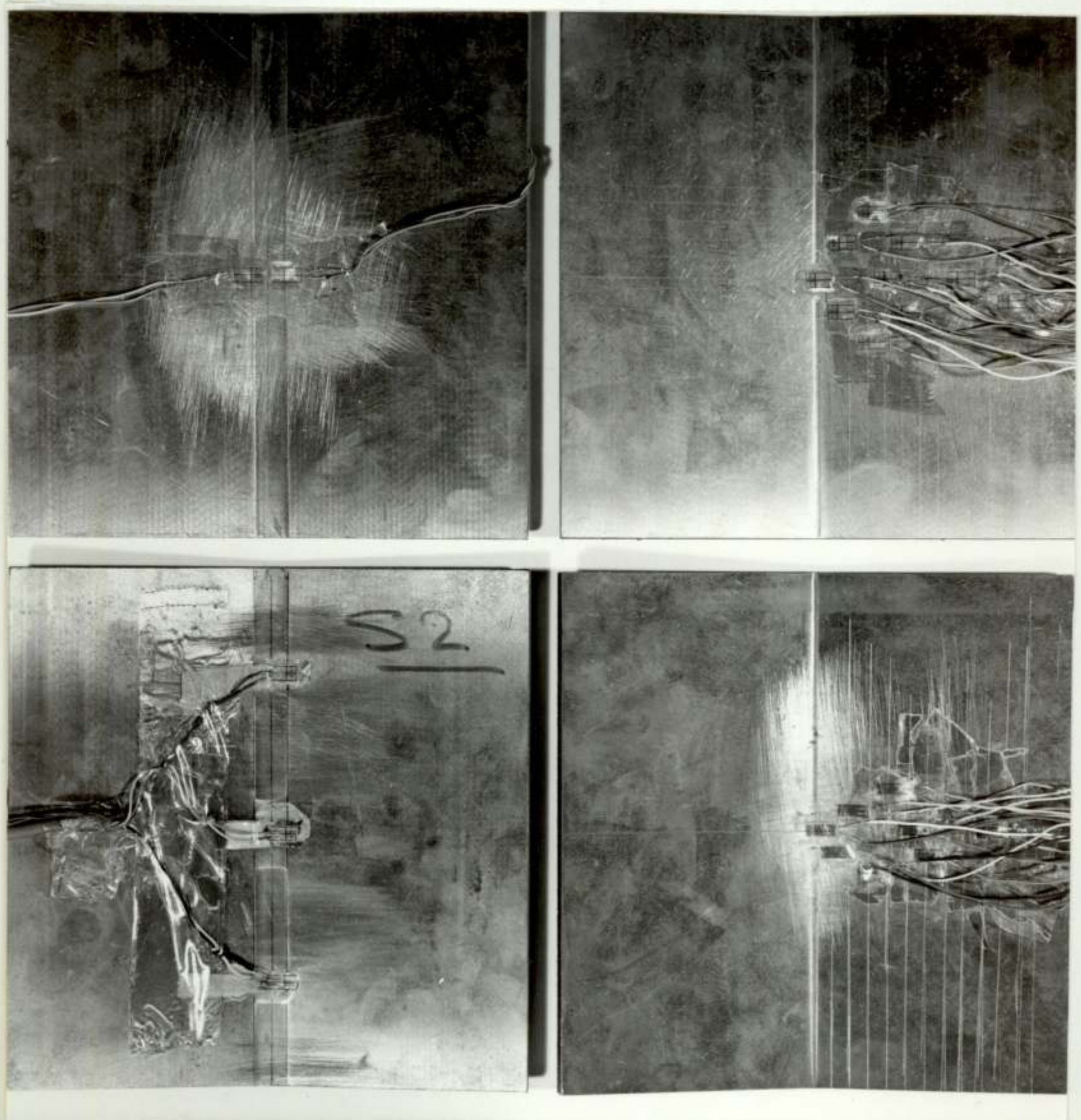

(c) (d)

Plate B.2 Disposition of strain gauges in the initial tests.

(a) Two strain gauges opposite to one another along the edge of the strip loading (10mm).

(b) Eleven strain gauges placed on one side of the knife-edge loading. Distance between gauges is shown in Fig. C.1.

(c) Three strain gauges along the edge of the strip loading (10mm).

(d) The same configuration as in (b).

Scale 1 : 2.2

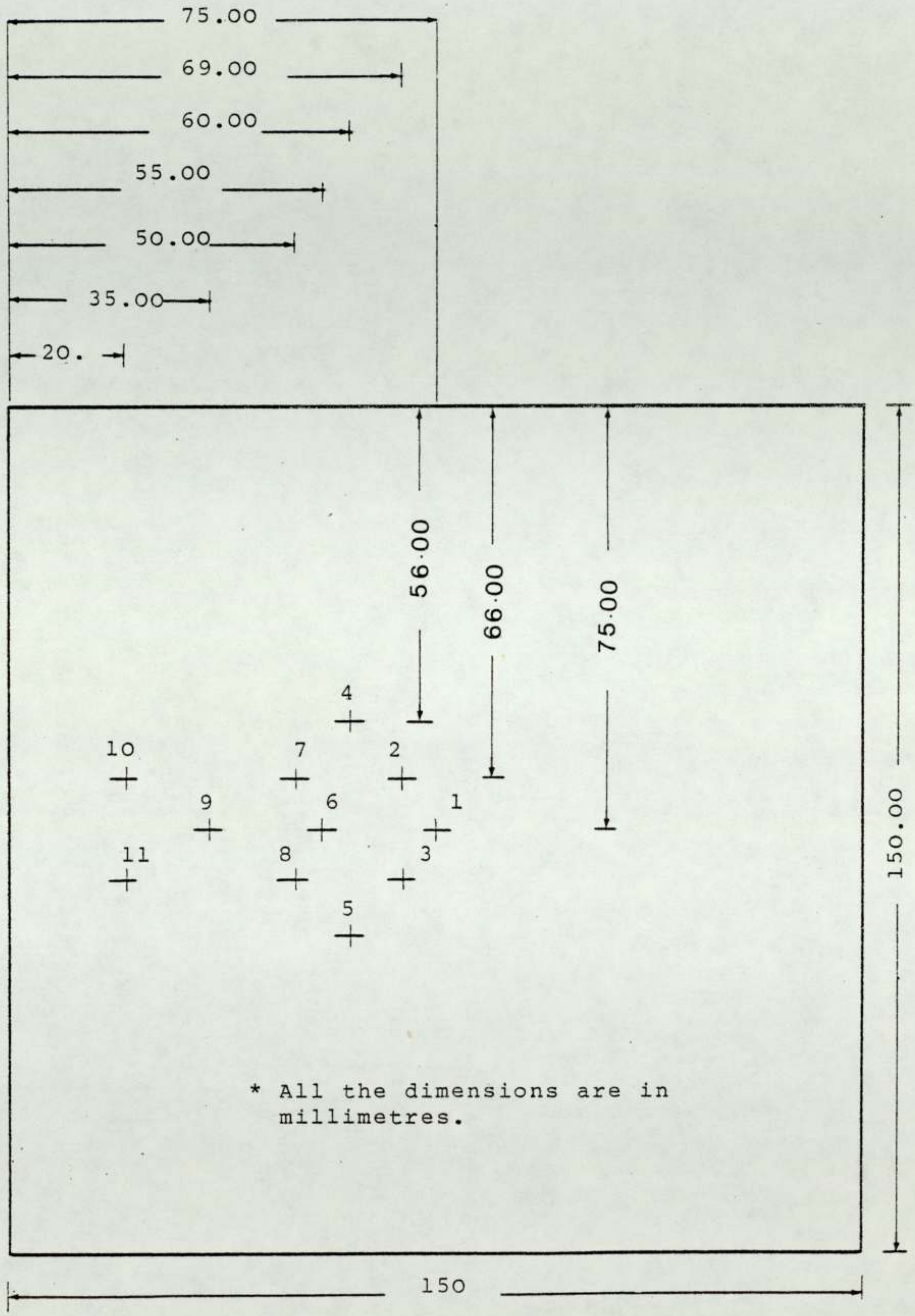

Fig. B.1 Disposition of strain gauges on the base plate 4. mm thick.

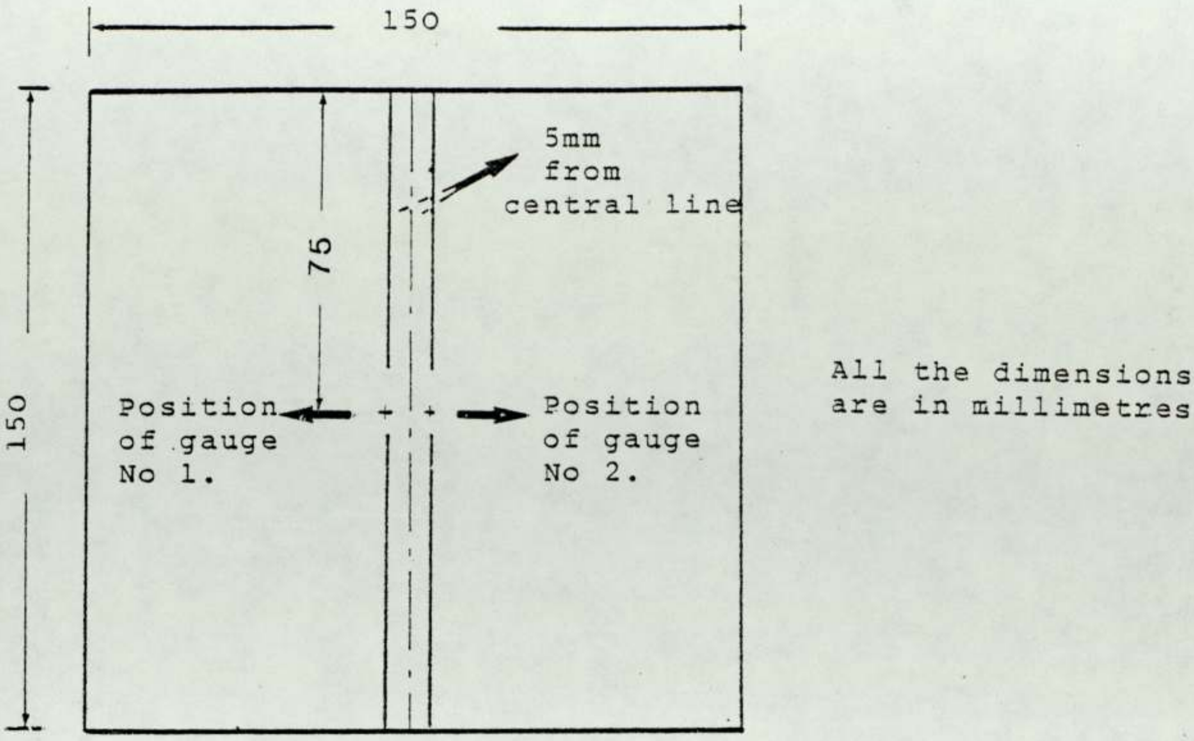

Fig B.2 The disposition of strain gauges on the base plate along the two edges of the loading piece (150x10)

Load	Stress in Steel Base Plate N/mm^2	
KN	Gauge No 1	Gauge No 2
0.00	00.00	00.00
2.50	18.27	19.30
10.00	24.36	20.30
20.00	28.42	27.40
30.00	34.51	30.45
40.00	40.60	38.57
50.00	50.75	46.70
60.00	58.87	54.80
70.00	68.00	60.90
80.00	77.14	70.04
100.00	105.56	93.38
120.00	148.19	138.00
130.00	172.55	156.30
140.00	194.88	182.70
150.00	221.27	203.00
160.00	253.73	245.63
180.00	454.70	448.60
200.00	U S	U S
205.00	U S	U S

Table B.2 Concentric strip loading on 150 mm cube through 4 mm thick steel base plate (strain gauges were fixed as shown in Fig. B.2).

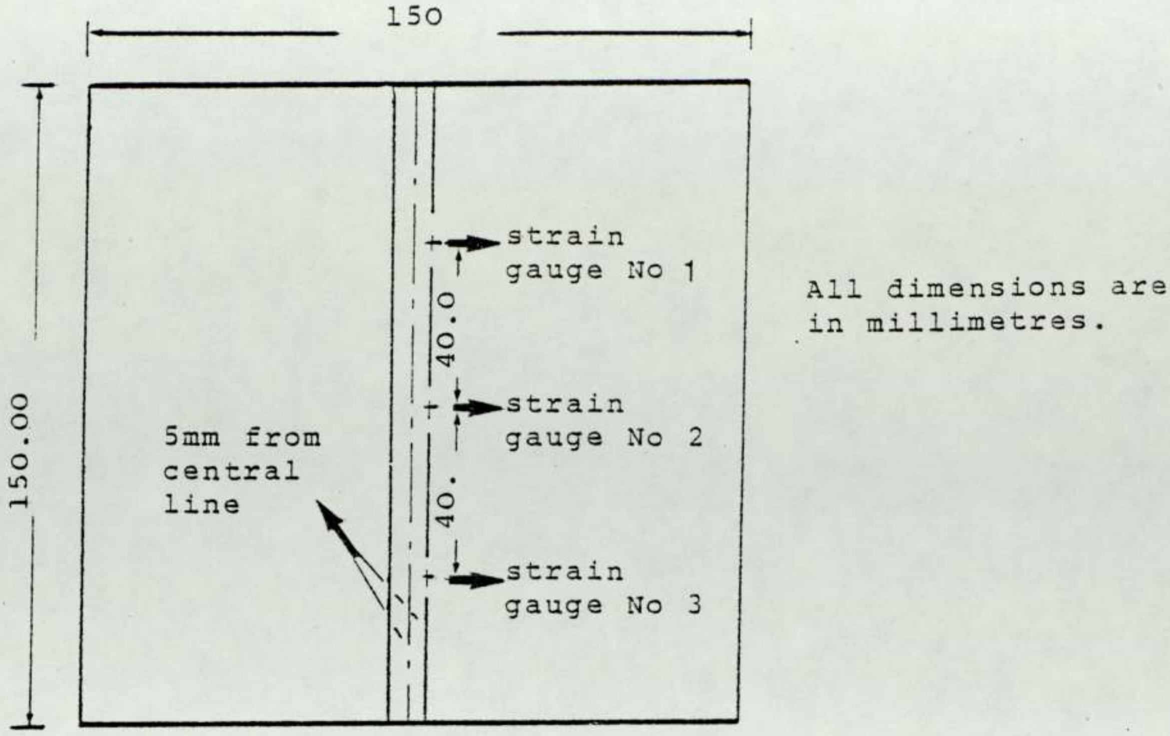

Fig B.3 The disposition of strain gauges on the base plate along the one edge of the loading piece (150x10)

Load	Stress in Steel Base Plate N/mm^2		
KN	Gauge no 1	Gauge No 2	Gauge NO 3
00.0	00.00	00.00	00.00
2.5	21.20	17.00	19.20
10.0	26.36	20.30	24.20
20.0	28.40	27.00	26.00
30.0	35.50	31.40	32.40
40.0	41.70	37.60	38.70
50.0	48.30	46.00	46.20
60.0	59.80	54.30	55.40
70.0	67.20	68.30	64.20
80.0	78.20	74.60	76.20
100.0	107.60	102.40	106.20
120.0	138.00	134.00	136.60
130.0	169.20	154.70	158.60
140.0	186.30	192.40	190.30
150.0	215.00	225.00	218.30
160.0	243.70	238.20	241.30
180.0	495.00	422.00	465.00
200.0	U S	U S	U S
209.0	U S	U S	U S

Table B.3 Concentric strip loading on 150 mm cube through 4 mm thick steel base plate (strain gauges were fixed as shown in Fig. B.3) .

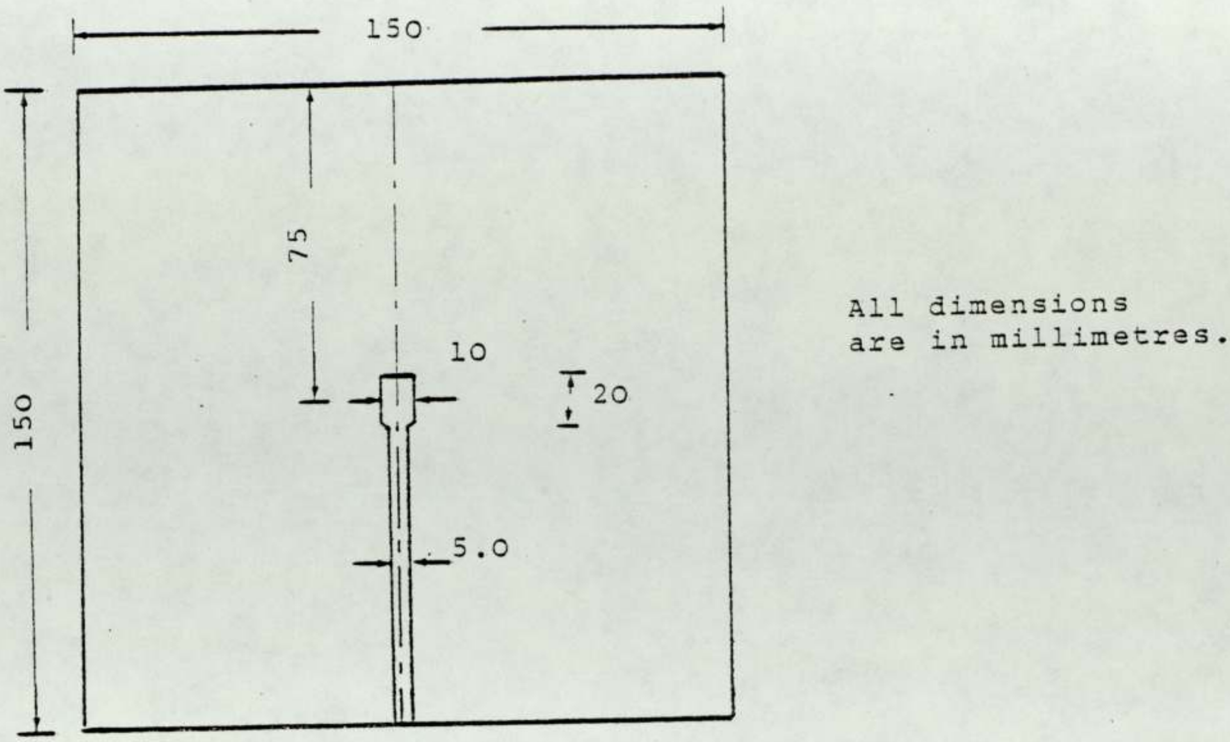

Fig. B.4 Plan view of 150mm concrete cube showing the gaps made on its surface for the strain gauges and leads

Load KN	Stress in Steel Base Plate (N/mm^2) Upper Face	Lower Face
0.00	00.00	0.00
2.50	18.27	-17.86
5.00	20.30	-18.88
10.00	24.36	-20.50
15.00	30.04	-24.80
20.00	38.57	-32.10
25.00	48.72	-42.22
30.00	52.78	-46.28
35.00	60.90	-53.39
40.00	72.06	-64.55
45.00	79.17	-70.64
50.00	97.44	-89.93
55.00	107.59	-100.10
60.00	121.80	-114.29
67.00	147.78	-139.66
Released	3.10	-2.20

Table B.4 Concentric knife-edge loading through 4 mm thick base plate with gauges fixed on the lower and upper faces

* Negative sign indicates tension.

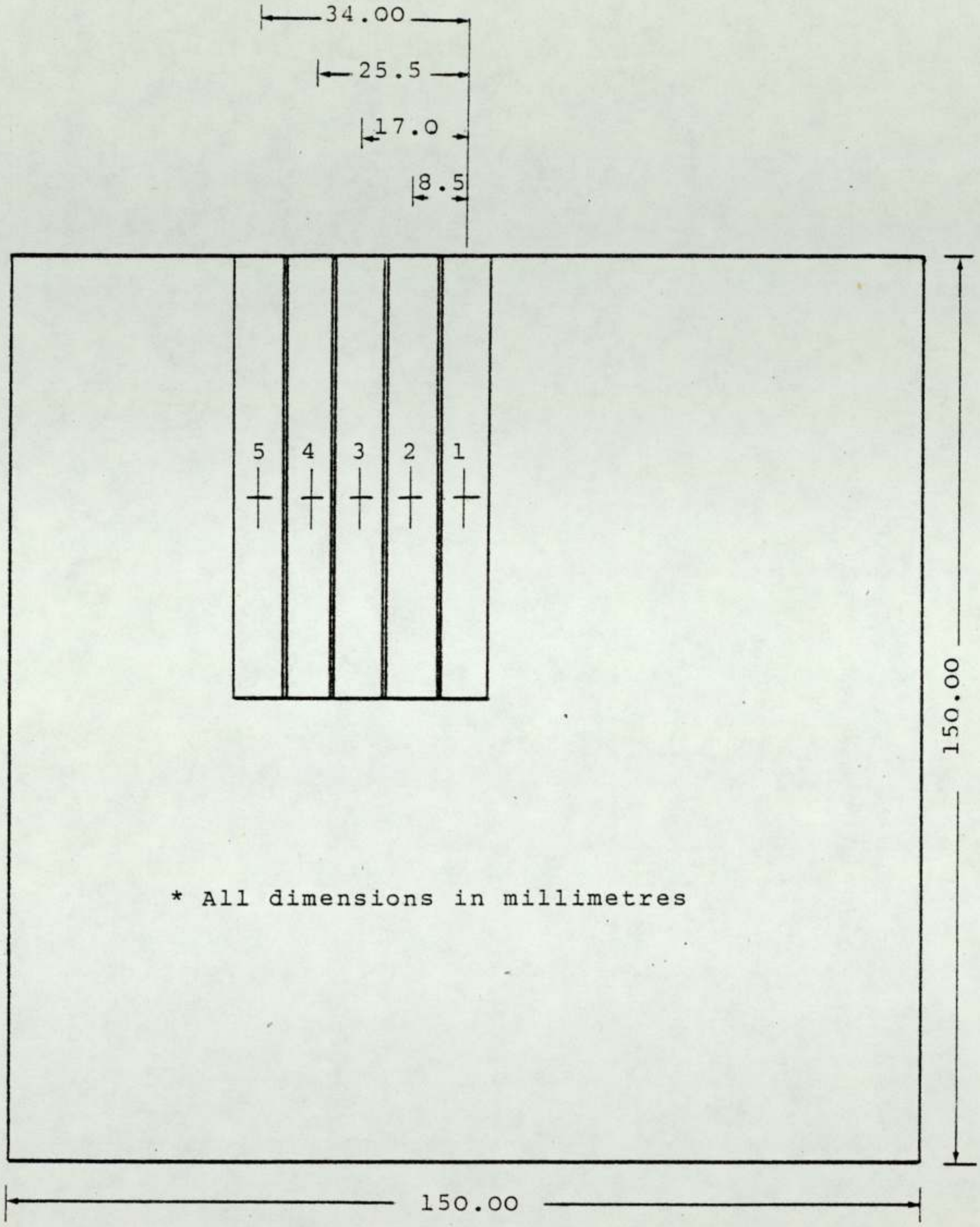

Fig. B.5 Disposition of strain gauges on the concrete cubes.

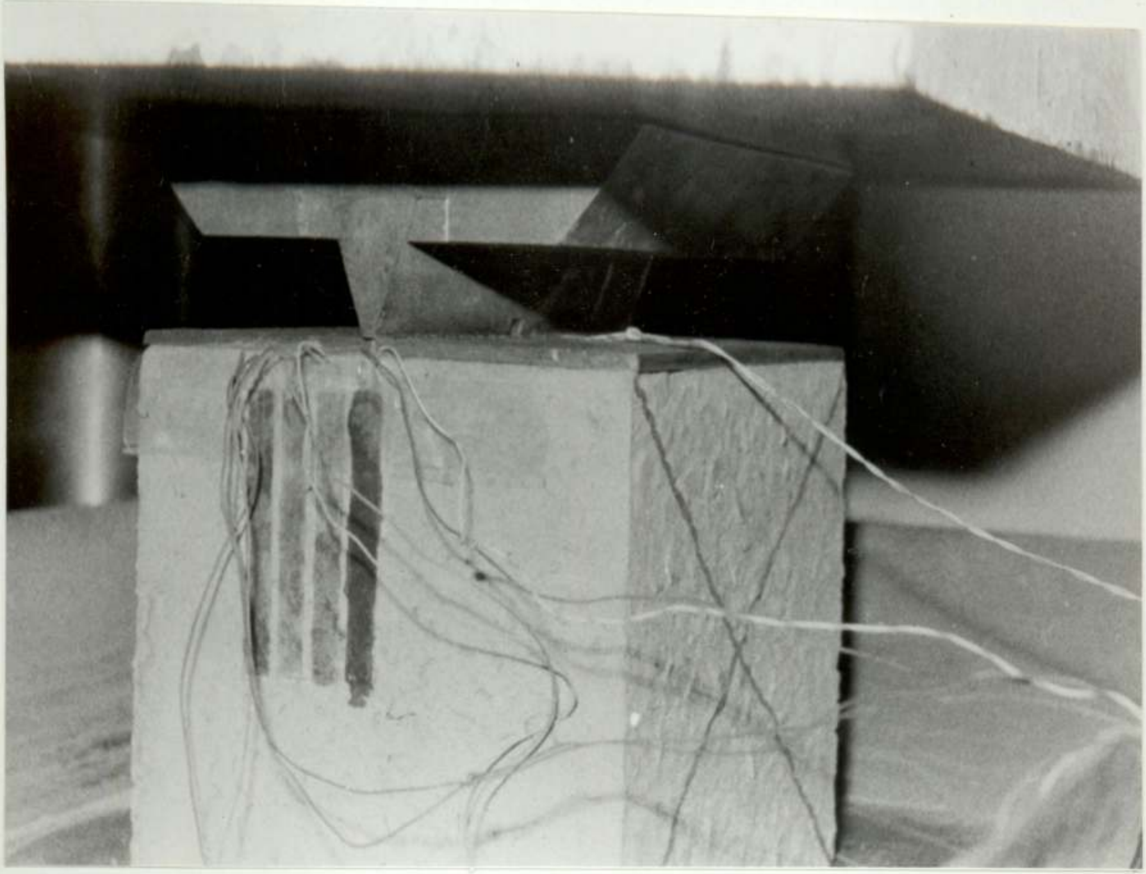

Plate B.3 Disposition of strain gauges on a concrete cube and a base plate 4mm thick

(Scale 1:3)

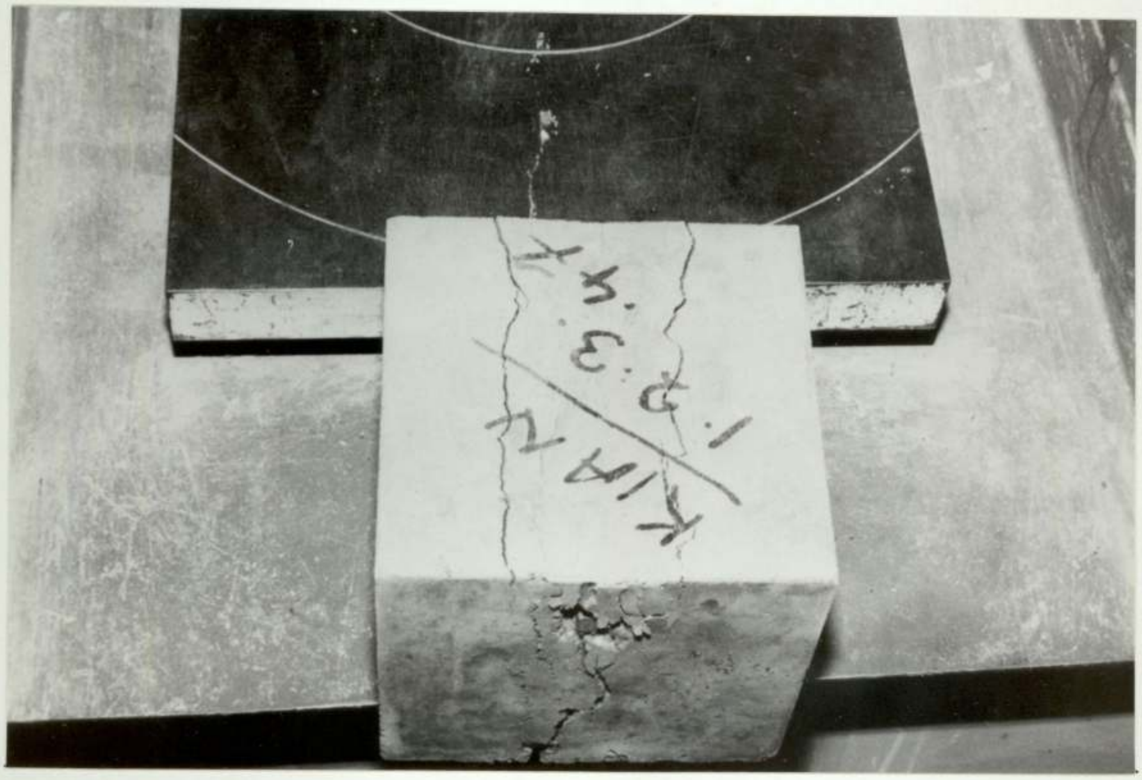

Plate B.4 Mode of failure of 150mm cube, loaded concentrically through a knife edge loading piece.

(Scale 1:3)

Load KN	Stress in concrete at five different positions N/mm^2 1	2	3	4	5
0.00	0.00	0.00	0.00	0.00	0.00
2.50	0.00	0.00	0.00	0.00	0.00
7.50	0.00	0.00	0.00	0.00	0.00
15.00	-.20	0.00	0.00	0.00	0.12
25.00	-.10			0.00	0.00
35.00	0.00	F	F	0.00	0.12
40.00	0.26	A	A	0.34	0.48
50.00	0.83	U	U	3.16	4.26
55.00	1.10	L	L	4.54	7.01
60.00	1.51	T	T	7.98	14.72
65.00	2.20	Y	Y	10.73	20.77
70.00	2.34	GAUGES		14.17	26.28
75.00	4.26			22.00	22.15
80.00	U S.			U S.	U S.

Table B.5- Concentric knife-edge loading through a 4mm steel base plate on a 150mm concrete cube (f_{cu} = 10.9N/mm^2).

Load KN	Stress in concrete at five different positions N/mm² 1	2	3	4	5
0.0	0.00	0.00	0.00	0.00	0.00
2.5	1.86	1.86	1.49	1.20	0.78
5.0	2.48	2.17	1.80	1.24	0.78
10.0	5.20	3.88	3.04	2.33	1.55
20.0	6.51	6.05	4.74	3.41	2.02
30.0	8.22	7.60	5.89	4.34	2.64
40.0	10.40	9.60	7.40	5.43	3.45
50.0	12.70	11.87	8.99	6.45	4.19
60.0	14.60	13.50	10.30	7.40	4.80
70.0	16.40	15.00	11.40	8.10	5.20
80.0	18.00	16.60	12.30	8.70	5.70
90.0	19.50	17.80	13.10	9.30	6.10
100.0	21.50	19.50	14.30	9.90	6.70
110.0	23.70	21.40	15.60	10.90	7.30
120.0	25.60	22.80	16.40	11.80	7.80
130.0	27.60	24.70	17.50	12.30	8.20
140.0	29.80	26.50	18.90	13.00	8.80
150.0	34.10	29.00	19.90	14.00	9.30
160.0	36.00	31.80	21.30	14.60	9.80
170.0	38.80	34.70	22.40	15.20	10.20
180.0	43.40	38.90	23.80	16.00	10.70
190.0	47.70	42.60	25.40	16.90	11.30
200.0	53.60	47.70	26.60	17.40	11.60
210.0	64.80	56.00	27.80	17.10	11.30
220.0	77.20	65.30	29.70	17.20	10.90
230.0	U S.	U S.	U S.	U S.	U S.
240.0	U S.	U S.	U S.	U S.	U S.
260.0	U S.	U S.	U S.	U S.	U S.

Table B.6- Concentric knife-edge loading through a 6mm steel base plate on a 150mm concrete cube (f_{cu} = 40.0N/mm²).

APPENDIX C TO CHAPTER FIVE

Table c.1	Details of the results presented in Table 5.4, correlated the Author's tests to the design load recommended by AISC
Table C.2	Details of the results presented in Table 5.5, correlated the Author's tests to the design load recommended by Draft of Steel Code
Table C.3	Details of the results presented in Table 5.6, correlated the Author's tests to the design load recommended by BS 449

Test Series	Test No	Concrete Strength f_{cu} N/mm^2	Loading Section B mm	D mm	Effective Cantilever Length a_e Eq.(5.5) mm	b_e Eq.(5.6) mm	Effective Column Base X Eq.(5.7) mm	Y Eq.(5.8) mm	Design Load F_w Eq.(5.9) KN
(I)	I1	27.9	10	76	13.3	13.3	34.5	98.7	20.2
on 150mm	I2	27.9	22	76	13.3	13.3	44.1	98.7	23.8
cubes	I3	27.9	36	76	13.3	13.3	55.3	98.7	32.4
t=4mm	I4	27.9	61	76	13.3	13.3	75.3	98.7	44.1
	I5	27.9	76	76	13.3	13.3	87.3	98.7	51.1
(II)	II1	34.0	10	151	11.8	11.8	31.5	167.0	38.0
on 250mm	II2	30.0	30	151	12.5	12.5	49.1	168.5	52.7
cubes	II3	30.0	50	151	12.5	12.5	65.1	168.5	69.9
t=4mm	II4	34.0	70	151	11.8	11.8	79.5	167.0	96.0
	II5	34.0	90	151	11.8	11.8	95.5	167.0	111.3
	II6	30.0	110	151	12.5	12.5	113.1	168.5	121.4
	II7	34.0	130	151	11.8	11.8	127.5	167.0	153.9
	II8	30.0	151	151	12.5	12.5	145.9	169.0	158.7
(III)	III1	34.4	10	162	23.4	23.9	54.8	200.7	80.4
on 250mm	III2	26.0	50	162	26.9	26.9	93.8	207.7	106.7
cubes	III3	26.0	70	162	26.9	26.9	109.8	207.7	126.0
t=8mm	III4	34.4	90	162	23.4	23.9	118.8	200.7	174.3

Table C.1 Details of the results presented in Table 5.4, correlated the Author's tests to the design load recommended by AISC.

(CONTINUED)

Test Series	Test No	Concrete Strength	Loading Section		Effective Cantilever Length		Effective Column Base		Design Load
		f_{cu} N/mm^2	B mm	D mm	a_e Eq.(5.5) mm	b_e Eq.(5.6) mm	X Eq.(5.7) mm	Y Eq.(5.8) mm	F_w Eq.(5.9) KN
	III5	34.4	110	162	23.4	23.9	134.8	200.7	197.7
	III6	26.0	130	162	26.9	23.9	157.8	207.7	181.1
	III7	26.0	150	162	26.9	26.9	173.8	207.7	199.5
(IV)	IV1	26.0	50	162	41.1	41.1	122.2	236.1	159.3
on 250mm	IV2	26.0	70	162	41.1	41.1	138.2	236.1	180.2
cubes	IV3	26.0	90	162	41.1	41.1	154.2	236.1	201.1
t=12mm	IV4	26.0	110	162	41.1	41.1	170.2	236.1	221.9
	IV5	26.0	130	162	41.1	41.1	186.2	236.1	242.8
	IV6	26.0	150	162	41.1	41.1	202.2	236.1	263.7

Table C.1 Details of the results presented in Table 5.4, correlated the Author's tests to the design load recommended by AISC.

Test Series	Test No	Concrete Strength	Loading Section		Effective Cantilever Length		Effective Column Base		Design Load
		f_{cu} N/mm^2	B mm	D mm	a_e Eq.(5.11) mm	b_e Eq.(5.10) mm	X Eq.(5.12) mm	Y Eq.(5.13) mm	F_u Eq.(5.14) KN
(I)	I1	27.9	10	76	12.2	11.3	32.5	98.6	35.7
on 150mm	I2	27.9	22	76	16.1	11.3	49.8	98.6	54.8
cubes	I3	27.9	36	76	20.6	11.3	69.9	98.6	79.9
t=4mm	I4	27.9	61	76	22.6	11.3	94.1	98.6	103.3
	I5	27.9	76	76	22.6	11.3	106.1	98.6	116.7
(II)	II1	34.0	10	151	11.4	10.2	30.8	171.5	71.2
on 250mm	II2	30.0	30	151	18.3	10.9	60.6	172.8	125.7
cubes	II3	30.0	50	151	24.7	10.9	89.4	172.8	185.4
t=4mm	II4	34.0	70	151	30.6	10.2	117.2	171.5	273.3
	II5	34.0	90	151	37.0	10.2	145.9	171.5	340.4
	II6	30.0	110	151	43.9	10.9	175.8	172.8	364.6
	II7	34.0	130	151	49.3	10.2	202.5	171.5	472.3
	II8	30.0	151	151	49.0	10.9	218.9	172.8	453.8
(III)	III1	34.4	10	162	20.4	20.4	48.7	202.7	135.8
on 250mm	III2	26.0	50	162	34.7	23.4	109.5	208.8	237.7
cubes	III3	26.0	70	162	41.1	23.4	138.3	208.8	300.2
t=8mm	III4	34.4	90	162	45.1	20.4	162.2	202.7	452.3

Table C.2 Details of the results presented in Table 5.5, correlated the Author's tests to the design load recommended by DSC.

(CONTINUED)

Test Series	Test No	Concrete Strength	Loading Section		Effective Cantilever Length		Effective Column Base		Design Load
		f_{cu} N/mm^2	B mm	D mm	a_e Eq.(5.11) mm	b_e Eq.(5.10) mm	X Eq.(5.12) mm	Y Eq.(5.13) mm	F_u Eq.(5.14) KN
	III5	34.4	110	162	49.6	20.4	187.2	202.7	522.0
	III6	26.0	130	162	48.5	23.4	201.0	208.8	436.5
	III7	26.0	150	162	48.5	23.4	207.0	208.8	471.3
(IV)	IV1	26.0	50	162	44.4	35.1	128.2	232.2	309.6
on 250mm	IV2	26.0	70	162	44.4	35.1	144.8	232.2	349.8
cubes	IV3	26.0	90	162	44.4	35.1	160.8	232.2	388.4
t=12mm	IV4	26.0	110	162	44.4	35.1	176.8	232.2	427.1
	IV5	26.0	130	162	44.4	35.1	192.8	232.2	465.7
	IV6	26.0	150	162	44.4	35.1	208.8	232.2	504.3

Table C.2 Details of the results presented in Table 5.5, correlated the Author's tests to the design load recommended by DSC.

Test Series	Test No	Concrete Strength	Loading Section		Effective Cantilever Length		Effective Column Base		Design Load
		f_{cu} N/mm^2	B mm	D mm	a_e Eq.(5.15) mm	b_e Eq.(5.16) mm	X Eq.(5.17) mm	Y Eq.(5.18) mm	F_w Eq.(5.19) KN
(I)	I1	27.9	10	76	11.9	11.9	33.8	99.8	23.5
on 150mm	I2	27.9	22	76	11.9	11.9	45.8	99.8	31.9
cubes	I3	27.9	36	76	11.9	11.9	59.8	99.8	41.6
t=4mm	I4	27.9	61	76	11.9	11.9	84.8	99.8	59.0
	I5	27.9	76	76	11.9	11.9	99.8	99.8	69.5
(II)	II1	34.0	10	151	10.8	10.8	31.6	172.6	46.4
on 250mm	II2	30.0	30	151	11.5	11.5	53.0	174.0	69.2
cubes	II3	30.0	50	151	11.5	11.5	73.0	174.0	95.3
t=4mm	II4	34.0	70	151	10.8	10.8	91.6	172.6	134.4
	II5	34.0	90	151	10.8	10.8	111.6	172.6	163.7
	II6	30.0	110	151	11.5	11.5	133.0	174.0	173.6
	II7	34.0	130	151	10.8	10.8	151.6	172.6	222.4
	II8	30.0	151	151	11.5	11.5	174.0	174.0	227.1
(III)	III1	34.4	10	162	21.4	21.4	52.8	204.8	93.0
on 250mm	III2	26.0	50	162	24.7	24.7	99.4	211.4	136.6
cubes	III3	26.0	70	162	24.7	24.7	119.4	211.4	164.1
t=8mm	III4	34.4	90	162	21.4	21.4	132.8	204.8	233.9

Table C.3 Details of the results presented in Table 5.6, correlated the Author's tests to the design load recommended by BS449.

(CONTINUED)

Test	Test	Concrete Strength	Loading Section		Effective Cantilever Length		Effective Column Base		Design Load
Series	No	f_{cu} N/mm^2	B mm	D mm	a_e Eq.(5.15) mm	b_e Eq.(5.16) mm	X Eq.(5.17) mm	Y Eq.(5.18) mm	F_w Eq.(5.19) KN
	III5	34.4	110	162	21.4	21.4	152.8	204.8	269.1
	III6	26.0	130	162	24.7	24.7	179.4	211.4	246.5
	III7	26.0	150	162	24.7	24.7	199.4	211.4	274.0
(IV)	IV1	26.0	50	162	37.0	37.0	124.0	236.0	190.2
on 250mm	IV2	26.0	70	162	37.0	37.0	144.0	236.0	220.9
cubes	IV3	26.0	90	162	37.0	37.0	164.0	236.0	251.6
t=12mm	IV4	26.0	110	162	37.0	37.0	184.0	236.0	282.2
	IV5	26.0	130	162	37.0	37.0	204,0	236.0	312.9
	IV6	26.0	150	162	37.0	37.0	224.0	236.0	343.6

Table C.3 Details of the results presented in Table 5.6, correlated the Author's tests to the design load recommended by BS449.

REFERENCES

1. BAUSCHINGER,J : Versuche Mit Quedern Aus Naturstein, Mechanischen und Technischen Laboratorium denkge, Technischen Hochschule, Munich, Germany, vol.6, 1876.P.13

2. MEYERHOF,G.G. : The Bearing Capacity of Concrete and Rock. Magazine of Concrete Research. Vol.4, No 12. April 1953. pp.107-116.

3. GRAF,O : Versuch Mit Betonquadern Zu Brucken-gelenken und Auflagern. Berlin, Verein Deutscher Ingenieure. Mitteilungen uber Forschungsarbeiten. No.232. 1921. P.68

4. SHELSON,W : Bearing Capacity of Concrete. Journal of the American Concrete Institute. Proceedings Vol.54, No.12. June 1958. PP.1183-1189.

5. PARKER,W : Loading Tests on Limit Area of Concrete Specimen, Report Lo 40424, Research Division, Hydro-Electric Power Commission of Ontario, 1947

6. TUNG AU : D.CAMPBELL-ALLEN PLEWES,W.G ROYER,M Discussion of "Bearing Capacity of Concrete," ACI Journal, V.29, No.12, June 1958 (Proceedings V.54), PP.1183-1189.

7. TUNG AU : BAIRD,D.L Bearing Capacity of Concrete Blocks. Journal of the American Concrete Institute. Proceedings Vol.56, No.9. March 1960. PP.869-879.

8. ŨGUR ERSOY : HAWKINS, N.M — Discussion of "Bearing Capacity of Concrete." ACI Journal, Vol.56, Part 2. September 1960. PP.1467 -1479.

9. MUGURUMA, H : OKAMOTO, S — Study on Bearing Capacity of Concrete. Proceedings of the Eighth Japan Conference on Testing Materials - Non-Metallic Materials. March 1965.

10. HAWKINS, N.M. : The Bearing Strength of Concrete Loaded Through Rigid Plates. Magazine of Concrete Research. Vol.20, No.62. March 1968. PP.31-40.

11. COWAN, H.J. : The Strength of Plain, Reinforced and Prestressed Concrete Under The Action of Combined Stresses, With Particular Reference to the Combined Bending and Torsion of Rectangular Sections. Magazine of Concrete Research. Vol.5, No.14, December 1953. PP.75-86.

12. HAWKINS, N.M : The Bearing Strength of Concrete for Strip Loadings. Magazine of Concrete Research. Vol.22, No.71. June 1970. PP.87-98.

13. HAWKINS, N.M : The Bearing Strength of Concrete Loaded Through Flexible Plates. Magazine of Concrete Research. Vol.20, No.63. June 1968. PP.95-102.

14. CHEN, W.F : DRUCKER, D.C — Bearing Capacity of Concrete Blocks or Rock. Proceedings of the American Society of Civil Engineering, Journal of the

Engineering Mechanics Division. Vol.95, No.EM4. August 1969. PP.955-978.

15. DRUCKER,D.C, PRAGER,W GREENBER,H.J : Extended Limit Design Theorems for Continuous Media, Quarterly of Applied Mathematics, Vol.9, PP.381-389. 1952.

16. GRAF,O : Versuch Mit Betungquadern zu Bruckengelenken und Auflagern, Berlin, Verein Deutscher Ingenieure, Mitteilungen uber Forschungsarbeiten, No.232, P.68, 1921. Uber Einige Aufgaben der Eisenbetonforschung Aus Alterer und Neuerer Zeit, Beton und Eisen, ol.33, No.11, PP.165-173, June 1934.

17. HYLAND,M.W CHEN,W.F : Bearing Capacity of Concrete Blocks. Journal of the American Concrete Institute. Proceedings Vol.67, No.3. March 1970. PP.228-236.

18. NIYOGI,S.K : Bearing Strength of Concrete Geometric Variations. Proceedings of the American Society of Civil Engineers, Journal of The Structural Division. Vol.99, No.517. July 1973 PP.1471-1490.

19. NIYOGI,S.K : Concrete Bearing Strength - Support, Mix, Size Effect. Proceedings of the American Society of Civil Engineers, Journal of the Structural Division. Vol.100, No.518. August 1974. PP.1685-1702.

20. DE-WOLF,M ASCE : Axially Loaded Column Base Plates. Journal of the

Structural Division. Vol.104, No.st5. May 1978. PP.781-792.

21. WILLIAMS,A : The Bearing Capacity of Concrete Loaded Over A Limited Area. Wesham Springs, Cement and Concrete Association, August 1979, P.70. Technical Report 526 (Publication 42.526).

22. BRITISH STANDARDS INSTITUTION : The Structural Use of Concrete. Part.1 : Design, Materials and Workmanship. London, 1972. 154. PP.CP 110:Part 1.

23. CEB-FIP : Model Code for Concrete Structural. Paris, Comite Euro-internationale du Beton, 1978. PP.348.

24. GERMAN COMMITTEE for REINFORCED CONCRETE : Concrete and Reinforced Concrete Structures : Design and Construction. Koln, 1972. Translated and published by the British Standards Institute. DIN 1045.

25. SOCIETE de DIFFUSION des TECHNIQUES du BATIMENT et des TRAVAUX PUCS : Technical Rules for Design and calculations Relating to Reinforced Concrete Structures and Buildings. Paris, 1968. Translated and published by the British Standards Institute. Rules CCBA 68.

26. REPUBLIQUE FRANCAISE : Conception et Calcul du Beton Precontraint. (Conception and design of prestressed concrete.) Provisional Instruction of 13th August 1973. Available in English translation.

27. American Concrete Institute : Building Code Requirements for Reinforced Concrete (ACI 318-77). Chapter 10. Included in ACI Manual of Concrete Practice 1978, Part 2. Detroit.

28. BRITISH STANDARD INSTITUTE : Method of testing concrete, part 4 - methods for testing concrete for strength. BS 1881 : 1970, part 4. LONDON. 1970.

29. AMERICAN INSTITUTE OF STEEL CONSTRUCTION Specification for the design, fabrication and erection of structural steel for buildings. AISC, New York, 7th Edition, 1973

30. BRITISH STANDARD INSTITUTION Draft standard specification for the structural use of steelwork in building. Part 1. November 1977.

31. BRITISH STANDARD INSTITUTION The use of structural steel in building. BS 449 : 1967.

32. ROWE, R.E : ZIELINSKI, J An Investigation of the Stress Distribution in the Anchorage Zone of Post-Tensioned Concrete Members. Research Report No.9. C & C.A. 1960.

33. SUNDARA, K.T : IYENGAR, R Two Dimensional theories of Anchorage Zone Stresses in Post- Tensioned Prestressed Beams. Jour. A.C.I. Oct, 1962, Vol.59, No.10.

34. MÖRSCH, E : Uber Die Berechnug de Gelenkquaden Beton und Eisen 1924, No. 12, pp. 156-161.

35. BORTCH,R : Die Spannungen in Walzgelenkguadern, Beton und Eisen, Feb. 1935, Vol. 35, No.4, pp. 61-66.

36. MAGNEL,G : Design of the Ends of Prestressed Concrete Beams. Concrete and Construction Engineering, May 1949, Vol.44, No.5, pp. 141-148.

37. GUYON,Y Contraintes dans les Piece Prismatiques Sourmises a des Forces Appliques Surleur Bases, au Voisinages Deces Bases. Publications, I.A.B.S.E. 1951, Vol.11. pp. 165-226.

38. TIMOSHENKO,S GOODIER,J.N Theory of Elasticity, 2nd Edn. 1951, Mc GrawHill Book CO. Inc.

39. CHRISTODOULIDES,S.P A Three Dimensional Investigation of the Stresses in the End Anchorage Blocks of a Prestressed Concrete Gantry beam.

40. CHRISTODOULIDES,S.P A Two Dimensional Investigation of the End Anchorages of Post-Tensioned Concrete Beams. The Structural ENgineer, April 1955, Vol.33, PP. 120-133.

41. BLEICH,F Der Gerade Stab Mit Rechteckguerschnitt als ebenes Problem. Der Bauingeniur. No. 9. 1923. , pp. 255-259, No. 10, pp. 304-307.

42. BAN,S MUGURUMA,H OGAKI,Z Anchorage Zone Stress Distributions in Post-tensioned Concrete Members. Proceedings, World Conference on Prestressed

Concrete, San Francisco, July 1957, pp.16-1 - 16-4.

43. SIEVERS,H Uber den spannungszustand im bereich der ankerplatten von spanngliedern vorgespannter stahlbeton-konstruktionren. Der bauingenieur. Vol. 31, No.4. April 1956. pp. 134-135

44. CHEN,W.F Plasticity in Reinforced Concrete, 1st Edn. 1982, Mc Graw-Hill Book CO.Inc.

45. GUYON,Y Limit-State Design of Prestressed Concrete, Vol 1. 1972, Applied Science Publisher LTD, LONDON.

46. ROCKEY,K.C EVANS,H.R GRIFFITHS,D.W The Finite Element Method, 1st Edn. 1975, Granada Publishing Limited.

47. BRAY,K.H.M A Computer Analysis of Large Civil Engineering Strctures. Thesis, the University of Aston for the Degree of Ph.D. 1973.

48. ZIELINSKI,J ROWE,R.E The Stress Distribution Associated With Groups of Anchorages in Post-tensioned Concrete Members. Cement and Concrete Association, Research Report No.13, Oct 1962.

49. REYNOLDS,C.E Reinfoced Concrete Desiners Handbook, 6th Edition, Concrete Publications Ltd, LONDON 1961, pp. 238.

50. NEVILLE,A.M Properties of Concrete, 3rd Edition, Pitman & Sons Ltd., LONDON 1963.

51. ZIENKIEWICZ,C.O The finite element method, 3rd

Edition. 1977 Mc Graw-Hill book
Co.Inc.